Experimental Testing and Analytical Modeling of Driven Steel Pile Bridge Bents

by

Jonathon A. Campbell

A thesis submitted to the Graduate Faculty of
Auburn University
in partial fulfillment of the
requirements for the Degree of
Master of Science

Auburn, Alabama
December 12, 2015

Lateral Load Testing, Bridge Engineering, Analytical Modeling, Soil-Structure Interaction

Approved by

Justin D. Marshall, Chair, Associate Professor of Civil Engineering
J. Brian Anderson, Ph.D., P.E. Associate Professor of Civil Engineering
Robert W. Barnes, Associate Professor of Civil Engineering

Abstract

One of the most common bridge types in Alabama is the multi-span bridge with precast girders and intermediate bents consisting of driven steel piles and a reinforced concrete cap. Due to its common use, effective analysis procedures for these types of bridges would result in the most sustainable use of resources. Driven pile bridge bents represent a soil-structure interaction and the bents are highly indeterminate; therefore assumptions made in analysis of these bents regarding certain boundary conditions including level of composite activity and pile-to-cap fixity are very important. ALDOT had recently highlighted issues with the analysis and design of steel pile bents where design pile forces were significantly higher than anticipated especially under cases involving lateral loads. The assumptions made in the analysis of these bents can have a significant impact on the numerical results. The research presented in this thesis sought to determine the appropriate boundary conditions to use in analysis of these bents through a series of lateral load tests on new construction and in-service bridges. Following testing of these bridges, analytical models were developed in SAP 2000 to determine a correlation between the field results and the models, and to simulate bridge behavior that was difficult to measure in the field.

It was concluded that the largest bending moments in the piles of the steel pile bents are developed near the top of the pile which is embedded into the cap, indicating the connection between the pile and the cap acts more as a fixed condition than a pinned condition. In cases where the piles were encased in concrete, the overall lateral stiffness of the bent is increased significantly due to the large moment of inertia of the encasements. Furthermore, during tests performed in

which an ALDOT load truck was used to apply gravity load, it was found that the live load induced a lateral deflection opposite in direction than the deflections from the tests without the truck. As a result, smaller net deflections were measured in the load tests with the load truck. These results were similar in the analyses performed in the SAP models as well.

Acknowledgments

First I would like to thank the members of my committee for their guidance and help throughout the duration of my research efforts. I would like to thank Dr. Anderson for his insight and knowledge during the field testing portion of the project. Thank you for helping make ideas for load tests on a piece of paper become a reality. I would like to especially thank Dr. Marshall, my major professor, for his constant guidance, help and patience throughout this entire project.

I would like to personally thank Dan Jackson, Lester Lee, Patrick Koch, Joseph Broderick, Jeremy Herman, Taylor Rawlinson, Adam Carroll and Pavlo Voitenko for their help during the field testing portion of this load test. Without your help, our field tests would never have happened as smoothly as they did. I would especially like to thank my research partner throughout this project, Zach Skinner. This project has truly been a collaborative effort and it has been a great privilege having him as a research partner and as a friend. I also must extend a special thanks to the people at LC Technology International for their help in recovering more than 8 months' worth of data analysis from a corrupted flash drive.

Finally, I would like to thank my parents for their love and support during my time at Auburn. They were always there for me every step of the way and have always supported my every move.

Table of Contents

Chapter 1 Introduction 1
1.1 Overview 1
1.2 Problem Statement 3
1.3 Research Objectives 3
1.4 Research Scope 4
1.4.1 Field Testing Overview 4
1.4.2 Computer Modeling and Design Methodologies 5
1.5 Organization of Thesis 5
Chapter 2 Background and Literature Review 7
2.1 Background and Description of Pile Bent Substructures 7
2.1.1 Pile Bent Description 8
2.1.2 Construction Process for Pile Bents 9
2.2 Lateral Load Testing Background 15
2.2.1 ASTM D3966 Provisions and Requirements 15
2.2.2 Testing Methods 16
2.3 Theoretical Behavior of Deep Foundations Under Lateral Loads 18
2.4 Analysis Methods for Deep Foundations 19
2.4.1 P-y Method 19
2.4.2 Broms's Methods for Determining Deflections and Ultimate Pile Capacity 20
2.4.3 Elastic Continuum Theory 21
2.5 Pile to Cap Modeling 22
2.6 Software Implementation 25
2.6.1 SAP 2000 25
Chapter 3 Field Test 1-Macon County Bridge 27
3.1 Introduction 27
3.2 Instrumentation 29
3.2.1 Instrumentation Layout 29
3.2.2 Installation of Electrical Resistance Gages on Steel Piles 35
3.2.3 Installation of Electrical Resistance Gages to Concrete Surfaces 40
3.2.4 Sister Bar Strain Gages 41
3.2.5 Displacement Wirepots 42
3.3 Testing Equipment and Setup 43
3.3.1 Reaction Frame Configuration 43
3.3.2 Hydraulic Jacks 45
3.3.3 Threaded Rods/Anchorage 46
3.3.4 Reference Frame for Wirepots 49
3.3.5 Data Acquisition 50
3.4 Testing Procedure 51
3.4.1 Load Monitoring During Test 51
3.4.2 Static Lateral Load Test 52
3.5 Analysis, Results, and Discussion of Load Test 53
3.5.1 Strains 53
3.5.2 Axial Force and Bending Moment Calculations from Strain Data 60

3.5.3 Axial Forces 65
3.5.4 Bending Moments 65
3.5.5 Displacement String Pots 69
3.5.6 Bridge Bent Behavior 71
3.6 Chapter Summary 72
Chapter 4 Field Test 2 – Macon County Bridge 73
4.1 Introduction 73
4.2 Instrumentation 74
4.3 Testing Equipment and Setup 74
4.3.1 Reaction Frame Configuration 74
4.3.2 Hydraulic Jacks 75
4.3.3 Threaded Rods/Anchorage 75
4.3.4 Truck Live Load 75
4.3.5 Reference Frame For Wirepots 77
4.3.6 Data Acquisition 77
4.4 Testing Procedure 77
4.4.1 Static Lateral Load Test 77
4.4.2 Combined Lateral and Gravity Load Test – Truck Centered in Roadway 78
4.4.3 Combined Lateral and Gravity Load Test – Truck Positioned at Edge of Roadway 80
4.5 Analysis, Results and Discussion of Load Test 82
4.5.1 Strains 83
4.5.2 Axial Force and Bending Moment Calculations from Strain Data 83
4.5.3 Axial Forces 84
4.5.4 Bending Moments 84
4.5.4.1 Lateral Only 85
4.5.4.2 Combined Lateral and Gravity with Truck Centered on Roadway 88
4.5.4.3 Combined Lateral and Gravity with Truck at Edge of Roadway 91
4.5.5 Displacement String Pots 94
4.5.6 Bridge Bent Behavior 97
4.6 Chapter Summary 97
Chapter 5 Field Test 3 – US 331 Bridge 99
5.1 Introduction 99
5.2 Instrumentation 99
5.2.1 Instrumentation Layout 99
5.2.2 Installation of Electrical Resistance Gages to Concrete Surfaces 101
5.2.3 Displacement Wirepots 104
5.3 Testing Equipment and Setup 105
5.3.1 Reaction Against Adjacent Bent 105
5.3.2 Hydraulic Jacks 106
5.3.3 Truck Live Load 107
5.3.4 Threaded Rods/Anchorage 108
5.3.5 Reference Frame for Wirepots 111
5.4 Testing Procedure 112
5.4.1 Load Monitoring During Test 112
5.4.2 Combined Gravity and Lateral Load Test 113
5.4.3 Static Lateral Load Test 115

5.5 Analysis, Results and Discussion of Load Test 115
5.5.1 Strains 116
5.5.2 Calculation of Axial Forces and Bending Moments 116
5.5.3 Test Bent Axial Forces – Combined Gravity and Lateral 119
5.5.4 Test Bent Bending Moments – Combined Gravity and Lateral 123
5.5.5 Reaction Bent Axial Forces – Combined Gravity and Lateral 130
5.5.6 Reaction Bent Bending Moments – Combined Gravity and Lateral 132
5.5.7 Test Bent Axial Forces – Lateral Load Only 135
5.5.8 Test Bent Bending Moments – Lateral Load Only 139
5.5.9 Reaction Bent Axial Forces – Lateral Load Only 145
5.5.10 Reaction Bent Bending Moments – Lateral Load Only 147
5.5.11 Displacement Wirepots 150
5.5.12 Bridge Bent Behavior 153
5.6 Chapter Summary 154
Chapter 6 Analytical Modeling of Tested Bridges 156
6.1 Introduction 156
6.2 Geometric Properties 156
6.3 Material and Frame Section Properties 157
6.4 Modeling of Soil Interaction 160
6.5 Loads 165
6.6 Analysis Results 169
6.6.1 Macon County Bent Without Deck 169
6.6.2 Macon County Test with Deck 180
6.6.3 US 331 Test 195
6.7 Chapter Summary 214
Chapter 7 Summary, Conclusions, and Recommendations 217
7.1 Summary 217
7.2 Conclusions 217
7.3 Recommendations 219
References 221
Appendix A. Threaded Rod Calibration Data A-1

List of Tables

Table 3-1 Concrete Properties 64
Table 6-1 Macon County Bent Spring Constants 164
Table 6-2 US 331 Bent Spring Constants 165
Table 6-3 Macon County Bent Loading Summary 168
Table 6-4 US 331 Bent Loading Summary 169

List of Figures

Figure 1-1 Typical Pile Bent Substructure with One-Story Sway Bracing 2
Figure 2-1 Typical Pile Bent with Galvanized Steel HP Piles and Reinforced Concrete Cap 8
Figure 2-2 Driven Steel Pile Bridge Bent with Concrete Encasements 9
Figure 2-3 Diesel Hammer Rig Used for Driving Piles 10
Figure 2-4 Diesel Hammer Being Lowered Into Driving Template 11
Figure 2-5 Piles Following Cut-Offs at Top of Pile Elevation 12
Figure 2-6 Driven HP Pile Following Excavation for Encasement Placement 13
Figure 2-7 Bent Cap Formwork Being Positioned 14
Figure 2-8 Cap Reinforcement Cage Prior to Concrete Placement 14
Figure 2-9 Casting of Concrete Bent Cap 15
Figure 2-10 Lateral Load Testing Methods by Pushing (ASTM 2007) 17
Figure 2-11 Lateral Load Testing Configuration by Pulling (ASTM 2007) 18
Figure 2-12 Solutions to Pile Deflections and Forces as a Function of Depth (Reese and Wang 2006) 19
Figure 3-1 Macon County Bridge Overall Plan (Weatherford & Associates 2013) 28
Figure 3-2 Elevation View of Bent 5 (Weatherford & Associates 2013) 29
Figure 3-3 Strain Gage Layout at Typical Instrumented Section 30
Figure 3-4 Steel Pile Instrumentation Layout Facing Old Town Creek 31
Figure 3-5 Steel Pile Instrumentation Layout Facing Away from Old Town Creek 32
Figure 3-6 Protective Angle Welded to Pile Flange 33
Figure 3-7 Concrete Encasement Instrumentation Layout Facing Old Town Creek 34
Figure 3-8 Sister Bar Layout Inside Bent Cap Facing Old Town Creek 34
Figure 3-9 Wirepot Configuration 35
Figure 3-10 Treated Steel Surface Prior to M-Bond Application 36
Figure 3-11 Installed Electrical Resistance Gage with Lead Wire Protection 37
Figure 3-12 Strain Gage with Soldered Connection to Three-Wire Cable 38
Figure 3-13 Electrical Resistance Gage with M-Coat J Surface Protection 39
Figure 3-14 Field-Installed Concrete Surface Gage 41
Figure 3-15 Sister Bar Tied into Bent Cap Reinforcing Cage 42
Figure 3-16 Field-Installed Wirepot 43
Figure 3-17 Reaction Frame Configuration 44
Figure 3-18 Threaded Rod End Anchorage at Reaction Frame 45
Figure 3-19 Enerpac Center-Hole Hydraulic Cylinders and Pump 46
Figure 3-20 Coupled Threaded Rod Sections 47
Figure 3-21 Steel Anchor Plate with Bearing Pad at Jack End 47
Figure 3-22 Gaged Threaded Rod Calibration 48
Figure 3-23 Field-Installed Threaded Rods with Instrumentation 49
Figure 3-24 Wooden Reference Frame for Wirepot Installation 50
Figure 3-25 Campbell Scientific CR1000 Datalogger (Campbell Scientific 2015) 51
Figure 3-26 Field Test Setup 52

Figure 3-27 Pile 1 Lower Section Strain Profile 55
Figure 3-28 Pile 1 Lower Section Strain Profile 55
Figure 3-29 Pile 2 Upper Section Strain Profile 56
Figure 3-30 Pile 2 Upper Section Strain Profile 56
Figure 3-31 Pile 2 Lower Section Strain Profile 57
Figure 3-32 Pile 2 Lower Section Strain Profile 57
Figure 3-33 Pile 3 Upper Section Strain Profile 58
Figure 3-34 Pile 3 Upper Section Strain Profile 58
Figure 3-35 Pile 4 Upper Section Strain Profile 59
Figure 3-36 Pile 4 Upper Section Strain Profile 59
Figure 3-37 Composite Cross-Section Geometry 62
Figure 3-38 Pile 1 Bending Moment Profile 66
Figure 3-39 Pile 1 Bending Moment Profile 66
Figure 3-40 Pile 2 Bending Moment Profile 67
Figure 3-41 Pile 2 Bending Moment Profile 67
Figure 3-42 Pile 3 Bending Moment Profile 68
Figure 3-43 Pile 3 Bending Moment Profile 68
Figure 3-44 Pile 4 Bending Moment Profile 69
Figure 3-45 Pile 4 Bending Moment Profile 69
Figure 3-46 Load-Deflection Plot – Macon County Test 1 70
Figure 4-1 Typical Roadway Cross Section (Weatherford & Associates 2013) 74
Figure 4-2 ALDOT Load Truck LC-5 Configuration (ALDOT) 76
Figure 4-3 LC-5 Geometry and Axle Loads 76
Figure 4-4 ALDOT Load Truck Centered in Roadway 79
Figure 4-5 Position of Load Truck Centered Over Roadway 79
Figure 4-6 ALDOT Load Truck Positioned at Edge of Roadway 81
Figure 4-7 Position of Load Truck Over Exterior Girder 82
Figure 4-8 Pile 3 Bending Moment versus Total Lateral Load Comparison 86
Figure 4-9 Pile 2 Bending Moment Profile 87
Figure 4-10 Pile 3 Bending Moment Profile 87
Figure 4-11 Pile 4 Bending Moment Profile 88
Figure 4-12 Pile 2 Bending Moment Profile 89
Figure 4-13 Pile 2 Bending Moment Profile 89
Figure 4-14 Pile 3 Bending Moment Profile 90
Figure 4-15 Pile 3 Bending Moment Profile 90
Figure 4-16 Pile 4 Bending Moment Profile 91
Figure 4-17 Pile 4 Bending Moment Profile 91
Figure 4-18 Pile 2 Bending Moment Profile 92
Figure 4-19 Pile 2 Bending Moment Profile 92
Figure 4-20 Pile 3 Bending Moment Profile 93
Figure 4-21 Pile 3 Bending Moment Profile 93
Figure 4-22 Pile 4 Bending Moment Profile 94
Figure 4-23 Pile 4 Bending Moment Profile 94
Figure 4-24 Load-Displacement with No Load Truck 95
Figure 4-25 Load-Displacement with Truck Centered on Roadway 95
Figure 4-26 Load-Displacement with Truck at Edge of Roadway 96

Figure 4-27 Load-Displacement Comparison of Three Tests 96
Figure 5-1 Test Bent Instrumentation Layout 100
Figure 5-2 Reaction Bent Instrumentation Layout 101
Figure 5-3 Wirepot Layout on Bent Cap Face 101
Figure 5-4 PL-60-11-3LT Concrete Strain Gage (Texas Measurements) 102
Figure 5-5 Installed Concrete Surface Strain Gage 103
Figure 5-6 Installed Concrete Surface Gage with Strain Relief 104
Figure 5-7 Field-Installed Wirepots 105
Figure 5-8 Hydraulic Cylinders and Pump Seen From Bridge Deck 107
Figure 5-9 ALDOT Load Truck in Configuration LC-5 108
Figure 5-10 Threaded Rods Anchored on Jack End 109
Figure 5-11 End Anchorage at Reaction Bent 110
Figure 5-12 Intermediate Bracing for Threaded Rods 111
Figure 5-13 Wooden Reference Frame for Wirepots 112
Figure 5-14 Load Truck Positioned Over Test Bent 113
Figure 5-15 Load Truck Positioning Over Exterior Girder 114
Figure 5-16 Composite Pile Cross Section 117
Figure 5-17 Pile 1 Axial Force vs. Lateral Load 120
Figure 5-18 Pile 2 Axial Force vs. Lateral Load 121
Figure 5-19 Pile 3 Axial Force vs. Lateral Load 121
Figure 5-20 Pile 4 Axial Force vs. Lateral Load 122
Figure 5-21 Pile 5 Axial Force vs. Lateral Load 122
Figure 5-22 Pile 6 Axial Force vs. Lateral Load 123
Figure 5-23 Pile 1 Bending Moment Profile 124
Figure 5-24 Pile 1 Bending Moment Profile 125
Figure 5-25 Pile 2 Bending Moment Profile 125
Figure 5-26 Pile 2 Bending Moment Profile 126
Figure 5-27 Pile 3 Bending Moment Profile 126
Figure 5-28 Pile 3 Bending Moment Profile 127
Figure 5-29 Pile 4 Bending Moment Profile 127
Figure 5-30 Pile 4 Bending Moment Profile 128
Figure 5-31 Pile 5 Bending Moment Profile 128
Figure 5-32 Pile 5 Bending Moment Profile 129
Figure 5-33 Pile 6 Bending Moment Profile 129
Figure 5-34 Pile 6 Bending Moment Profile 130
Figure 5-35 Pile 7 Axial Force vs. Lateral Load 131
Figure 5-36 Pile 8 Axial Force vs. Lateral Load 131
Figure 5-37 Pile 9 Axial Force vs. Lateral Load 132
Figure 5-38 Pile 7 Bending Moment Profile 133
Figure 5-39 Pile 7 Bending Moment Profile 133
Figure 5-40 Pile 8 Bending Moment Profile 134
Figure 5-41 Pile 8 Bending Moment Profile 134
Figure 5-42 Pile 9 Bending Moment Profile 135
Figure 5-43 Pile 9 Bending Moment Profile 135
Figure 5-44 Pile 1 Axial Force vs. Lateral Load 136
Figure 5-45 Pile 2 Axial Force vs. Lateral Load 136

Figure 5-46 Pile 3 Axial Force vs. Lateral Load 137
Figure 5-47 Pile 4 Axial Force vs. Lateral Load 137
Figure 5-48 Pile 5 Axial Force vs. Lateral Load 138
Figure 5-49 Pile 6 Axial Force vs. Lateral Load 138
Figure 5-50 Pile 1 Bending Moment Profile 139
Figure 5-51 Pile 1 Bending Moment Profile 140
Figure 5-52 Pile 2 Bending Moment Profile 140
Figure 5-53 Pile 2 Bending Moment Profile 141
Figure 5-54 Pile 3 Bending Moment Profile 141
Figure 5-55 Pile 3 Bending Moment Profile 142
Figure 5-56 Pile 4 Bending Moment Profile 142
Figure 5-57 Pile 4 Bending Moment Profile 143
Figure 5-58 Pile 5 Bending Moment Profile 143
Figure 5-59 Pile 5 Bending Moment Profile 144
Figure 5-60 Pile 6 Bending Moment Profile 144
Figure 5-61 Pile 6 Bending Moment Profile 145
Figure 5-62 Pile 7 Axial Force vs. Lateral Load 146
Figure 5-63 Pile 8 Axial Force vs. Lateral Load 146
Figure 5-64 Pile 9 Axial Forces vs. Lateral Load 147
Figure 5-65 Pile 7 Bending Moment Profile 148
Figure 5-66 Pile 7 Bending Moment Profile 148
Figure 5-67 Pile 8 Bending Moment Profile 149
Figure 5-68 Pile 8 Bending Moment Profile 149
Figure 5-69 Pile 9 Bending Moment Profile 150
Figure 5-70 Pile 9 Bending Moment Profile 150
Figure 5-71 Load-Deflection with Load Truck Positioned at Road Edge 151
Figure 5-72 Load-Deflection with No Load Truck 152
Figure 5-73 Load Deflection Comparison of Both Load Tests 152
Figure 6-1 SAP Model Geometry for Macon County Bent 159
Figure 6-2 SAP Model Geometry for US 331 Bent 160
Figure 6-3 Preliminary FB Multipier Model of Macon County Bent (Skinner 2015) 161
Figure 6-4 Preliminary FB Multiper Model of US 331 Bent (Skinner 2015) 162
Figure 6-5 Macon County Bent Soil Profile (Skinner 2015) 163
Figure 6-6 US 331 Bent Soil Profile (Skinner 2015) 163
Figure 6-7 Loading Diagram for First Macon County Test 167
Figure 6-8 Macon County Bent with no Deck Deflected Shape at 75 kips 170
Figure 6-9 Macon County Bent with no Deck Moment Diagram at 75 kips 171
Figure 6-10 Pile 1 Bending Moment Comparisons 173
Figure 6-11 Pile 2 Bending Moment Comparison 174
Figure 6-12 Pile 3 Bending Moment Comparison 175
Figure 6-13 Pile 4 Bending Moment Comparisons 176
Figure 6-14 Pile 1 Axial Load versus Lateral Load 177
Figure 6-15 Pile 2 Axial Load versus Lateral Load 178
Figure 6-16 Pile 3 Axial Force versus Lateral Load 178
Figure 6-17 Pile 4 Axial Force versus Lateral Load 179
Figure 6-18 Load Deflection Comparison from Macon County Test with no Bridge Deck 180

Figure 6-19 Pile 1 & 2 Bending Moment Comparisons with no Load Truck 182
Figure 6-20 Pile 3 & 4 Bending Moment Comparisons with No Load Truck 183
Figure 6-21 Pile 1 SAP Bending Moment Profiles with Load Truck Centered on Roadway 185
Figure 6-22 Pile 2 Bending Moment Comparisons with Load Truck Centered on Roadway.... 186
Figure 6-23 Pile 3 Bending Moment Comparisons with Load Truck Centered Over Roadway 187
Figure 6-24 Pile 4 Bending Moment Comparisons with Load Truck Centered Over Roadway 188
Figure 6-25 Pile 1 & 2 Bending Moment Comparisons with Load Truck Positioned at Edge of Roadway 190
Figure 6-26 Pile 3 & 4 Bending Moment Comparisons with Truck Positioned at Edge of Roadway 191
Figure 6-27 Pile 1 Axial Force versus Lateral Load..... 192
Figure 6-28 Pile 2 Axial Force versus Lateral Load..... 193
Figure 6-29 Pile 3 Axial Force versus Lateral Load..... 193
Figure 6-30 Pile 4 Axial Force versus Lateral Load..... 194
Figure 6-31 Load-Deflection Comparisons of Macon County Bent with Bridge Deck..... 195
Figure 6-32 Pile 1 Bending Moment Comparisons with Truck at Edge of Roadway 198
Figure 6-33 Pile 2 Bending Moment Comparisons with Truck at Edge of Roadway 199
Figure 6-34 Pile 3 Bending Moment Comparisons with Truck at Edge of Roadway 200
Figure 6-35 Pile 4 Bending Moment Comparisons with Truck at Edge of Roadway 201
Figure 6-36 Pile 5 Bending Moment Comparisons with Truck at Edge of Roadway 202
Figure 6-37 Pile 6 Bending Moment Comparisons with Truck at Edge of Roadway 203
Figure 6-38 Pile 1 Bending Moment Comparisons with no Load Truck 205
Figure 6-39 Pile 2 Bending Moment Comparisons with no Load Truck 206
Figure 6-40 Pile 3 Bending Moment Comparisons with no Load Truck 207
Figure 6-41 Pile 4 Bending Moment Comparisons with no Load Truck 208
Figure 6-42 Pile 5 Bending Moment Comparisons with no Load Truck 209
Figure 6-43 Pile 6 Bending Moment Comparisons with no Load Truck 210
Figure 6-44 Pile 1 Axial Force versus Lateral Load Comparison 212
Figure 6-45 Pile 2 Axial Force versus lateral Load Comparison..... 212
Figure 6-46 Pile 3 Axial Force versus Lateral Load Comparison 213
Figure 6-47 Pile 4 Axial Force versus Lateral Load Comparison 213
Figure 6-48 Pile 5 Axial Force versus Lateral Load Comparison 214
Figure 6-49 Pile 6 Axial Force versus Lateral Load Comparison 214
Figure A-1 Black Rod Calibration Data A-1
Figure A-2 Red Rod Calibration Data A-2

Chapter 1 Introduction

1.1 Overview

One of the most common types of bridges in Alabama is the multi-span bridge with precast/prestressed concrete girders and pile bents consisting of a cast-in-place, reinforced concrete bent cap and driven steel HP piles. Typically, the exterior piles are battered at a 1.5:12 slope. When the bent is located within the flow channel, the steel piles are encased in non-structural concrete three feet above the mudline. The pile encasements are typically extended at least five feet below the projected ground elevation. These concrete encasements serve as protection to prevent section loss of the steel piles. If the clear height of the piles is greater than 14 feet, welded sway bracing is used in order to provide sufficient lateral stiffness and strength. The welded sway bracing can be configured as one-story as shown in Figure 1-1 or two-story. This bridge type is very common for the Alabama Department of Transportation (ALDOT); therefore, effective analysis and design procedures for these bridges are a necessity to provide efficient bridge designs.

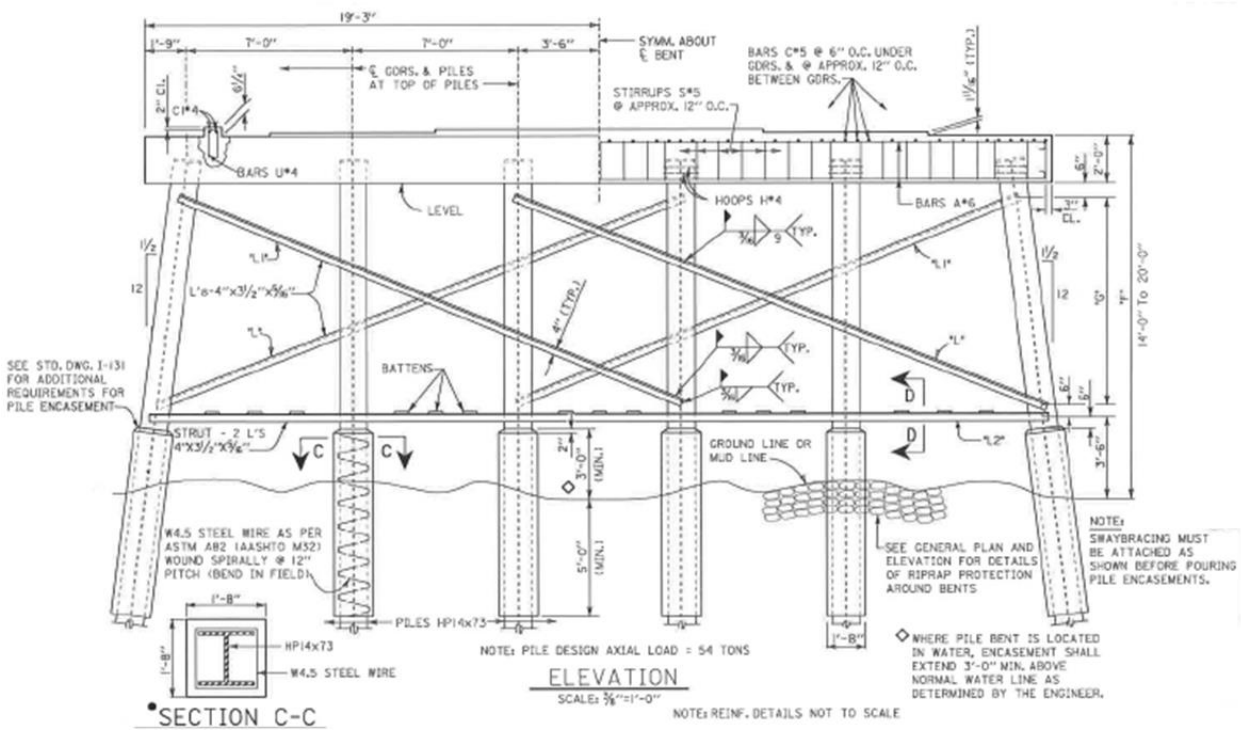

Figure 1-1 Typical Pile Bent Substructure with One-Story Sway Bracing

Driven steel pile bridge bents are efficient structures, but are difficult to model correctly. The steel piles play a part in the resistance of both gravity and lateral loads. Due to the combination of flexural and axial effects on the piles, the overall structure is highly indeterminate. Changes in stiffness in the elements can therefore cause significant changes in the element forces. The stiffness of the piles is dependent on a number of assumptions including but not limited to the degree of composite behavior between the steel pile and concrete encasement, the rigidity of the connection between the steel pile and the cast-in-place bent cap, and the interaction between the steel pile and the surrounding soil. The piles' flexural stiffness, end fixities, and unbraced lengths have a significant impact on the bent's overall lateral stiffness; therefore these critical assumptions play a key part in performing the analysis accurately.

A better understanding of how these pile bents perform under gravity and lateral load is necessary to validate analysis methods and design procedures and model the pile bents correctly.

In order to better gain this understanding, a series of load tests were performed on newly constructed and existing bridges. The tested pile bents were instrumented during testing to determine forces and moments in the piles and bent cap and also the degree of composite behavior of the concrete encasement. The results from these tests were then used to calibrate numerical models which can be used to analyze existing pile bent designs and develop recommendations for assumptions to be made in analysis and design procedures for Load and Resistance Factor Design (LRFD) of pile bent bridge substructures.

1.2 Problem Statement

Recent correspondence with the ALDOT Bridge Bureau indicated an issue with the analysis and design of a steel pile bridge bent without sway bracing. An independent consultant submitted a design package for a pile bent that included significantly higher pile design forces than were anticipated by ALDOT designers. An additional analysis was performed by a different consultant who was unable to determine the reason for the discrepancy in the pile forces. He did indicate, however, that assumptions made in the analysis could significantly affect the pile forces and that the design forces came from load combinations including lateral loads. The research detailed in this thesis examines the behavior of steel pile bents under gravity and lateral loading and calibrate analytical models to include proper assumptions listed in the previous section.

1.3 Research Objectives

• Identify the gravity and lateral load transfer mechanism within the steel pile bridge bent including the cast-in-place bent cap, driven steel HP piles and concrete encasement.

• Develop calibrated analytical models in SAP2000 (CSI 2011) which will be used to determine appropriate boundary conditions, including soil-pile interaction, composite behavior and pile-to-cap connection including connection springs for steel pile bent bridge models.

•Use calibrated analytical models to validate findings in experimental load tests of new construction and existing pile bent bridges.

1.4 Research Scope

The project scope included four field tests of instrumented steel pile bridge bents using the ALDOT load trucks for gravity load application and reaction pile groups or an adjacent steel pile bent for lateral loads. Analysis of the results of the field tests were then used to calibrate analytical models to evaluate the tested pile bents as well as other existing pile bents.

1.4.1 Field Testing Overview

A series of field tests were performed on existing and newly constructed driven steel pile bridge bents. The first two field tests were conducted during the construction of a multi-span pile bent bridge in Macon County, AL. The first test occurred after the girders spanning both directions had been set, and the second test occurred after the bridge deck had been cast. For this test, the steel piles were instrumented prior to being driven to obtain information at sections below the ground surface. Once the piles were driven, instrumentation was installed on the piles at sections above ground and also to the concrete encasements at the same sections along the height of the piles. Sections of steel reinforcing bars were also instrumented and tied in to the main reinforcement cage of the bent cap before casting in order to obtain forces and moments in the cap during testing.

The second field test was performed on an existing bridge in Montgomery, AL. The bridge was supported by several different pier types including steel pile bents. The bent tested consisted of driven steel piles with square concrete encasements. For this test, the adjacent bridge was used as a reaction bent to apply the lateral load. Sensors were installed on the pile concrete encasements of both the test bent and the reaction bent in order to obtain forces and moments in the piles during testing.

The final test was performed on two pile bents constructed at the Auburn University National Geotechnical Experimentation Site (AUNGES) co-located at the National Center for Asphalt Technology (NCAT) Test Track. One of the test bents included only vertical piles and the other consisted of exterior battered piles. The bents in this test were loaded to failure to observe nonlinear behavior of the structures.

The research project was a collaborative effort; however, this thesis focuses on the instrumentation, testing procedure and analysis and results from the load tests performed on the Macon County and US 331 bridges.

1.4.2 Computer Modeling and Design Methodologies

Finite element structural analysis software was implemented following experimental testing in order to validate the results from each of the tests. Two dimensional pile bent models were created in SAP 2000 v17 (CSI 2011) to determine the correlation between the field test results and analytical results. These models included soil-structure interaction through the development of linear springs at incremental levels. These springs were developed from models created in FB Multipier (BSI 2004), which gives force-displacement information at different soil layers along the length of the pile. From the structural models created in SAP 2000, appropriate assumptions for the analysis of these pile bent bridges were determined. Having an understanding of soil-structure interaction, level of composite behavior of the encased piles, and connectivity of the pile to cap connection is essential for the design of pile bent substructures.

1.5 Organization of Thesis

This thesis is divided into seven chapters. Chapter 1 is an introductory chapter providing the motivation for the research project, objectives and a summary of the research performed. Chapter 2 provides a background on steel pile bridge bents and an overview of theoretical behavior of deep foundations under lateral loads and analysis methods. Chapter three details the testing, analysis

and results of a new construction pile bent bridge constructed in Macon County Alabama. Chapter four details a second field test performed on the new construction bridge in Macon County. Chapter five details the testing, analysis and results of an in service pile bent bridge in South Montgomery, Alabama located on US Highway 331 South. Chapter 6 details the analytical models created in SAP2000 for verification of findings during the aforementioned load tests. Finally chapter 7 summarizes the findings in each of the load tests and provides conclusions and recommendations for analysis procedures for driven steel pile bridge bents.

Chapter 2 Background and Literature Review

2.1 Background and Description of Pile Bent Substructures

The multi-span bridge with precast-prestressed concrete girders and intermediate bents consisting of driven steel piles and a reinforced concrete bent cap is widely used in the state of Alabama. This section provides a detailed description of pile bent substructures and the typical construction process for pile bents with driven steel HP piles.

Pile bents are a part of the substructure of the bridge system. The elements of a bridge system can be divided into two separate groups: superstructure and substructure. The superstructure of a bridge is made up of all components above the bridge's supports including the bridge deck, girders, and intermediate diaphragms. The substructure of a bridge is comprised of all the bridge elements required to support the bridge superstructure (Tonias & Zhao, 2007). Substructure elements can include piers, abutments, bearings, pedestals and backwalls. Pile Bents fall into the category of piers. Piers act as intermediate supports for the bridge superstructure located at discrete points along the length of bridge. The most common types of piers are column bents and pile bents. This thesis focuses on pile bents. A typical pile bent can bee seen in Figure 2-1.

Figure 2-1 Typical Pile Bent with Galvanized Steel HP Piles and Reinforced Concrete Cap

2.1.1 Pile Bent Description

Typical intermediate pile bents consist of either precast or steel piles driven into the ground by means of a hydraulic, diesel or air hammer. The exterior piles in these bents are typically battered at a 1.5:12 slope. Steel HP piles are one of the most common pile sections used in pile bent substructures. The flanges and webs of these sections are of equal thickness, and they are proportioned this way to reduce the hard driving stresses which they are subjected to (Bowles 1996). These steel HP piles are typically encased in non-structural concrete to prevent section loss. The cross section of these encasements can be either circular or square. Alternatively, galvanized piles have become used by ALDOT for corrosion protection. The bent shown in Figure 2-1 consists of galvanized steel HP piles. The other primary element of a typical pile bent is a cast-in-place reinforced concrete bent cap, which is cast following pile driving. The top of the piles are typically

embedded a minimum of 12 inches into the bottom of the bent cap. In cases where encasements are used, a two-inch embedment of the encasement into the cap is used which eliminates the need for chairs for the reinforcement cage of the cap. This thesis focuses on pile bents where steel HP piles encased in non-structural concrete were utilized. The bent focused on is shown in Figure 2-2.

Figure 2-2 Driven Steel Pile Bridge Bent with Concrete Encasements

2.1.2 Construction Process for Pile Bents

Piles are installed early on in the construction process of a multi-span bridge. Once initial grading and sitework is completed, the piles are then driven. Marks are generally made on the piles every one foot along the length of the pile, as seen in Figure 2-1, for the inspector to have a visual representation of how far the pile has been driven. A driving log is also kept during the pile-driving process, in which the number of hammer blows per foot of driving depth is recorded. The piles are driven using either a hydraulic, diesel, or air hammer. Piles may also be driven using a vibratory hammer depending on the soil conditions, but not typically for bearing applications. An image of a diesel hammer used for pile driving can be seen in Figure 2-3.

Figure 2-3 Diesel Hammer Rig Used for Driving Piles

The piles are laid out in plan using surveying equipment. Once the piles locations are determined, a template is arranged in order for the crane operator to lower the piles into their proper locations. Appropriate measures are taken in cases where the piles are battered to ensure the correct slope. After the template is set, the crane operator picks up the pile with the winch attached to the hammer rig and lowers the pile into place in the driving template. A few initial blows are usually performed to adequately seat the piles in the soil. An image of a driving rig with pile attached being lowered into place in the driving template can be seen in Figure 2-4.

Figure 2-4 Diesel Hammer Being Lowered Into Driving Template

Once the piles are driven to the required depth, the excess pile lengths are cut off using a blow torch. The top of pile elevations are located using surveying equipment. An image of the piles following top cut-offs can be seen in Figure 2-5. Notably, the tops of the battered piles are cut parallel to the bottom face of the bent cap.

Figure 2-5 Piles Following Cut-Offs at Top of Pile Elevation

In cases where concrete encasement is used as the means of section loss protection, a specified depth is excavated below grade so that the encasement formwork can be positioned. Encasements usually extend 5 ft below finished grade. An image of the excavated area surrounding a driven pile can be seen in Figure 2-6. Once excavation is compete, the encasement forms are lowered into place and the concrete is cast around the piles. Following casting of the encasements, a layer of rip-rap is placed in the excavated area up to the original grade. The layer of rip rap surrounding the encased piles can be seen in Figure 2-2.

Figure 2-6 Driven HP Pile Following Excavation for Encasement Placement

After the piles are driven and encased and the layer of rip rap is placed, the bent cap is then cast. The main reinforcement cage for the cap is fabricated on-site. Prior to casting of the bent cap, the formwork for the cap is positioned appropriately using two steel piles as a base support with 4x4's and plywood decking placed on top of the piles. An image of the bent cap formwork being formed can be seen in Figure 2-7. Once the formwork is set, the reinforcement cage is lowered by crane into the appropriate position. An image of the reinforcement cage being lowered into place can be seen in Figure 2-8.

Figure 2-7 Bent Cap Formwork Being Positioned

Figure 2-8 Cap Reinforcement Cage Prior to Concrete Placement

Once the reinforcement cage is lowered into place, the ends of the cap are sealed using pieces of plywood board similar to the other formwork. Anchor bolt holes are then placed in line with the

piles, where the girders will be anchored to the bent cap. The concrete bent cap is then cast and finished at the appropriate elevation. The bent cap being cast can be seen in Figure 2-9.

Figure 2-9 Casting of Concrete Bent Cap

2.2 Lateral Load Testing Background

This section details lateral load testing procedures commonly performed on single piles and pile groups. It also details the requirements for lateral load tests on pile foundations per ASTM D3966 including design of the testing apparatus, testing configurations and instrumentation recommendations.

2.2.1 ASTM D3966 Provisions and Requirements

Lateral load testing of piles and pile groups is commonly performed on new construction projects where pile foundations are being implemented. Field tests provide the most reliable relationship between the applied load and the foundation's lateral movement (ASTM 2007). The reference standard these load tests must follow is ASTM D3966 "Standard Test Methods for Deep

Foundations Under Lateral Loads". This specification provides guidelines and recommended procedures for lateral load tests performed on deep foundations.

The specification provides requirements for the loading apparatus used for the test as well as minimum requirements for the testing configuration. The testing area must be excavated to the approximated elevation of the finished grade for a radius of the test pile or pile group. When pile groups are tested, the group must be capped at an elevation above ground surface. Recommendations for the design of the loading apparatus and the reaction group used for testing are also made within the specification. Steel plates are suggested to be used at bearing surfaces of the hydraulic jacks onto the test piles and are to be designed to adequately carry anticipated loads in the test. Reaction piles are to be designed so that the number of piles provides sufficient reaction to the anticipated loads while not deflecting excessively. A clear distance of at least five times the maximum pile diameter must be provided between the test piles and the reaction piles. The loading apparatus should be constructed so that loads applied are in line with the central axis of the pile or the pile cap to prevent any eccentric loading of the piles.

The ASTM specification also provides requirements and provisions on the use of hydraulic jacks for lateral load testing of piles. The jacks used must conform to ASME B30.1 and should have a capacity exceeding the anticipated loading of the test by at least 20 percent. If multiple jacks are used, the jacks are to be of the same make and model and should have the ability to apply equal pressure to prevent the occurrence of load imbalance and eccentric loading. The specification also provides guidance on jacks used in load tests where the load is applied by pulling, stating that the jacks should be capable of applying a constant force over the test increment durations.

2.2.2 Testing Methods

Testing methods covered in ASTM D3966 are divided into two separate categories: load applied by pushing and load applied by pulling. For cases where the load is applied by pushing,

reaction piles or a deadman system can be used. Examples of each of these loading configurations can be seen in Figure 2-10. A deadman system consists of using heavy blocks or timber cribbing to provide reaction for the applied loads. The hydraulic jack is anchored to the deadman setup and the ram is extended to push the test pile or pile group away from the deadman. In a reaction pile system, a group of piles is driven some distance from the test pile or pile group and capped at or above ground surface to provide a bearing location for the hydraulic cylinder. The same loading technique is then used, extending the ram of the cylinder to push on the test pile or pile group and react against the reaction pile or reaction pile group.

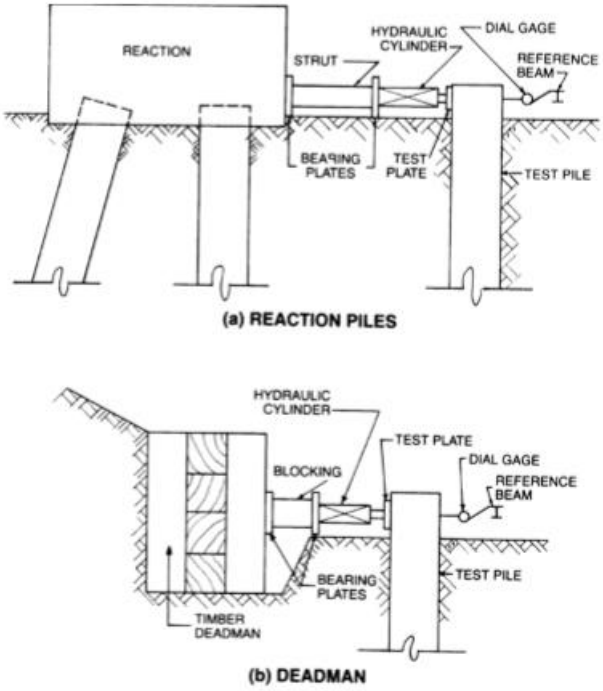

Figure 2-10 Lateral Load Testing Methods by Pushing (ASTM 2007)

The second method for applying lateral load per ASTM D3966 is by pulling. In this load application method, a reaction system and center-hole hydraulic cylinders are commonly used. High strength tension rods are extended between the test pile or pile group and the reaction piles and are anchored on each end by a reaction beam and a clamp or nut on the end of the center-hole

cylinder as seen in Figure 2-11. The lateral load is then applied by extending the hydraulic ram which pulls the test piles and the pile group toward each other. The ASTM document also provides requirements for load applied by pulling, stating that if two tension members are used, they must be spaced equidistant from the centerline of the pile in order to minimize eccentric loading of the pile or pile group.

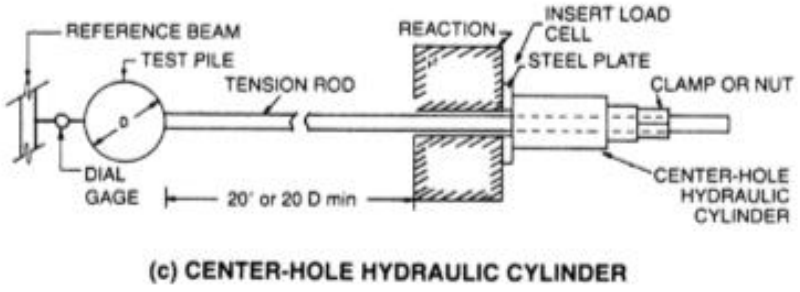

Figure 2-11 Lateral Load Testing Configuration by Pulling (ASTM 2007)

For each of the load tests reported on in this thesis, the lateral load was applied by pulling, and a reaction pile group was used. All loading configurations and apparatuses were designed and configured in accordance with ASTM D3966. All deviations, deletions or additions to the load testing apparatus and test schedule were validated with calculations. The loading configurations and apparatuses used are detailed later in this thesis.

2.3 Theoretical Behavior of Deep Foundations Under Lateral Loads

Piles, like other structural elements are designed for strength and serviceability limit states. They are designed so that they have adequate strength under ultimate loads, but also so that excessive deflections do not occur under service level loads. In a majority of cases, the maximum tolerable deflection will control the design of piles (Poulos and Davis 1980). Lateral loading of a pile is a soil-structure interaction problem in which the deflection of the pile and the lateral resistance of the soil are interdependent (Reese and Wang 2006). A knowledge of the relationships between pile deflection, slope, shear and bending moment is important in the design of pile

foundations. Piles are checked for adequate strength against the maximum bending moments from ultimate loads and are checked to ensure the maximum deflection is less than the allowable under service loads. A figure of the relationship of the deflection, slope, bending moment, shear force and soil reaction as a function of pile depth can be seen in Figure 2-12.

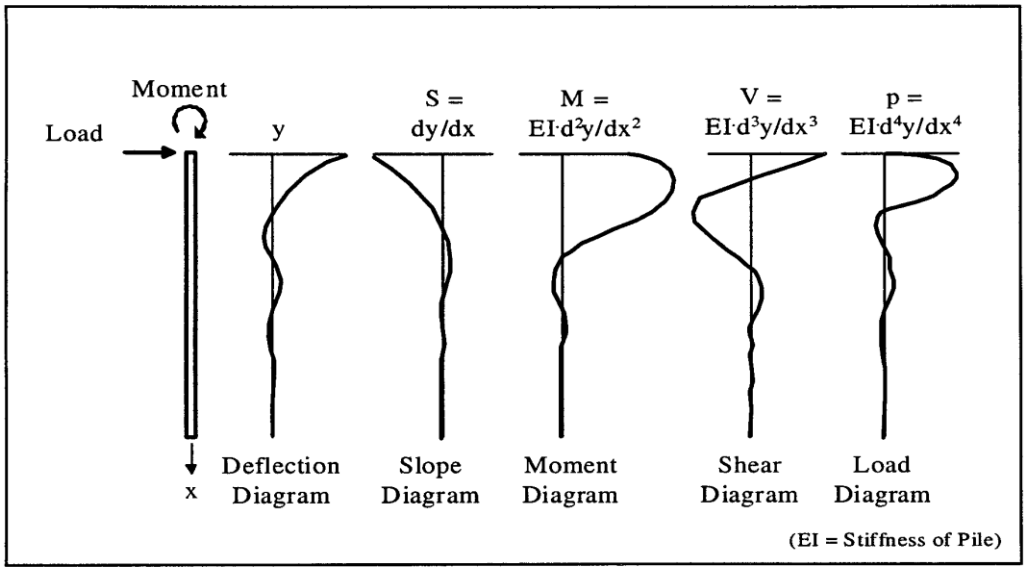

Figure 2-12 Solutions to Pile Deflections and Forces as a Function of Depth (Reese and Wang 2006)

2.4 Analysis Methods for Deep Foundations

There are multiple solutions for analyzing the behavior of deep foundations under lateral load, the most common being the beam on elastic foundation approach (or the Winkler approach), the empirical method by Broms, elastic continuum theory by Poulous, and the finite element method. The most commonly used method used for analyzing deep foundations under lateral loads is the Winkler Method also known as the p-y method. The Winkler method is only used in the case of laterally loaded foundations.

2.4.1 P-y Method

Soil-structure interaction is accounted for by either treating the soil mass around the pile as a continuum or by substituting springs located at a discrete points along the length of the pile to represent the soil. The latter method is referred to as the p-y method, and is the most commonly used method for determining deflections under working loads (Salgado 2008). The governing differential equation for the p-y method is manipulated from the differential equation 1-1 for bending moment used by Hetenyi (1946) from classical beam theory. A relationship between the pile deflection and the lateral soil stiffness is used to develop p-y curves.

$$M = E_p I_p \frac{d^2y}{dz^2} \qquad \text{(Equation 1-1)}$$

Where E_p is the modulus of elasticity of the pile, I_p moment of inertia of the pile, y is the lateral displacement of the pile and z is the pile depth. The relationship between the lateral soil resistance, p and the pile deflection, y is given by the following:

$$p = ky \qquad \text{(Equation 1-2)}$$

where k is the modulus of subgrade reaction. The modulus of subgrade reaction is assumed to vary linearly with depth for a normally consolidated clay and constant with depth for sands and overly consolidated clay (Hsiung and Chen 1997). Using this relationship between soil resistance and pile deflection, the governing differential equation can be rewritten as the following:

$$E_p I_p \frac{d^4y}{dz^4} + ky = 0 \qquad \text{(Equation 1-3)}$$

The solution to the differential equation is used to create curves of horizontal soil reaction, p versus horizontal displacement, y. The Winkler approach ignores the axial load effect on the piles and treats the soil as series of springs rather than a continuous layer. However, it is easily implemented and widely accepted for analyzing pile foundations under lateral loads.

2.4.2 Broms's Methods for Determining Deflections and Ultimate Pile Capacity

Broms presented methods for determining the lateral deflection of pile groups under working loads and determining the ultimate lateral resistance of pile groups in a series of papers. He provided a number of empirical formulas for the lateral deflection of laterally loaded piles in cohesive (1964a) and cohesionless soils (1964b). The ultimate lateral resistance of the pile could be computed relatively easily by using formulas and tabulated values based on experimental testing. Broms' methods for computing lateral deflection assumed that the coefficient of subgrade reaction increased linearly with pile depth. The analysis methods are based on the assumed failure modes for short piles and for long piles. His equations for deflection assumed that the failure mode of short piles is dependent on the embedment length of the pile and the failure mode of long piles occurs when a plastic hinge occurs at the location of the maximum bending moment of the pile. Broms' method is very readily implemented by hand, but typically provides calculated deflections that are conservative and is rarely used in practice.

2.4.3 Elastic Continuum Theory

Poulos (1971a) developed an approach for analyzing single piles and pile groups under lateral loading by treating the soil surrounding the piles as an elastic continuum. The pile is assumed to be an infinitely thin, linearly elastic strip embedded in an elastic media. The pile is divided into elements and a uniform pressure, p is applied across the width of the pile. The displacement along the length of the pile is a function of the uniformly applied pressure and the soil reaction modulus. The soil modulus is assumed to be constant with depth in this method. The piles are assumed to be prismatic and the soil is assumed to have the same properties along the entire depth of the pile. Poulos considered fixed-and free-head pile heads in his approach. The lateral displacement for a free-head pile is given as:

$$y_0 = I_h \frac{P}{E_s L} + I_m \frac{M}{L^2} \qquad \text{(Equation 2-4)}$$

Where I_h is a displacement influence factor for lateral load only, P is the applied lateral load, E_s is the soil reaction modulus, L is the length of the pile, I_m is a displacement influence factor for applied moment only, and M is the applied moment. The lateral displacement of a fixed-pile is given as:

$$y_0 = I_f \frac{P}{E_s L} \qquad \text{(Equation 2-5)}$$

Where I_f is a displacement influence factor for a fixed-head pile with an applied lateral load.

2.5 Pile to Cap Modeling

Pile groups which consist of a pile cap are typically modeled as a fixed-head condition, meaning the rotation of the top of the pile which is embedded into the cap is fully restrained. Lateral load tests by Gerber and Rollins (2009) showed that the piles groups that are capped do not behave as fully fixed in terms of load and deflection, but somewhere between unrestrained and fully restrained. A nine-pile group was constructed and loaded without a cap, then following the first test, the group was capped and reloaded. It was found that the deflections of the piles decreased by 40% in the test where the piles had been capped and the lateral resistance of the pile group increased by 51%. Analyses were performed using a fixed-head and free-head condition and then compared to the results from the load tests. According to theoretical results, the deflection of the pile group with the cap should have been approximately 25% of the measured deflection of the pile group without the cap; however, the actual deflection of the group with the cap was 60 % of the deflection of the group without the cap. The cap appeared to provide some rotational restraint of the pile heads, but not full restraint. No results on bending moments in the piles were produced for this particular load test. Modeling the piles as fully restrained will result in pile deflections which are less than actual results, but will result in bending moments in the cap that are overly conservative.

Mokwa and Duncan (2003) developed a practical approach for approximating the level of moment restraint provided by the pile cap at the top of a pile group. A fully fixed-head condition is rarely achieved in the field; therefore assuming a fully restrained pile-head can lead to under estimations of lateral deflections of the pile and overly conservative values of bending moments in the cap. Suggested methods for calculating a rotational restraint coefficient, $K_{M\theta}$, are presented by Mokwa and Duncan to improve the estimates of deflections of pile groups under lateral load. The coefficient to modify rotational restraint was completely dependent on the axial stiffness of the piles. The pile cap rotational stiffness coefficient is defined by:

$$K_{M\theta} = \frac{\Delta M}{\Delta \theta} \qquad \text{(Equation 2-6)}$$

where ΔM is the increment of moment on the cap and Δθ is the resulting rotation of the cap. When lateral load is applied to the cap, rotation of the cap occurs causing the trailing side of the cap to displace upward and the leading side of the cap to displace down, inducing compressive axial loads in the leading piles and tensile axial loads in the trailing piles. The cap will tend to rotate about the center of the cap. The increment of moment on the cap is determined by summing moments created by the axial loads in the piles about the center of rotation of the cap. The rotation of the cap is related to the axial displacement of the piles and is computed as:

$$\Delta\theta = tan^{-1}\frac{\Delta y_i}{(x_i - a)} \qquad \text{(Equation 2-7)}$$

Where y_i is the vertical pile displacement, x_i is the horizontal distance from the center of the last trailing row of piles, and a is the distance from the center of the last trailing row of piles to the point of rotation of the pile cap.

The effective accuracy of these rotational restrain coefficients were tested using experimental data from pile load tests compared against results from analytical models (Mokwa and Duncan 2003). Values of $K_{M\theta}$ using approximate pile axial stiffness applied to the results from the

analytical models assuming a fixed-head conditions gave results that correlated seemingly well with the results measured in the field test in terms of deflections and cap rotations. The pile axial stiffness can only be approximated using the methods presented, but still tend to provide a more accurate estimation of deflections and rotations. The method is also limited to working level loads and does not account for any nonlinearity.

Richards et al. (2011) performed experimental tests on concrete filled pipe pile groups to determine the performance of the pile-to-cap connection with varying cap reinforcing and pile embedment lengths. The studies performed suggested that pile-to-cap connections with shallow embedment may have greater capacity than design formulas previously developed. Four full-scale pile groups with a reinforced concrete cap were tested with the pile embedment and degree of pile-to-cap reinforcing varying. Three different failure modes were investigated for the pile groups: failure of the soil surrounding the piles, failure of the piles, and failure in the cap. An analysis using the program Group (Ensoft 2000) was performed to determine the correlation between analytical and test results. Two non-linear analyses were performed; one assuming a pinned connection between the pile and cap and one assuming a fixed condition between the pile and cap. The load-deflection response from the test results appeared to correlate well with the results from the fixed head analysis performed. During the testing, none of the piles yielded, so the discussion regarding the failure mode was limited to failure in the cap. Concrete crushing in the cap and shear failure in the cap were the two anticipated failure modes. From the test results, it was determined that the piles were able to develop significant moments even with minimal pile embedment, and that piles designed as pinned at the top may develop moments closer to a fixed head condition. It was also determined that longer embedment may be used to minimize shear reinforcement within the cap even though minimum embedment provides adequate flexural reinforcement.

2.6 Software Implementation

In order to validate findings from experimental testing, computer software programs were used in this research study to create structure models which simulated the geometry and loading conditions from the field tests. Two software programs were used to create models to analyze the tested bridge bents. Preliminary models were built in FB-Multipier (BSI 2004) to determine the lateral loads to apply to the bents to ensure that strength limit states would not be reached and that excessive deflections would not occur. Following load testing, structural models were created in SAP 2000 to validate the results of the field tests. The models would represent the as-built geometry of the bents at the time of testing as well as material properties determined from laboratory testing. The models would also include pile-to-cap connections which would simulate the behavior of the bents during the load testing. Soil-pile interaction would be included in the model by linear springs located along the length of the pile. The loads applied to the these bents simulate the actual loading conditions during each of the load tests including the effects of lateral loads applied and wheel loads from the load trucks used during the tests.

2.6.1 SAP 2000

The primary analysis software used to determine the correlation between results from the field tests and theoretical values was SAP 2000. The program was chosen based on its availability and user prior knowledge of the software interface. SAP is a useful product for performing simple static, linear elastic analyses to complex dynamic, non-linear inelastic analyses (CSI 2011). Object based models are created in the program and converted to element based models in order to perform the finite element analysis. For each of the models created and reported on in this thesis, static linear-elastic and nonlinear displacement based analyses were performed. Two- dimensional frame models were developed using SAP's predefined 2D frame templates. The frame section

designer and element springs tools were used in creating these models to simulate the actual cross-sections of the piles in each of the test bents.

Chapter 3 Field Test 1-Macon County Bridge

3.1 Introduction

A multi-span bridge under construction in Macon County, Alabama was used for the first field test for this research project. The bridge was a replacing bridge spanning over Old Town Creek on Macon County Road 9 in Shorter, AL. The bridge consists of six 40 ft spans with four AASHTO Type I girders spaced at 8 ft on center. A plan view of the overall bridge plan can be seen in Figure 3-1. The intermediate bents consisted of a reinforced concrete cap beam with 4 driven HP14x89 steel piles spaced at eight feet on center. The two exterior piles in the bent were battered at a 1.5:12 slope. The piles in bents 3 and 4 were galvanized while bents 2, 5, and 6 were encased in non-structural concrete. The pile encasements in bents 2, 5 and 6 were circular with a diameter of 30 in. Bent 5 was used as the test bent for the first lateral load test. A figure of the bent geometry with dimensions taken from the design drawings can be seen in Figure 3-2.

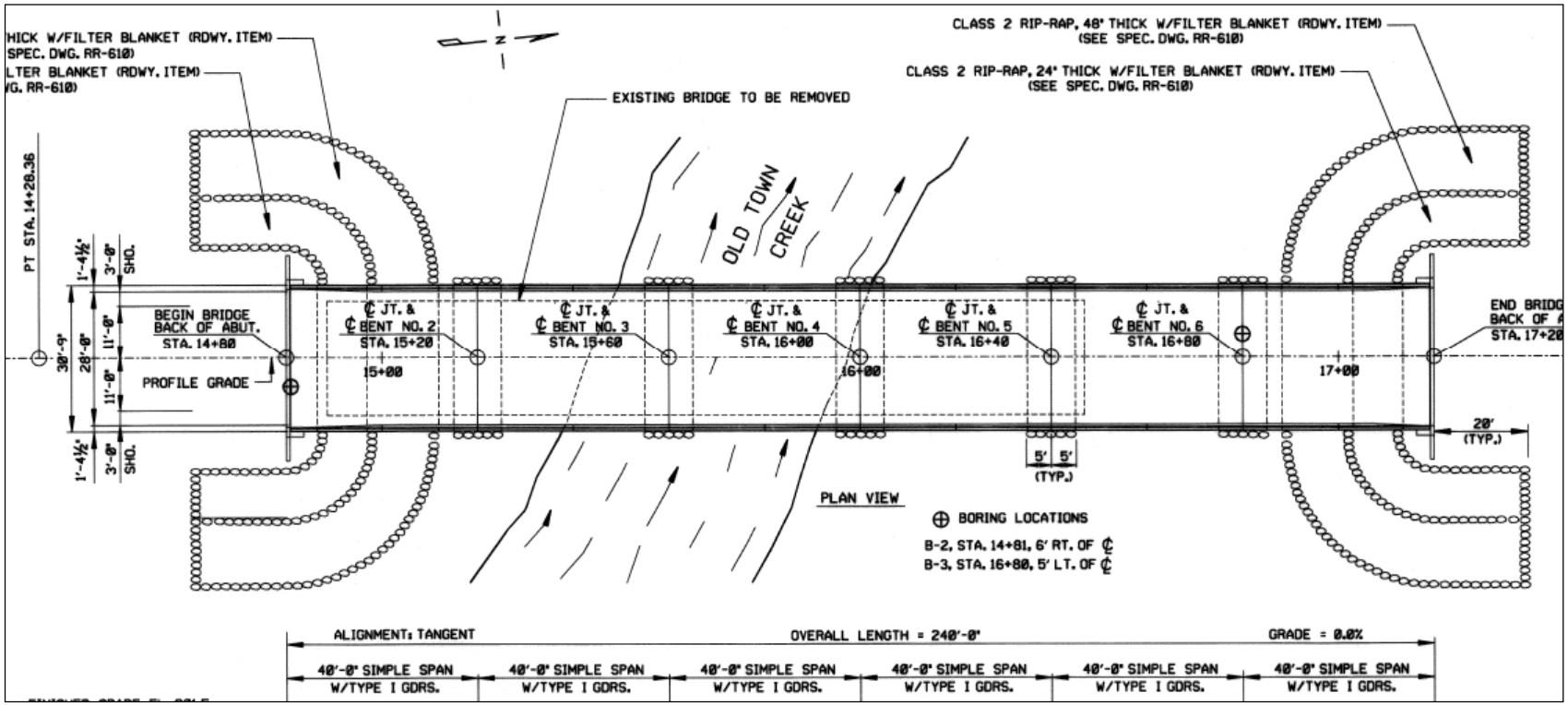

Figure 3-1 Macon County Bridge Overall Plan (Weatherford & Associates 2013)

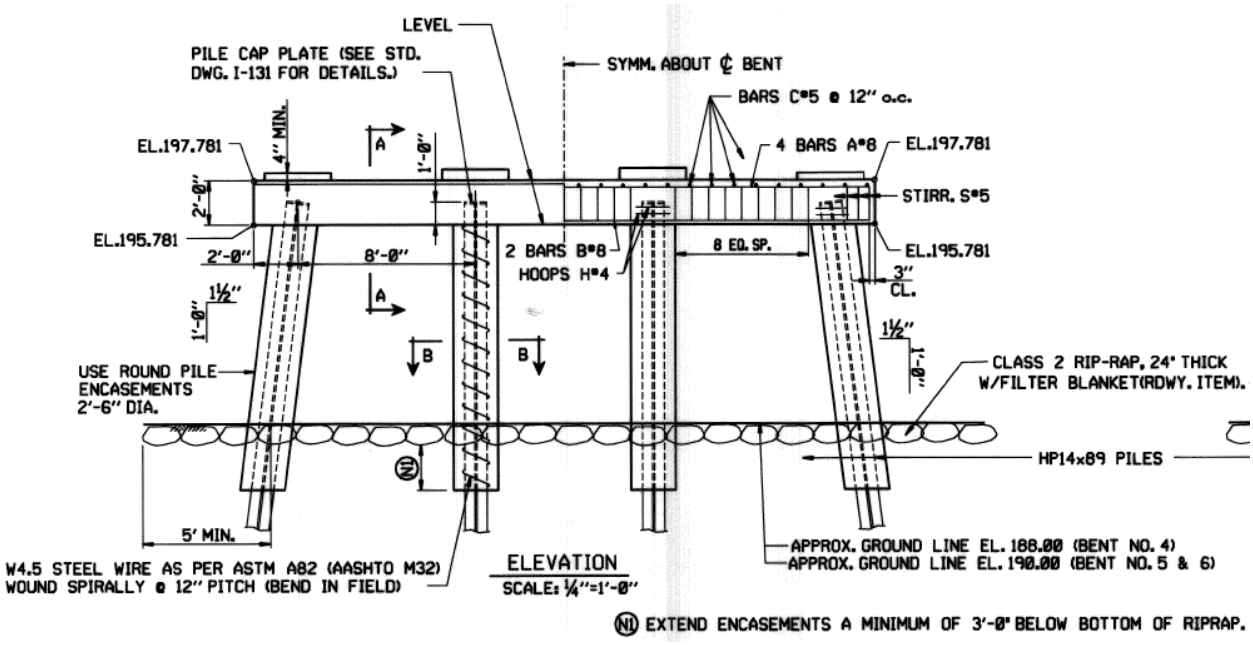

Figure 3-2 Elevation View of Bent 5 (Weatherford & Associates 2013)

This chapter details how the driven pile bent bridge in Macon County was tested as well as the analysis and results from that test. It contains sections on instrumentation, testing configurations, and the procedure used for testing. It also contains the results and analysis from the test as well as a discussion of the results.

3.2 Instrumentation

This section details how the test bent was instrumented. It contains the instrumentation layout for the bent, the different types of instrumentation used, and how each of the different types of instrumentation was installed.

3.2.1 Instrumentation Layout

In order to measure axial forces and bending moments in the driven piles, electrical resistance strain gages were installed on the inside of flanges on both sides of the web. A pair of gages was installed at each instrumented location in order to properly measure weak axis bending, which was the direction in which the piles were displaced. To obtain a moment versus depth profile for each

of the piles, four total sections along the length of the piles were instrumented. An image showing the instrumentation configuration at a single section can be seen in Figure 3-3. The instrumentation configuration shown in Figure 3-3 is representative of the instrumented sections above grade. The sections below grade were instrumented similarly, but a gage for measuring weak axis bending (green gage) was not installed and the gages were installed on the inside of the pile flanges so that they were protected during driving of the piles. The instrumentation layout for the gages installed along the length of the steel piles can be seen in Figure 3-4. The cables connected to each of the gages were color coded so that they could be easily identified during the tests. The gages above grade were connected using red wires while the gages below grade were connected with blue wires. The highest instrumented section above grade was labeled as black and the lower section was labeled as red. This labeling convention was used for the above and below grade conditions. The piles in the bent were labeled Piles 1, 2, 3 and 4 with pile 1 being the far right pile facing Old Town Creek and Pile 4 being the far left pile facing Old Town Creek. This numbering convention will be used henceforth in this chapter.

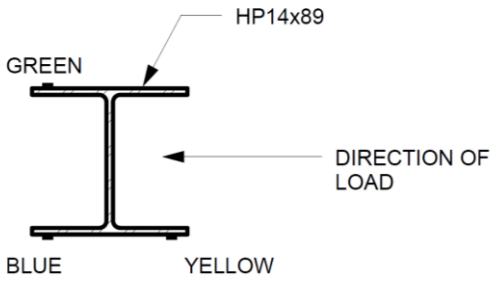

Figure 3-3 Strain Gage Layout at Typical Instrumented Section

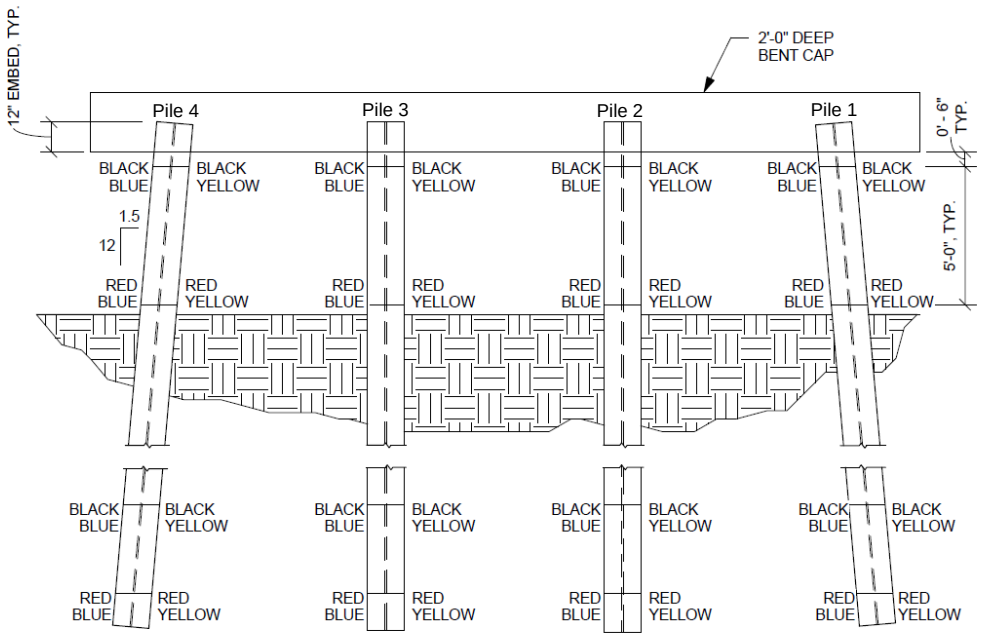

Figure 3-4 Steel Pile Instrumentation Layout Facing Old Town Creek

Figure 3-4 only shows the gages used for moment calculations about the axis in which they were loaded. A single gage (shown as the green gage in Figure 3-3) was installed at each section on the opposite flange for strong axis moment calculations. The instrumentation layout for the single gages installed to monitor strong axis bending can be seen in Figure 3-5.

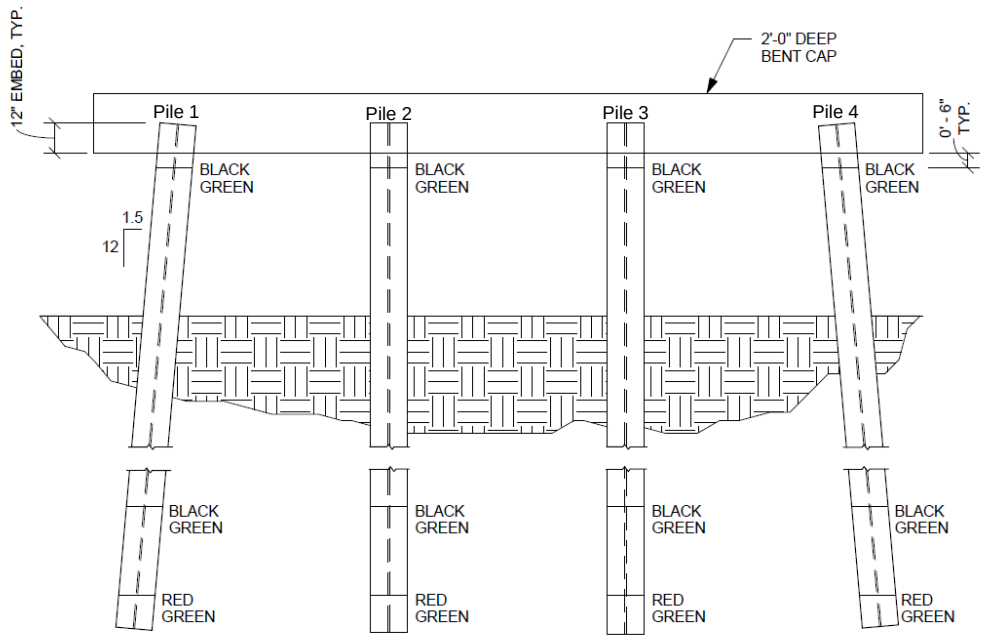

Figure 3-5 Steel Pile Instrumentation Layout Facing Away from Old Town Creek

As seen in the instrumentation layouts above, two sections below grade were instrumented and two sections above grade were instrumented. The gages at the section below grade were installed prior to driving. They were installed on the inside of the flanges to decrease the frictional resistance between the soil and the pile during the driving process. Two five-foot lengths of L2x2x3/8 were welded to the inside of the flanges over the sections where strain gages were installed to provide additional protection during the driving process. The ends of the angles were cut at an angle and a plate was welded at the ends to act as a driving tip. An image of the protective angle with the welded end plate can be seen in Figure 3-6.

Figure 3-6 Protective Angle Welded to Pile Flange

After concrete encasements were cast around the driven piles and rip rap was placed, a pair of electrical resistance strain gages were installed on the concrete surface at the same sections as the previously installed steel gages. These gages were installed so that a strain profile over the entire composite cross section could be obtained. A total of 12 concrete surface strain gages were installed: four on piles 1 and 2 and two on piles 3 and 4. The instrumentation layout for the concrete surface strain gages can be seen in Figure 3-7.

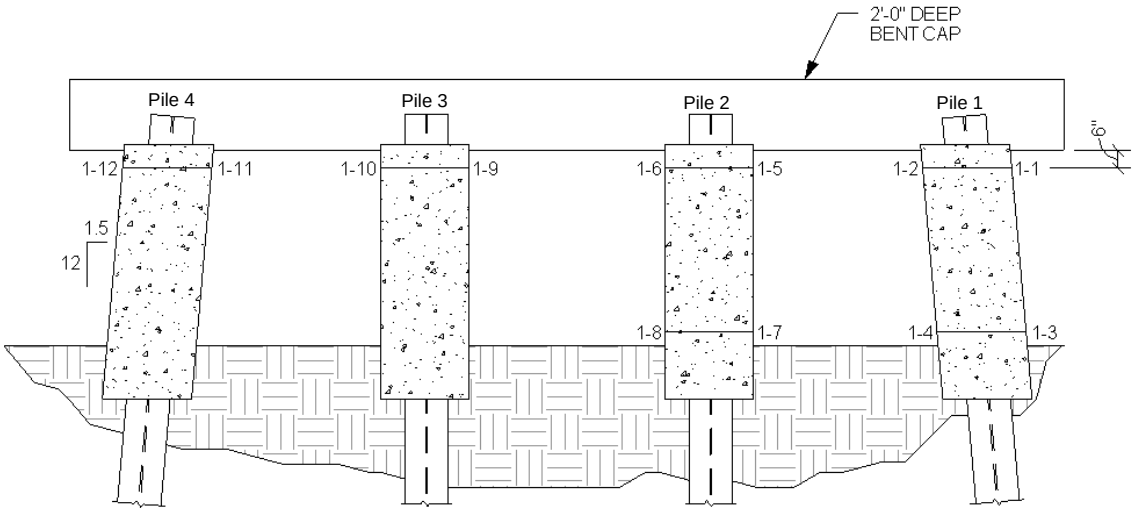

Figure 3-7 Concrete Encasement Instrumentation Layout Facing Old Town Creek

Electrical resistance gages were also installed on pieces of steel reinforcing bars which were tied into the reinforcement cage of the bent cap. These gages were installed in order to measure bending moment inside the cap. An instrumentation layout of the instrumented rebar in the cap can be seen in Figure 3-8.

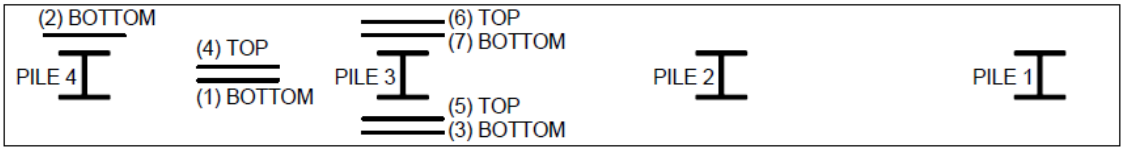

NOTES:
1. (#) INDICATES GAGE NUMBER ON WIRE
2. BOTTOM/TOP INDICATES WHETHER BAR IS TIED INTO TOP OR BOTTOM STEEL IN REINFORCEMENT CAGE

Figure 3-8 Sister Bar Layout Inside Bent Cap Facing Old Town Creek

In addition to strain monitoring, WDS P-60 series draw wire sensors from Micro-Epsilon with a 1000 mm (39”) range were installed on the bent cap to measure the total lateral deflection of the cap during the load test. These draw wire sensors will be referred to as wirepots for the remainder

of this thesis. Four wirepots were installed at each corner of the bent cap cross section. An image of the wirepot configuration on the cap can be seen in Figure 3-9.

Figure 3-9 Wirepot Configuration

3.2.2 Installation of Electrical Resistance Gages on Steel Piles

Once the piles for the test bent arrived on site, electrical resistance gages were installed at two sections along the length of the piles that were to be below finished grade. The first section was located 19 feet from the bottom of the pile and the second section was located 22 feet from the bottom of the pile. The HP14x89 pile sections used were 35 feet in total length.

Prior to gage installation, a smooth treated surface was prepared at each section to be instrumented. First, the mill scale was removed using a Dremel tool with a circular grinding bit. Next, the smoothed surface was prepared in accordance with techniques described by Vishay Micro-Measurements Instruction Bulletin B-129-8. This procedure included degreasing with CSM-2 Degreaser, wet abrading with an acidic solution, M-Prep Conditioner A, and neutralizing using a liberal amount of M-Prep Neutralizer A and a cotton tipped applicator.

A 125LW strain gage from Vishay Micro-Measurements was installed on the treated surface following surface preparation. The installation procedure described by Vishay Micro-

Measurements Instruction Bulletin B-127-14 was used to install the strain gages. This procedure consisted of removing the gage with a pair of tweezers and placing a piece of PCT-2M gage installation tape over the gage and terminal, ensuring that the gage is centered on the tape. The gage and tape assembly was then aligned over the treated section. The gage end of the tape was then lifted at a shallow angle until the entire gage is lifted off of the steel surface. M-Bond 200 catalyst was then applied to the gage surface to ensure proper hardening of the adhesive. After the catalyst was applied, one or two drops of M-Bond 200 adhesive were applied at the fold at where the tape meets the specimen surface. An image of a treated gage location on the steel piles prior to application of M-Bond 200 can be seen in Figure 3-10.

Figure 3-10 Treated Steel Surface Prior to M-Bond Application

Once the adhesive was applied, the tape was rotated so that the gage is directly over the installation area. With a single stroke, the thumb was slid over the tape pressing the gage into the adhesive. The adhesive was spread over the installation area to ensure no air bubbles form, and pressure was held over the gage for at least ten seconds to ensure adequate bond. Following gage installation, a piece of mastic tape was placed under the lead wires to ensure they did not make

contact with the specimen surface. An installed gage with mastic placed under the lead wires is shown in Figure 3-11.

Figure 3-11 Installed Electrical Resistance Gage with Lead Wire Protection

For data acquisition, the electrical resistance gages had to be connected to three-wire cables which were wired into a CR1000 Campbell Scientific datalogger. This connection was made by soldering the exposed lead wires to the ends of the three-wire cable. Two of the wires were wired together while the third served as the "power" wire to complete the quarter bridge circuit. An image of a strain gage with the soldered connection to the three-wire cable can be seen in Figure 3-12. After the cable wires were adequately connected to the leads, a piece of electrical tape was then placed around each of the soldered connections to prevent the two lead wires from touching. After this layer of electrical tape was placed, a piece of mastic tape was placed over the exposed gage to serve as an initial layer of weather protection and strain relief.

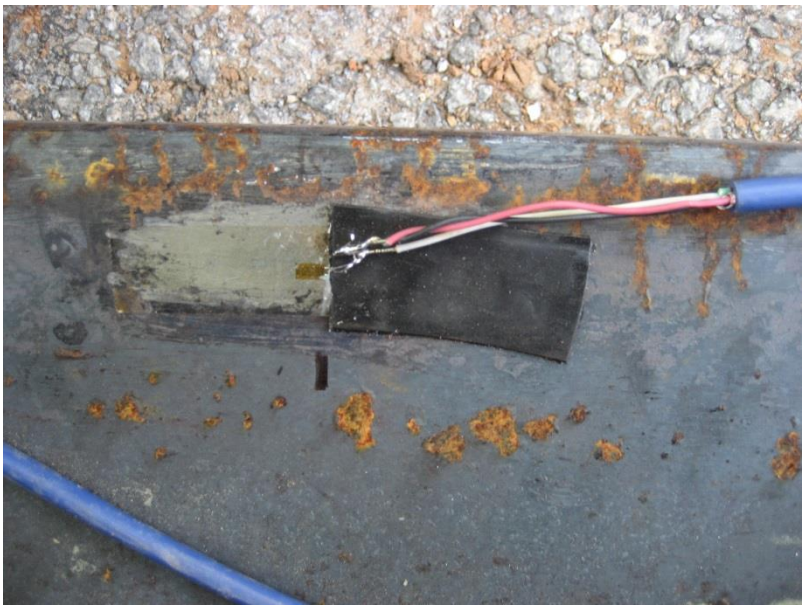

Figure 3-12 Strain Gage with Soldered Connection to Three-Wire Cable

To provide additional protection from weather and water exposure, M-Coat J protective coating was used. This coating was prepped and applied using Micro-Measurements Instruction Bulletin B-147-5. The coating was prepared by mixing the resin and cuing agent with a paint scraper for approximately 5 minutes until the substance became brown in color and developed a thick consistency. Once it was adequately mixed, the coating was dispensed onto an aluminum plate and applied over the gages, covering the entire layer of mastic tape on top of the gage and a portion of the attached three-wire cable. An image of an installed gage with M-Coat J protective coating can be seen in Figure 3-13.

Figure 3-13 Electrical Resistance Gage with M-Coat J Surface Protection

Once the gages were installed on all four piles, two five foot sections of L2x2x3/8 were welded to the piles covering the strain gages to provide protection and strain relief of the gages during the driving process. Once the piles were driven, each of the gages were checked using the P3 Strain Indicator to ensure the gages were functioning correctly. 17 of the 24 gages that were installed survived.

After the piles were driven, gages were installed at two sections above finished grade. The first section was located 18 inches from the top of the pile, which was six inches below the bottom of the bent cap. The next section was located five feet below the first section. The installation surfaces were prepared and the gages were installed using the procedure outlined in Section 3.2.2. The gages were checked using the P3 Strain Indicator after the concrete encasements were cast over the piles. 12 of the 20 gages installed above ground survived.

3.2.3 Installation of Electrical Resistance Gages to Concrete Surfaces

Once the concrete encasements were cast over the driven piles, concrete surface electrical resistance strain gages were installed at the same locations along the height of the pile as the steel gages that were previously installed. The concrete surfaces were prepared and the gages were installed according to procedures described in Vishay Micro-Measurements Application Note TT-611. A bristled brush was used to remove any surface irregularities then the surface was dusted to remove excessive concrete dust. Next, a coat of M-Bond AE-10 was used to fill any voids in the concrete. Once the adhesive had cured, the installation area was abraded with a 320 grit paper until the concrete was exposed. A 40CBY strain gage from Vishay Micro-Measurements with a four inch gage length was then removed from its casing using a pair of tweezers and centered on a piece of PCT-2M gage installation tape. A layer of five minute epoxy was applied to the concrete surface and the gage was installed by pressing and holding the gage onto the epoxy for at least five minutes, spreading the epoxy over the gage and tape assembly to ensure no air bubbles had formed. A layer of mastic tape was applied over the exposed gage, as well as a layer of M-Coat J to provide additional weather protection. An installed concrete surface gage can be seen in Figure 3-14.

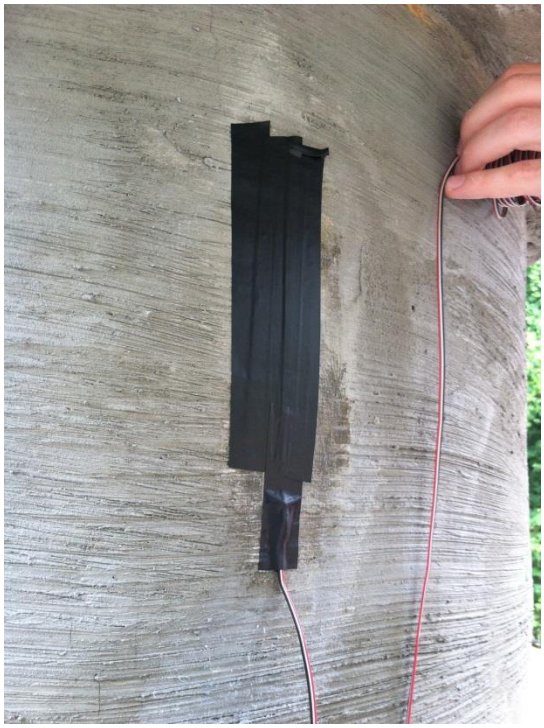

Figure 3-14 Field-Installed Concrete Surface Gage

3.2.4 Sister Bar Strain Gages

Sister bar strain gages were created by installing a 125LW strain gage from Vishay Micro-Measurements to a smooth, prepared surface in the middle of a two foot long #3 reinforcing bar. Prior to casting of the bent cap, these sister bars were tied into the reinforcement cage of the cap at appropriate locations. An installed sister bar can be seen in Figure 3-15.

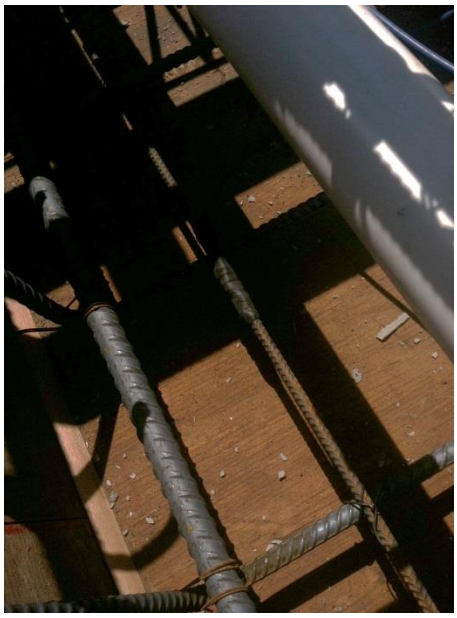

Figure 3-15 Sister Bar Tied into Bent Cap Reinforcing Cage

The surface of the sister bars were treated and the gages were installed using the same procedures listed in Section 3.2.2. When creating the surface of these bars, a minimal amount of steel was removed, so that the cross sectional area of the bar was not significantly decreased. Once the gages were installed, a layer of electrical tape followed by a layer of mastic tape was applied over the gage to ensure water tightness. Once the cap had been cast, the sister bar gages were tested in the P3 Strain Indicator. Six of the seven sister bar gages survived installation.

3.2.5 Displacement Wirepots

To measure lateral deflection of the test bent, wirepots were installed onto each corner of the bent cap face. These wirepots were attached to the bent by drilling a small hole into the end face of the bent cap, screwing in a small eyebolt and filling the hole with epoxy to ensure that the bolt would not move as the bent deflected. The wirepots were mounted to a wooden frame that would act as a reference beam. Four wirepots, one at each corner of the cap were installed to gain an average lateral deflection of the bent and to measure whether twisting of the cap occurred. An installed wirepot can be seen in Figure 3-16.

Figure 3-16 Field-Installed Wirepot

3.3 Testing Equipment and Setup

This section includes details on the testing configuration used for this load test. It also includes details on the reaction frame used, the hydraulic jacks and threaded rods used to apply the lateral load, the reference beam used to mount the wirepots, and the data acquisition system used.

3.3.1 Reaction Frame Configuration

A frame consisting of two driven HP14x89 piles was used to react against the bridge bent during the lateral load test. The load was applied by pulling the bent and the reaction frame together using high-strength steel threaded rods and center-hole hydraulic jacks. A cut-off section of pile was used as a diagonal brace to achieve frame action in the system. This cut-off section was welded to the two vertical piles in the reaction frame. Two pile cut-offs were welded to the top of the vertical members of the frame. These horizontal members were used to anchor the threaded rods to the reaction frame. The reaction frame configuration used for this load test can be seen in Figure 3-17.

Figure 3-17 Reaction Frame Configuration

Twelve foot sections of 1 1/8 in. diameter threaded rod with a yield strength of 105 ksi were connected using high strength steel coupling nuts to span the entire length of the bent cap. The threaded rods were anchored to the reaction frame using pieces of HSS6x6x1/2. These pieces of HSS6x6x1/2 spanned between the flanges of the horizontal members of the frame as seen in Figure 3-18. The rods were anchored using a nut and washer combination, and were hand tightened prior to lateral load application to ensure adequate bearing of the tube to the flanges of the horizontal members of the reaction frame.

Figure 3-18 Threaded Rod End Anchorage at Reaction Frame

3.3.2 Hydraulic Jacks

The threaded rods used to apply the lateral load spanned the length of the bent cap and were fed through two center-hole hydraulic cylinders that were connected to the end face of the bent cap. Two Enerpac #RRH-3010 long stroke hydraulic cylinders were used for the test. Each cylinder had a capacity of 30 tons (60 kips). The cylinders were connected to an Enerpac ZU4 Class ZU4408JB pump fitted with valves to provide equal pressure on both of the cylinders. The hydraulic cylinders and pump can be seen in Figure 3-19.

Figure 3-19 Enerpac Center-Hole Hydraulic Cylinders and Pump

3.3.3 Threaded Rods/Anchorage

Threaded rods were used as tension members to apply lateral load to the bridge bent. High-strength 1 1/8 in. diameter steel rods with a yield strength of 105 ksi were used in this load test. Twelve foot long segments were used to span the length of the bent cap. These twelve foot segments were joined using high-strength steel hex coupling nuts. The rods were threaded to the coupling nuts from both ends and hand tightened to ensure the full strength of the rods could be adequately developed. Two coupled rods can be seen in Figure 3-20.

Figure 3-20 Coupled Threaded Rod Sections

Two 1 ¾”x12”x1-0” A36 steel anchor plates were used as bearing plates on the jack end of the bent cap. A 1” elastomeric bearing pad was placed between the bent cap and the anchor plate to promote an even load distribution over the end face of the concrete bent cap. The anchor plates were designed using a maximum jack load of 120 kips and an allowable concrete stress of $0.85f'_c$. A conservative concrete compressive strength of 3 ksi was used for the allowable concrete stress at the face of the bent cap. The jack end anchorage can be seen in Figure 3-21.

Figure 3-21 Steel Anchor Plate with Bearing Pad at Jack End

The rods were anchored to the reaction frame using two pieces of HSS6x6x1/2 that spanned between the top and bottom flanges of the horizontal members of the frame. The pieces of steel tube were anchored using a nut and washer combination and hand tightened prior to the application of lateral load.

Two threaded rods were instrumented with electrical resistance gages in order to monitor the lateral load being applied to the bent during testing. The gages were installed using procedures previously mentioned in 3.2.2. Prior to testing, the rods were calibrated using the Tinius Olsen Universal Testing Machine to measure axial force and the P3 strain indicator to read axial strain in the rods. The load and strain measurements were used to create stress vs. strain curves for each of the rods from which calibration factors were created for accurate load monitoring during the load test. The rods loaded into the Tinius Olsen machine can be seen in Figure 3-22 and the rods installed in the field test setup can be seen in Figure 3-23.

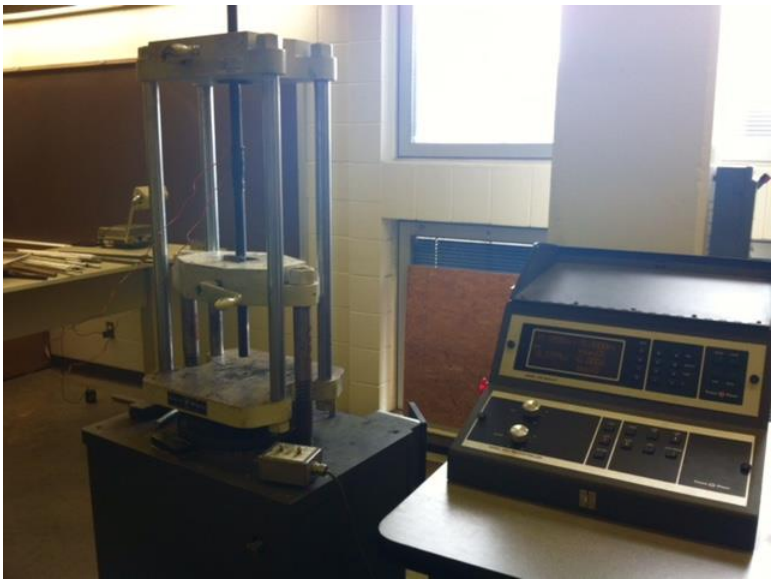

Figure 3-22 Gaged Threaded Rod Calibration

Figure 3-23 Field-Installed Threaded Rods with Instrumentation

3.3.4 Reference Frame for Wirepots

For measurement of lateral displacement of the bent cap during testing, displacement wirepots were utilized. A reference beam was necessary to anchor the wirepots. A wooden frame was constructed to anchor the wirepots and serve as a reference. The frame consisted of two vertical "A-frames" tied together by two horizontal 2x4's at the bottom of the frames and two along the height of the frame. Two diagonal braces were used at the bottom of the legs of the frames to resist in-plane side-sway. A ½" plywood board was connected to the frame for the wirepots to be anchored to and a piece of cut-off HP14x89 was placed on top of the frames in order to prevent vertical and lateral movement during the test. The wooden reference frame can be seen in Figure 3-24.

Figure 3-24 Wooden Reference Frame for Wirepot Installation

3.3.5 Data Acquisition

A Campbell Scientific datalogger was used to record data from the electrical resistance gages on the steel piles, concrete pile encasements, sister bars, and threaded rods. The datalogger was also used to record data from the displacement string pots. During the lateral load test, data was recorded once every 15 seconds for the entirety of the test. The Campbell Scientific datalogger used for this load test can be seen in Figure 3-25.

Figure 3-25 Campbell Scientific CR1000 Datalogger (Campbell Scientific 2015)

Four multiplexers were used to wire in the strain gages and displacement pots. The first three multiplexers were programmed for 120 ohm resistance gages. The strain gages installed on the steel piles and the sister bars were wired into these first three multiplexers. The fourth multiplexer was programmed for 350 ohm resistance gages. The remainder of the strain gages installed on the concrete pile encasements and the threaded rods were wired into this multiplexer. The wire pots were wired directly into the datalogger.

3.4 Testing Procedure

This section consists of the procedures used during testing. One set of data was recorded for this test. The data set included strain, load, and displacement measurements for the entire load test.

3.4.1 Load Monitoring During Test

The datalogger was programmed so that the output received from the electrical resistance strain gages installed on the threaded rods was in pounds. A laptop connected to the datalogger was used to graphically display the outputs from each of the gaged threaded rods so that the load in the system could be monitored throughout the duration of the load test. Each gaged threaded rod consisted of two strain gages located on opposite sides of the rod. The relative strains in each of the gages were averaged and converted to stresses then force based on their elastic modulus and cross sectional area. A calibration factor was also built into the program within the Campbell

Scientific datalogger. A display of the force in both rods was monitored to ensure that each of the jacks was exerting a relatively equal load to prevent major eccentric loading of the bent cap.

3.4.2 Static Lateral Load Test

On June 27, 2014 a static lateral load test was performed on the test bent. At the time of testing, the girders on both the forward and back spans had been set. The strategy for the load test was to load the bent in 10 kip increments up to 60 kips, holding each load increment for five to ten minutes, and then unloading the bent in two to three unloading increments and holding each unloading increment for three to five minutes. An image of the entire test setup can be seen in Figure 3-26.

Figure 3-26 Field Test Setup

Both load and displacement were monitored throughout the entirety of the test to ensure that excessive displacements did not occur and that the load in one jack was not significantly higher than the other. During the loading phases, the pressure in the jacks was increased using a hand-held remote which extended and retracted the pistons. For the loading phases, the pump was in extend mode and for the unloading phases, the pump was in retract mode.

The bent was loaded in 10 kips increments up to 60 kips, holding at each increment for ten minutes. The bent was then unloaded to 35 kips in three increments, holding at each increment for five minutes. After observation of small displacements at the 60 kip load increment, it was decided to reload the bent in five kip increments up to a total lateral load of 75 kips. The load was held for five minutes at each load increment for this reloading phase. Once the 75 kip load increment was completed, the bent was unloaded in four increments. The pump was put into retract mode to unload the bent. The piston pressure was released and the load was held for three minutes at each unloading increment and the load level was recorded. This process was repeated until the load in each of the jacks returned to its initial level.

3.5 Analysis, Results, and Discussion of Load Test

This section contains measured data as well as results from the full lateral load test. The methods and assumptions made for calculating axial forces and bending moments is also outlined in this section.

3.5.1 Strains

Strains at cross section above ground and below ground were observed in order to determine the functionality of the instrumentation. At sections above ground, strain data was captured on both the concrete encasement surfaces as well as the steel piles embedded within the encasements. The strain distribution across the composite section was of major interest, seeing that it had an effect on the method of calculating axial forces and bending moments at the section. For all strain

data, compressive strains are considered positive and tensile strains are considered negative. An average of the strains at each loading increment was used in developing the strain profiles since data was recorded for five to ten minutes at each load.

Upon observation, it was clear that the sections above ground in which concrete and steel surfaces were instrumented, were not behaving fully composite. The strain profile across the entire cross section was not linear, indicating that a perfect bond between the steel piles and the concrete encasement did not exist. Notably, the steel section was straining significantly more than the concrete. Strain profiles at each of the above ground sections in which concrete and steel surfaces were instrumented for graphical representation of the non-composite behavior. Strain profiles at each cross section can be seen in Figure 3-27 through Figure 3-36. The instrumented sections on the concrete surface occur at +/- 15 in. on each of the plots. The strain profiles for each pile are divided into two separate plots ranging from 10-40 kips and 50-75 kips in order to better determine behavior between load increments.

Upon observation, none of the concrete surface gages installed on the upper section of pile 1 were functioning correctly; therefore, this section was not considered in the calculations of axial forces and moments. As stated previously, the upper instrumented sections were located six inches from the bottom of the bent cap and the lower instrumented sections were located five feet below the upper instrumented sections. Concrete encasements were only instrumented at the upper locations on piles 3 and 4, therefore strain profiles at the lower sections for these piles are not included in the figures below.

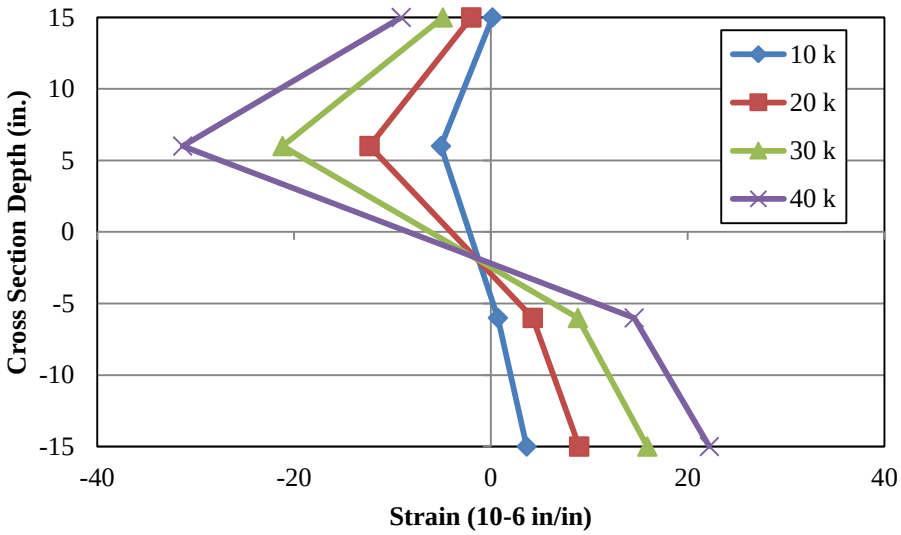

Figure 3-27 Pile 1 Lower Section Strain Profile

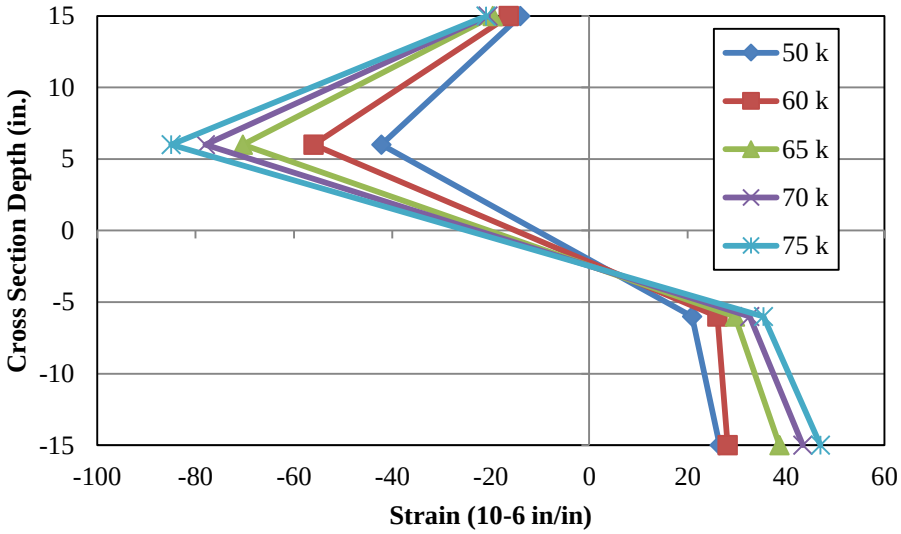

Figure 3-28 Pile 1 Lower Section Strain Profile

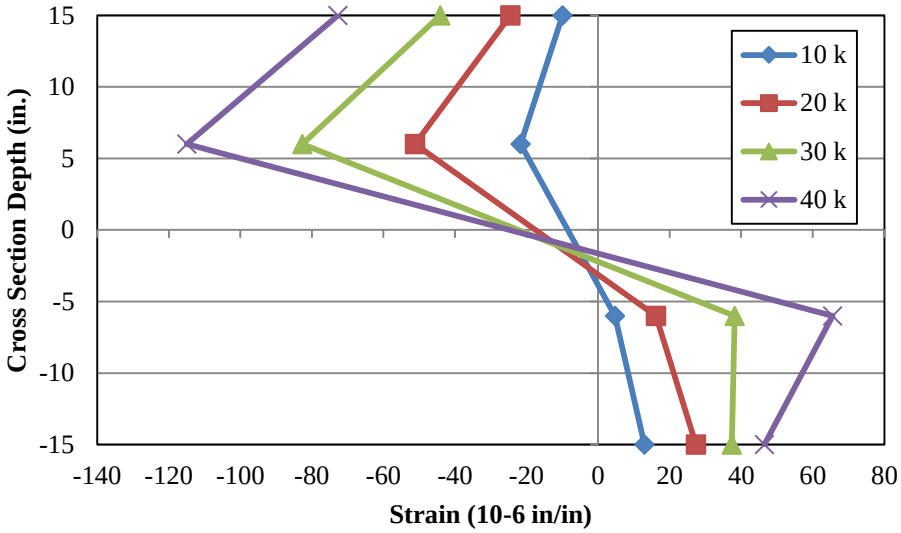

Figure 3-29 Pile 2 Upper Section Strain Profile

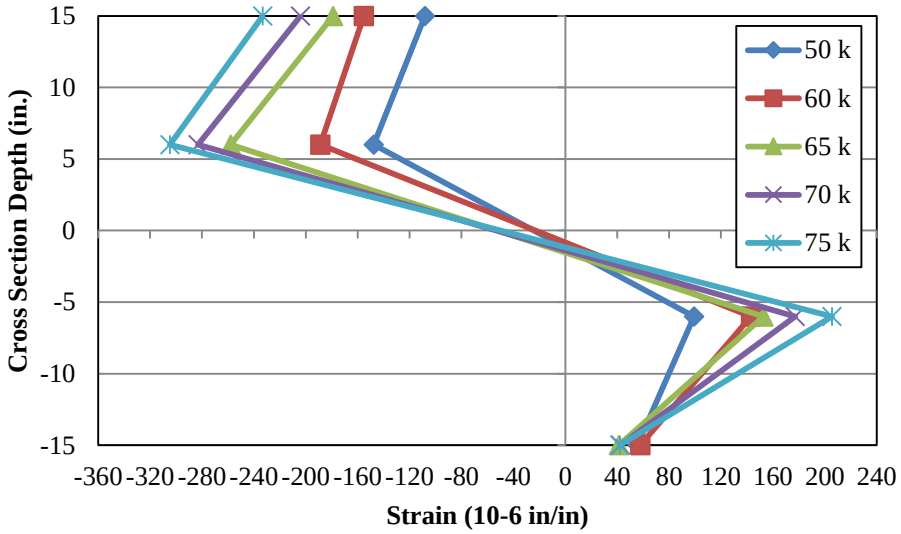

Figure 3-30 Pile 2 Upper Section Strain Profile

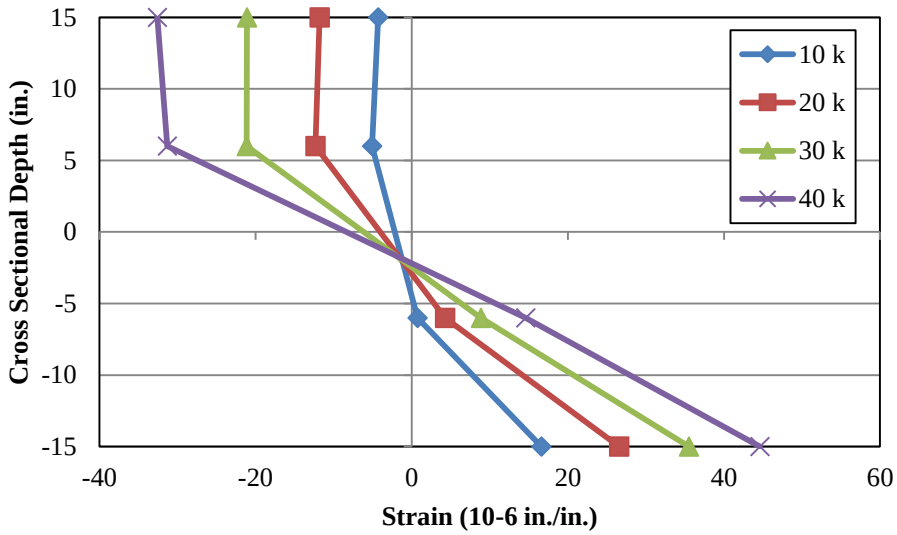

Figure 3-31 Pile 2 Lower Section Strain Profile

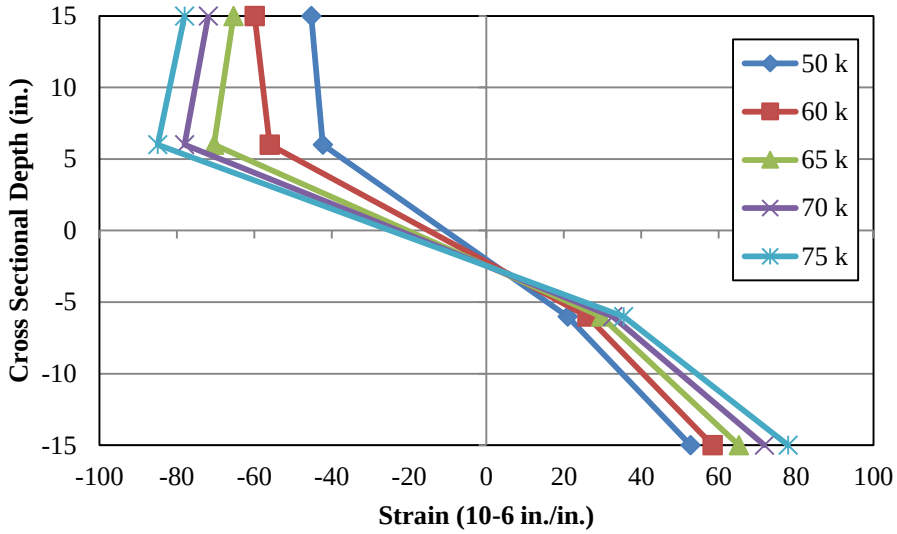

Figure 3-32 Pile 2 Lower Section Strain Profile

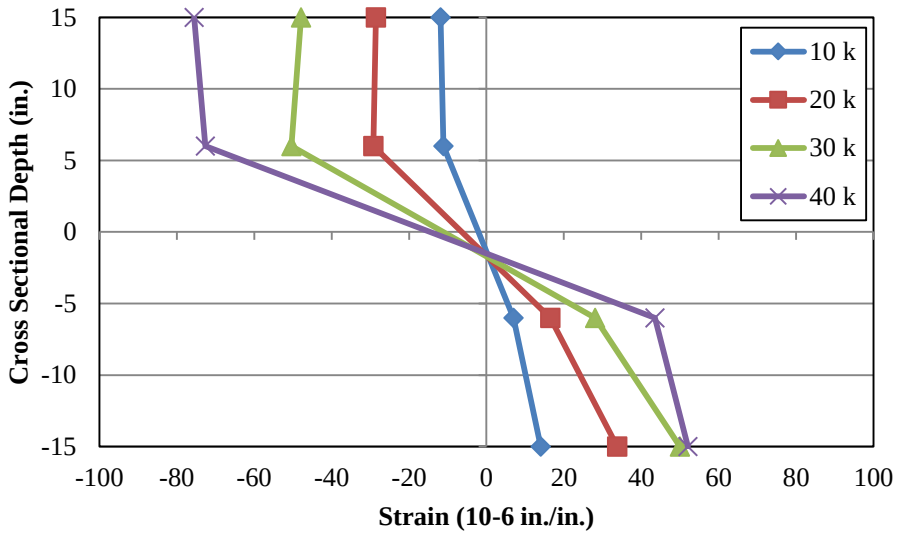

Figure 3-33 Pile 3 Upper Section Strain Profile

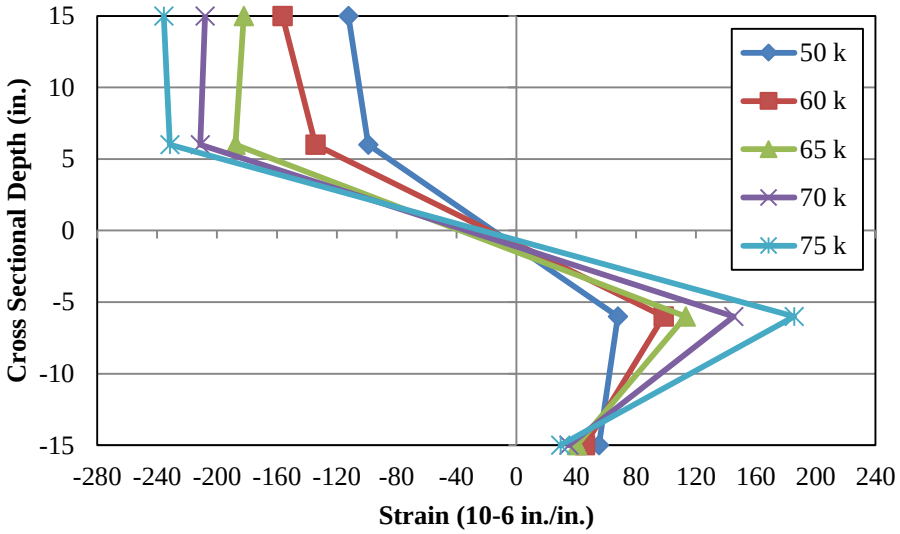

Figure 3-34 Pile 3 Upper Section Strain Profile

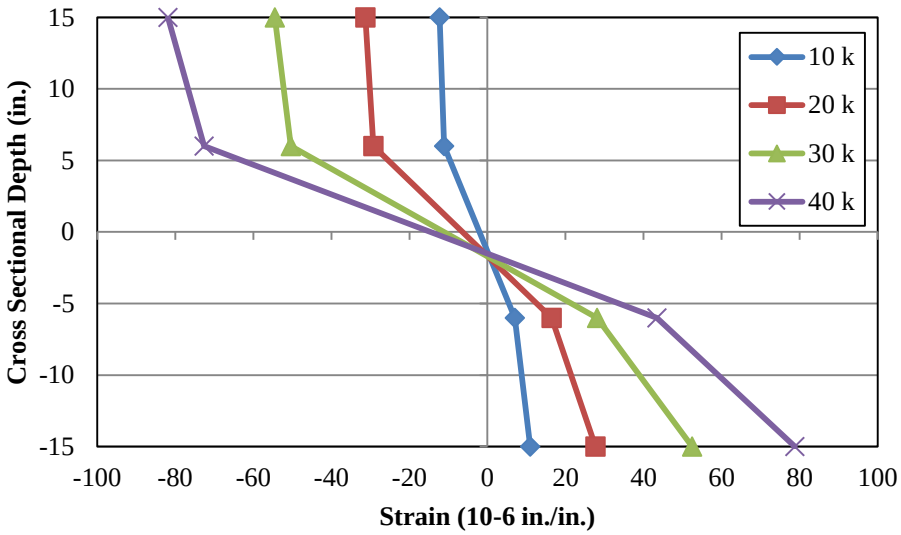

Figure 3-35 Pile 4 Upper Section Strain Profile

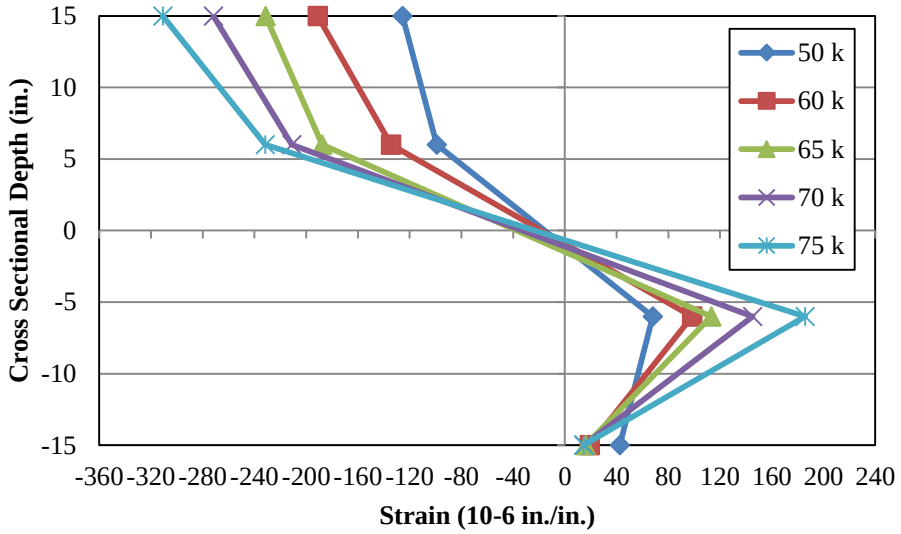

Figure 3-36 Pile 4 Upper Section Strain Profile

A number of different factors can be attributed to the piles not behaving perfectly composite. It is likely that the cracks had formed in the concrete due to the concrete being restrained by the steel pile. These restrain cracks would have formed prior to the piles being displaced during the tests. The locations of these cracks are very difficult to determine; therefore, the gages installed on the tension faces of the encasements have extremely variable results as the applied load increases.

Once the concrete cracks, bond stresses between the concrete and the steel are developed which can cause slipping.

The level of composite behavior, however, is of little concern to bridge designers seeing that they do not account for the stiffness or strength of the concrete encasements in their pile design. The encasements are in place primarily to prevent section loss of the steel piles in cases where the bent is located within the flow channel.

3.5.2 Axial Force and Bending Moment Calculations from Strain Data

For axial force and bending moment calculations at instrumented pile sections, two different approaches were used. As previously mentioned, the instrumented sections where both steel and concrete surfaces were instrumented did not behave perfectly composite. The method for computing axial forces and bending moments at this location became more involved due to the non-linear strain profile over the cross section. This section details how axial forces and bending moments were calculated at sections with and without concrete encasements.

The axial stress at cross sections where the piles were not encased in concrete was computed by taking the average of the compressive and tensile strains on the cross section and multiplying it by the modulus of elasticity of the steel pile. The force was then computed by multiplying the axial stress by the gross cross-sectional area of the steel pile. The method used for computing the axial force in the steel pile can be seen in Equation 3-1.

$$P = \left(\frac{\varepsilon_c + \varepsilon_t}{2}\right) E A_g \qquad \text{(Equation 3-1)}$$

Where:

P = axial load in pile (kips)

ε_c=compressive strain (in./in.)

ε_t=tensile strain (in./in.)

E = modulus of elasticity (ksi)

A_g = gross cross-sectional area (in.^{2})

For these computations, the modulus of elasticity used for the steel piles was assumed to be 29,000 ksi and the gross cross-sectional area used for HP14x89 was 26.1 in.^{2}.

At sections where the steel piles were not encased in concrete, bending moment calculations are performed assuming a linear strain distribution over the pile cross section. Using the two measured strains on the tension and compression sides of the pile flange, the curvature of the cross section can be computed using Equation 3-2.

$$\varphi = \frac{\varepsilon_c - \varepsilon_t}{h} \qquad \text{(Equation 3-2)}$$

Where:

φ=curvature (in.$^{-1}$)

ε_c=compressive strain (in./in.)

ε_t=tensile strain (in./in.)

h=distance between measured strains (in.)

The curvature was then used to calculate bending moments at the cross section using Equation 3-3.

$$M_b = \varphi EI \qquad \text{(Equation 3-3)}$$

Where:

M_b = bending moment (kip-in)

E = modulus of elasticity (ksi)

I = moment of inertia (in.^{4})

The piles were being loaded in the weak axis direction, therefore I_y of the HP14x89 was used as the moment of inertia used for calculation of bending moment, which was 326 in^4.

A different approach was necessary for computing axial forces and bending moments at the instrumented sections where both steel and concrete strains were measured. Had the sections behaved in a truly composite manner, i.e. the strain profile over the cross section was linear, then a transformed section analysis could have been used to compute the bending moments on the cross section.

A basic integration approach was considered for axial force and bending moment calculations. The cross section was divided into six areas, and the strains at the centroid of these areas were linearly interpolated based on the measured strains. Figure 3-37 shows the cross section divided into these six areas. The trapezoidal rule for integration was used to calculate these areas. For concrete stress calculations where steel areas were also present, the areas of the steel were subtracted from the concrete area.

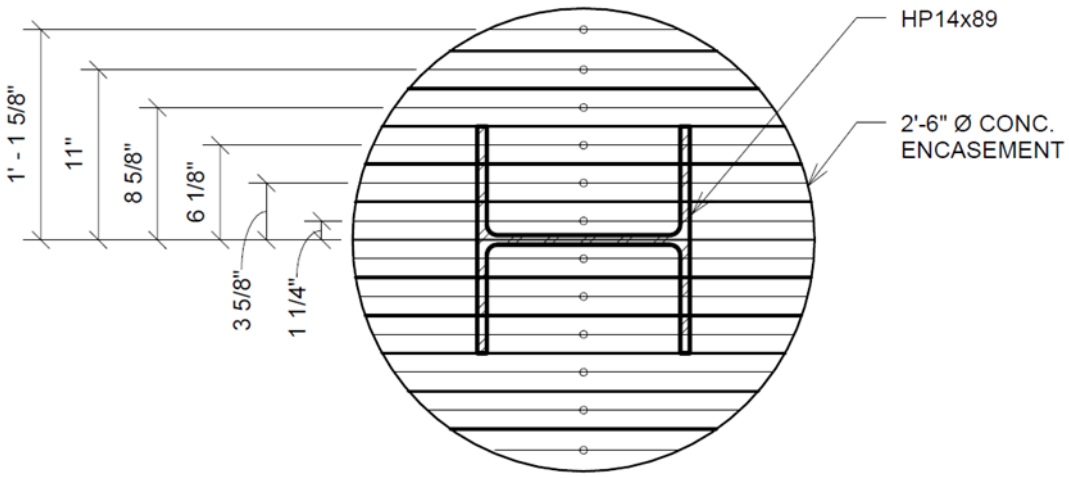

Figure 3-37 Composite Cross-Section Geometry

Axial Stresses at each of these locations were computed using Hooke's Law. This assumption was made assuming the section remained uncracked during the load tests. Equation 3-3 was used to calculate the axial force on the cross section.

$$P = \int_A \sigma dA \qquad \text{(Equation 3-4)}$$

The strains and cross sectional areas of both the concrete and steel were used for this calculation. Implementing Hooke's Law and separating the steel and concrete terms, equation 3-4 can be shown as:

$$P = \sum(\varepsilon_{i,c} E_c A_{i,c}) + \sum(\varepsilon_{i,s} E_s A_{i,s)} \qquad \text{(Equation 3-5)}$$

Where:

P = axial force on cross section (kips)

$\varepsilon_{i,c}$= strain in concrete (in./in.)

E_c = modulus of elasticity of concrete (ksi)

$A_{i,c}$ = incremental area of concrete (in^2)

$\varepsilon_{i,s}$= strain in steel (in./in.)

E_s = modulus of elasticity of steel (ksi)

Moment equilibrium was used in order to calculate the bending moment on the cross section. Moments were summed about the center of the composite cross section using the forces calculated using equation 3-5. Equation 3-6 was used to calculate bending moments at each instrumented cross section where steel and concrete surfaces were instrumented.

$$M_b = \int_A \sigma y dA \qquad \text{(Equation 3-6)}$$

Similar to axial forces computation, the cross section was divided into incremental areas. The strain at the centroid of each of these areas was determined using linear interpolation, and the incremental area was calculated using the trapezoidal rule. The moment arm, y, for this calculation was the distance from the centroid of the incremental area to the centroid of the composite cross section. The relationship in equation 3-6 simplifies to equation 3-7. This equation was used to compute bending moments on the composite cross section where d_i is the distance from the centroid of the incremental area to the centroid of the composite cross section.

$$M_b = \sum \varepsilon_{i,c} E_c * d_i * A_{i,c} + \sum \varepsilon_{i,s} E_s * d_i * A_{i,s} \qquad \text{(Equation 3-7)}$$

The modulus of elasticity used for the concrete encasements was based on cylinder tests performed by the contractor for the new construction bridge. The approximated concrete modulus of elasticity was calculated using Equation 3-8. This equation was simplified from the equation for approximated modulus of elasticity in ACI 318-11 (ACI 2011), assuming normal weight concrete with a unit weight of 150 pcf. For this computation, the measured compressive strength from cylinder breaks at 28 days was used and the lightweight concrete factor was taken as 1.0.

$$E_c = 57{,}000\lambda\sqrt{f'_c} \qquad \text{(Equation 3-8)}$$

Where:

E_c = concrete modulus of elasticity (psi)

λ=lightweight concrete factor

f'_c = specified 28-day concrete compressive strength (psi)

Cylinder breaks were made at 8 and 28 days. The 28-day tests were performed on June 16, nine days before the load test was performed. For all calculations from this load test, the measured compressive strengths from the 28-day cylinder tests were used. An average of the two cylinder strengths was used in computing the modulus of elasticity of the concrete encasements. Table 3-1 shows the cylinder test results for the concrete encasements used in bent 5 at the Old Town Creek Bridge.

Table 3-1 Concrete Properties

Test Date	Age (days)	Specified Compr. Strength (psi)	Actual Compr.Strength (psi)
05/2714	8	3000	3590
06/16/14	28	3000	4720
06/16/14	28	3000	4780

The specified 28 day compressive strength for these pile encasements was 3000 psi. These encasements are typically used to prevent pile section loss in terms of corrosion, and are not used in structural calculations for the piles. The actual measured compressive strengths from these cylinder tests at 28 days indicated that the concrete used for the encasements exceeded their specified compressive strength considerably. The value of E_c used from the average of the measured compressive strengths was 3928 ksi.

3.5.3 Axial Forces

The axial forces calculated were found to be well beyond theoretical values. Due to the large cross sectional area of the concrete encasements, minor changes in strain result in a large change in axial forces. The forces that were calculated were not feasible considering equilibrium therefore they were deemed too inaccurate to report.

3.5.4 Bending Moments

Bending moment profiles for each pile can be seen in Figure 3-38 through Figure 3-45. The pile depth is measured from the top of the pile head, which is embedded one foot into the cast-in-place bent cap. The first instrumented section occurred six inches below the bottom of the cap, therefore the first point on each of the bending moment profile occurs at -1.5 feet. The top of the rip-rap varied slightly at each pile location, but occurred at an average of -7.0 feet. The ground elevation below the rip-rap layer occurs at approximately -10.0 feet. Negative moments at below ground cross sections indicates curvature reversal meaning the pile flanges that were in tension or compression at sections instrumented above ground were now opposite. The stiffness of the concrete section was much larger relative to the steel pile section, therefore the bending moments carried by the concrete section are transferred into the ground at the level in which the encasements terminate. A small amount of bending moment is shed into the pile itself at the location which the

encasements stop. Therefore, the bending moments carried by the steel section below ground are very small in comparison to the above ground composite moments.

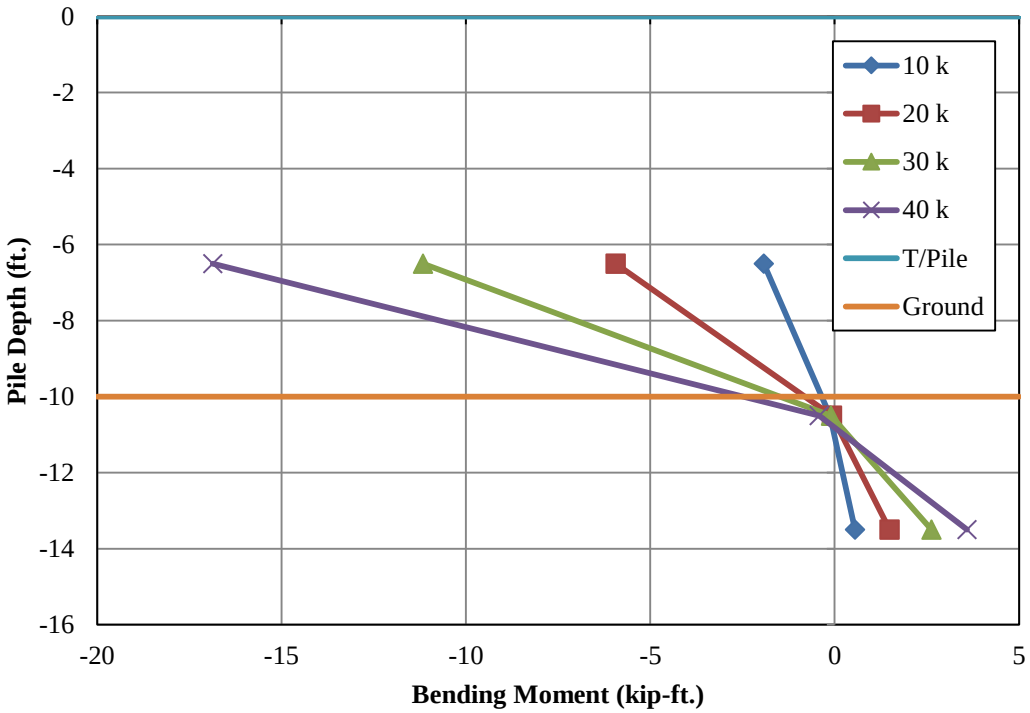

Figure 3-38 Pile 1 Bending Moment Profile

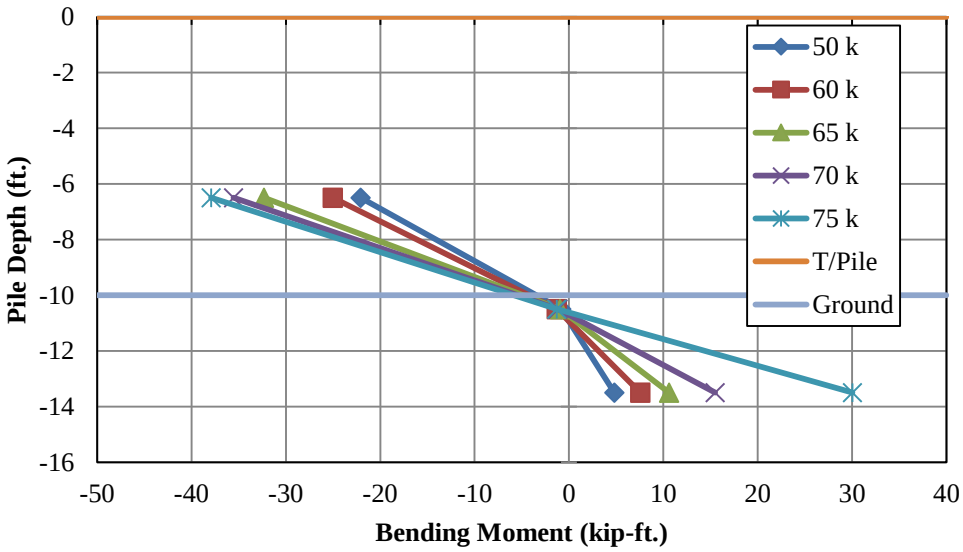

Figure 3-39 Pile 1 Bending Moment Profile

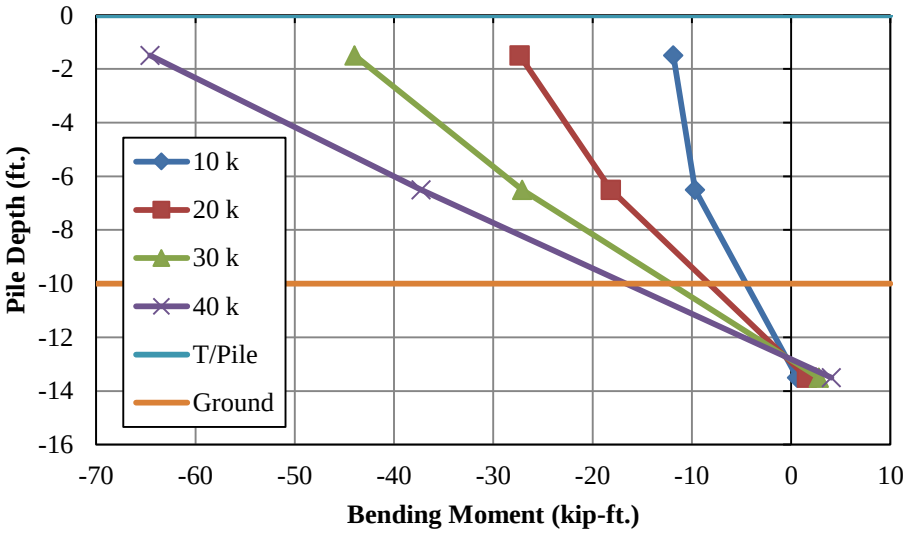

Figure 3-40 Pile 2 Bending Moment Profile

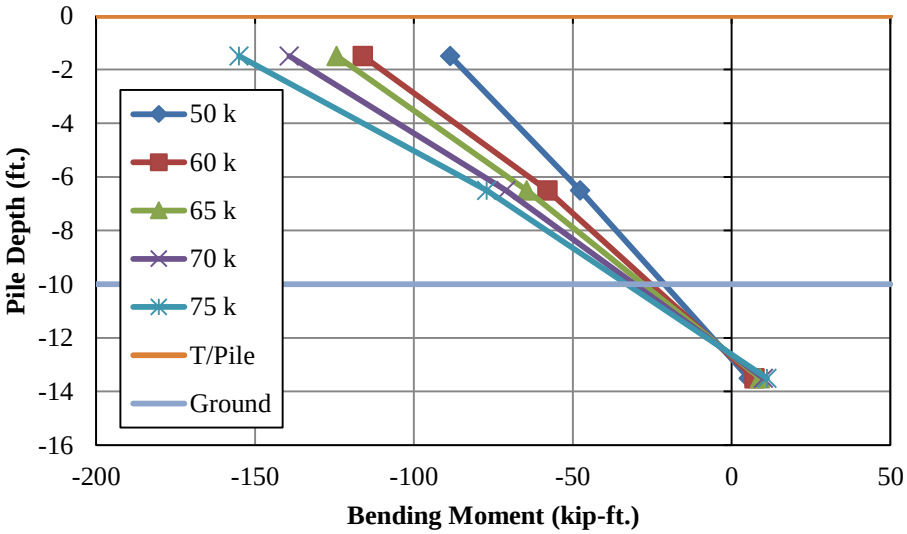

Figure 3-41 Pile 2 Bending Moment Profile

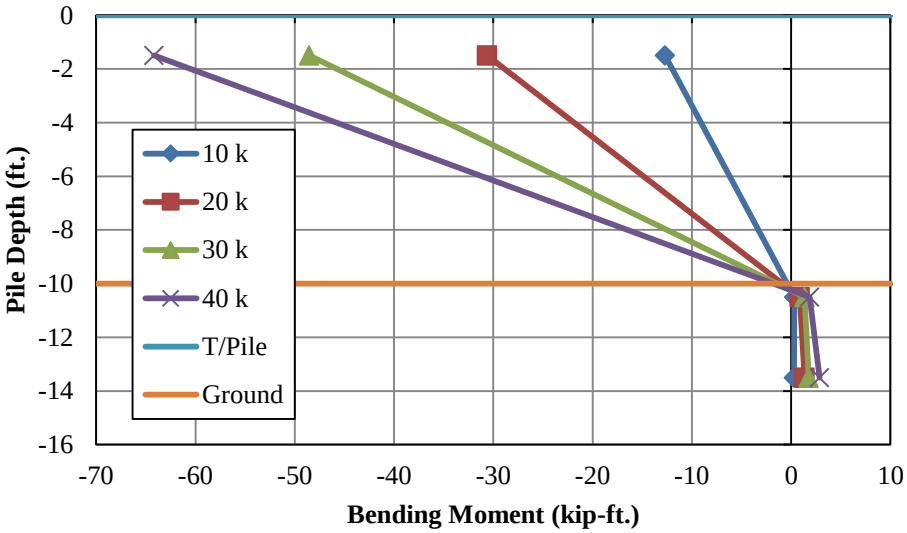

Figure 3-42 Pile 3 Bending Moment Profile

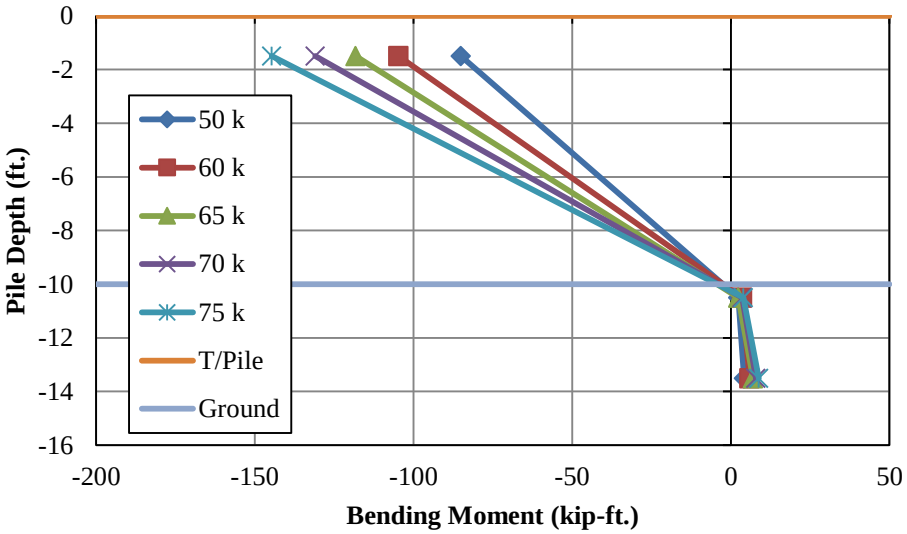

Figure 3-43 Pile 3 Bending Moment Profile

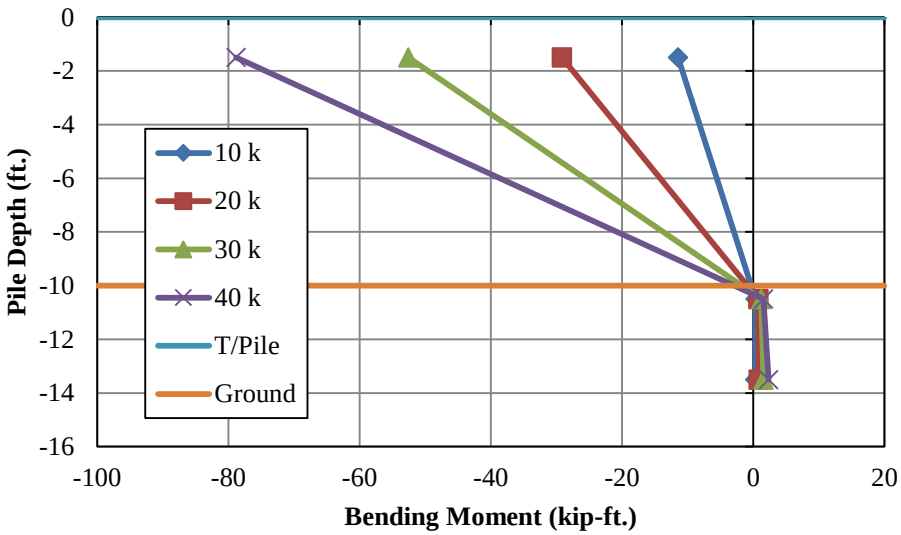

Figure 3-44 Pile 4 Bending Moment Profile

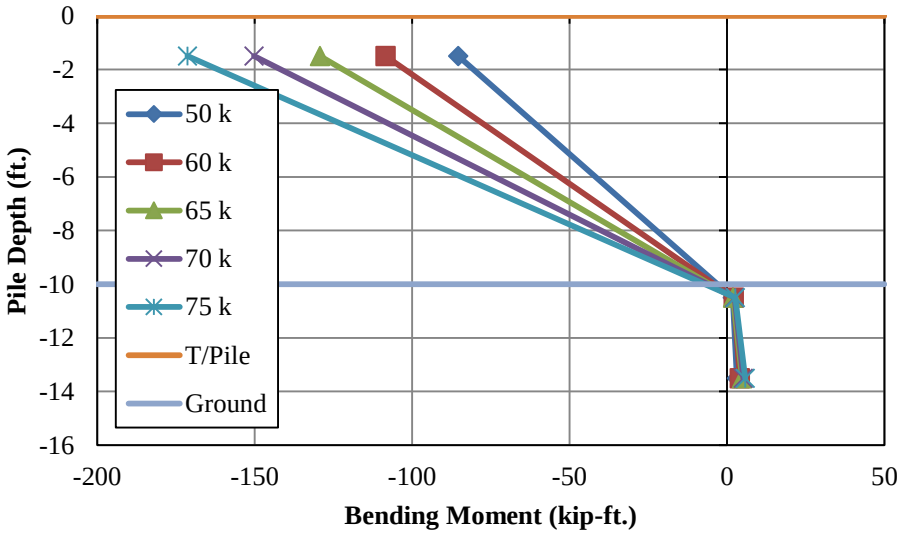

Figure 3-45 Pile 4 Bending Moment Profile

3.5.5 Displacement String Pots

Lateral displacement data was recorded during the load test using displacement wirepots. Wirepots were installed in each corner of the bent cap to obtain a load versus average lateral deflection relationship for the pile bent substructure. Four wirepots were also used to ensure that no significant twisting of the cap was present due to eccentric loading. The load versus deflection

plot for the load test can be seen in Figure 3-46. The recorded displacement for each of the four wirepots as well as the average deflection can be seen in the figure.

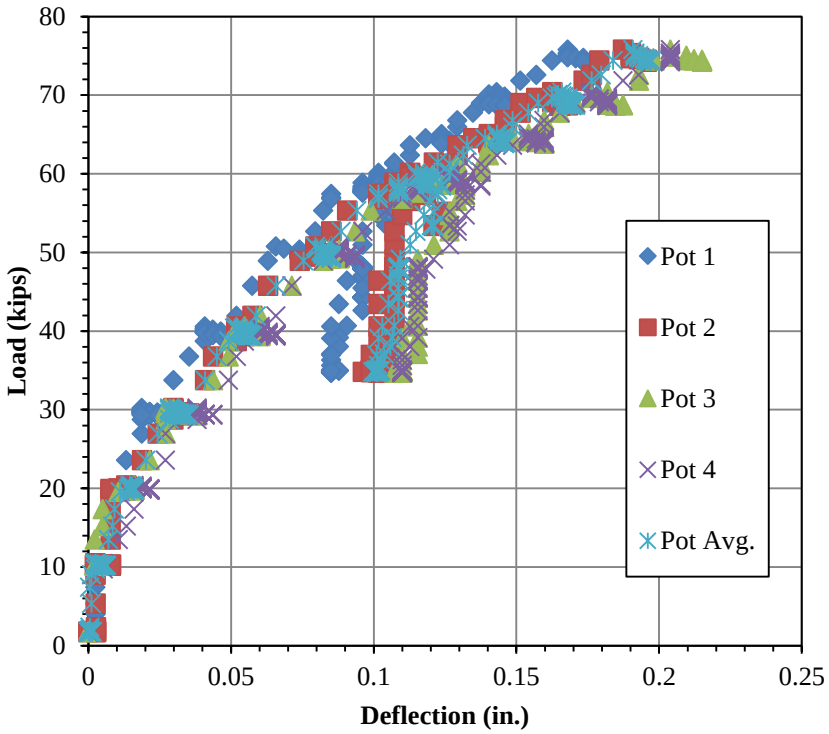

Figure 3-46 Load-Deflection Plot – Macon County Test 1

The recorded deflection for each of the four plots is very similar for the entire duration of the load test. This similarity in deflections is important in that there was little effect due to eccentric loading, meaning that the load in each of the hydraulic jacks remained virtually the same throughout the duration of the test. This similarity in each of the wirepots also proved that there was little very little twisting of the cap.

The bent deflected an average of 0.2 in. at a maximum lateral load of 75 kips. The large overall stiffness of the bent can be attributed to a number of reasons. The lateral stiffness of the pile bent structure is heavily dependent on the stiffness of the vertical elements which in this case are the piles. The flexural stiffness of a single pile with respect to a concentrated load is a function of the unbraced length cubed. The test bent for the Macon County Bridge had pile clear heights of

around 5 feet, making the bridge extremely stiff. The stiffness is also a function of the modulus of elasticity of the elements and their moment of inertia. For the encased steel piles, the moment of inertia of the concrete section alone is 487 times greater than the moment of inertia of the steel piles in the direction in which they were loaded in the test. This additional stiffness increases the overall stiffness of the bent significantly.

3.5.6 Bridge Bent Behavior

The Macon County Bridge bent was very stiff during the lateral load test. The high stiffness of the bent can be attributed to the small free height of the piles and the additional stiffness of the circular concrete encasements. The shape of the bending moment profile in each of the four piles during the load test was similar to the theoretical shape of the bending moment profile with the piles behaving in a fixed head condition with the maximum bending moment at the top of the pile. Although a complete profile was not captured with the instrumentation used, the curvature reversal of the piles below finished grade could clearly be seen. The bending moment dissipated quickly as the pile depth increased. This dissipation can be partially attributed to the load carried by the concrete encasement being transferred to the soil and the steel pile where it is terminated. Due to the large amount of load carried by the encasement relative to the steel pile, the remanding load transferred through the pile is small. The maximum bending moment that was calculated from measured strains was much smaller than the maximum bending moment at the bottom of the bent cap. This dissipation in moment can be attributed in part to the lateral load transfer from the pile to the soil at these depths. The lateral resistance of the soil results in shear forces in the pile, causing curvature reversal. From measured strains on the concrete encasements and the steel piles, it was observed that the piles were not acting perfectly composite indicating that slipping had occurred between the concrete and steel surfaces. This level of composite behavior can likely be attributed

to the presence of small shrinkage cracks developed due to the steel pile restraining the concrete. However, a cracked section analysis was not used.

3.6 Chapter Summary

The bent performed very well and was exceptionally stiff under lateral loads easily exceeding service level lateral loads. Bending moment values were relatively high for each of the four piles. The measured strains gave inconclusive results with regards to the axial forces in each of the piles under lateral loading. The pile section encased in concrete did not appear to act perfectly composite, but this level of composite behavior is of little interest to designers since they do not take into consideration the stiffness or strength of the concrete encasements in the design of the piles. The addition of these encasements only increases the performance and stiffness of the pile bents.

Chapter 4 Field Test 2 – Macon County Bridge

4.1 Introduction

The Macon County Route 9 replacement bridge under construction was also used for the second field test. The second test was completed following casting of the concrete roadway. The barrier rails had not yet been cast at the time of testing. The roadway consisted of a 7 in. concrete deck with a width of 30’-9”, a typical width for standard 12 ft. lanes. A typical roadway cross section can be seen in Figure 4-1. Three tests were performed in this test: a purely lateral load test and two combined gravity and lateral tests. ALDOT load trucks were used for application of gravity load. For the first combined gravity and lateral load test, the load truck was positioned in the center of the roadway with the back-center wheel axle centered over the bent. For the second combined lateral and gravity load test, the load truck was positioned on the edge of the roadway over the piles that were expected to be in axial compression due to overturning from lateral load. The instrumentation used in the first load test was also used for this second load test. Load transfer through the bridge deck was not within the scope of this research; therefore, the bridge deck was not instrumented prior to load testing.

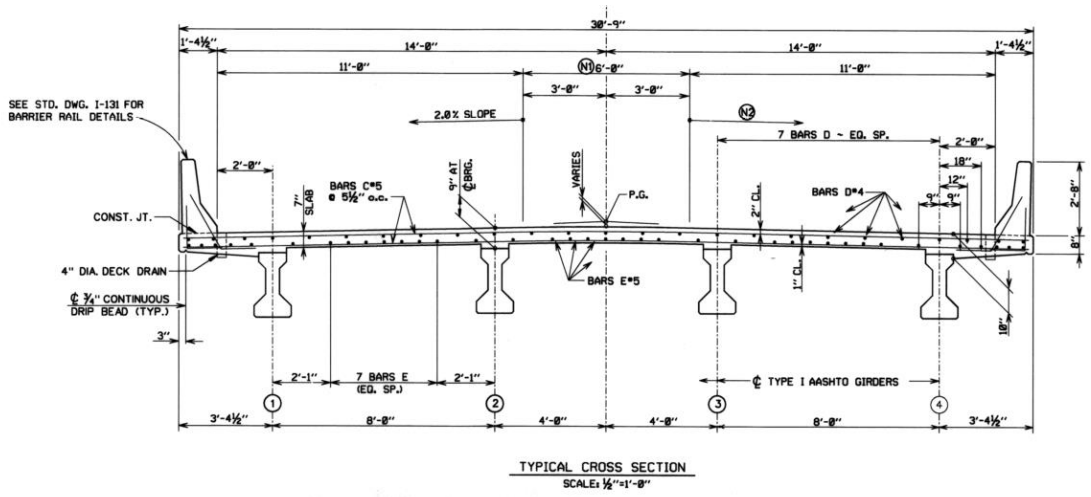

Figure 4-1 Typical Roadway Cross Section (Weatherford & Associates 2013)

This chapter details the instrumentation, testing methods, and equipment used for the second load test at the Macon County replacement bridge. This section also details the analysis, results and discussion of the data collected during the load tests.

4.2 Instrumentation

The instrumentation used for the first load test on the Macon County Bridge was also used for the second load test. The instrumentation installed on the steel piles, concrete encasements, and sister bars were used to calculate axial forces and bending moments during the tests. For instrumentation layouts, instrumentation used, and installation procedures, see Section 3.2.

4.3 Testing Equipment and Setup

This section details the setup used for this load test as well as the equipment used to apply the load and monitor forces, moments and deflections.

4.3.1 Reaction Frame Configuration

An A-frame configuration consisting of two HP14x89 vertical piles with an HP14x89 diagonal strut was used as a reaction frame for the second load test. Two horizontal pile cut-offs were

welded to the vertical members at the top of the frame so that the threaded rods could be adequately anchored. For more details on the reaction frame used for this load test, refer to Section 3.3.1.

4.3.2 Hydraulic Jacks

Two 60 ton Enerpac center-hole hydraulic cylinders were used for load application for this load test. The cylinders were connected to a hydraulic pump fitted with pressure valves to ensure equal pressure in each of the cylinders during the load test. For more details on the hydraulic cylinders and pump used for this test, refer to Section 3.3.2.

4.3.3 Threaded Rods/Anchorage

High-Strength steel threaded rods were used as tension members to apply the lateral load for this test. The rods were 1 1/8” in diameter with a yield strength of 105 ksi. The rods were coupled using steel coupling nuts. The rods were threaded into the coupling nuts from both ends and hand tightened to ensure adequate development. For images and more details on the threaded rods and end anchorages used for this test, refer to Section 3.3.3

4.3.4 Truck Live Load

For the combined lateral and gravity load tests, an ALDOT load truck was used for gravity load application. The load truck configuration used for this load test was LC-5. The load truck with this configuration weighed a total of 85,700 lbs. A figure of the LC-5 configuration can be seen in Figure 4-2 . The geometry and axle loads for the load truck in the LC-5 configuration can be seen in Figure 4-3. In this figure, the GVW shown in the total truck weight. The loads shown represent the total load for each of the three axles.

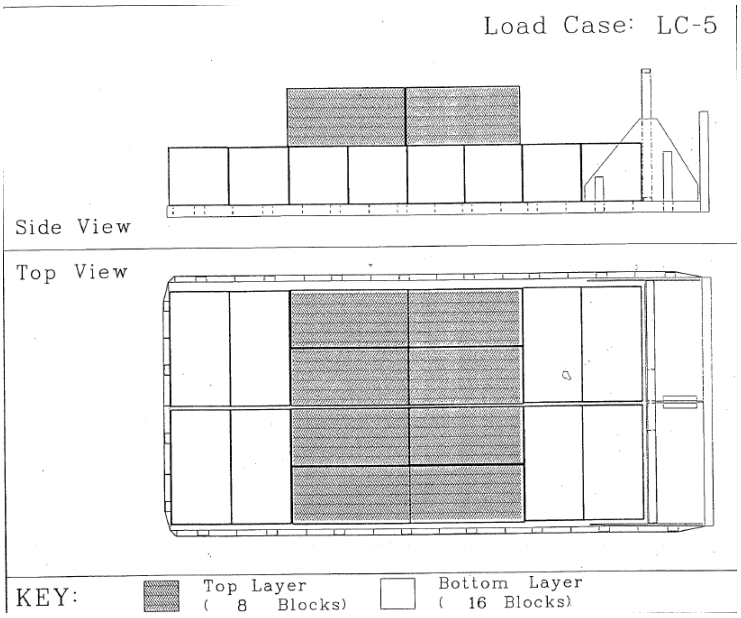

Figure 4-2 ALDOT Load Truck LC-5 Configuration (ALDOT)

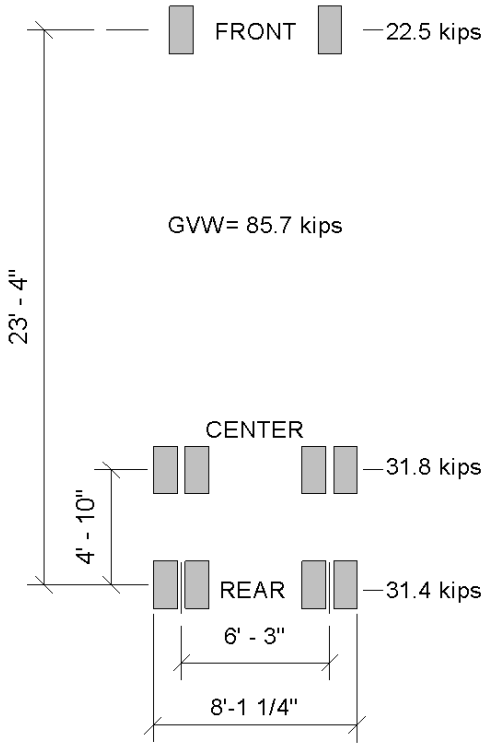

Figure 4-3 LC-5 Geometry and Axle Loads

During the test, the truck was positioned so that the center axle of the truck seen in Figure 4-3 was centered over the bent centerline. Two different tests were completed, with the transverse

position of the load truck varying. In each of these tests the longitudinal positioning of the load truck remained the same.

4.3.5 Reference Frame For Wirepots

Displacement wirepots were used in order to measure lateral deflection of the bent cap during the load tests. The wirepots were mounted onto a wooden frame which served as a reference frame for the wirepots. For more details on the reference frame used for this test, refer to Section 3.3.4.

4.3.6 Data Acquisition

A CR1000 datalogger from Campbell Scientific was used to record data from the electrical resistance gages on the steel piles, concrete pile encasements, sister bars, and threaded rods. Four multiplexers were used to wire in the instrumentation. For each of the three tests performed, data was recorded every 15 seconds. For more details on the data acquisition system for this load test, refer to Section 3.3.5.

4.4 Testing Procedure

This section details the procedure for each of the tests performed on the Macon County replacement bridge and how the loads and deflections were monitored during the testing of the bridge. Three separate load tests were performed. The first test performed was a purely lateral load test with the only axial load being the self-weight of the structure. The second and third tests were combined lateral and axial tests. An ALDOT Load Truck in configuration LC-5 was used for axial load application. The load truck's center of gravity was positioned directly over the bent for each test. The load truck was positioned in the center of the roadway for the first test and positioned so that the outside wheels were over the exterior girder for the second test.

4.4.1 Static Lateral Load Test

The first test performed on September 18, 2014 was a purely lateral load test with no ALDOT load truck. This test was executed similarly to the load test on the bent in Chapter 3. The bent was

loaded in ten kip increments up to a total lateral load of 60 kips. The load was held for five minutes at each loading increment to obtain a sufficient amount of data for each load. Once the total load was reached, the bent was unloaded in four unloading increments. The unloading was achieved by setting the hydraulic pump in "retract" mode, and releasing pressure. A specified load was not used in each of the unloading increments. However, the load at each unloading increment was recorded and held for three minutes to obtain a sufficient amount of data. The bent was unloaded in this manner until the load in the threaded rods was due to initial tension.

4.4.2 Combined Lateral and Gravity Load Test – Truck Centered in Roadway

The second test performed was a combined lateral and gravity test using an ALDOT load truck with the LC-5 configuration. The truck was centered over the roadway for the first test to theoretically distribute the truck load evenly to each of the four piles in the test bent. The back middle wheel axle was centered over the test bent to ensure that the truck load's center of gravity was directly over the bent. Data was recorded as the truck entered the bridge roadway and continued to be recorded for five minutes after it reached its intended position. The position of the load truck during the first combined lateral and gravity test can be seen in Figure 4-4.

Figure 4-4 ALDOT Load Truck Centered in Roadway

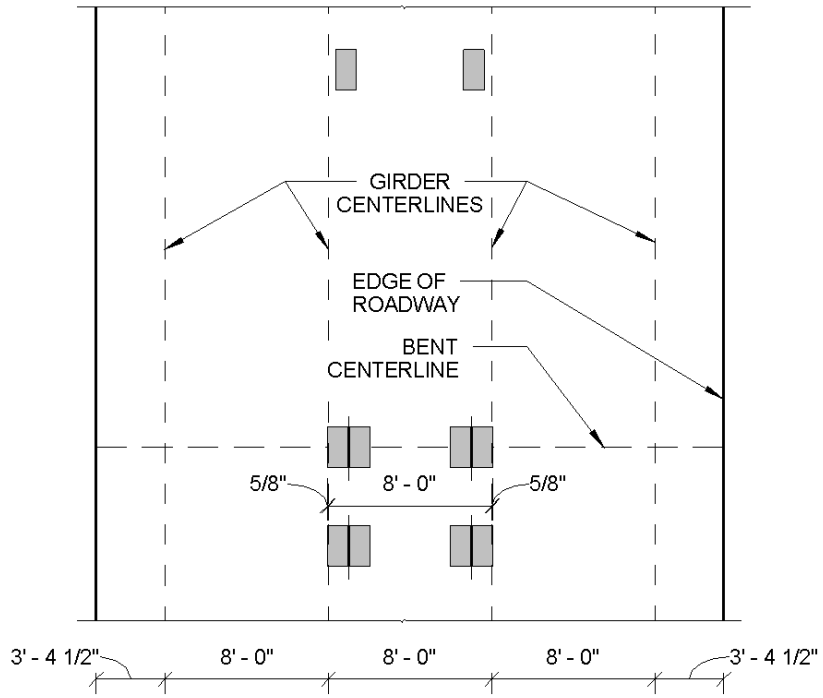

Figure 4-5 Position of Load Truck Centered Over Roadway

Once the truck was positioned correctly and sufficient data was recorded, the bridge was loaded laterally. The lateral load was applied by setting the hydraulic pump into "extend" mode and increasing the pressure using the hand-held remote. The bent was then loaded in 10 kip increments up to a total lateral load of 60 kips. Each load increment was held for five minutes to obtain a sufficient amount of data. Once the 60 kip load increment was reached, the bent was then loaded in 5 kips increments up to a total lateral load of 75 kips. Each load increment from 65 kips to 75 kips was also held for five minutes. Once the total load was reached, the bent was then unloaded in four unloading increments. The bent was unloaded by setting the hydraulic pump into "retract" mode, slightly releasing pressure. Each unloading increment was held for three minutes to obtain sufficient data. The bent was unloaded until the load in the threaded rods reached the initial load.

4.4.3 Combined Lateral and Gravity Load Test – Truck Positioned at Edge of Roadway

The third test performed was a combined lateral and gravity load test as well. For this test, the ALDOT load truck was positioned at the edge of the roadway with its outside wheel centered over the exterior girder. Similarly to the second test, the load truck's back center axle was centered over the test bent.

The truck was positioned over the side of the bent in which the piles were expected to be in axial compression due to overturning. The goal was to apply the gravity load to induce maximum compression in the exterior battered pile. The truck's positioning for the third test can be seen in Figure 4-6 and Figure 4-7.

Figure 4-6 ALDOT Load Truck Positioned at Edge of Roadway

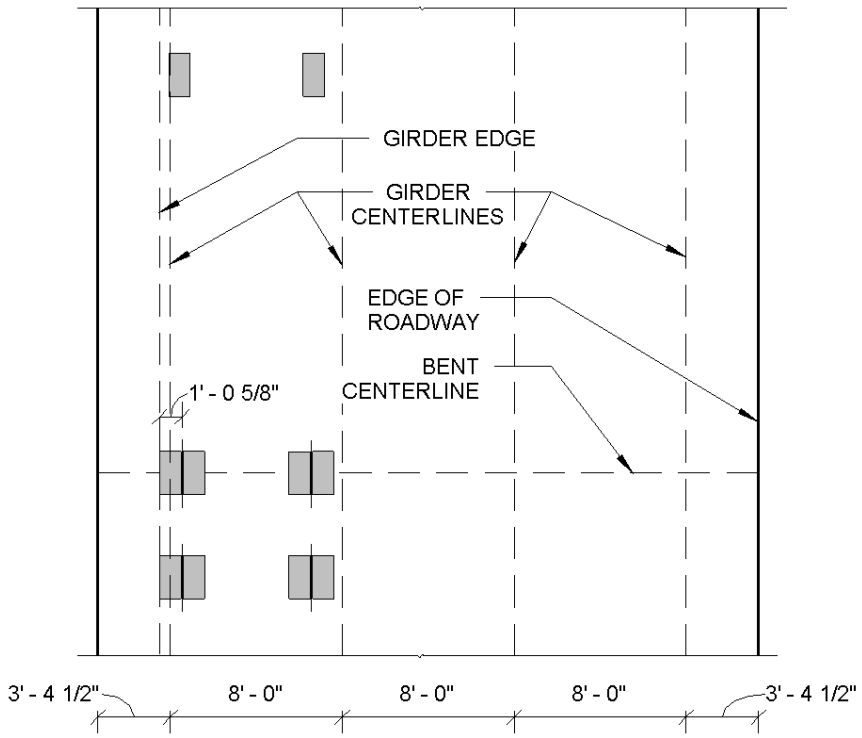

Figure 4-7 Position of Load Truck Over Exterior Girder

The truck was positioned appropriately and data was recorded for five minutes to obtain axial force information in the piles. The bent was then loaded laterally in 10 kip increments up to a total lateral load of 60 kips. The load was held for five minutes at each loading increment to obtain sufficient strain data. After the last loading increment was completed, the bent was then unloaded in a series of four increments. The bent was unloaded by setting the hydraulic pump to its "retract" setting and releasing pressure in the system. Each unloading increment was held for three minutes before proceeding to the next increment. The bent was unloaded until the force in the threaded rods reached its initial load.

4.5 Analysis, Results and Discussion of Load Test

This section contains measured data as well as results from the three load tests performed. The methods and assumptions made for calculating axial forces and bending moments is also outlined in this section.

4.5.1 Strains

Measured strains from gages instrumented on the concrete surface and the steel piles were observed in order to determine the functionality of the gages. At sections in which the concrete surface and the steel pile were both instrumented, the strain distribution across the composite cross section was inspected to determine whether or not the cross section was acting compositely. Similarly to the measured strains in the first load test outlined in Chapter 3, the encased sections did not appear to behave fully compositely. The strain distributions over the composite cross sections were not linear, indicating slipping between the concrete surface and the steel pile. This nonlinear strain distribution was accounted for when calculating axial forces and bending moments at the cross sections in which strains were measured on the concrete and the steel pile.

Upon observation, neither of the concrete surface gages on the upper instrumented section on Pile 1 appeared to be functioning correctly therefore they are not included in the bending moment profiles.

4.5.2 Axial Force and Bending Moment Calculations from Strain Data

Two different approaches for calculating bending moments and axial forces were implemented. The first approach was used for sections in which strains were measured on the concrete surfaces and the steel piles. This approach consisted of linearly interpolating the strains at discrete points along the cross section and integrating over the area. The second approach was used for calculating bending moments at instrumented cross sections not including concrete encasements. This approach used the curvature of the cross section based on measured strains and the bending moment was calculated by multiplying the curvature by their moment of inertia and their modulus of elasticity. The moment of inertia of the axis in which the piles were loaded about was used in these calculations. The concrete strengths used in the load test outlined in Chapter 3 were used again for axial force and bending moment calculations for the load tests in this chapter

as well. These concrete strengths were based on compressive tests performed at 28 days after placement of the encasements. A modulus test was not performed on cylinder samples from the concrete placed in the bent cap or the encasements; therefore the modulus of elasticity for the concrete encasements was approximated using the empirical equation given in chapter 3. For further details regarding the calculation of bending moments and axial forces, refer to Section 3.5.2.

4.5.3 Axial Forces

The axial forces calculated were found to be well beyond theoretical values. Due to the large cross sectional area of the concrete encasements, minor changes in strain result in a large change in axial forces. The forces that were calculated were not feasible considering equilibrium therefore they were deemed too inaccurate to report.

4.5.4 Bending Moments

The bending moment profiles for each of the piles for each load test are provided in this section. For calculation of bending moments for each of the piles, the strain at each gage location was averaged during each load increment to account for relaxation during loading. Both concrete surface gages on pile 1 located 6 inches from the bottom of the cap were found to be faulty during the test. The lower gages at the lowest instrumented section of pile 1 were also faulty leaving two functioning instrumented sections for pile 1. The bending moment profile for pile 1 is not included in the sections below due to a lack of sufficient data points. The instrumented sections on piles 3 and 4 located five feet from the bottom of the cap are not included in the bending moment profiles due to the lack of concrete surface gages at these locations. For all bending moment profiles shown in this section, zero elevation occurs at the top of the pile which occurs at the centerline of the bent cap. The first data point occurs at elevation -1.5 ft. which is located 6” below the bottom of the

cap. The top of the rip-rap layer occurs at approximately -7.0 ft. and the ground elevation below the rip rap layer occurs at approximately -10.0 feet.

4.5.4.1 Lateral Only

The bending moment profiles for piles 2, 3 and 4 for the lateral load test with no additional gravity load can be seen in Figure 4-9 through Figure 4-11. The maximum bending moments occurred at the instrumented location six inches from the bottom of the cap indicating a fixed head condition of the pile to the bent cap which was to be expected. The maximum bending moments ranged from 92 kip-ft to 137 kip-ft. The inflection point for each of the piles seemed to occur near the ground surface or slightly below ground surface. This observation is more apparent in piles 3 and 4 where gages at both instrumented sections below ground were functioning correctly. In pile 2 the lowest below ground instrumented section was the only section used in determining the bending moment profile; therefore the approximate inflection point observed from the bending moment profile is lower than expected. Theoretically the inflection point should occur near ground level, however the addition of the rip rap creates a difficult condition to effectively predict where the inflection point will occur. The slope of the moment diagram for pile three seems to change at the 30 kip load increment with the values of bending moment increasing significantly from the instrumented section above. Upon further inspection of the bending moments at this section plotted against applied load, it is clear that no apparent increase in bending moment begins to occur until the 30 kip load increment. This trend was especially apparent in the loading conditions in which the load truck was on the bridge, which can be seen in Figure 4-8.

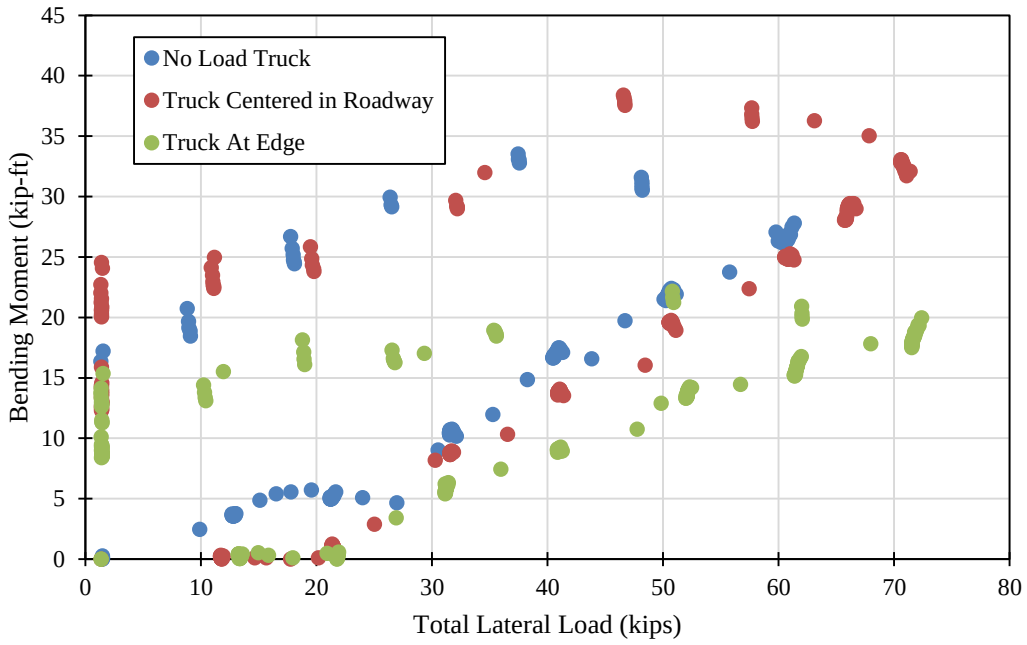

Figure 4-8 Pile 3 Bending Moment versus Total Lateral Load Comparison

The figure above carries out the bending moments through the unloading phases as well and clearly shows that the values of bending moment do not appear to return to zero. While this was the case with the majority of the instrumented sections, only this section on pile 3 did not return to within 10 kip-ft. The magnitude of the bending moment, however is very small at this section relative to the moments calculated at the section above ground. Only the lower instrumented section on Pile 3 (non-encased section) seemed to exhibit this behavior. In each of the other piles with the exception of Pile 1, the magnitude of the bending moment at the lowest instrumented section ranged from 2-10 kip-ft. during the duration of the tests.

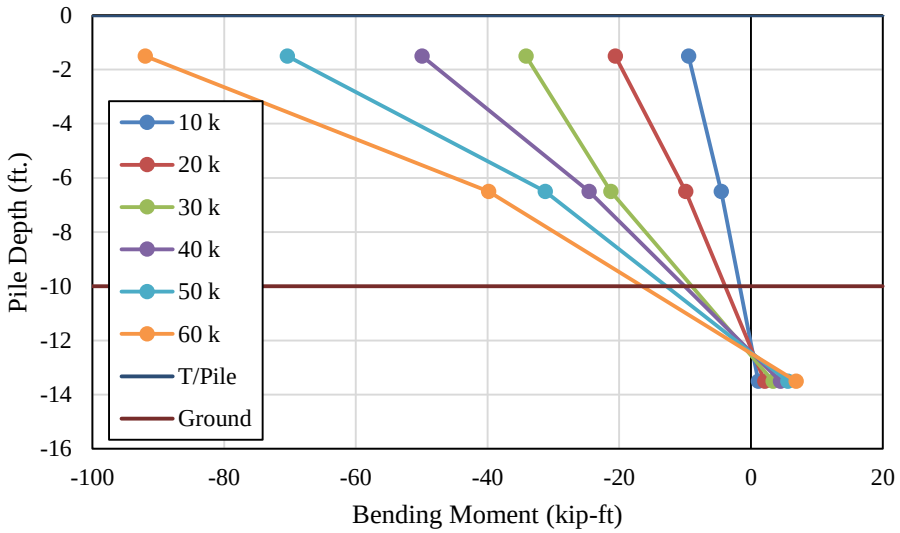

Figure 4-9 Pile 2 Bending Moment Profile

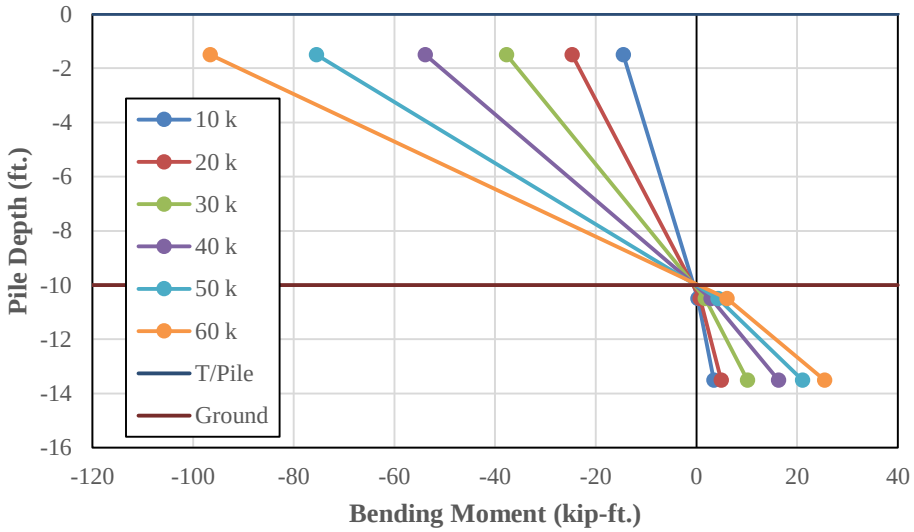

Figure 4-10 Pile 3 Bending Moment Profile

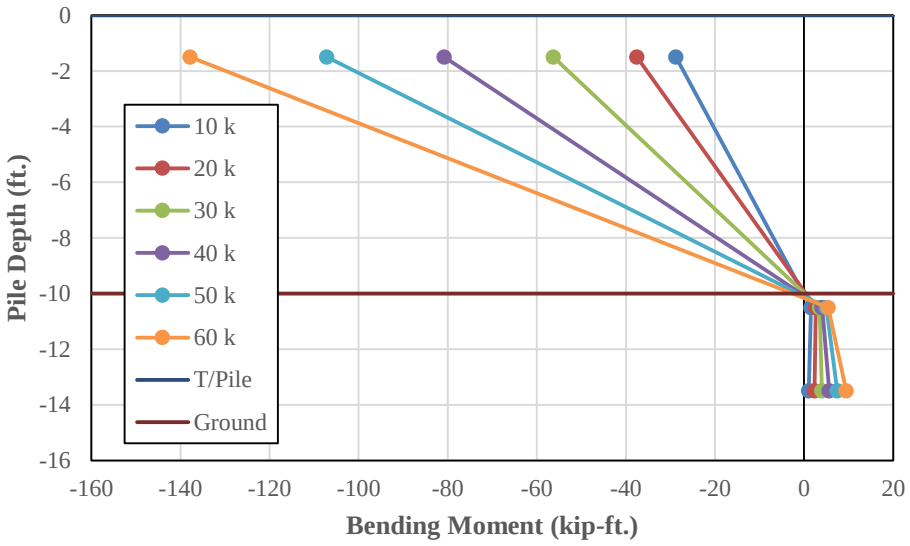

Figure 4-11 Pile 4 Bending Moment Profile

4.5.4.2 Combined Lateral and Gravity with Truck Centered on Roadway

The bending moment profiles for piles 2, 3 and 4 for the combined lateral and gravity load test in which the load truck was centered over the roadway can be seen in Figure 4-12 through Figure 4-17. The maximum bending moments, located at the instrumented section six inches below the bottom of the cap, ranged from 120 kip-ft. to 167 kip-ft. These bending moment values were relatively higher than the bending moments from the lateral load test in which no additional gravity load was applied.

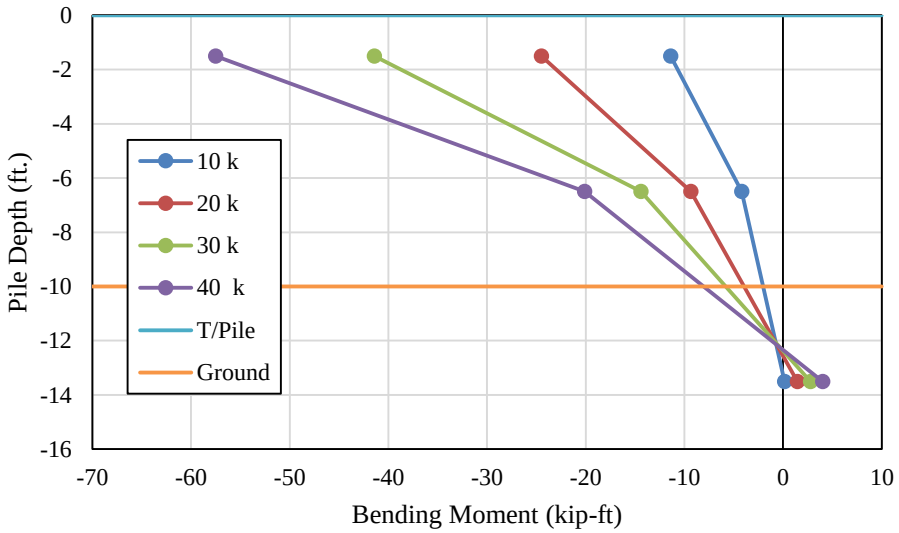

Figure 4-12 Pile 2 Bending Moment Profile

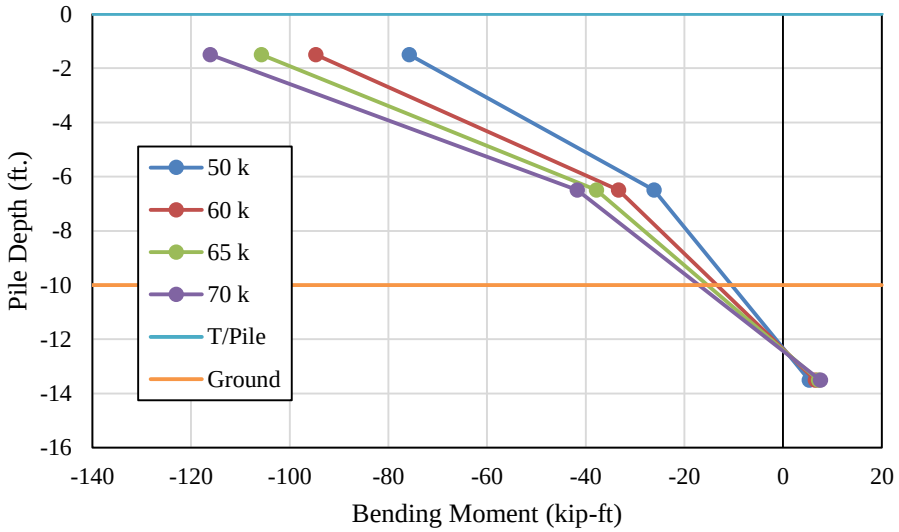

Figure 4-13 Pile 2 Bending Moment Profile

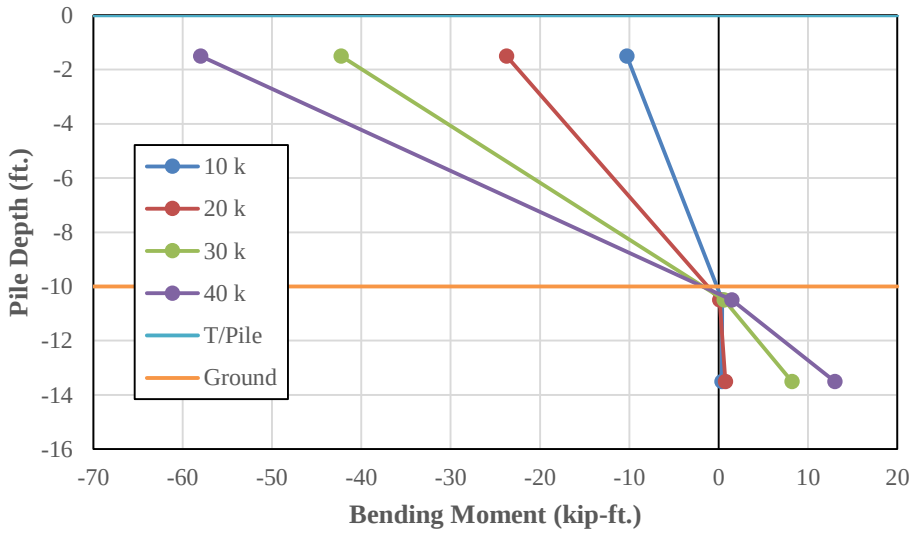

Figure 4-14 Pile 3 Bending Moment Profile

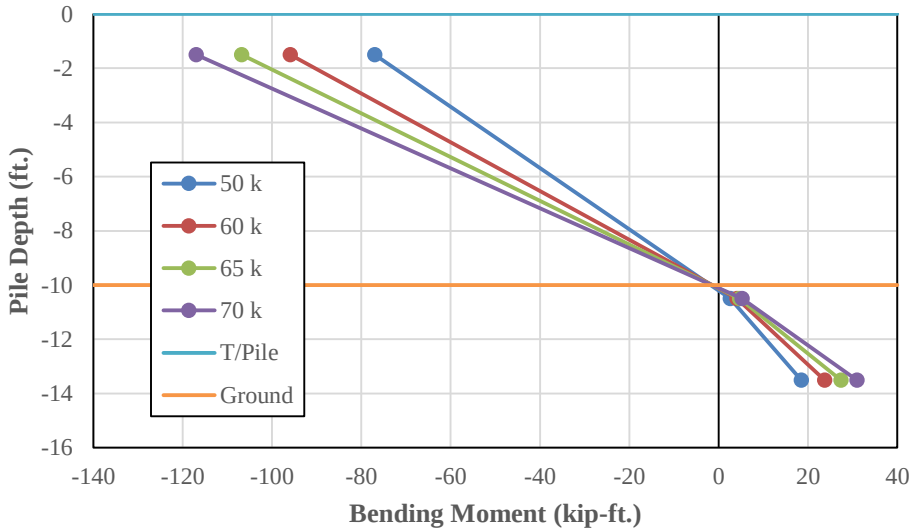

Figure 4-15 Pile 3 Bending Moment Profile

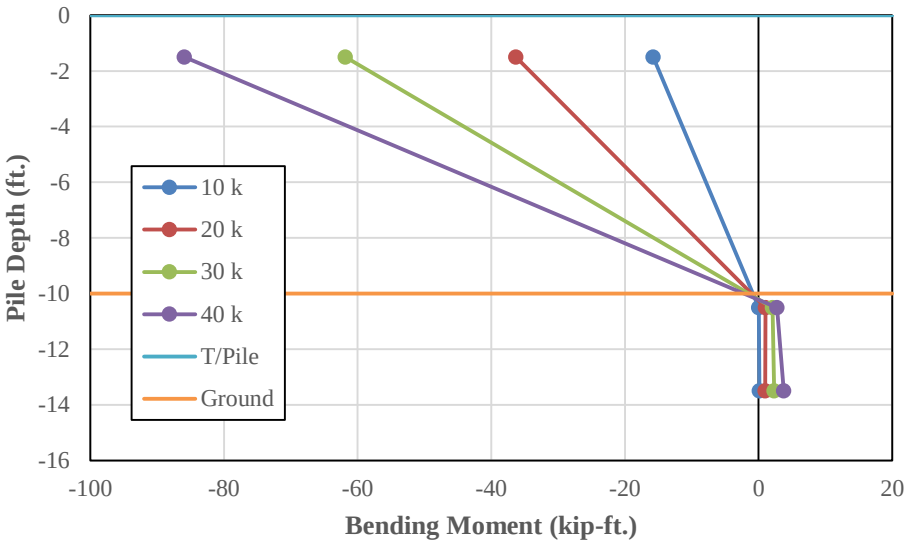

Figure 4-16 Pile 4 Bending Moment Profile

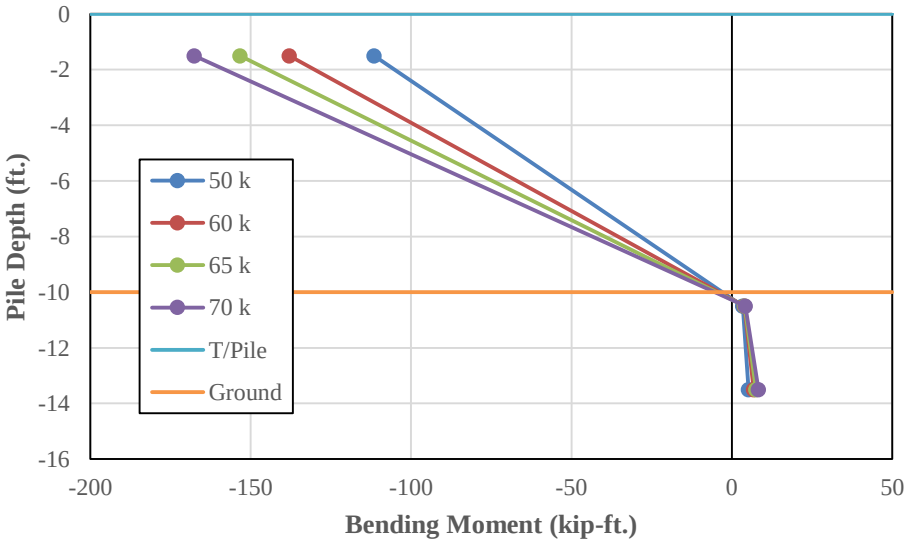

Figure 4-17 Pile 4 Bending Moment Profile

4.5.4.3 Combined Lateral and Gravity with Truck at Edge of Roadway

The bending moment profiles for piles 2, 3 and 4 for the combined lateral and gravity load test in which the load truck was positioned at the edge of the roadway can be seen in Figure 4-18 through Figure 4-23. The maximum bending moment values, located at the instrumented section six inches from the bottom of the cap ranged from 107 kip-ft. to 142 kip-ft. These bending moment

values fell in between the values from the lateral load test with no additional gravity load and the combined lateral and gravity load test in which the load truck was centered over the roadway. Notably, the maximum bending moments occurred in Pile 4 which is the leading pile in the load test meaning that his pile is expected to be in axial compression due to overturning.

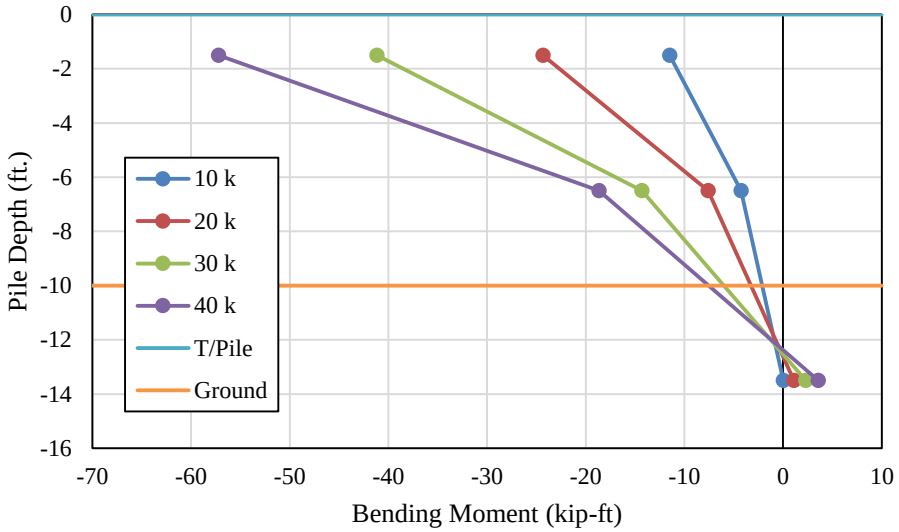

Figure 4-18 Pile 2 Bending Moment Profile

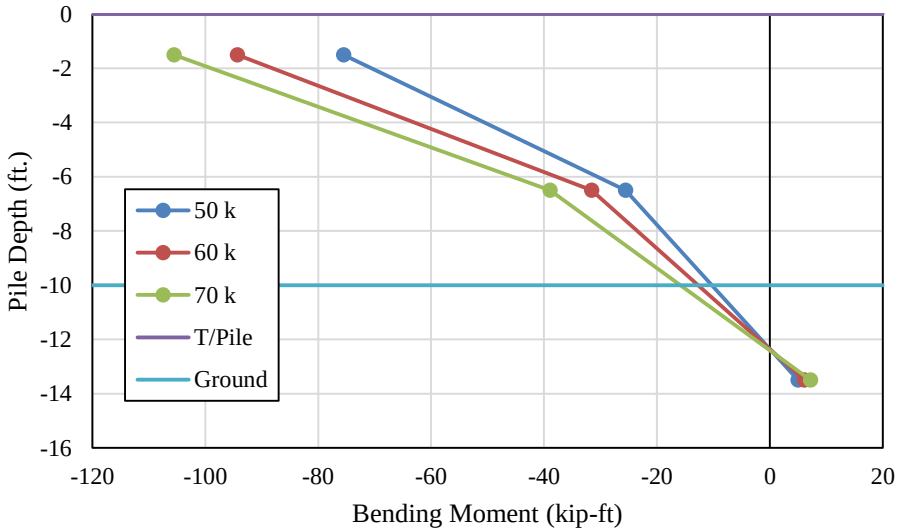

Figure 4-19 Pile 2 Bending Moment Profile

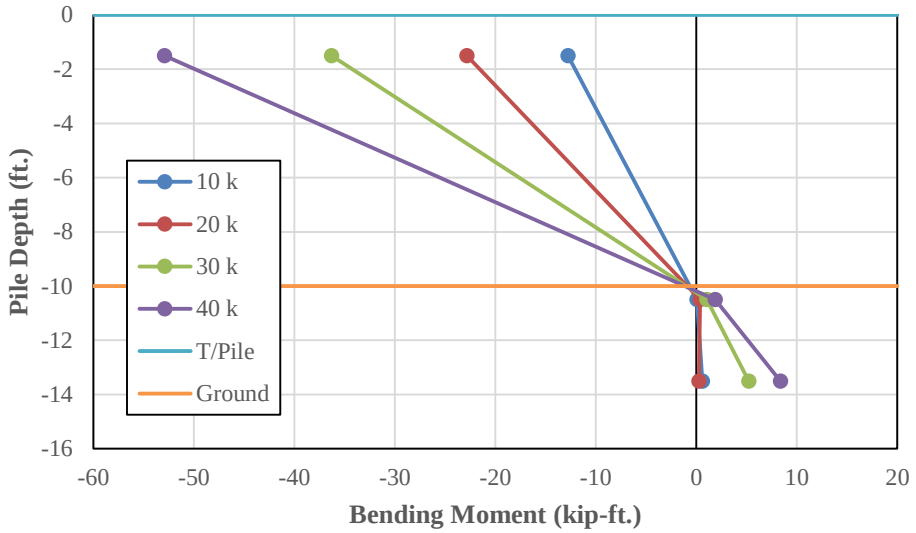

Figure 4-20 Pile 3 Bending Moment Profile

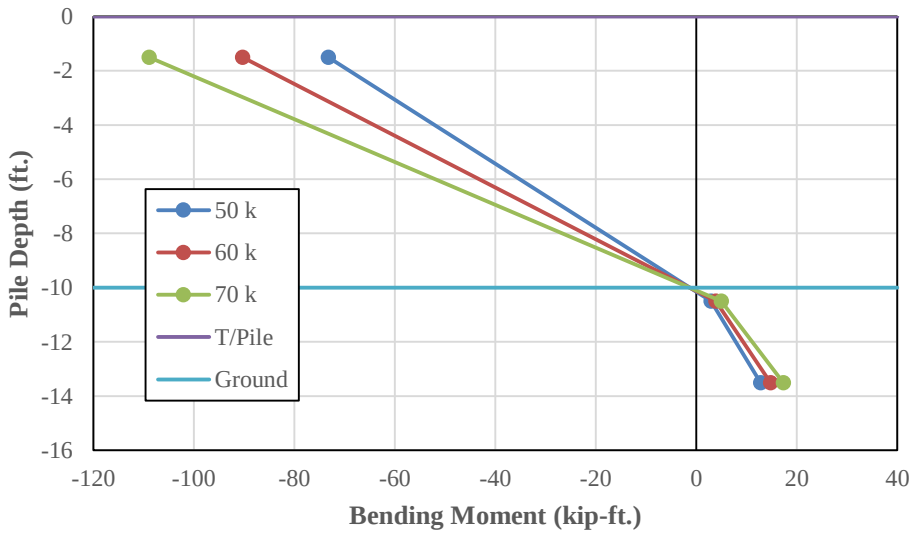

Figure 4-21 Pile 3 Bending Moment Profile

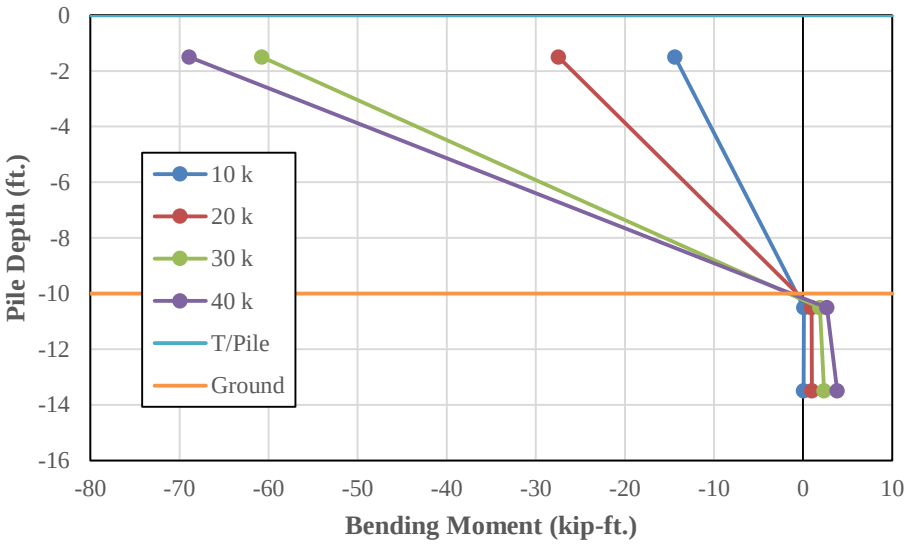

Figure 4-22 Pile 4 Bending Moment Profile

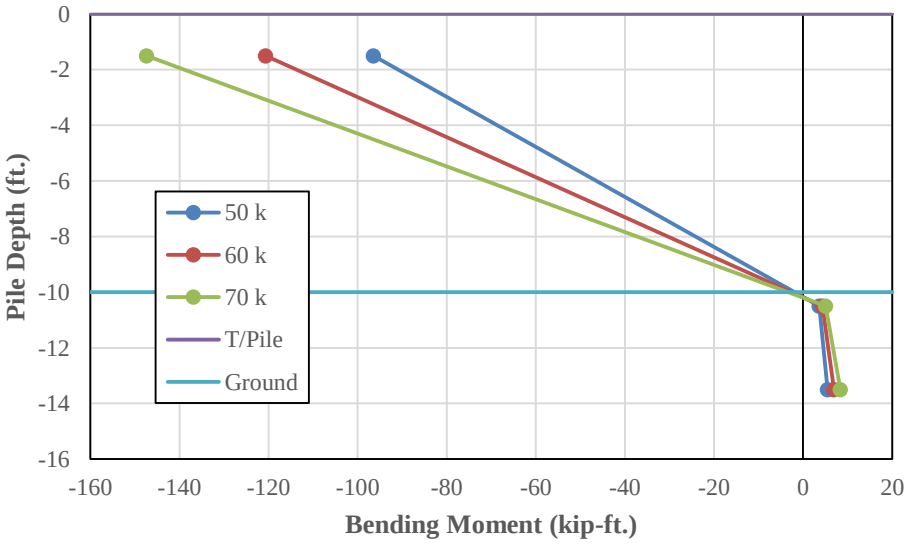

Figure 4-23 Pile 4 Bending Moment Profile

4.5.5 Displacement String Pots

Load versus displacement figures for each of the three load tests can be seen in Figure 4-24 through Figure 4-26. A comparison of the load versus average wirepot displacement for each of the three load tests can be seen in Figure 4-27. The bent appeared to be extremely stiff under each of the three loading conditions, deflecting around an average of 0.1” in each of the three tests. The

bent appeared to exhibit increased stiffness with the addition of gravity load. Notably, the bent was loaded to a total lateral load of 60 kips in the first load test as opposed to 70 kips in the second and third tests. Figure 4-27 contains the load-displacement data up to a total lateral load of 60 kips; the data from the 70 kips load increment is not included in this plot.

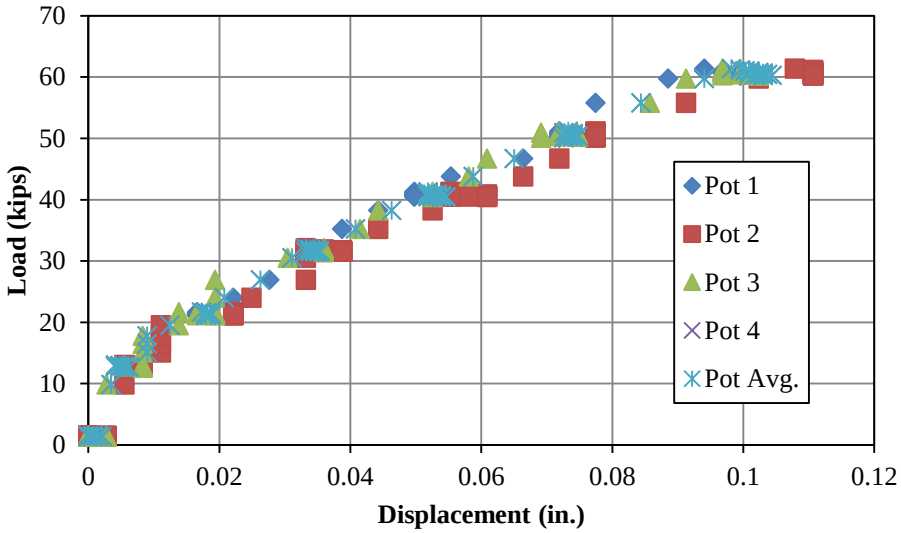

Figure 4-24 Load-Displacement with No Load Truck

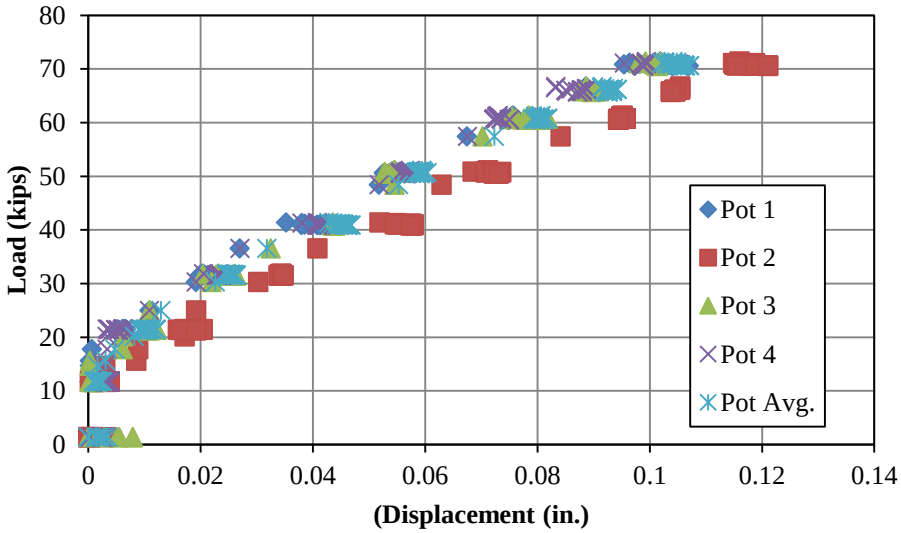

Figure 4-25 Load-Displacement with Truck Centered on Roadway

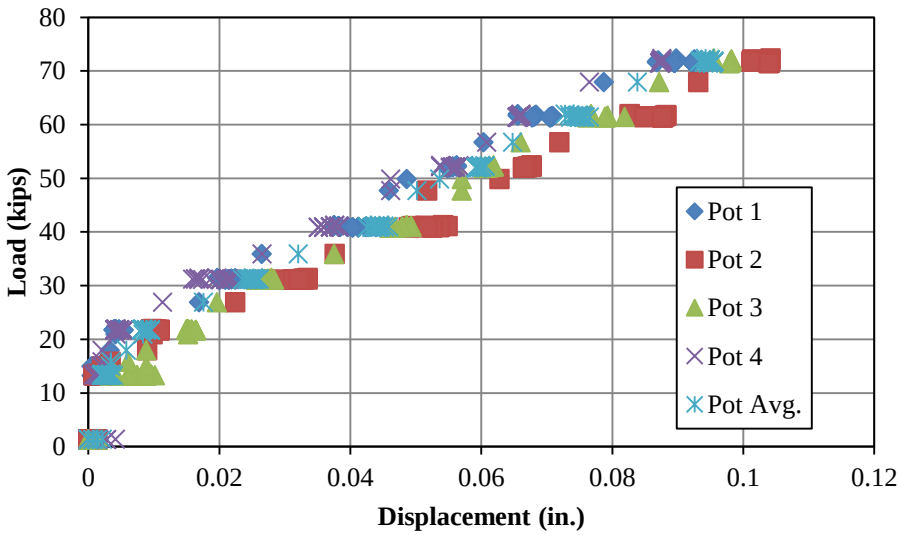

Figure 4-26 Load-Displacement with Truck at Edge of Roadway

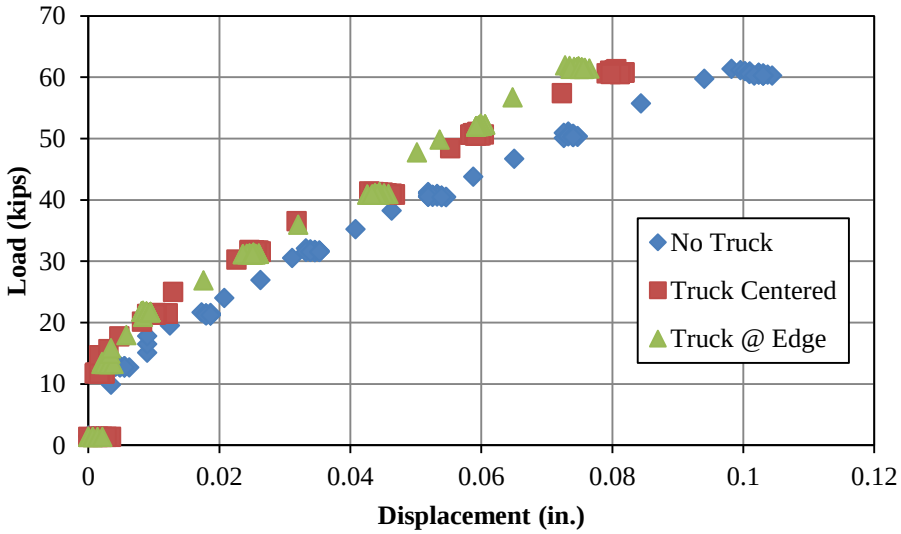

Figure 4-27 Load-Displacement Comparison of Three Tests

The bent behaved extremely stiff in each of the three load tests, however it is clear that the bent's stiffness increased slightly with the addition of gravity load. The total bent cap deflection with no truck was higher than the deflections in each of the combined lateral and gravity load tests; however these deflections were extremely small. There was likely lateral displacement caused by the truck loads in the opposite direction of the displacement caused by the lateral load. The

increased compressive force in the piles results in smaller lateral displacements. The cracks that were likely present in the encasements are not as effected when the compressive force in the piles is larger. The moment of inertia of the encased pile section is closer to the uncracked moment of inertia which results in a larger flexural stiffness.

4.5.6 Bridge Bent Behavior

The bridge bent appeared to behave extremely stiff under each of the three loading conditions described in this chapter. The bent deflected around 0.1" in each of the tests, and behaved slightly stiffer in each of the tests in which gravity load was also applied. The displacements during the lateral load test without gravity load were smaller than the displacements during the tests with the load truck. Due to the small changes in displacements it is determined that the addition of gravity load has very little effect on the lateral stiffness of the bridge bent. The total bent deflection was roughly half of the total deflection measured in the load test conducted before the bridge deck was placed, indicating that the addition of the bridge deck provides a significant amount of addition stiffness.

The bending moment profiles for each of the piles indicate a fixed head condition between the top of the pile and the bent cap which is to be expected. The maximum bending moments were relatively high in magnitude, ranging from 92 kip-ft. to 160 kip-ft. These large bending moments can be attributed to the large stiffness of the pile sections with concrete encasements. The inflection point of each of the piles appeared to occur at or below ground surface which is to be expected.

4.6 Chapter Summary

The bridge bent performed very well under each of the three loading conditions, behaving extremely stiff in each case. It can be determined that the addition of gravity load has little effect on the lateral stiffness of the bridge bent. The addition of the bridge deck clearly increased the

stiffness of the bent when comparing the displacements in each of the three tests conducted to the displacements from the test conducted before the bridge deck had been placed. The addition of gravity load, did however have an effect on the magnitude of the bending moments at the instrumented locations six inches from the bottom of the cap. The maximum bending moments were higher in each of the loading conditions with additional gravity load compared to the lateral load test without additional gravity load which is to be expected due to the increased flexural stiffness of the piles due to the larger compressive force.

Chapter 5 Field Test 3 – US 331 Bridge

5.1 Introduction

An existing multi-span bridge with driven steel pile bents was used for the third load test of the project. The bridge, located on US 331 in South Montgomery, Alabama, consisted of pile bents with 6 driven HP10x42 piles with 16 in. square concrete encasements. The two exterior piles in the bents were battered at a 1.5:12 slope. The bents consisted of a reinforced concrete bent cap, with a trapezoidal cross section of the same geometry as the cap used in the Macon County load test.

For this load test, both the north and south bound bridges were utilized. A bent on the southbound bridge was used as the test bent while the northbound bridge was used to react against. A loading mechanism similar to the Macon County test was used for the US 331 test, using threaded rods as tension members and hydraulic cylinders to essentially pull the two bridges together.

This chapter details how the driven pile bent bridge was tested as well as the analysis and results from that test. It contains sections on instrumentation, testing configurations, and the procedure used for testing. It also contains the results and analysis from the test as well as a discussion of the results.

5.2 Instrumentation

This section details how the test bent and reaction bent were instrumented. It contains the instrumentation layout for the two bents, the types of instrumentation used, and how each of the types of instrumentation was installed.

5.2.1 Instrumentation Layout

In order to determine axial forces and bending moments during the different load tests, electrical resistance strain gages were installed on piles in the test bent and the reaction bent. To

effectively capture the approximate bending moment profile in each of the piles, three sections were instrumented on the test bent. At each of these sections, a pair of strain gages was installed: one gage on each face of the piles. Strain gages were installed on the concrete encasements due to the inability to access the steel piles.

The piles were numbered with the far right pile being Pile 1 and the far left pile being Pile 6. This numbering scheme is looking South down the bridge. The instrumentation layout for the test bent can be seen in Figure 5-1. The reaction bent was also instrumented so that its behavior during the load tests could be monitored as well. This bent was not instrumented as heavily as the test bent. Three piles in the bent were instrumented with only two sections being instrumented. An image of the reaction bent instrumentation layout with the numbering scheme included can be seen in Figure 5-2. Note that this figure is also shown facing south which would be against traffic for this bridge.

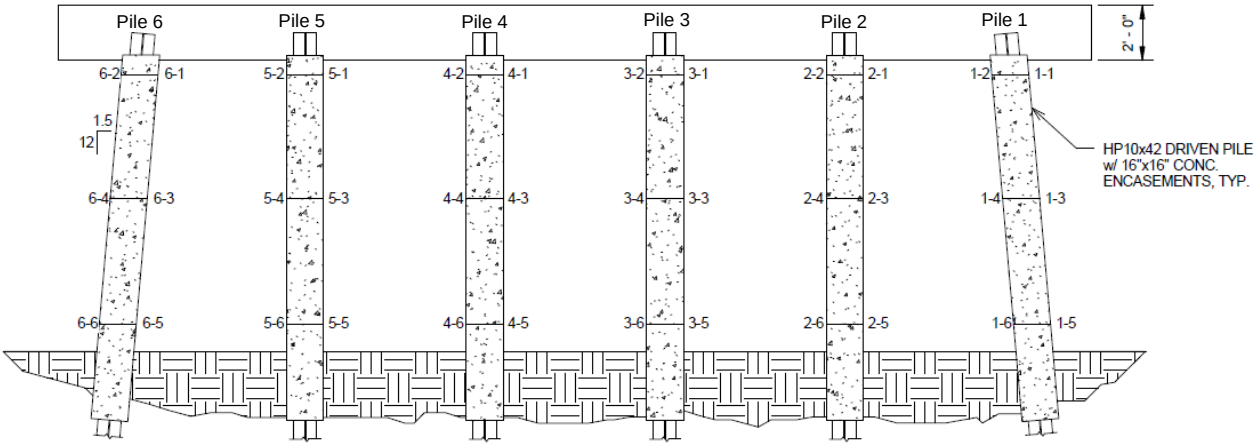

Figure 5-1 Test Bent Instrumentation Layout

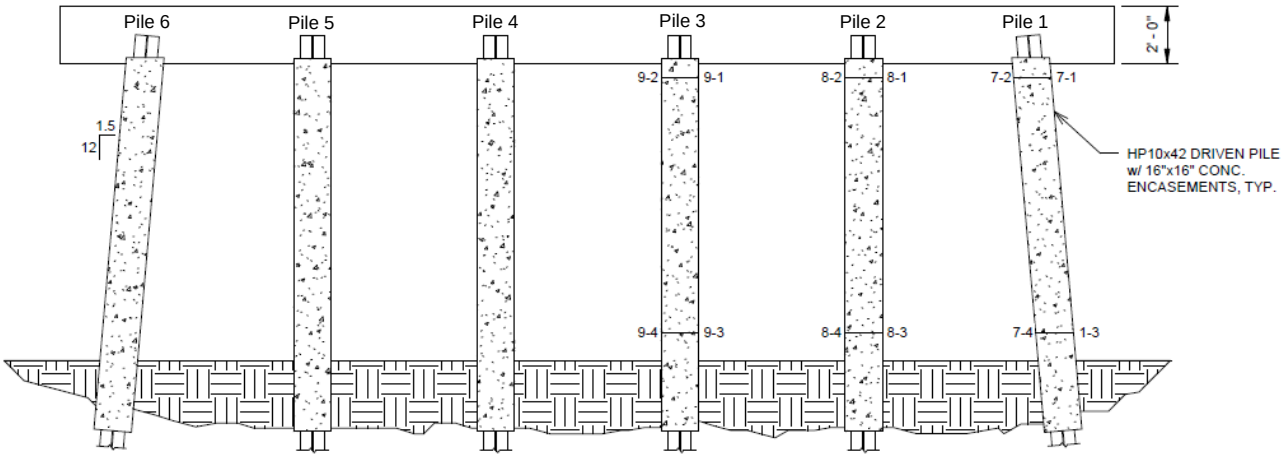

Figure 5-2 Reaction Bent Instrumentation Layout

Displacement wirepots were used in order to measure lateral deflection during the load tests. Two wirepots were installed on the outside face of the test bent and were installed on the same end as the hydraulic cylinders. One wirepot was installed on the top right corner of the bent cap face and the other was installed on the bottom left corner of the cap face. These locations were chosen to be able to obtain an average displacement of the bent cap and to determine whether or not the cap was twisting at all during the test. The wirepot layout on the bent cap can be seen in Figure 5-3.

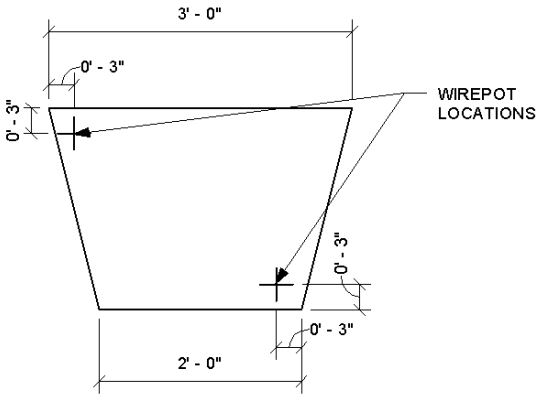

Figure 5-3 Wirepot Layout on Bent Cap Face

5.2.2 Installation of Electrical Resistance Gages to Concrete Surfaces

One day prior to load testing, concrete surface strain gages were installed at each of the locations shown in Figure 5-1 and Figure 5-2. PL-60-11-3LT strain gages from Texas Measurements were used for strain measurements at each of the instrumented sections. The selected gages were 60 mm in length, providing adequate length for averaging over the concrete surface. The gages came with pre-attached cables which allowed for an easier soldered connection to be made to cables which were connected to the data acquisition system. An image of a PL-60-11-3LT gage can be seen in Figure 5-4.

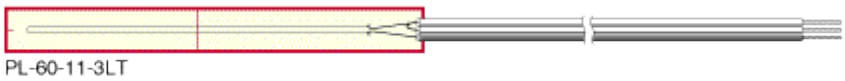

Figure 5-4 PL-60-11-3LT Concrete Strain Gage (Texas Measurements)

The instrumentation surfaces were prepared and the gages were installed using procedures described in Micro-Measurements Application Note TT-611. In order for the gages to function properly, the installation surface had to first be adequately treated. A bristled brush was used to remove any loose soil or excess paste on the surface of the concrete encasements. A CSM-2 degreaser was then used to remove surface irregularities. Once degreasing had taken place, all loose dust was blown from the surface. The surface was then conditioned using a generous amount of M-Prep Conditioner A, an acidic solution. The conditioner was placed on the surface and scrubbed with a bristled brush. The area was then washed thoroughly with clean water. The acidity of the surface was then reduced by applying a generous amount of M-Prep Neutralizer 5A, a basic solution. Once the neutralizer was applied and spread appropriately, the surfaced was rinsed with water and dried thoroughly. Following degreasing and conditioning, all voids on the surface were filled with a solids adhesive. M-Bond AE-10 was used as the adhesive for the treatment surface. Once the adhesive was properly mixed, it was applied over the gaging surface, filling all voids and

leveled to provide a smooth surface. Once the adhesive had cured, a 320-grit sand paper was used to smooth the surface until the base material was exposed. Once a proper gaging surface had been created, layout lines were drawn on the surface so that the gages could be placed in the proper location and at the correct orientation. M-Bond AE-10 was also used to bond the gages onto the installation surface. The gage was first picked up using a pair of tweezers and placed onto a piece of PCT-2M gage installation tape, ensuring that the gage was centered on the tape. The gage and tape assembly was then aligned over the installation surface, and the gage end of the tape was then lifted at a shallow angle until the entire gage is lifted off the treated surface. M-Bond AE-10 was then applied over the gage surface. The gage was then lowered over the installation surface and pressed down for approximately 30 seconds. An installed concrete surface strain gage can be seen in Figure 5-5.

Figure 5-5 Installed Concrete Surface Strain Gage

Following gage placement, a piece of mastic tape was placed over the gage area to provide an initial layer of strain relief and weather protection. Further waterproofing was deemed unnecessary

due to the load test being performed the following day and the bridge deck providing additional means of weather protection as well. After the layer of mastic was applied to the gages, a piece of duct tape was wrapped around the pile, below the instrumented sections so that both of the gages' pre-attached cables were held in placed. This tape layer provided one more layer of strain relief for the gages. A hook was installed at the highest sections for additional strain relief as well. The pre-attached strain gage cables were fed through the hook and secured with a layer of duct tape as previously mentioned. A completely installed strain gage with all strain relief measures in tact can be seen in Figure 5-6.

Figure 5-6 Installed Concrete Surface Gage with Strain Relief

5.2.3 Displacement Wirepots

Displacement wirepots were used to measure the lateral deflection of the test bent during the load tests. Two WDS P-60 wirepots with a 1 meter range from Micro-Epsilon were used in this test. The wirepots were installed to the bent by predrilling holes into the outside face of the bent cap using a concrete drill bit. Once the holes were drilled, a small metal hook was placed inside and the hole was filled with a five-minute epoxy to ensure that hook was properly anchored to the

face of the cap. Prior to the test, the wirepots were mounted onto a sheet of plywood attached to a wooden reference frame. The wirepots were attached using two 2 ½" wood screws. The clip on the end of the string of the wirepot was attached to the hook on the bent cap face. Two wirepots were installed for used during the load tests: one at the top right corner of the bent cap face and another on the bottom left corner. The installed wirepots can be seen in Figure 5-7.

Figure 5-7 Field-Installed Wirepots

5.3 Testing Equipment and Setup

This section includes details on the testing configuration used for this load test. It also details the reaction bent configuration, the hydraulic jacks and threaded rods used to apply the lateral load, the reference beam used to mount the wirepots, and the data acquisition system used.

5.3.1 Reaction Against Adjacent Bent

The bent adjacent to the test bent on the northbound bridge was used as a reaction bent for the load tests. Similar to the Macon County tests, high strength steel threaded rods were used as tension members. In these tests, the rods were anchored at the end of the test bent where the hydraulic

jacks were located and at end of the reaction bent. The rods spanned on each side of the bent cap and were held in place by 135 degree hooks made of steel reinforcing bars. The rods were anchored at the far end of the reaction bent by a piece of HSS6x6x1/2 with pre-punched holes. The rods continued through the HSS section and were anchored at each end using a nut and washer combinations.

Center-hole hydraulic cylinders were used on the far end of the test bent to apply the lateral load through the tension members. A "pulling" mechanism was used to apply the lateral load, similar to the Macon County tests.

5.3.2 Hydraulic Jacks

Center-hole hydraulic jacks were used to apply the lateral load in the load tests. The threaded rods were fed through these hydraulic jacks and were anchored on the end using a double nut and washer combination. Two Enerpac #RRH-3010 long stroke hydraulic cylinders were used for the test. Each cylinder had a capacity of 30 tons or 60 kips. The cylinders were connected to an Enerpac ZU4 Class ZU4408JB pump fitted with valves to provide equal pressure on both of the cylinders. An image of the two hydraulic cylinders and the pump shown from the bridge deck above can be seen in Figure 5-8.

Figure 5-8 Hydraulic Cylinders and Pump Seen From Bridge Deck

5.3.3 Truck Live Load

For the combined lateral and gravity load test, an ALDOT load truck was used for gravity load application. The load truck in configuration LC-5 was used for this test. The truck had a total weight of 87,500 pounds. During the test, the truck was positioned so that its center of gravity was directly over the test bent. The truck was placed in the left lane of the bridge so that the truck would be induce axial load in the piles that would be expected to be in axial compression due to the effect of lateral load. An image of the ALDOT load truck configured in LC-5 can be seen in Figure 5-9.

Figure 5-9 ALDOT Load Truck in Configuration LC-5

5.3.4 Threaded Rods/Anchorage

High strength steel threaded rods were used as tension members to apply the lateral load in these load tests. The threaded rods used were 1 1/8” in diameter and had a yield strength of 100 ksi. For the majority of the length that the rods spanned, 12 foot long sections were used and were coupled using steel hex coupling nuts. Shorter sections of threaded rod were used toward the hydraulic jack end and the anchored end of the reaction bent to avoid having to thread the nuts over a long portion of the rods a the anchored locations. Two instrumented sections of threaded rod, three feet in length, were coupled near the hydraulic cylinder end of the bridge bent. These instrumented rods were used to monitor the lateral load during each of the tests. They were placed near the hydraulic cylinders so that the cables from the instrumentation could be connected into the data acquisition system.

On the hydraulic cylinder end of the test bent, the rods were anchored by a section of HSS6x6x1/2 with pre-punched holes. The rods continued through the tube section and were fed

through the center-hole hydraulic cylinders. The two cylinders would bear directly on the tube sections and a ½" thick elastomeric bearing pad was placed between the tube and the bent cap in order to ensure an even load distribution over to bent cap face. The rods were anchored using a double nut and washer combination. Theses nuts were tightened so that they were flush with the piston of the cylinders. An image of the end anchorage at the hydraulic cylinder end of the test bent can be seen in Figure 5-10.

Figure 5-10 Threaded Rods Anchored on Jack End

The threaded rods spanned the entire length of the test bent and the reaction bent plus an additional 25 feet in between the bents. On the far end of the reaction bent, the threaded rods were anchored in a similar fashion as the hydraulic jack end. A piece of HSS6x6x1/2 with pre-punched holes spanned between the two rods with the rods continuing through the tube. A piece of ½" thick elastomeric bearing material was placed in between the tube and the face of the bent cap to ensure an even load distribution over the bearing area. The two rods were anchored using a nut and washer combination and were hand tightened until the nut was flush with the face of the tube section. An image of the end anchorage at the far end of the reaction bent can be seen in Figure 5-11.

Figure 5-11 End Anchorage at Reaction Bent

The threaded rods had to be suspended from the bent cap before they were tensioned in placed; therefore intermediate supports for the rods located at discrete locations along the length of the two caps were necessary. This was not an issue in the Macon County tests since the majority of the length of the rods were inside of the bent cap. The rods could not travel through the cap for this test; therefore, a method for supporting the rods in between the end anchorage locations had to be determined. The most efficient and cost effective method for supporting these rods prior to the test was to use steel reinforcing bars bent at a 135 degree angle to catch the rods at points along the length of the bent cap. A piece of number four steel reinforcing bar was bent with one bend being 90 degrees and the other being a 135 degree bend. The 90 degree bend was then placed between the girder pedestal and bottom of the girder, and wooden shims were used to wedge the hook into place. The rods were lifted over the hook and set on the steel hooks, and were then coupled at these locations to avoid having to lift long lengths of threaded rod at once. An image of a steel reinforcing bar used as an intermediate support can be seen in Figure 5-12.

Figure 5-12 Intermediate Bracing for Threaded Rods

5.3.5 Reference Frame for Wirepots

The displacement wirepots used to measure bent lateral deflection were anchored to a wooden reference frame. The frame consisted of two A-frames with a vertical member, diagonal kicker and horizontal member at the base. A diagonal brace was used in between the two A-frames in order to prevent movement of the frame in the transverse direction. A stiff frame was necessary for this test so that accurate lateral deflections were obtained from the wirepots. Two 2x4's spanning between the two A-frames were used so that a sheet of plywood could be connected to the frame. The wirepots would then anchor into this sheet of plywood. To provide additional stiffness, tie-backs were connected to the frame and staked into the ground. An image of the reference frame used to anchor the wirepots can be seen in Figure 5-13.

Figure 5-13 Wooden Reference Frame for Wirepots

5.4 Testing Procedure

This section contains the procedures followed for each of the load tests performed on the US 331 Bridge. Two tests were performed: the first was a combined lateral and gravity load test and the second was a purely lateral load test. This section also contains the means for monitoring the load during each of the tests.

5.4.1 Load Monitoring During Test

Steel threaded rods were used as tension members to apply lateral load to the system during each of the load tests. Having a means for monitoring the load at all times during the test was extremely important. A laptop which was connected to the data acquisition system was set up near the test bent. The output for the load in each of the hydraulic jacks, the total load in the hydraulic jacks, and the average wirepot displacement were displayed on the laptop for the entire duration of the test. These outputs were displayed to know when the target load increment had been reached.

Deflections were of interest during the test to ensure that the bridge remained linear elastic throughout the test and large lateral displacements did not occur.

5.4.2 Combined Gravity and Lateral Load Test

The first test performed was a combined gravity and lateral load test. An ALDOT load truck in load configuration LC-5 was used for gravity load application for this test. Since the test bridge was in service during the time of the test, traffic control was an important aspect of the test. When the load truck approached the bridge, traffic was stopped until the load truck was in its desired location so that initial data could be recorded with only the load truck on the bridge. The load truck was positioned so that its center of gravity was directly over the test bent. The truck was positioned in this location to ensure that most of the load was being transferred to the test bent and not the adjacent bents. The truck's position over the bent can be seen in Figure 5-14.

Figure 5-14 Load Truck Positioned Over Test Bent

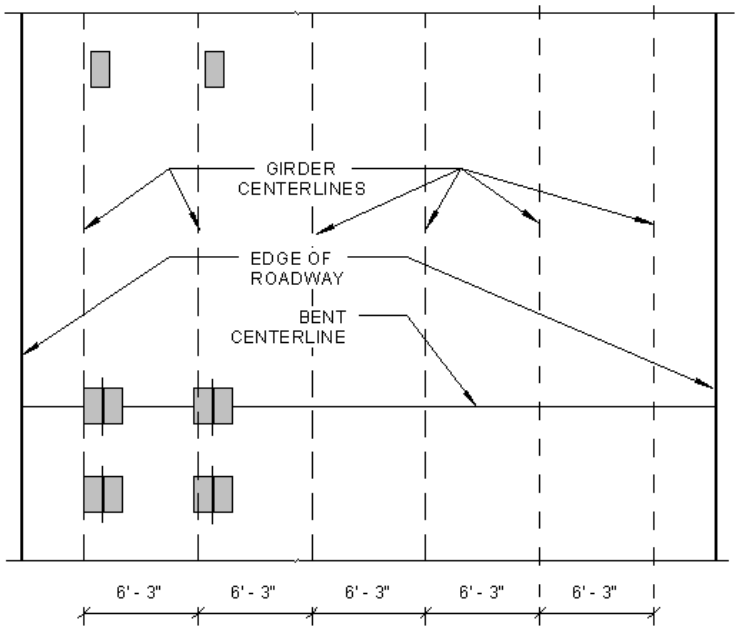

Figure 5-15 Load Truck Positioning Over Exterior Girder

In the transverse direction, the load truck was positioned so that its left wheel axle was over the left exterior girder of the test bent. This positioning was chosen so that the load truck would induce additional compression into the piles that would theoretically be in axial compression due to overturning of the bent under lateral loading.

Once the truck was positioned, traffic was stopped for three minutes and a data reading was taken with the truck in its intended position to simulate a gravity load only condition. Once this reading was taken, the bent was loaded laterally in 10 kip increments to a total load of 90 kips. Due to the rods between the test bent and reaction bent sagging initially, the end anchorage on the jack end and the reaction end had to be hand tightened prior to jack load being applied. This hand tightening procedure was performed instead of applying jack load to ensure that the stroke of the cylinders was not used prematurely to remove the sag out of the rods. An initial load of 12 kips was induced into the threaded rods due to hand tightening of the end anchorages. Therefore the

net load at the last increment was 80 kips. However, the loads reported are all total loads seeing that the bent was still subject to this initial 12 kip load.

The bent was loaded laterally by setting the hydraulic pump into "extend" mode and increasing the hydraulic pressure using a hand-held remote. Once the target load increment had been met, traffic was stopped for three minutes so that data could be recorded without additional noise due to traffic. Traffic was not stopped while the load was being increased however. Once the 90 kips load increment had been met, the bridge was unloaded in a series of three unloading increments. The bridge was unloaded by setting the hydraulic pump into "retract" mode and releasing hydraulic pressure from the system. The load in the jacks at each of these increments was properly recorded since there were no target loads for the unloading increments. The final unloading increment was when the load in the jacks was at the initial load of 12 kips.

5.4.3 Static Lateral Load Test

The second load test performed was a static lateral load test with no live load application. Before the load test began, traffic was stopped for three minutes so that data could be collected with no noise due to traffic. Following this initial reading, the bent was loaded in 10 kip increments up to a total lateral load of 90 kips, holding the load and stopping traffic for three minutes at each load increment. The bent was loaded using the same procedure described in section 5.4.2. Once data was recorded at the 90 kip load increment, the bridge was unloaded in a series of unloading increments. The hydraulic pump was set to "retract" mode and pressure was released incrementally until the load in the rods reached its initial value. The load in each jack and the total load was recorded at each unloading increment.

5.5 Analysis, Results and Discussion of Load Test

This section contains measured data as well as results from each of the load tests performed on the US 331 bridge. The methods and assumptions made for calculating axial forces and bending moments is also outlined in this section.

5.5.1 Strains

Strain gages were not instrumented on the steel pile sections for this series of load tests, therefore the level of composite behavior between the steel and concrete encasements was unable to be determined. Upon initial observations of strain profiles across the concrete encasement cross section, it was apparent that the tensile and compressive strains were very similar, indicating a bending condition due to lateral load effects. This was the case especially in piles 2 through 5. The tensile strains in pile 1 and the compressive strains in pile 6 were higher in absolute value than the opposite, indicating net axial compression or tension. Due to the batter of these exterior piles, this net axial load due to lateral load effects was to be expected.

5.5.2 Calculation of Axial Forces and Bending Moments

Axial forces and bending moments during the load tests were computed from the measured concrete strains on each of the six piles. A few basic assumptions needed to be made to take into account the stiffness of the steel piles since there was not instrumentation installed on the piles. From data analysis from the Macon County test, it was found that the concrete and steel strains at low load levels were quite similar meaning that small amounts of slipping occurred. The levels of strain at the highest instrumented locations on each of the piles were relatively small during each of the load tests performed. Therefore it was determined that linear interpolation of strain at the location of the flange tips could be used to determine the stresses, forces and bending moments in the steel piles. Although the exact locations of the steel piles within the concrete encasements were unknown, it was assumed that the piles were centered within the encasements. Figure 5-16 shows the assumed location of the steel piles flanges used for linearly interpolating strains for axial force

and bending moment calculation. The steel strains used were at the flange tips, three inches from the face of the concrete encasements.

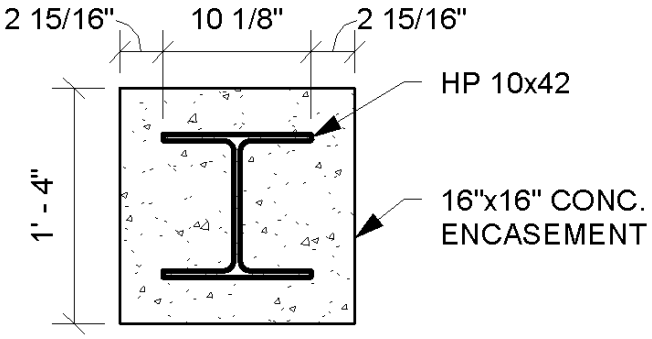

Figure 5-16 Composite Pile Cross Section

The axial force in the piles during the load tests were calculated by taking the average of the tensile and compressive interpolated steel strains and multiplying that value by the modulus of elasticity of the steel piles then multiplying that by the gross cross-sectional area of the HP10x42 pile. This axial load in the steel pile was then added to the axial load contribution of the concrete encasement. The total pile axial load was calculated using equation 5-1. Notably, the area used in computing the concrete contribution to the axial load is the gross cross-sectional area of the composite pile minus the cross-sectional area of the steel pile.

$$P = \left(\frac{\varepsilon_{c,s}+\varepsilon_{t,s}}{2}\right) E_s A_s + \left(\frac{\varepsilon_{c,con}+\varepsilon_{t,con}}{2}\right) E_c\left(A_g - A_s\right) \qquad \text{(Equation 5-1)}$$

Where:

P = total pile axial load (kips)

$\varepsilon_{c,s}$ = interpolated steel compressive strain (in./in.)

$\varepsilon_{t,s}$ = interpolated steel tensile strain (in./in.)

E_s = modulus of elasticity of steel (ksi)

A_s = steel pile cross-sectional area (in^2)

$\varepsilon_{c,con.}$ = measured concrete compressive strain (in./in.)

$\varepsilon_{t,con.}$ = measured concrete tensile strain (in./in.)

E_c = modulus of elasticity of concrete (ksi)

A_g = gross cross-sectional of composite pile ($in.^2$)

The bending moments at each cross section during each of the load tests was calculated by taking the curvature at the cross section and multiplying it by the stiffness at the section. A linear strain distribution over the cross section was assumed, so that the stiffness of the steel pile could be included in the moment calculation as well. The curvature for the cross section was calculated using equation 5-2.

$$\varphi = \frac{\varepsilon_{c,con.} - \varepsilon_{t,con.}}{h} \qquad \text{(Equation 5-2)}$$

Where:

φ = curvature at cross-section ($in.^{-1}$)

h = distance between two measured strains (in.)

The bending moment at each cross section takes into consideration the stiffness of the concrete encasement as well as the steel pile. One uncertainty in these calculations is the compressive strength of the concrete. No information regarding the specifications for structural or non-structural concrete used for this bridge during its construction was readily available, therefore an assumption had to be made regarding the strength of the concrete. A compressive strength of 5000 psi was used to determine the modulus of elasticity to use in the bending moment calculation. Calculations performed using the data from each of these tests also assumed the concrete was uncracked. The modulus of elasticity was approximated using equation 5-3, which was simplified from the equation for the approximate concrete modulus of elasticity from ACI 318-11 (ACI 2011). A modulus of elasticity of 4031 ksi was used for computation of bending moments and axial forces for each of the tests.

$$E_c = 57{,}000\sqrt{f'_c} \qquad \text{(Equation 5-3)}$$

Where:

E_c = approximate concrete modulus of elasticity (psi)

fc= specified 28 day concrete compressive strength (psi)

Equation 5-4 was then used to compute the bending moment at each instrumented cross section during each of the load tests. Note that since the steel strains were linearly interpolated from the measure concrete strains, the curvature over the cross section is constant.

$$M_b = \varphi\left(E_c\left(I_g - I_s\right) + E_s I_s\right) \qquad \text{(Equation 5-4)}$$

Where:

M_b = bending moment at specified cross-section

I_g = gross moment inertia of the composite section (in^4)

I_s = moment inertia of the steel pile (in^4)

5.5.3 Test Bent Axial Forces – Combined Gravity and Lateral

Axial forces in each of the piles in the test bent during the combined gravity and lateral load test were calculated from measured strains. The stiffness of the steel piles was taken into consideration in the calculation of these axial forces; however, due to the large stiffness of the concrete cross section relative to the steel pile, the contribution of the steel pile is small. The axial forces in each of the piles plotted against the total lateral load applied can be seen in Figure 5-17 through Figure 5-22.

Due to axial load effects, the bent will want to overturn meaning that the exterior pile on the jack end will be in axial tension and the exterior pile on the opposite end of the bent will be in axial compression. The exterior piles will tend to carry the largest amount of axial load due to overturning because of the batter in the piles. The interior vertical piles will tend to resist the load

through flexure and carry little axial load due to overturning. The data from this test indicates this prediction, with the exterior pile on the jack end having a significant amount of axial tension and the exterior pile on the opposite end having a significant amount of axial compression due to overturning. Note that in each of the axial load figures, negative values are assumed to be tension and positive values are assumed to be compression.

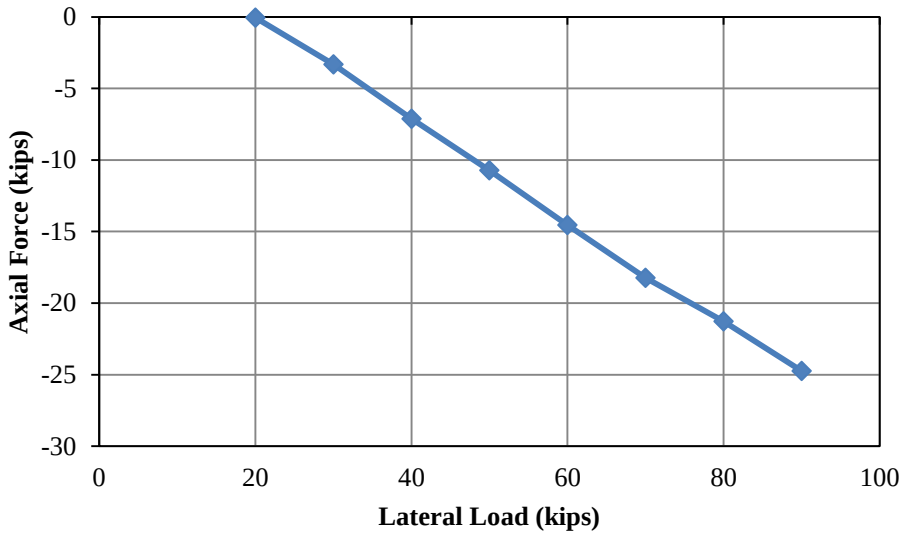

Figure 5-17 Pile 1 Axial Force vs. Lateral Load

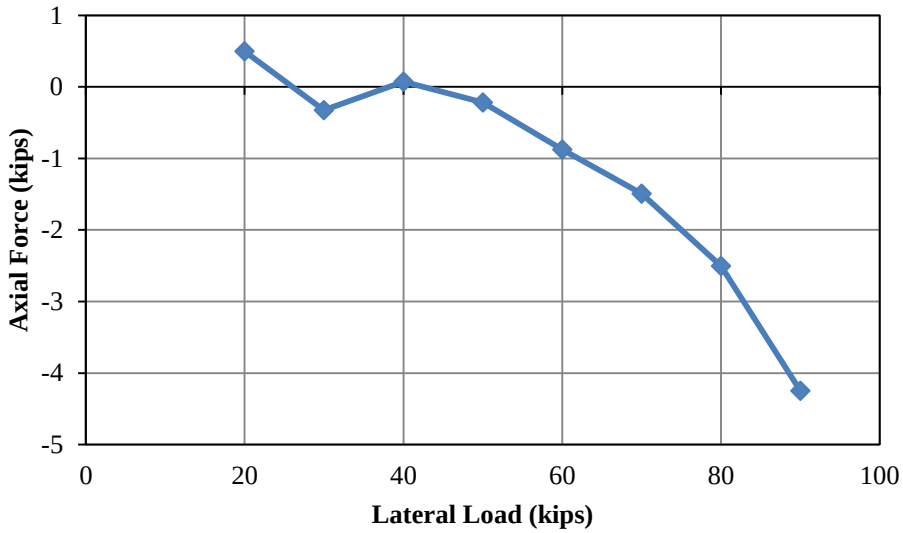

Figure 5-18 Pile 2 Axial Force vs. Lateral Load

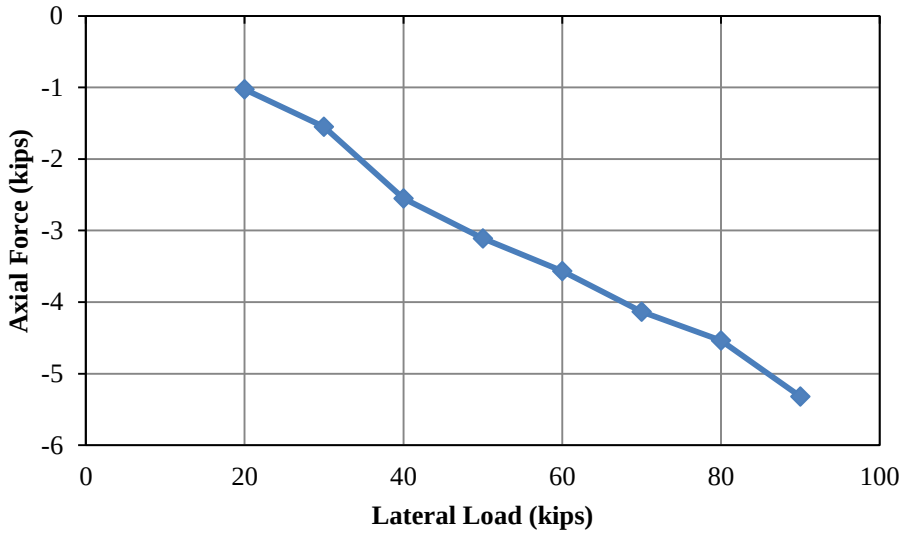

Figure 5-19 Pile 3 Axial Force vs. Lateral Load

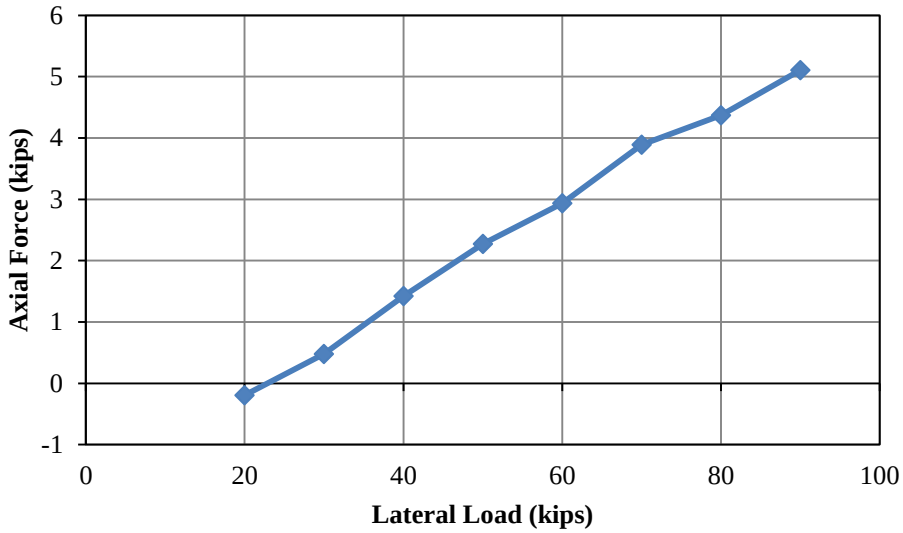

Figure 5-20 Pile 4 Axial Force vs. Lateral Load

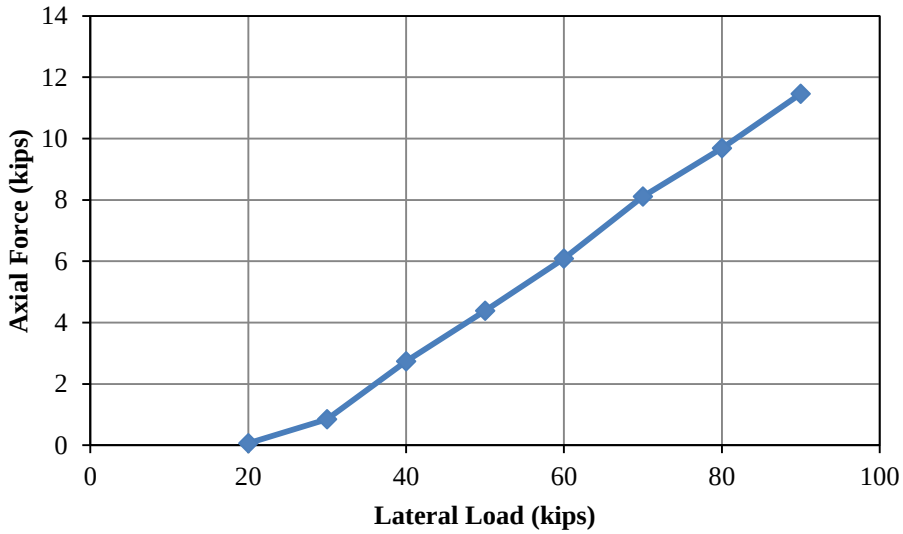

Figure 5-21 Pile 5 Axial Force vs. Lateral Load

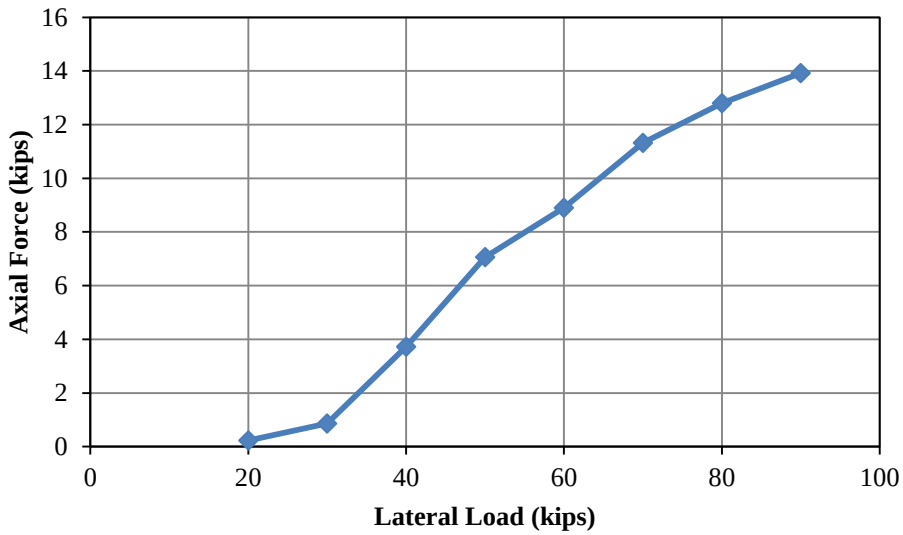

Figure 5-22 Pile 6 Axial Force vs. Lateral Load

The strain gage readings at the upper instrumented sections were used in order to calculate the axial forces in each of the piles. The axial load transfer from the bent cap to the pile is of most interest to designers which was why this location was chosen to calculate axial forces.

5.5.4 Test Bent Bending Moments – Combined Gravity and Lateral

Bending moment profiles in each of the piles during the combined gravity and lateral load test can be seen in Figure 5-23 through Figure 5-34. For each of the plots, zero elevation is considered to be the centerline of the bent cap. The initial bending moment profile represents the condition with only the load truck on the bridge and no lateral load applied. The shape of the moment profiles for each of the piles is relatively linear over the three instrumented sections. The bending moment appears to begin as a positive values in the piles near where the load truck was positioned. The moment decreases in magnitude as the lateral load is increased, eventually transitioning from positive to negative moment around the 30-50 kip load increment. Piles 1-3 are not as significantly affected by the load truck. The magnitude of the moment becomes more negative as the lateral load increases. Bending moment values calculated during the load test were much less than

expected, with the maximum moment six inches below the top of the pile around 14.5 kip-ft. Note that only the concrete encasements were instrumented during these tests; it is very difficult to gage how the steel pile is behaving relative to the concrete encasements. Data from the Macon County tests indicates that the piles do not behave purely composite, meaning that the steel pile strains a significant amount more than the concrete encasement. Due to the lack of instrumentation on the steel piles, it was decided to assume a linear strain distribution across the composite cross section, interpolating the strain values at the steel piles. For a bending moment calculation, the contribution of the steel pile relative to the concrete section is small due to the large difference in moment of inertias of the two sections. This large difference in stiffness would mean that the strain differential between the concrete surface and the steel pile would have to be very large as well to compensate.

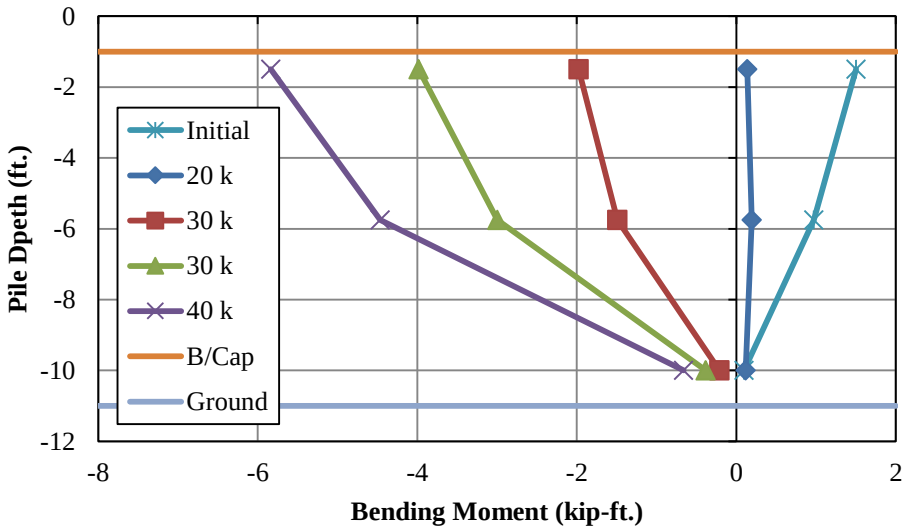

Figure 5-23 Pile 1 Bending Moment Profile

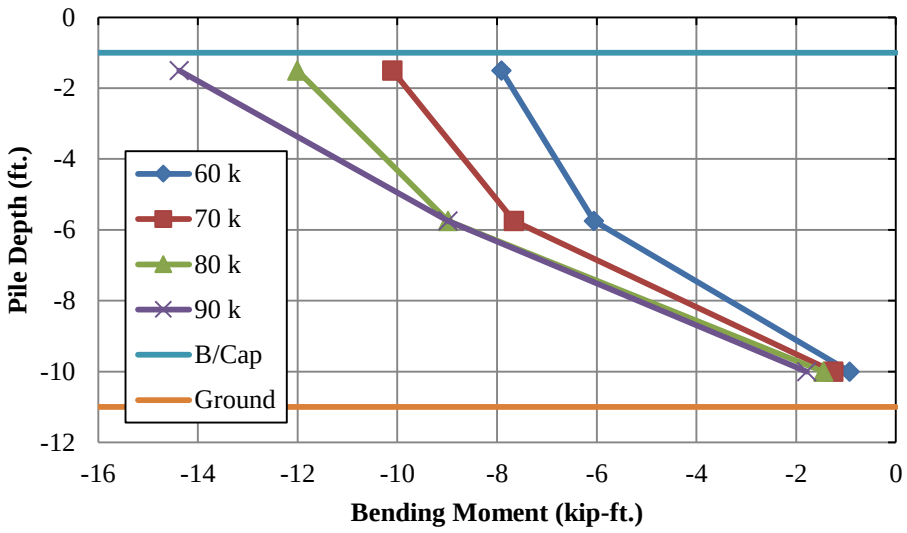

Figure 5-24 Pile 1 Bending Moment Profile

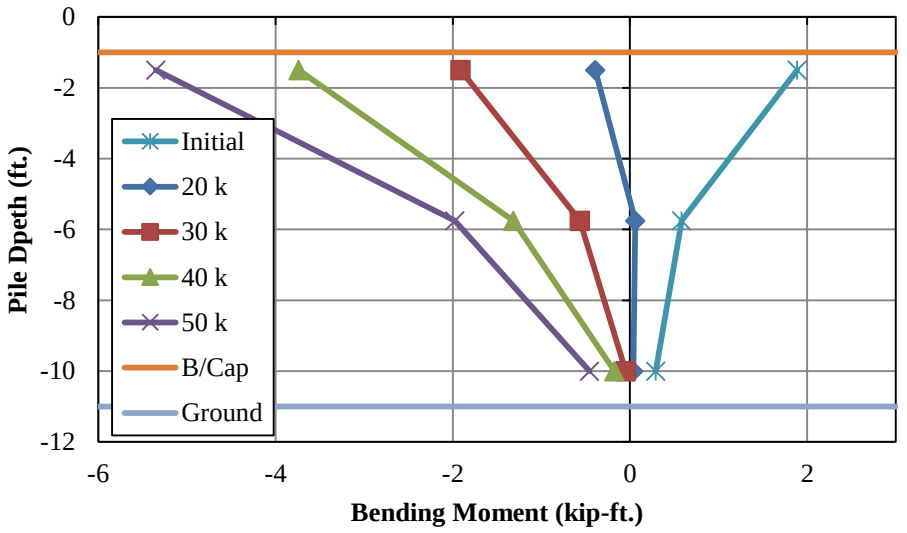

Figure 5-25 Pile 2 Bending Moment Profile

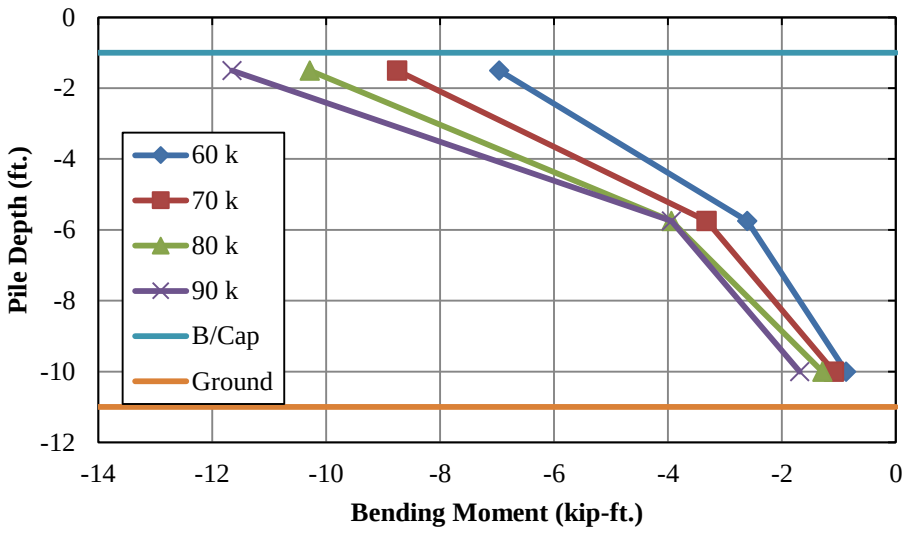

Figure 5-26 Pile 2 Bending Moment Profile

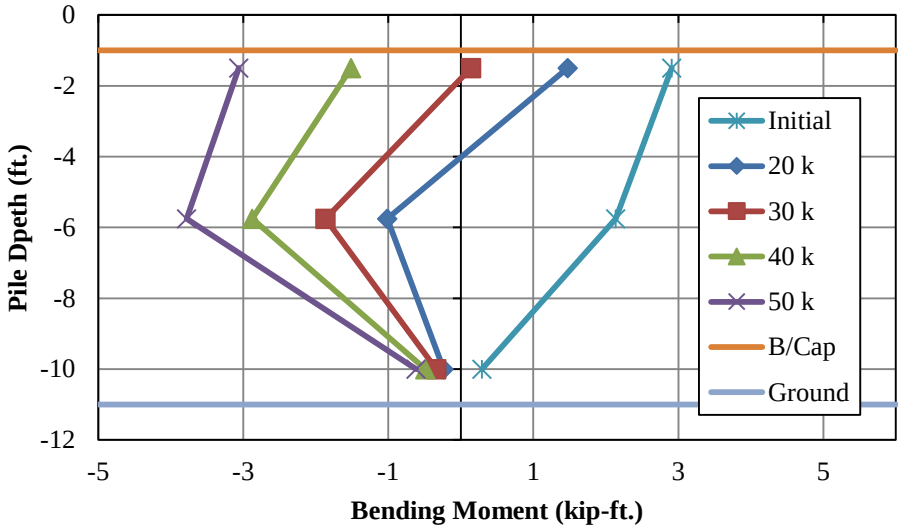

Figure 5-27 Pile 3 Bending Moment Profile

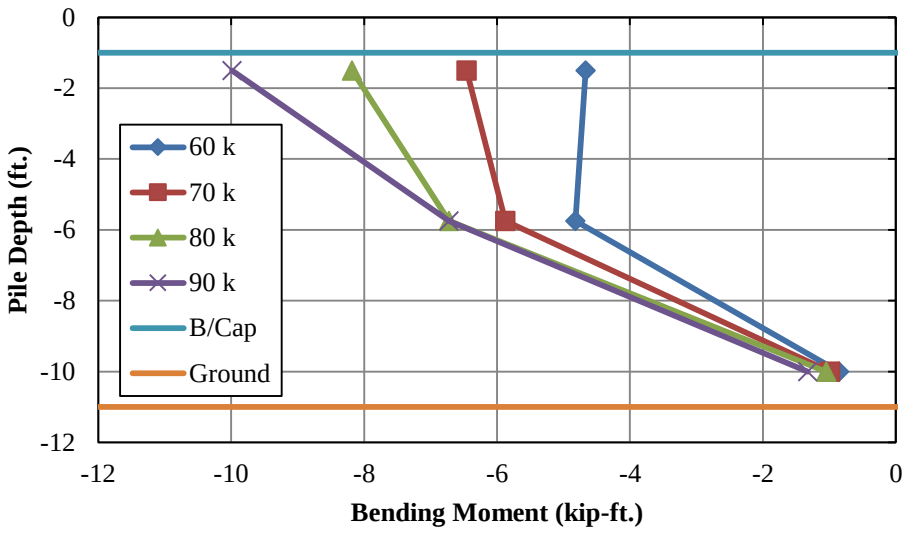

Figure 5-28 Pile 3 Bending Moment Profile

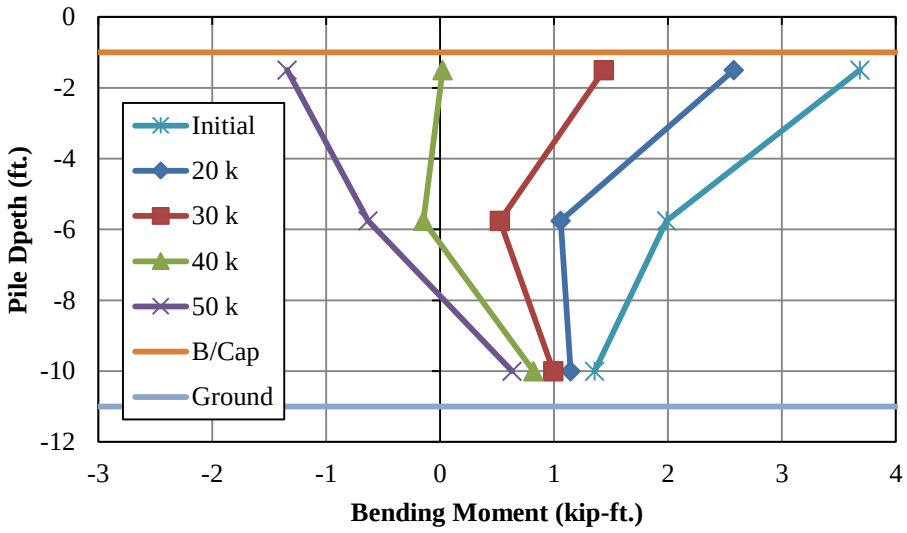

Figure 5-29 Pile 4 Bending Moment Profile

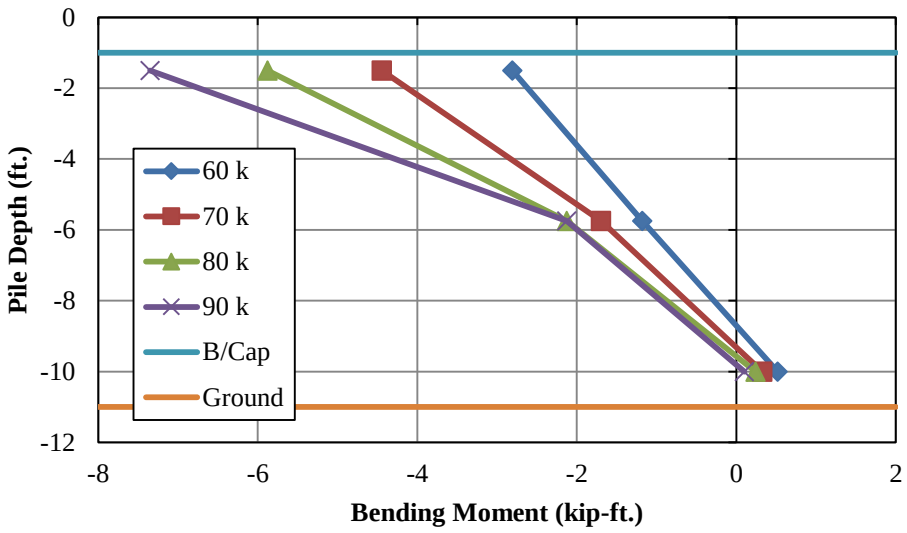

Figure 5-30 Pile 4 Bending Moment Profile

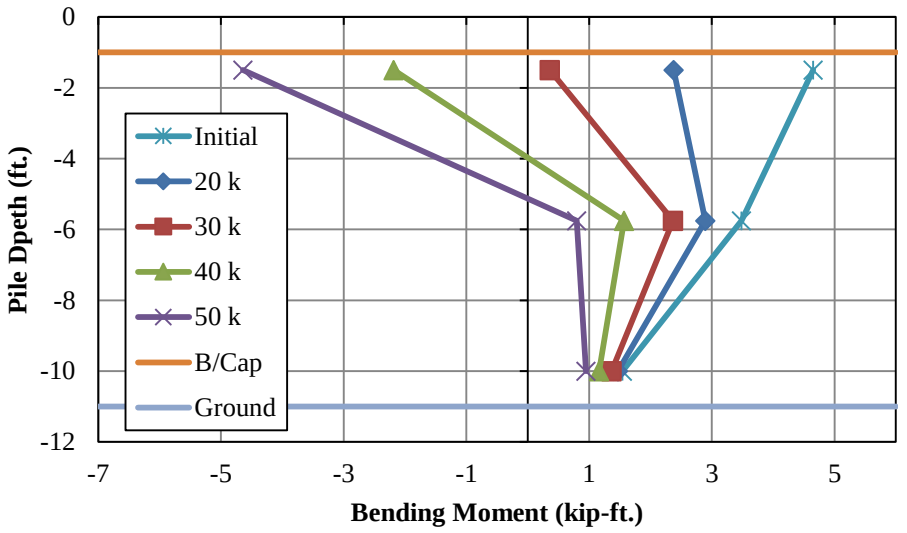

Figure 5-31 Pile 5 Bending Moment Profile

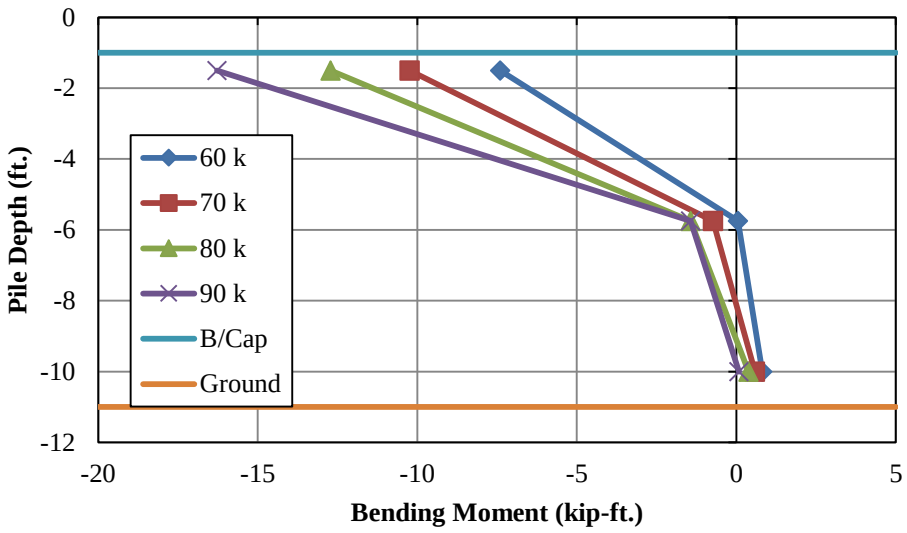

Figure 5-32 Pile 5 Bending Moment Profile

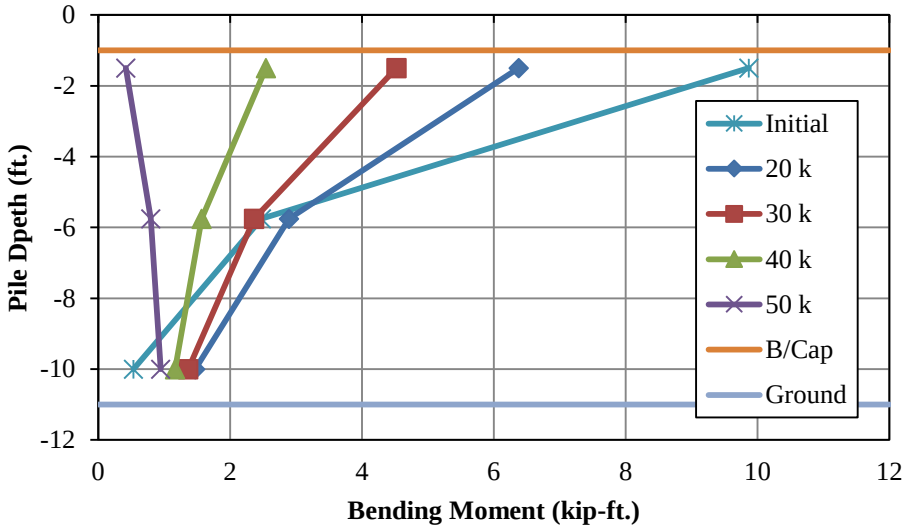

Figure 5-33 Pile 6 Bending Moment Profile

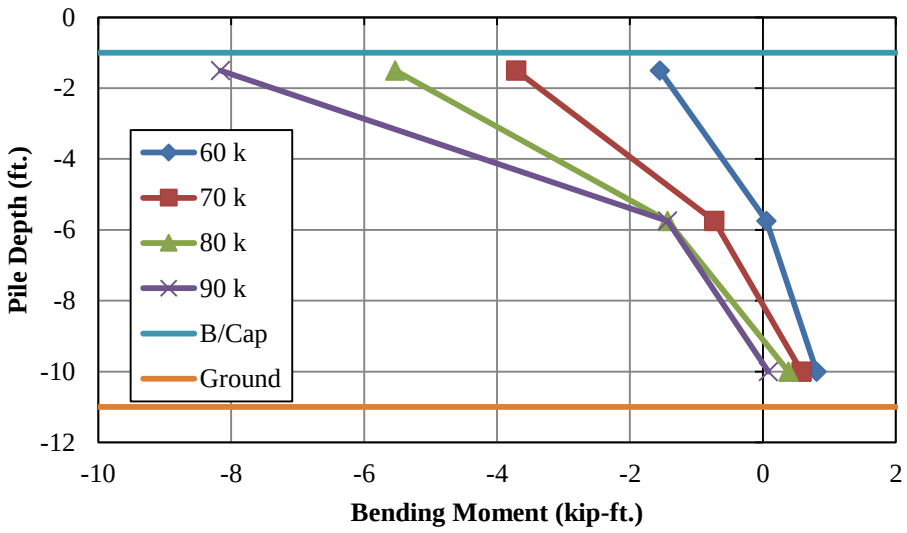

Figure 5-34 Pile 6 Bending Moment Profile

5.5.5 Reaction Bent Axial Forces – Combined Gravity and Lateral

The three exterior piles in the reaction bent looking south were instrumented in order to compare the performance of the reaction bent to the test bent during the load tests. Axial forces vs. applied lateral load in each of the instrumented piles in the reaction bent can be seen in Figure 5-35 through Figure 5-37. Similar to the calculations for axial load for the test bent, the upper instrumented section in each of the piles in the reaction bent was used to calculate the axial force.

The bents were loaded by essentially pulling them together, meaning that the bents would tend to overturn towards each other. This overturning would result in the exterior piles closest to the reaction bent which were instrumented being in axial compression due to overturning from the lateral load. The results indicate that each of the three instrumented piles were in axial compression with Pile 7, the exterior battered pile, having the highest value of axial compression.

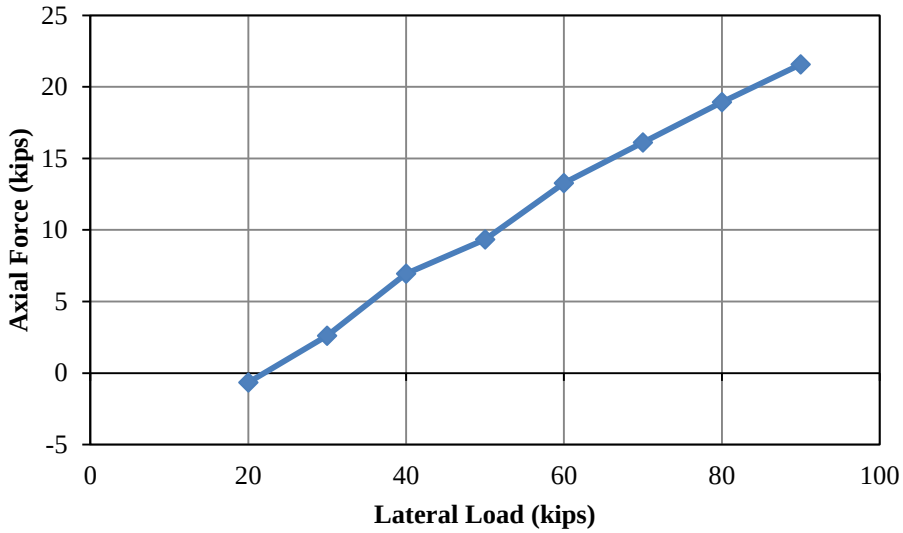

Figure 5-35 Pile 7 Axial Force vs. Lateral Load

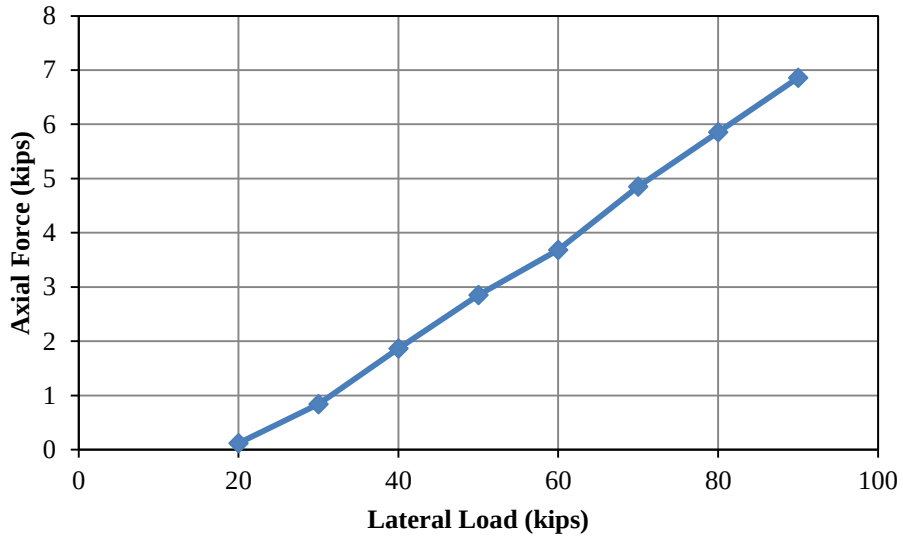

Figure 5-36 Pile 8 Axial Force vs. Lateral Load

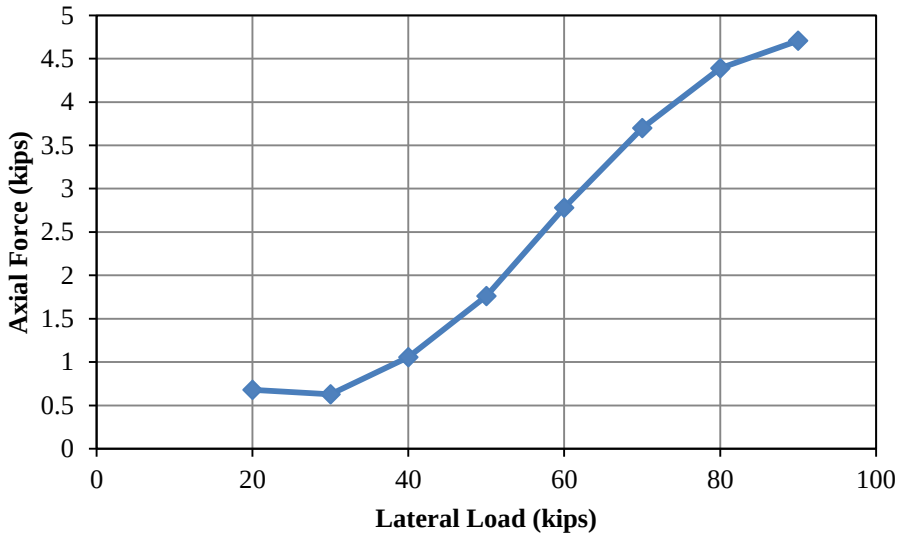

Figure 5-37 Pile 9 Axial Force vs. Lateral Load

5.5.6 Reaction Bent Bending Moments – Combined Gravity and Lateral

The bending moment profiles for each of the instrumented piles in the reaction bent can be seen in Figure 5-38 through Figure 5-43. Note that only two sections along the length of the pile were instrumented in the reaction bent. The maximum moment near the bottom face of the bent cap and the lowest instrumented section were used to compare the bending moment profiles of the instrumented piles in the reaction bent to the piles in the test bent. Similar to the test bent, the lowest instrumented sections on the reaction bent piles were found to be located near the inflection point, with the value of the bending moment close to zero. The maximum bending moments at the upper instrumented sections ranged from about 5 kip-ft. to about 10 kip-ft at a total load of 90 kips. These maximum values are less than the moment values in the test bent, most notably in Pile 7, the exterior battered pile. The compressive axial force in this pile, however, is much greater than the compressive axial force in Pile 6 in the test bent. This indicates that Pile 6 resisted the lateral load more through axial forces transfer rather than flexure.

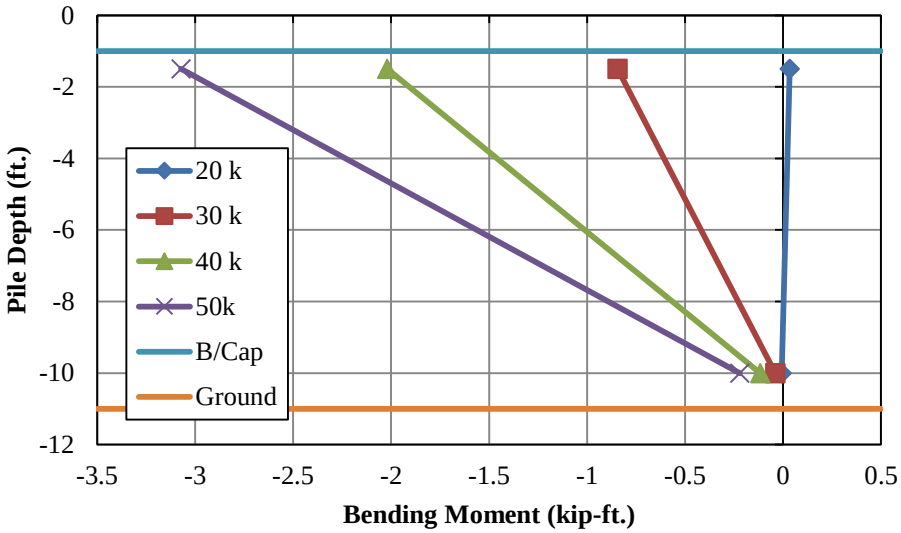

Figure 5-38 Pile 7 Bending Moment Profile

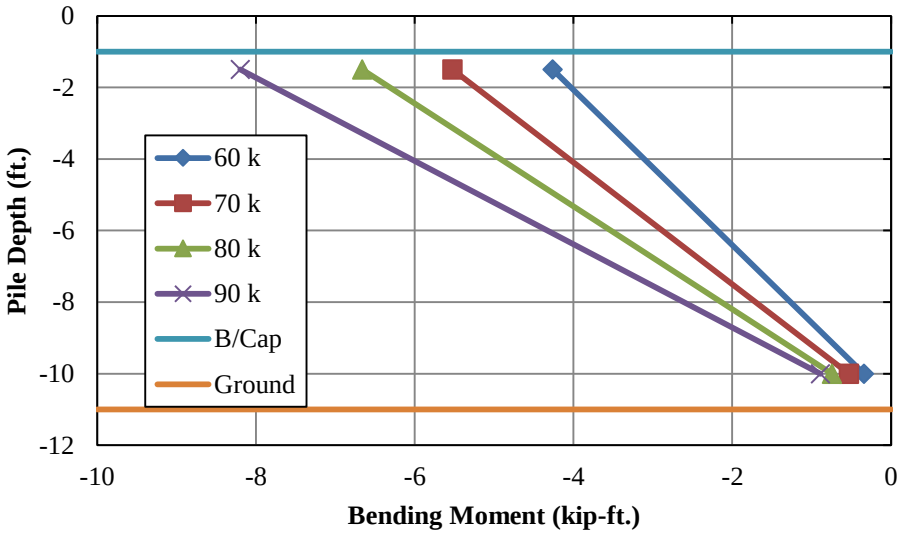

Figure 5-39 Pile 7 Bending Moment Profile

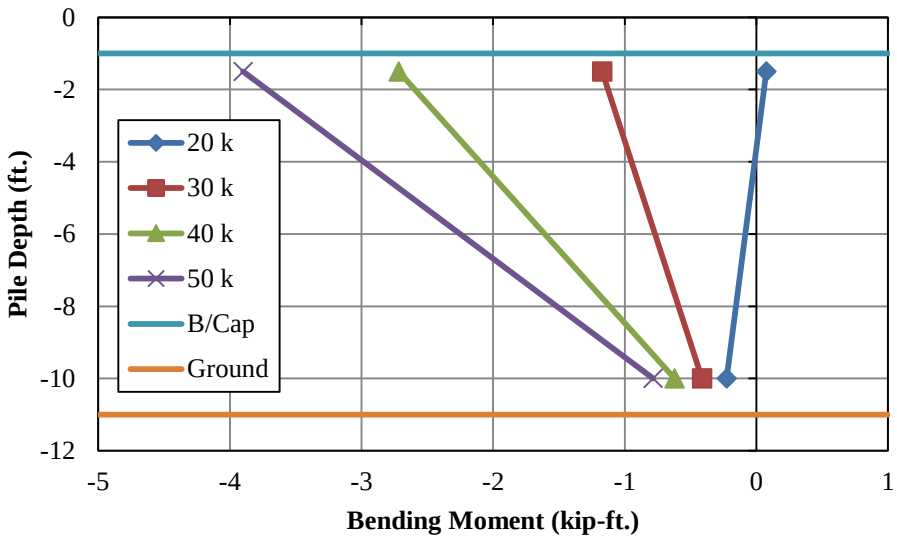

Figure 5-40 Pile 8 Bending Moment Profile

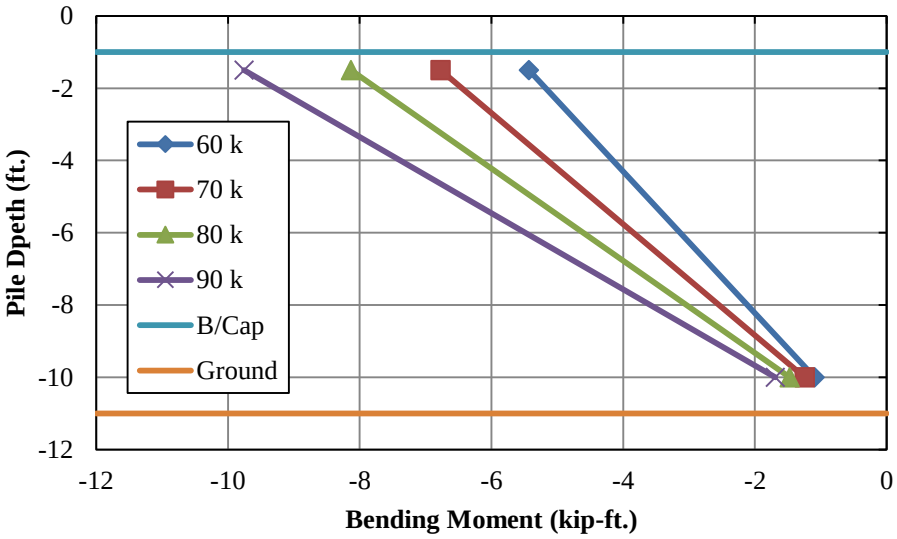

Figure 5-41 Pile 8 Bending Moment Profile

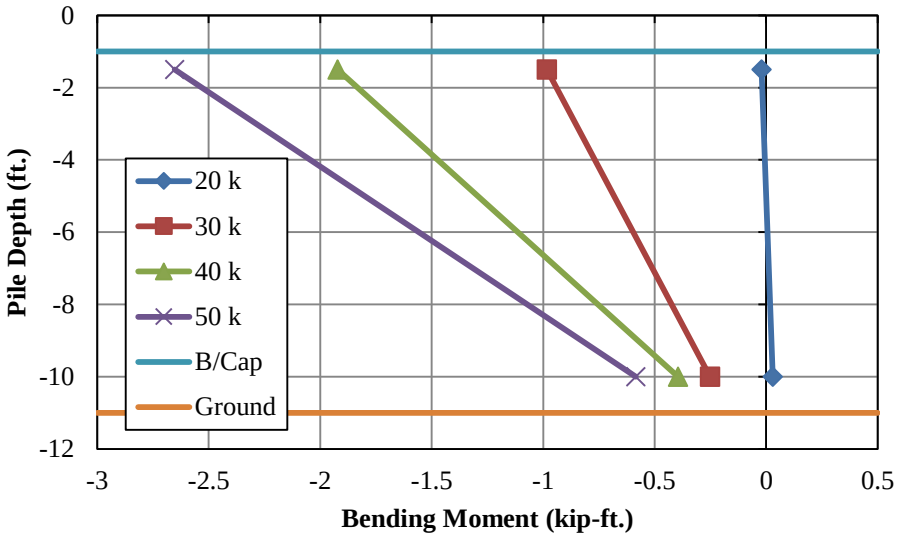

Figure 5-42 Pile 9 Bending Moment Profile

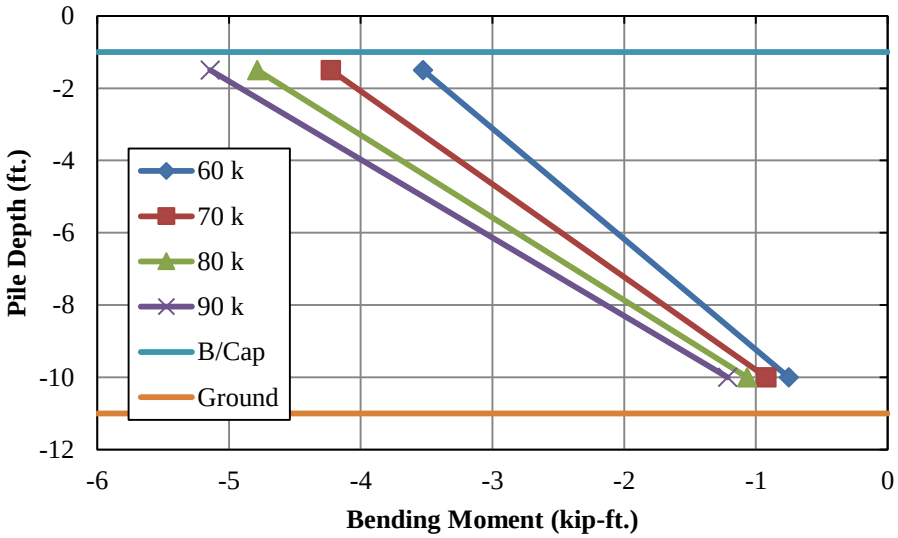

Figure 5-43 Pile 9 Bending Moment Profile

5.5.7 Test Bent Axial Forces – Lateral Load Only

Axial force vs. Lateral load plots for each of the six piles in the test bent during the lateral only load test can be seen in Figure 5-44 through Figure 5-49. The piles indicated similar behavior during the lateral only load test as the combined gravity and lateral test with the exterior piles

carrying a majority of the axial load due to their batter. Piles 1, 2, and 3 seemed to be in net axial tension while piles 4, 5 and 6 were in net axial compression due to overturning. These results were to be expected. Notably, the compressive axial force in pile 6 was considerably larger than the tensile axial force in pile 1.

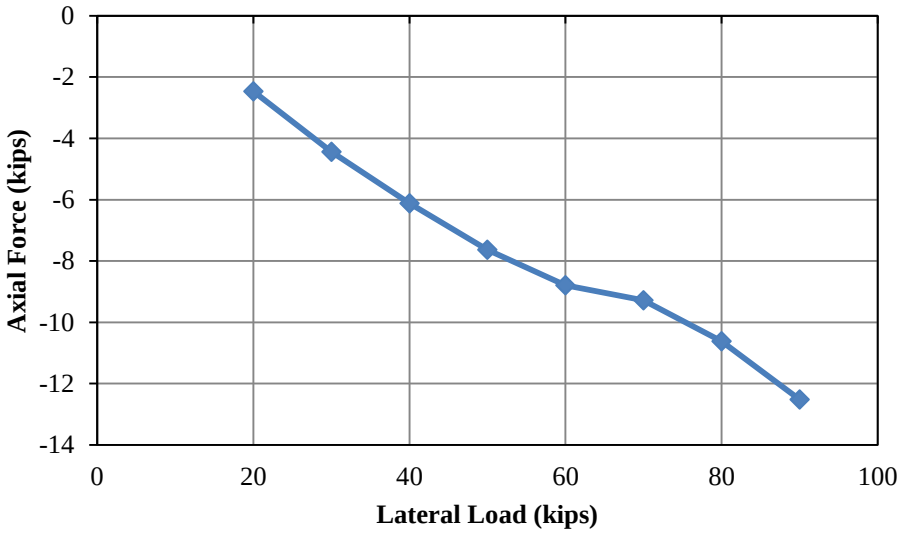

Figure 5-44 Pile 1 Axial Force vs. Lateral Load

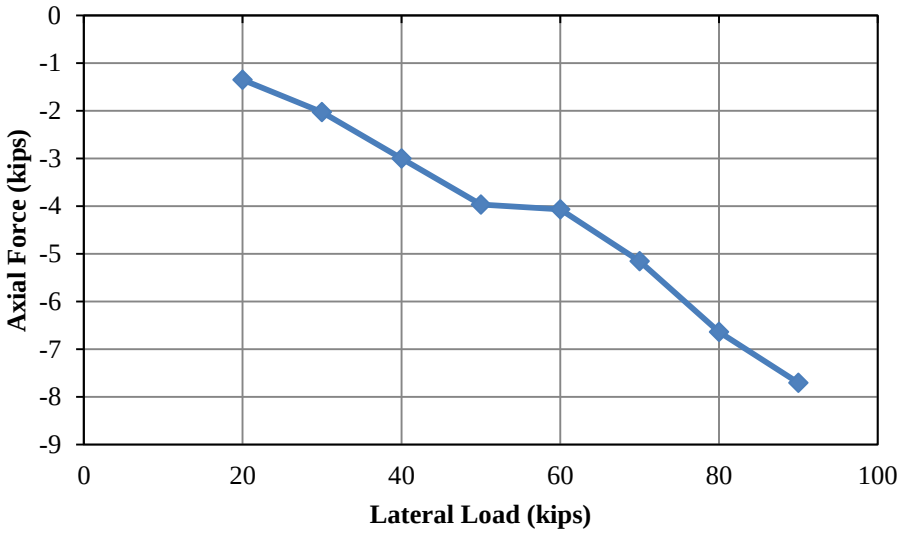

Figure 5-45 Pile 2 Axial Force vs. Lateral Load

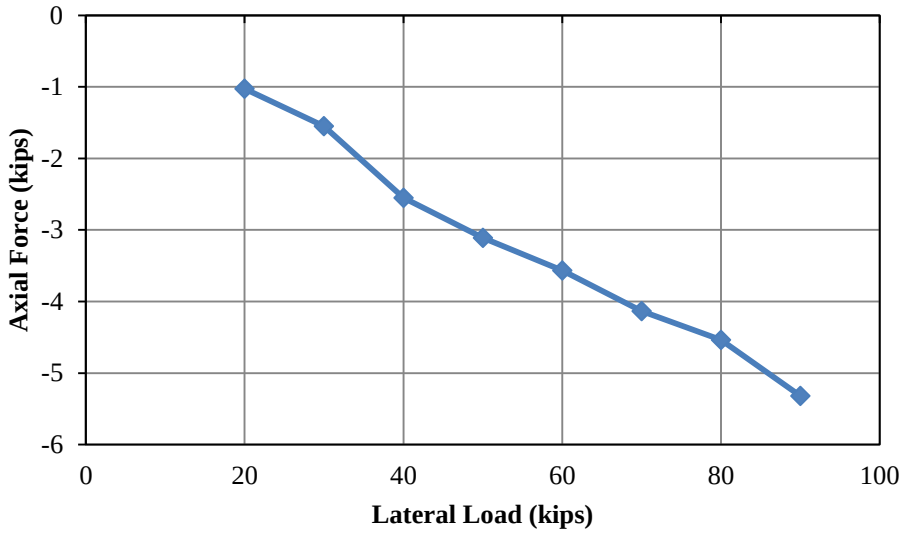

Figure 5-46 Pile 3 Axial Force vs. Lateral Load

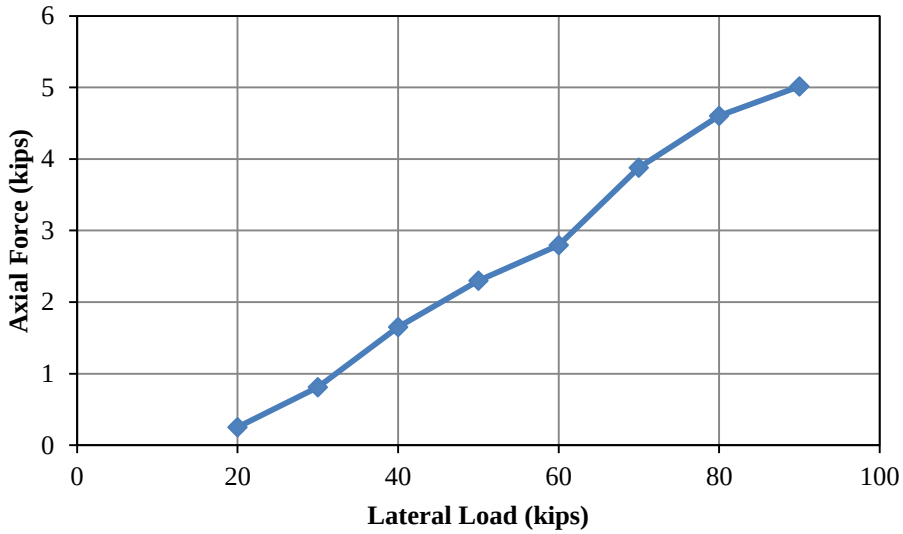

Figure 5-47 Pile 4 Axial Force vs. Lateral Load

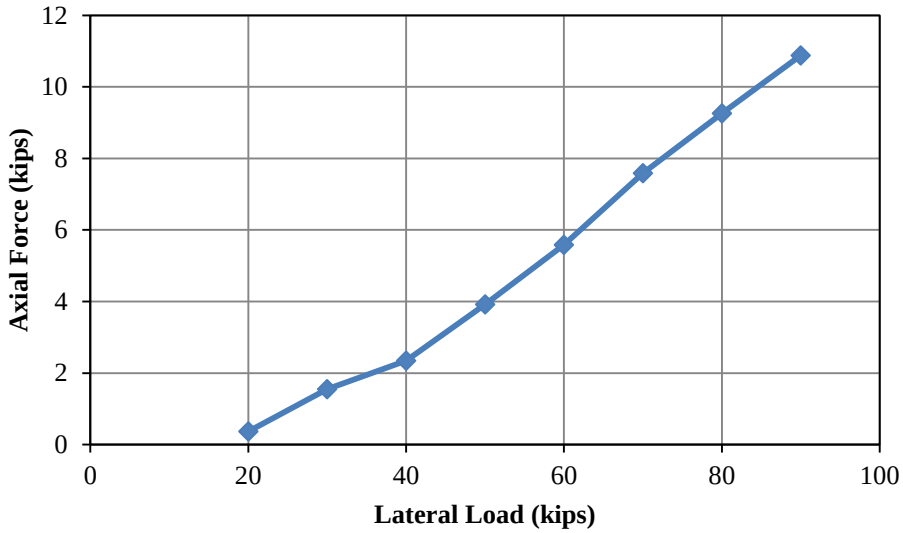

Figure 5-48 Pile 5 Axial Force vs. Lateral Load

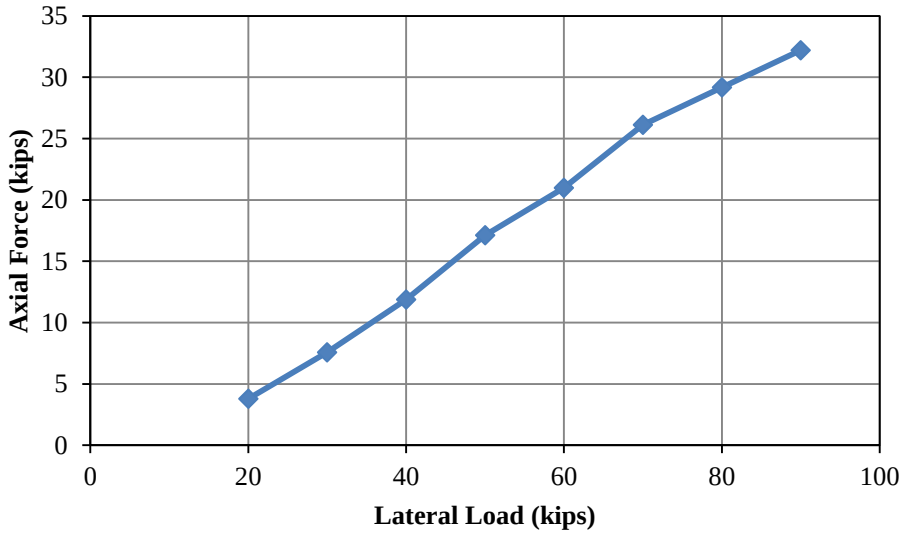

Figure 5-49 Pile 6 Axial Force vs. Lateral Load

The upper instrumented section was used in computing the axial forces in the piles. The transfer of load from the bent cap into the piles is of most importance to designers; therefore, this location was chosen. The axial force diagram over the length of the pile should remain relatively constant over the length of the pile until the pile enters the ground where the load will then be transferred into the subsurface.

5.5.8 Test Bent Bending Moments – Lateral Load Only

Bending moment profiles in each of the piles during the combined gravity and lateral load test can be seen in Figure 5-50 through Figure 5-61. The shape of the bending moment profile for each of the piles is similar to the combined gravity and lateral load test with the maximum bending moment appearing to be located near the bottom of the bent cap. The magnitude of the bending moments for the piles during the lateral load test with no additional gravity load are small, but similar to the moments calculated during the combined gravity and lateral test. The maximum calculated moments ranged from 11 kip-ft. to 20 kip-ft.

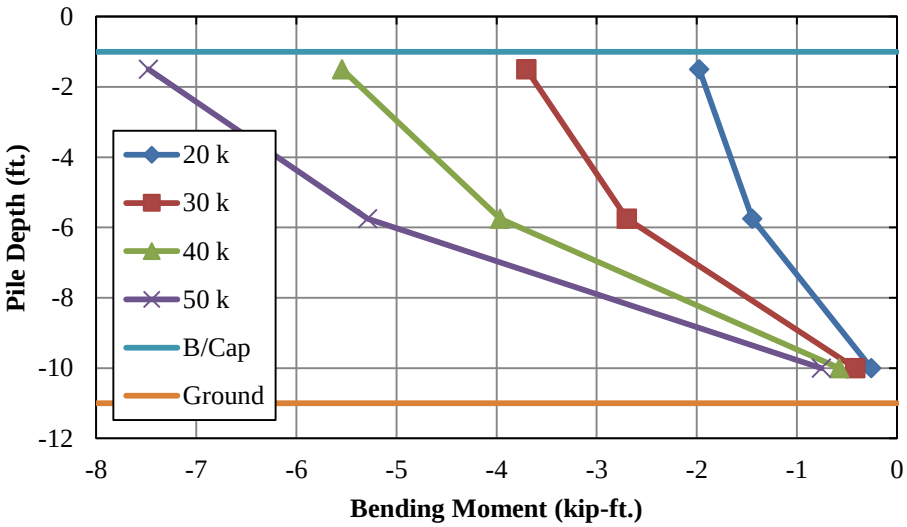

Figure 5-50 Pile 1 Bending Moment Profile

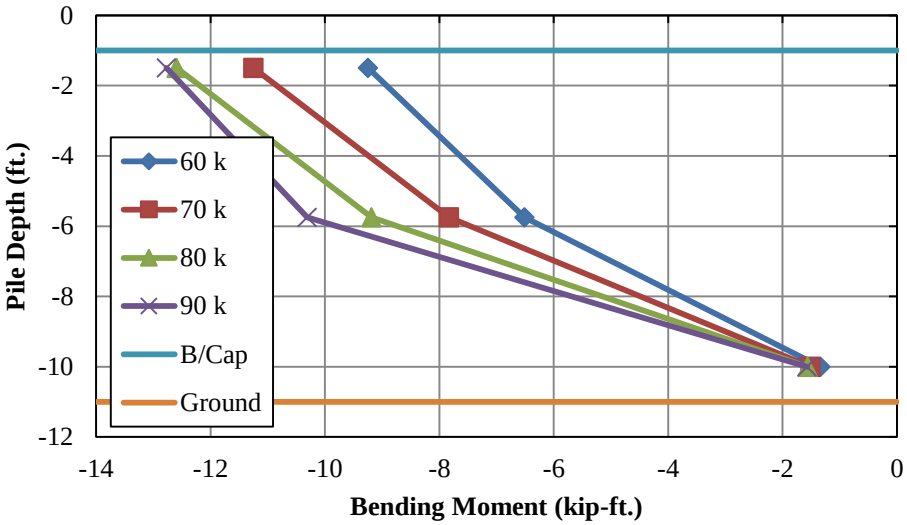

Figure 5-51 Pile 1 Bending Moment Profile

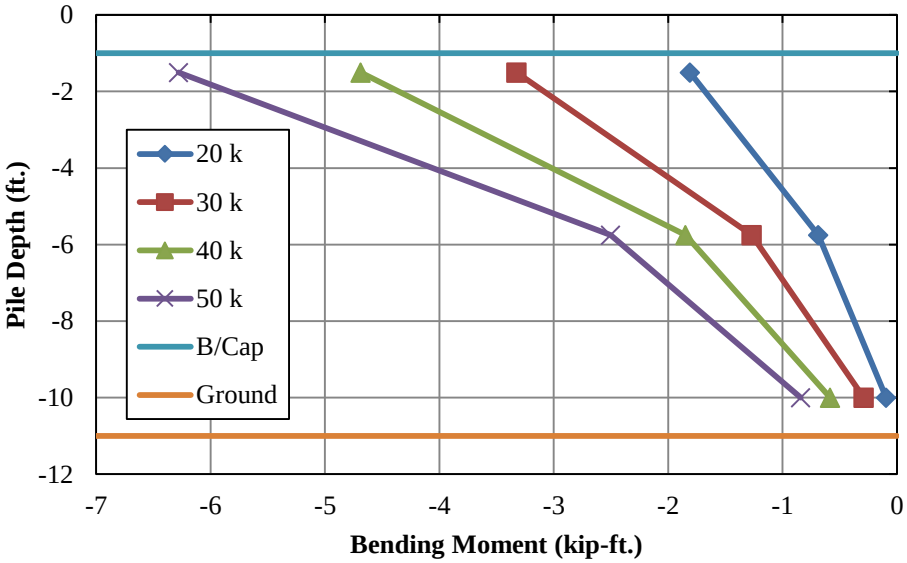

Figure 5-52 Pile 2 Bending Moment Profile

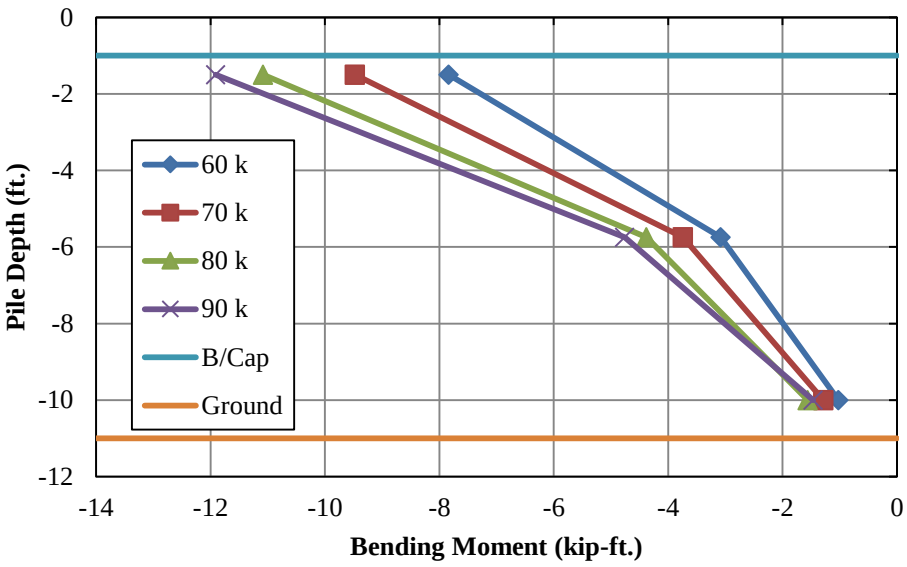

Figure 5-53 Pile 2 Bending Moment Profile

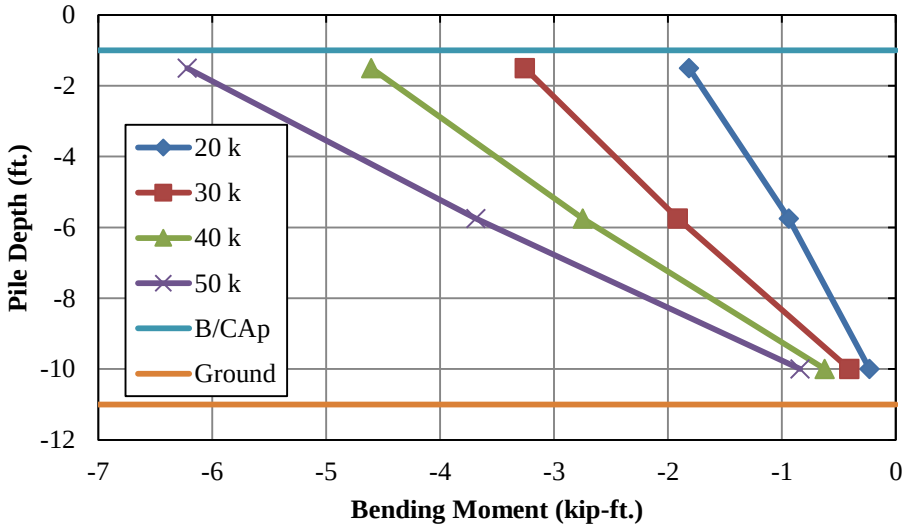

Figure 5-54 Pile 3 Bending Moment Profile

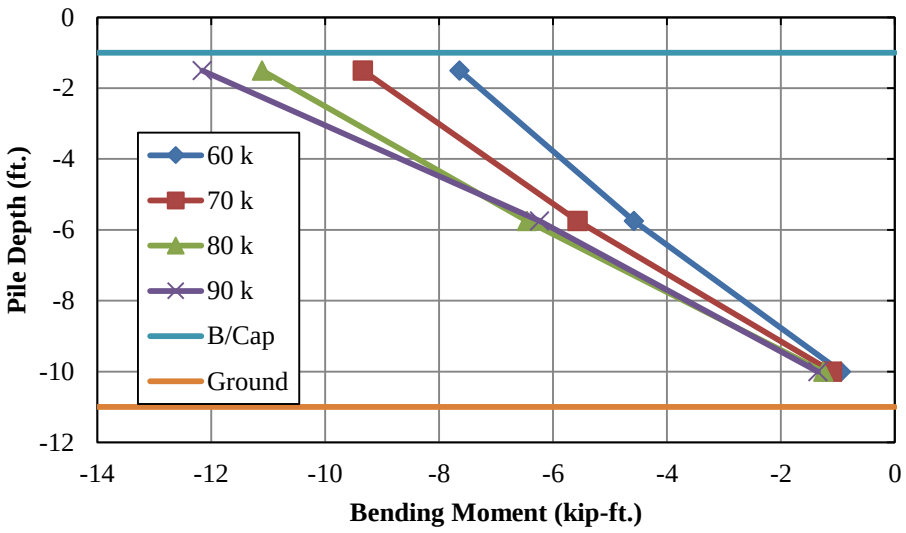

Figure 5-55 Pile 3 Bending Moment Profile

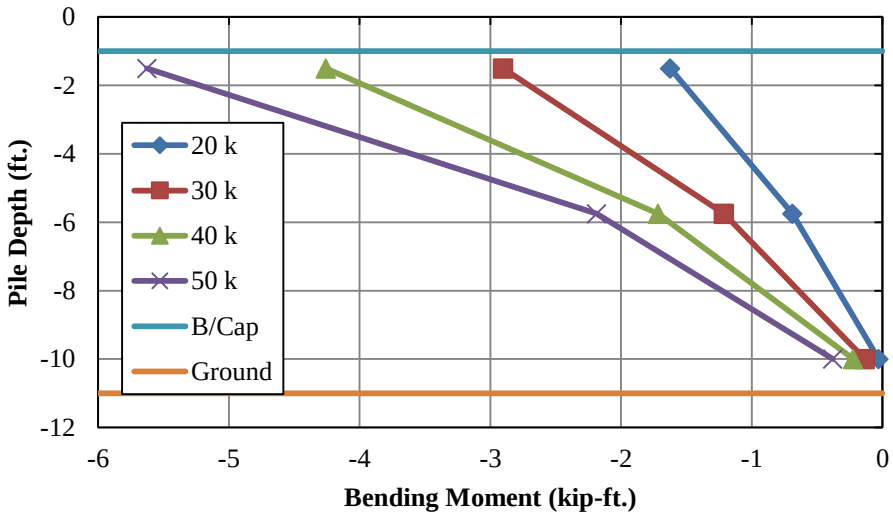

Figure 5-56 Pile 4 Bending Moment Profile

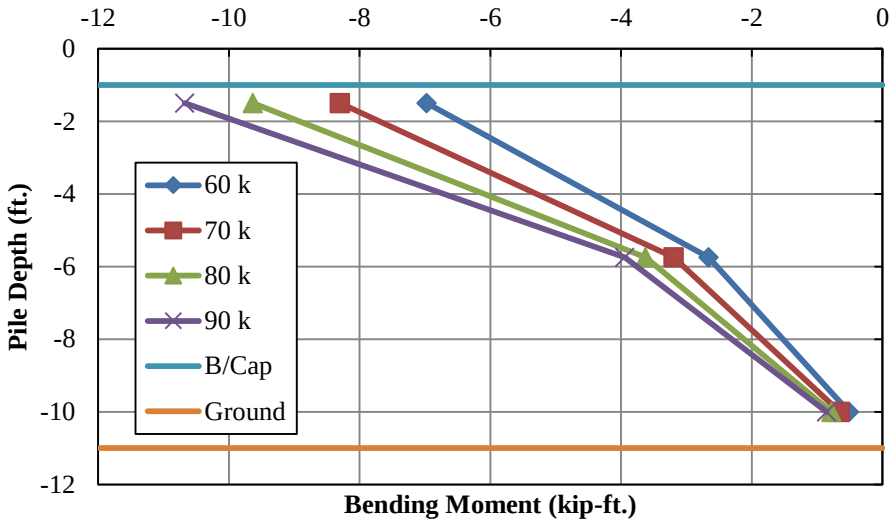

Figure 5-57 Pile 4 Bending Moment Profile

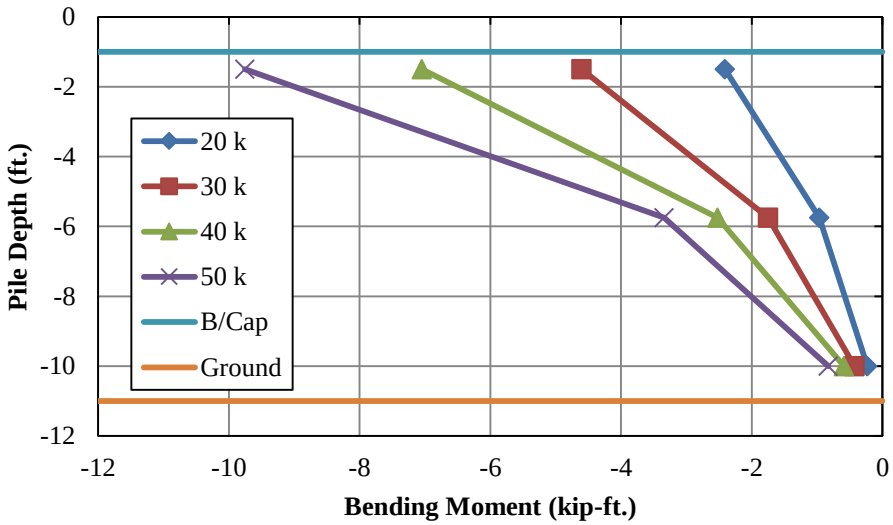

Figure 5-58 Pile 5 Bending Moment Profile

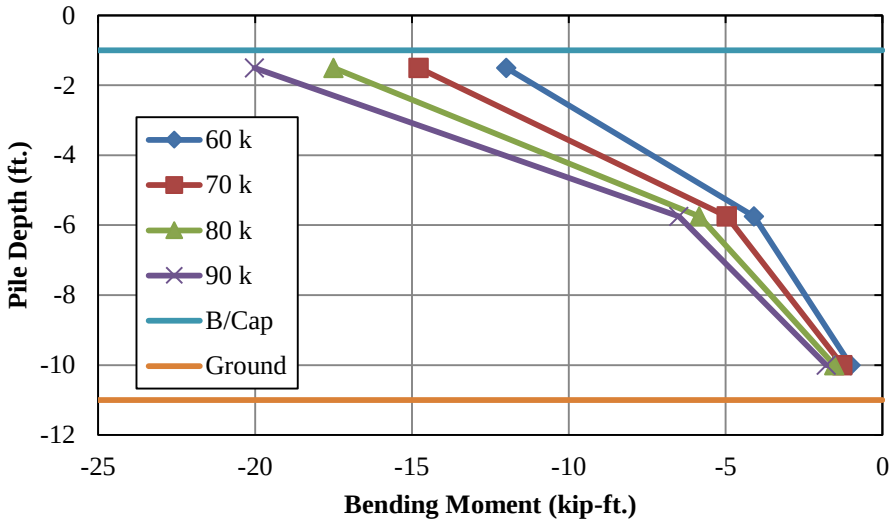

Figure 5-59 Pile 5 Bending Moment Profile

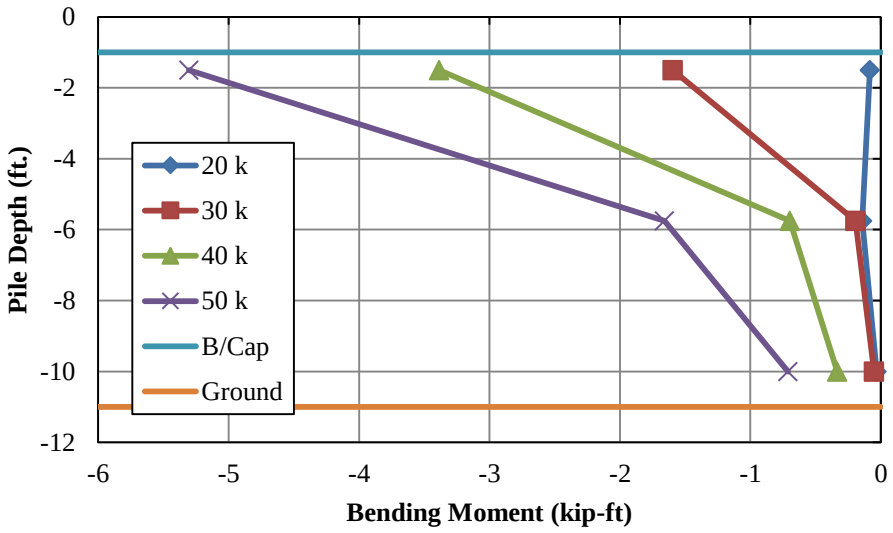

Figure 5-60 Pile 6 Bending Moment Profile

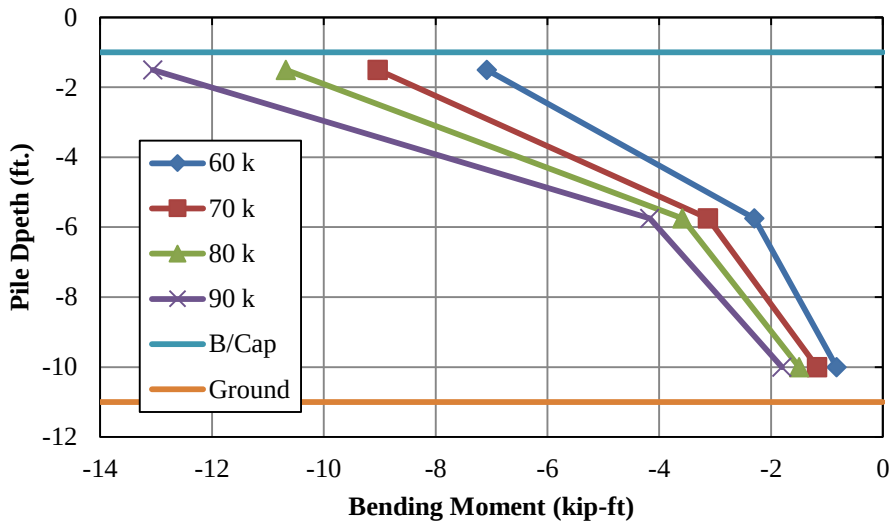

Figure 5-61 Pile 6 Bending Moment Profile

5.5.9 Reaction Bent Axial Forces – Lateral Load Only

Axial force versus applied lateral load for piles 7, 8 and 9 of the reaction bent during the lateral load test with no additional gravity load can be seen in Figure 5-62 through Figure 5-64. The instrumented section located six inches from the bottom of the cap were used to calculate axial forces. The axial load in pile 7 of the reaction bent appeared to have the highest magnitude during the load test, which was to be expected. Each of the instrumented piles in the reaction bent were in axial compression due to lateral load effects. The magnitude of the axial load in piles 8 and 9 were considerably smaller than in pile 7.

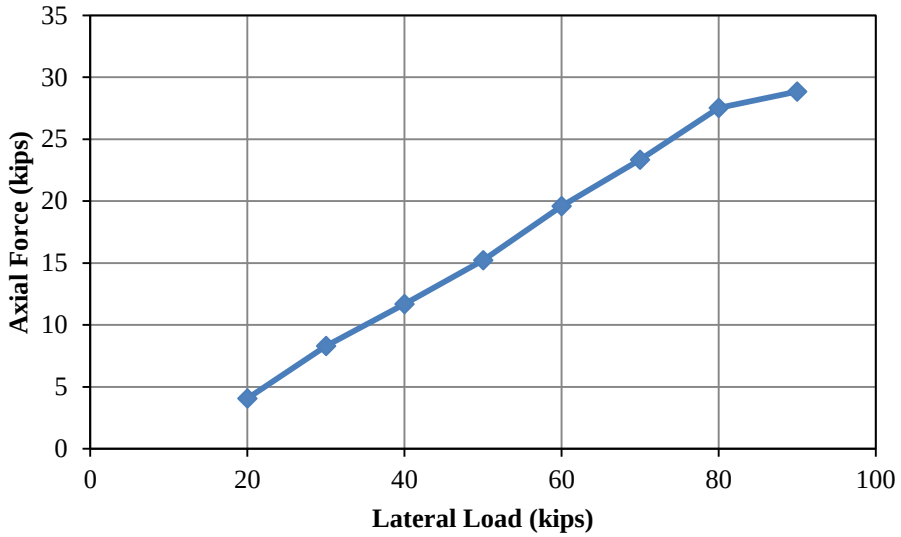

Figure 5-62 Pile 7 Axial Force vs. Lateral Load

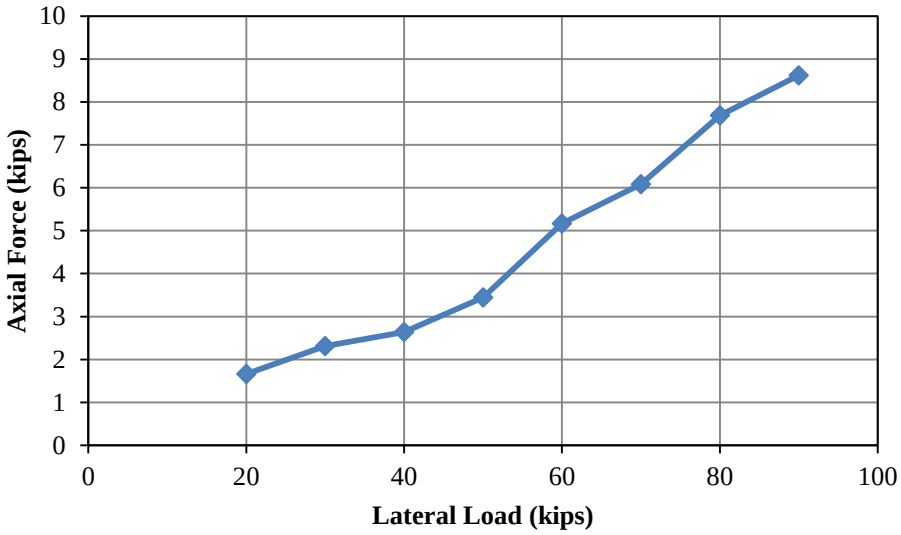

Figure 5-63 Pile 8 Axial Force vs. Lateral Load

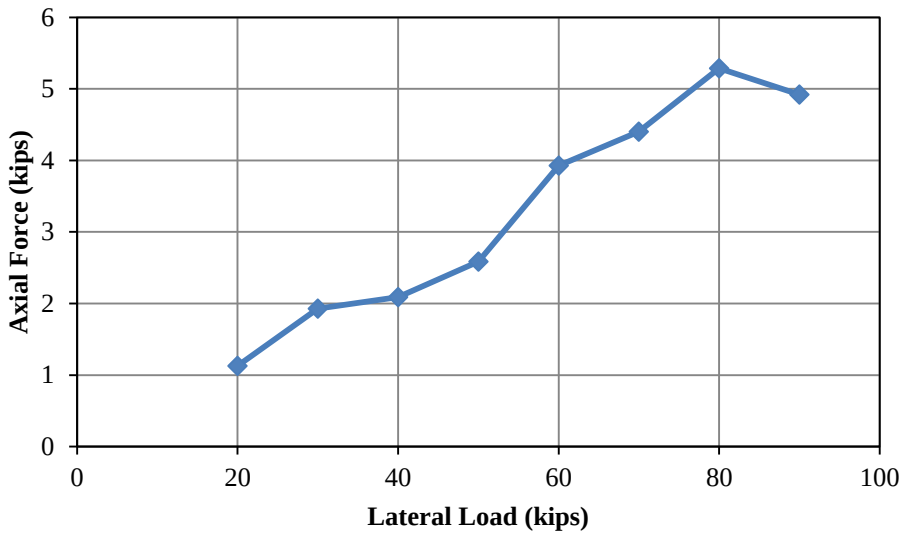

Figure 5-64 Pile 9 Axial Forces vs. Lateral Load

5.5.10 Reaction Bent Bending Moments – Lateral Load Only

The bending moment profiles for each of the instrumented piles in the reaction bent can be seen in Figure 5-65 through Figure 5-70. The maximum bending moments at the total lateral load increment ranged from 7 kip-ft. to 12 kip-ft. The magnitude of the bending moments are still relatively small, but comparable to the magnitude of the bending moments calculated in the test bent at the same load levels.

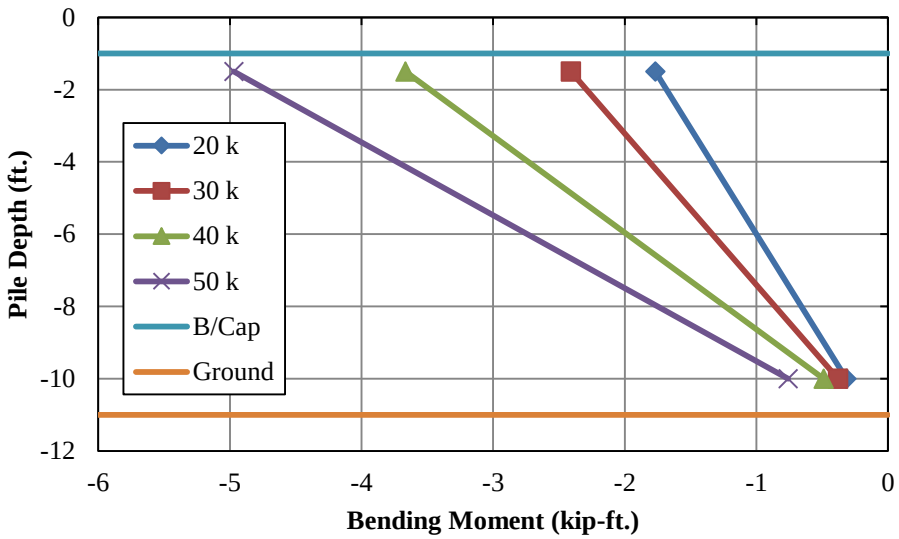

Figure 5-65 Pile 7 Bending Moment Profile

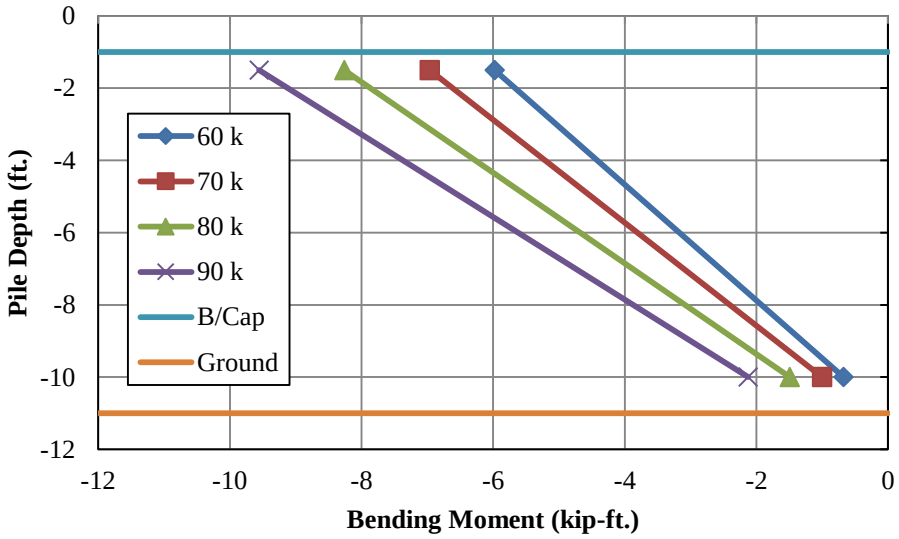

Figure 5-66 Pile 7 Bending Moment Profile

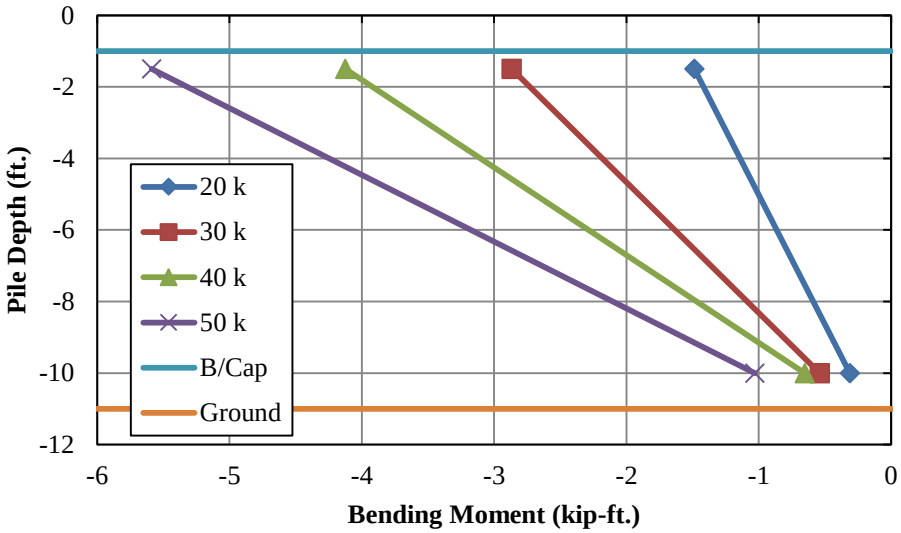

Figure 5-67 Pile 8 Bending Moment Profile

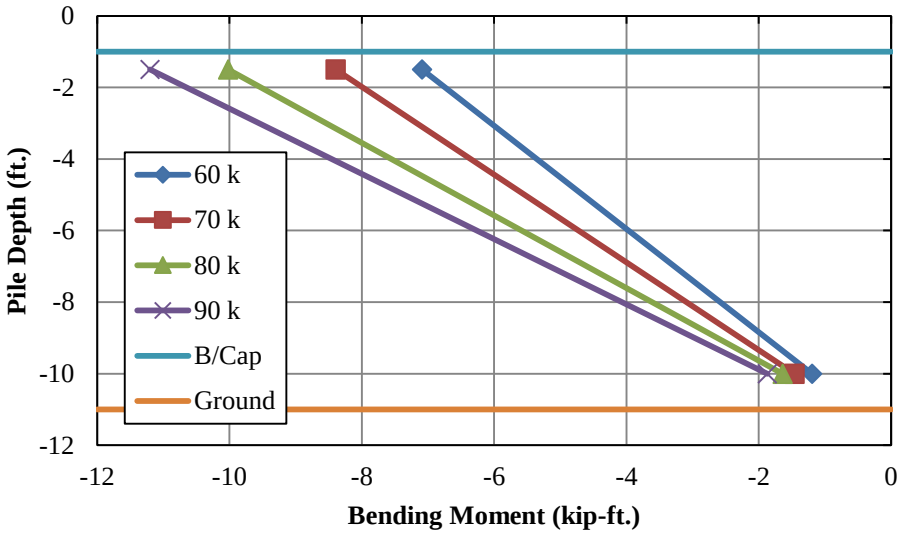

Figure 5-68 Pile 8 Bending Moment Profile

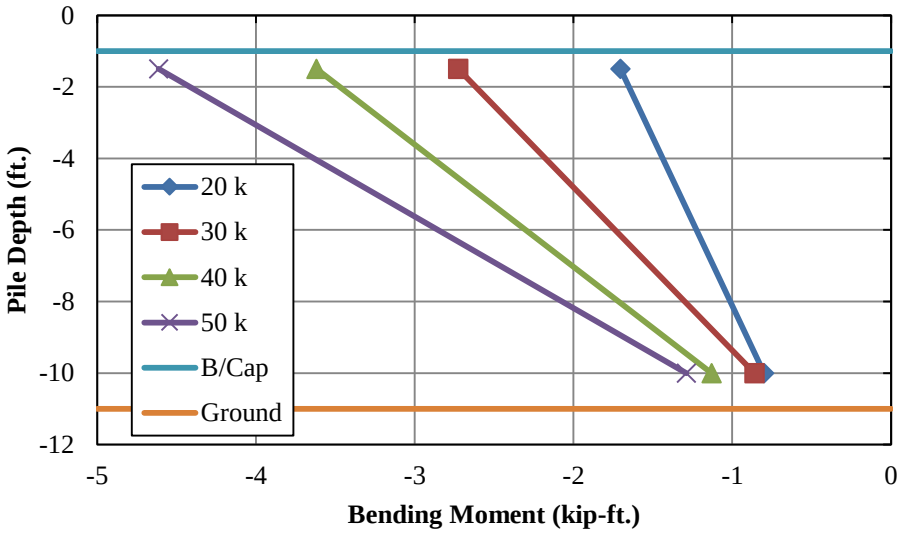

Figure 5-69 Pile 9 Bending Moment Profile

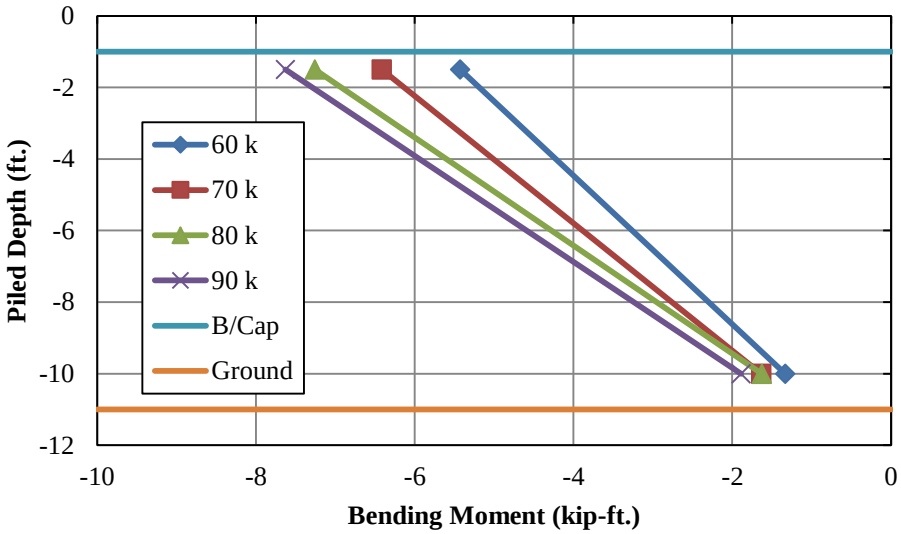

Figure 5-70 Pile 9 Bending Moment Profile

5.5.11 Displacement Wirepots

Two displacement wirepots were installed to the end face of the bent cap to measure lateral deflection of the bent during each of the load tests. One wirepot was located in the top right corner of the cap and the other was located in the bottom left corner so that an average total deflection of the cap during the tests could be obtained.

The load vs. deflection curve for the combined gravity and lateral load test can be seen in Figure 5-71. The measured deflection in each of the two wirepots as well as the average deflection of the two is shown in the figure. The measured deflections in each of the two wirepots are very similar during this test indicating that there was little twisting of the cap during the load test. The bent was extremely stiff during the test, deflecting a maximum of less than 0.1 in. at 90 kips of total applied lateral load.

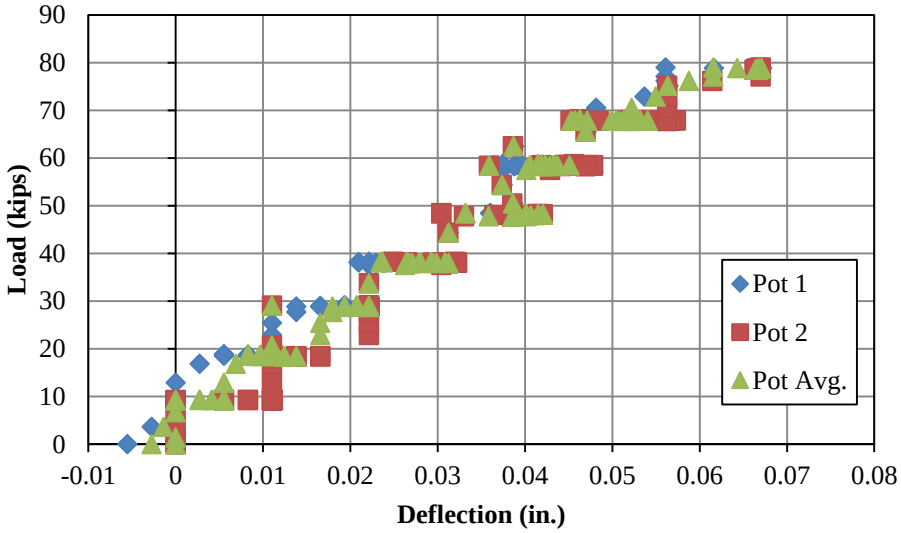

Figure 5-71 Load-Deflection with Load Truck Positioned at Road Edge

The load vs. deflection curve for the test bent during the lateral only load test can be seen in Figure 5-72. The average total deflection of the bent at a total lateral load of 90 kips was again under 0.1 in. indicating an extremely stiff response to the lateral load test.

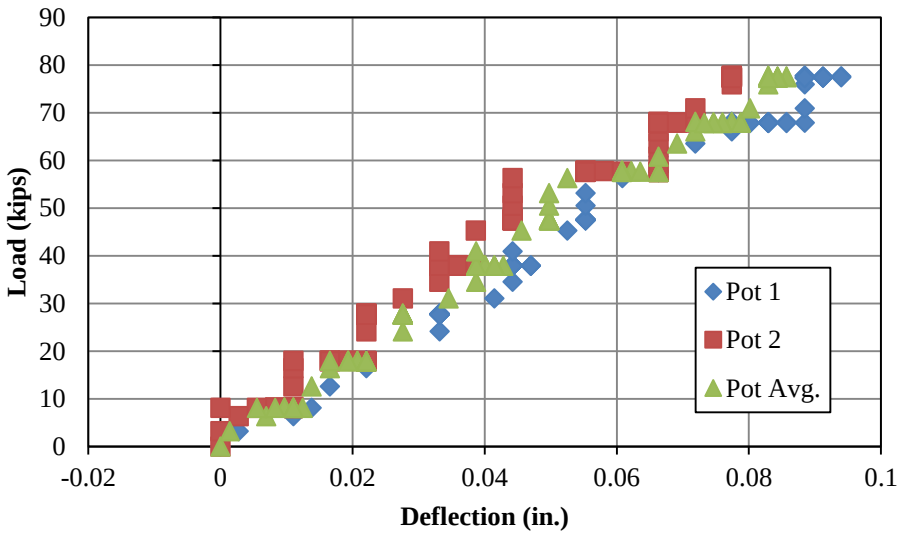

Figure 5-72 Load-Deflection with No Load Truck

A comparison of the average load vs. deflection curves for each of the two load tests performed can be seen in Figure 5-73. The average total deflection was greater with no additional truck load. However, in each load test, the bent was extremely stiff, deflecting less than 0.1 in. in each case.

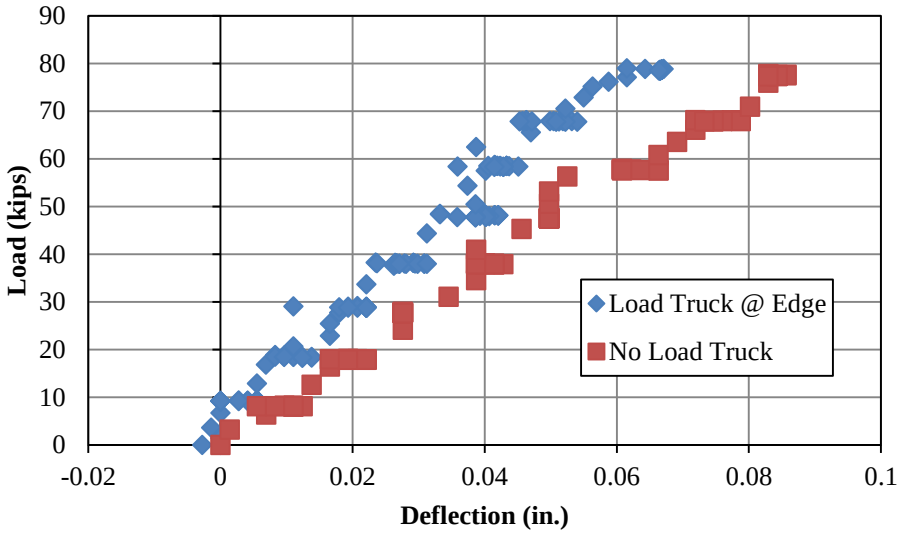

Figure 5-73 Load Deflection Comparison of Both Load Tests

The stiffness of the bents can be attributed to a number of factors. Even though the clear height of the piles is over 11 feet, the number of piles in the bent increases the lateral stiffness

dramatically. The shedding of load to the adjacent bents can also attribute to the large stiffness of a single bent. The load-deflection response of the test bent appeared to be linear throughout the duration of each of the test which was to be expected at the intended load levels.

5.5.12 Bridge Bent Behavior

The test bent in the US 331 bridge was extremely stiff during each of the two load tests performed. The bent deflected less than 0.1 in. during each of the two tests. The extreme stiffness can be attributed to the number of piles in the bent and the additional stiffness from the adjacent bents. The bridge superstructure essentially ties the bents together allowing a portion of the lateral load to be transferred to each of the bents on the forward and back spans of the test bent through the intermediate diaphragms and bearing pad connection. The bent deflected approximately 20% more without the load truck on the bridge. The decrease in deflection during the test with the load truck on the bridge can be attributed to the lateral deflection in the opposite direction due to the truck load. The initial negative displacement results in a smaller net displacement at each lateral load increment. The increased flexural stiffness of the bent can also be attributed to the effects of cracking of the pile encasements. The moment of inertia of the encased piles is larger with the addition of compressive force which will result in a larger flexural stiffness.

The values of the computed bending moments were lower than expected with the maximum bending moments being between 10 and 18 kip-ft. The change in bending moment magnitude from the 80 kip to 90 kip load increment was smaller than the change in moment between the other load increments. This small change can also be seen in the load-deflection response. The change in deflection between these two load increments was also small relative to the other load increment. The moment in the piles is related to the pile displacement meaning that a small change in displacement will result in a small change in moment.

Due to instrumentation only being installed on the concrete encasement surfaces, it was nearly impossible to monitor the behavior of the steel piles during the load tests. A linear strain distribution over the cross section was assumed to interpolate the strains at the flange tips of the steel pile and therefore consider their effects in axial force and bending moment calculation. The shape, however, of the moment diagrams was as expected with the maximum bending moment being at the bottom of the bent cap suggesting a fixed head condition for the piles. The moment diagram decreased linearly along the height of the piles which was instrumented with the lowest instrumented section being relatively close to the inflection point. The inflection point was expected to be close to the ground surface; therefore this observation is considered to be reasonable. The bending moments calculated in the piles in the reaction bent during each of the tests were significantly less than the calculated bending moments in the test bent. The axial compressive force in the leading pile of the reaction bent were higher in magnitude than the compressive force in the test bent.

5.6 Chapter Summary

The test bent performed well during each of the three load tests performed and was extremely stiff, deflecting less than 0.1 in. in each loading condition. The bending moments calculated from measured strains on the concrete encasements were very low in magnitude. The moments that were calculated included an approximated stiffness of the steel piles; however, the behavior of the steel piles during each of the load tests is uncertain. The shape of the moment diagram above the ground surface for each of piles was as to be expected with the maximum bending moments occurring near the bottom of the bent cap and the approximate inflection point being at or near the ground surface. The location of the maximum bending moment clearly indicates a fixed head condition at the pile to pile cap connection.

The load-displacement response for the test bent remained fairly consistent during each of the combined gravity and lateral load tests as well as the test with no additional gravity load applied. The lateral stiffness of the bent did appear to increase by a small margin with the addition of gravity load; however, this increase in stiffness or decrease in displacement is seemingly negligible. Therefore it can be determined that addition of gravity loads in the service level range causes minimal effects on the lateral stiffness of bridge bent.

Chapter 6 Analytical Modeling of Tested Bridges

6.1 Introduction

Finite Element structural models were created in order to determine how well the results from the field tests correlated with analytical results. The models were also used in order to determine behavior of the bent that was unable to be instrumented in field testing. Two-dimensional bridge bents were developed using SAP 2000. The bents tested in both Macon County and on US 331 remained well within the elastic range during the tests; therefore, a linear elastic static analysis was deemed to be acceptable. The models created in SAP 2000 simulated the geometry of the as-built bents. Composite cross-sectional elements and soil-structure interaction were also included in the models. The loads applied to the models simulated the actual applied loads to the bents during each of the load tests performed on the Macon County and US 331 Bent.

6.2 Geometric Properties

The structural models were created based on geometry obtained from construction documents and physical measurements taken from the as-built structure. A two-dimensional frame model was used to develop each of the bents, therefore the XZ plane remained the primary working plane. Vertical grids in the Z plane were first created at each of the pile locations, with the reference point being at the far left pile. Horizontal grids in the X plane were then created at the level of the ground surface and the centerline of the bent cap with the ground level being the point of reference. Horizontal grids were then drawn at each elevation in which a linear soil spring was to be added. The addition of these grids made for easier modeling of battered piles. For the Macon County test, the actual pile lengths for the as-built bent were known and were modeled accordingly. The pile lengths for the US 331 bridge were unknown; therefore an approximate pile length of 35 ft. was assumed. In most cases, the bending moment is dissipated well before the bottom of the pile

making the assumed pile length reasonable. The piles were then manually drawn at each of the previously drawn grid locations. Once the piles were drawn in at their respective locations, the local axes of the piles were rotated by 90 degrees so that the piles would be oriented in the same direction as they were in the field. Grid points were created to the left and right of the exterior pile locations at the base of the piles at an offset distance correlating to a 1.5:12 slope over the total pile length. The exterior piles were then manually drawn at their correct batter. Once the piles were drawn in, linear springs were applied at the pile tips in the z-direction. These properties of these springs were determined from models created in FB-Multipier by Skinner (2015). The axial reaction at the tip of the pile was divided by the vertical displacement of the pile tip in order to compute an axial spring at the pile tip. Grid points were then offset in the X plane away from the exterior pile grids at the distance to the edge of the bent cap. The bent cap was then manually drawn in as one continuous frame element. Due to the piles having an embedment of 12 in. into the 24 in. deep cap, a centerline model with the pile heads connected to the centerline of the bent cap was determined to be acceptable. This centerline model eliminated the need for additional connection springs or link elements to model the pile to cap connection. The results from the field test indicated that the maximum bending moment occurred at the top of the pile and decreased linearly; therefore it was deemed acceptable to fully restrain rotation at the connection between the piles and the bent cap. Results from load tests by Richards et al. (2011) and Gerber and Rollins (2009) indicated that a fully fixed head condition is difficult to achieve; however, piles embedded into a cap behave very similar to a fixed condition under working level loads when there is no apparent non-linear behavior. Once the bent geometry was drawn in, linear springs were added along the length of the piles at the grid elevations previously drawn.

6.3 Material and Frame Section Properties

Once the geometry of the bents was in place, the frame sections and material properties for the bents were modified so that the elements in the bents reflected their as-built condition. The default material properties and user-generated material properties were used in the models.

For the bent elements in the Macon County bridge, the material properties were much easier to model due to the availability of information from the as-built structure. Concrete cylinder breaks performed at 7 days and 28 days from the concrete encasements and the bent cap were used in the Macon County model. Modulus of elasticity tests were not performed; therefore, the modulus of elasticity of the concrete encasements and the bent cap was approximated using the empirical equation shown in Chapter 3.

The bent cap was modeled using the section designer within SAP 2000. The trapezoidal cross-section of the bent cap was drawn within the section designer and was assigned the appropriate material property based on concrete strengths recorded from cylinder breaks at 28 days. Modeling the composite cross section including the steel pile and the concrete encasement proved to be fairly challenging. The piles were split into two separate elements at the location in which the encasements terminated. Below the termination of the encasements, which occurred five feet below finished grade, the piles were modeled using the HP14x89 section from the SAP 2000 AISC 14 database. The local axes of the piles were rotated 90 degrees to ensure that they were loaded about the same axis in which they were loaded in the experimental tests. The composite cross section including the concrete encasements was modeled using the section designer within SAP 2000. A 30 in. diameter concrete cross section was drawn in and given the appropriate material properties, then a steel I-section was drawn in on top of the concrete cross-section to ensure that it was included appropriately in the calculation of areas and moments of inertia about each of its axes. The dimensions of the piles were manually entered in accordance with the AISC

Manual for Steel Construction (AISC 2011) and the piles were assigned as A992 Grade 50 steel. An isometric view of the SAP 2000 model of the Macon County Bent including the overall geometry can be seen in Figure 6-1.

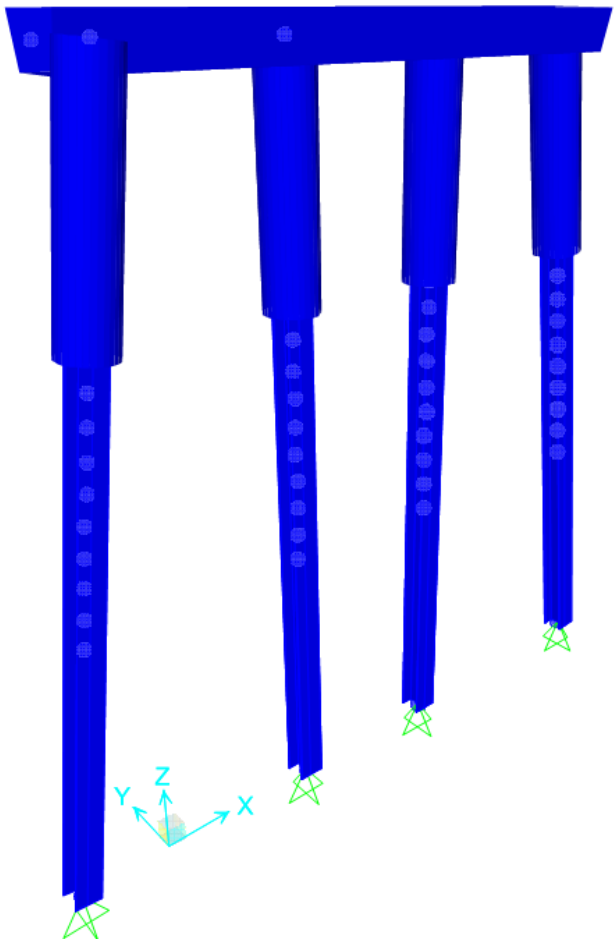

Figure 6-1 SAP Model Geometry for Macon County Bent

The model for the US 331 Bent was built similarly to the Macon County Bent. The overall geometry of the bent was built, and then the frame elements were designated their appropriate material and section properties. The trapezoidal cross section of the concrete bent cap was built using the section designer within SAP 2000 so that the exact geometry of the cap could be simulated. The depth of the encased piles was unknown, so an assumption as to how deep the piles were embedded into the ground had to be made. A typical embedment of the encasements is five

feet; therefore, this embedment was used in the SAP model. The encased pile sections were also built in the section designer. A 16 in. x 16 in. square concrete section was input first. A structural steel I-shape was then placed on top of the square concrete section. The depth, flange width, flange thickness and web thickness of the steel section were taken from the section properties listed for an HP10x42 in the AISC Manual for Steel Construction. For the pile depth below the encased pile section, the HP10x42 section from the AISC 14 pro database within SAP 2000 was used. After the pile sections were input, the local axes of the piles were rotated 90 degrees so that the piles would be loaded about the axis they were loaded during the load tests. An isometric view of the overall geometry of the model for the US 331 bent can be seen in Figure 6-2

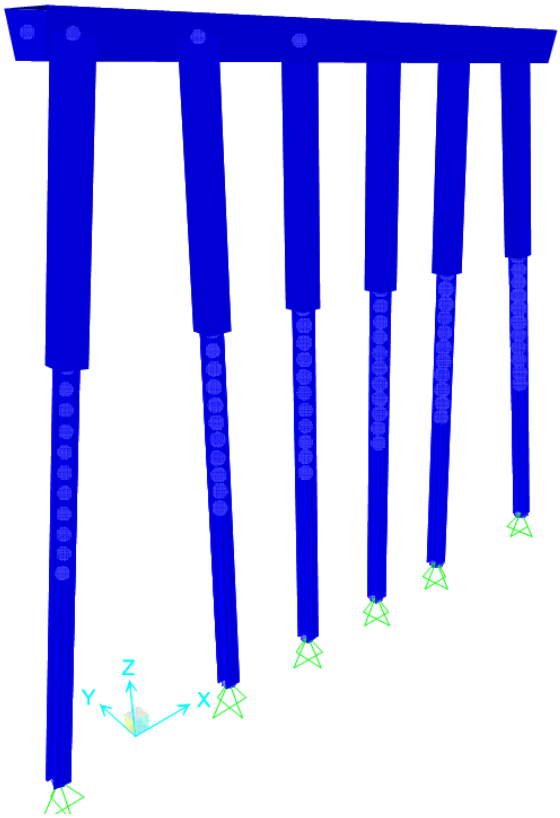

Figure 6-2 SAP Model Geometry for US 331 Bent

6.4 Modeling of Soil Interaction

To approximately model the interaction between the piles and the soil, linear springs were applied at discrete locations along the length of the piles. The properties of these springs were dependent on the soil properties at different pile depths. Prior to each of the load tests, preliminary models were developed in FB Multipier in order to determine maximum loading targets that would result in an acceptable deflection that would not cause permanent damage to the steel piles, the encasements or the overall bent itself. The preliminary models created in Multipier considered soil properties, concrete encasement and embedment depth into the concrete bent cap. An image of the preliminary models for the Macon County Bent and the US 331 Bent can be seen in Figure 6-3 and Figure 6-4 respectively.

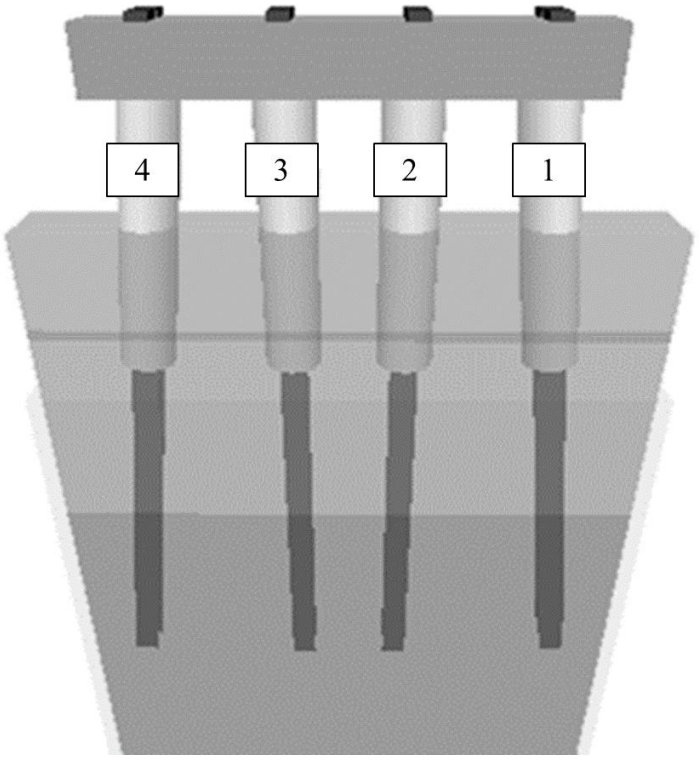

Figure 6-3 Preliminary FB Multipier Model of Macon County Bent (Skinner 2015)

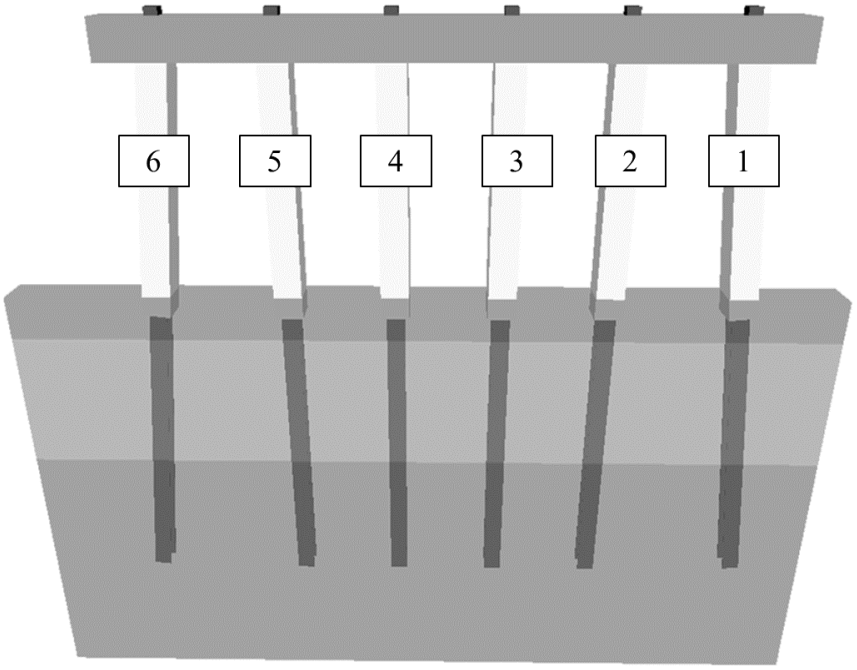

Figure 6-4 Preliminary FB Multiper Model of US 331 Bent (Skinner 2015)

The FB multipier model consisted of soil data taken from boring logs from design drawings of the bridges. Soil layers were input into the model at the elevations determined from the boring logs. Each soil layer contains its appropriate properties, as seen in Figure 6-5 and Figure 6-6.

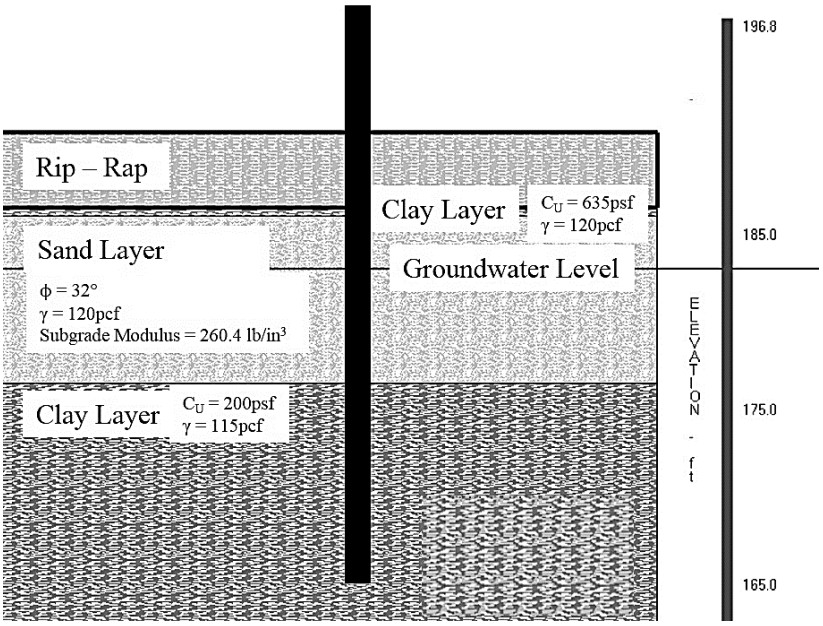

Figure 6-5 Macon County Bent Soil Profile (Skinner 2015)

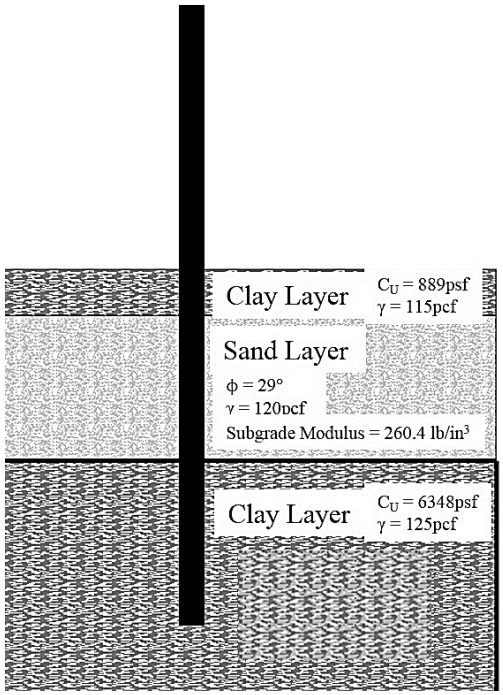

Figure 6-6 US 331 Bent Soil Profile (Skinner 2015)

The springs were applied to simulate lateral resistance of the soil in the X-direction, which was the direction of loading for the bent models. The magnitudes of these springs were input with units

of kips/in. at locations along the lengths of each of the piles. The springs were determined by taking the shear force from the FB-Multipier model in the pile at a given depth and dividing it by the lateral displacement of the pile at that particular depth. The lateral displacement was essentially equal in each of the piles at every load increment; therefore it was deemed adequate to take an average of the spring magnitude for each pile and apply that spring magnitude to all piles at each location along the length of the pile. The first spring was placed at ground level and springs were placed in roughly one foot intervals along the remaining pile length. A summary of the average soil spring constants used for the Macon County test and the US 331 Bent can be seen in Table 6-1 and Table 6-2.

Table 6-1 Macon County Bent Spring Constants

Depth (ft.)	Average Spring Constant (k/in.)
10.78*	144.5
12.11	137.8
13.44	92.4
14.78	27.1
16.11	131.2
17.44	703.3
18.77	1742.2
20.1	3243.8
21.44	659.4
22.77	353.4
24.1	682.7
25.43	35.9
26.76	24.4
28.1	256.4
29.43	4.41
30.76	2.72

*Indicates average ground surface not including 5 feet of rip-rap

Table 6-2 US 331 Bent Spring Constants

Depth (ft.)	Average Spring Constant (kip/in.)
12*	47.5
13	53.9
14	25.7
15	256.2
16	6541.3
17	974.6
18	387.8
19	110.8
20	77.2
21	67.3
22	66.8
23	289.3
24	485.7
25	75.6
26	49.5

*Indicates average ground surface

6.5 Loads

Loads applied to the models created for the Macon County Bent and the US 331 Bent to simulate the actual loads applied during the load tests. Static loads were applied to the Macon County Bent model to simulate the lateral load from the hydraulic cylinder. Due to the uncertainty of the lateral load transfer to other structural elements of the US 331 Bent, it was decided to perform a displacement-based analysis. Nodal displacements equal to the displacements measured during the field tests were applied to the US 331 bridge to simulate the lateral load applied by the hydraulic cylinders. In each of the models, the wheel loads from the load truck, and the self-weight dead load from the girders and bridge deck were simulated by applying static point loads applied at the girder locations. Three separate types of load pattern were created: Dead, Truck Live, and

Lateral. The dead load case consisted of the self-weight of the piles and bent cap, the girders framing into the bent, and the bridge deck. For the first load test on the Macon County Bridge, the deck weight was not included because the deck had not yet been cast. The truck live load case consisted of the wheel loads from the load truck. The truck wheel loads were applied as point loads at the girder locations. A deck strip was analyzed at each of the axle locations to determine the wheel load reaction on the each of the girders. The girders were then analyzed as a simple span beam to determine the reactions at the bent. The wheel load reactions for the center axle were not analyzed in a beam run, but applied directly to the bent since the center axle was positioned directly over the bent. Lateral load cases were developed for each lateral load increment for each of the tests. The lateral loads were applied as point loads at the centroid of the face of the bent cap.

For the test performed on the Macon County Bent prior to the deck being case, the only loads applied were the lateral load due to the hydraulic jacks and the self-weight reactions of the girders on either side of the bent. The self-weight of the girders was calculated using the cross-sectional area of a Type I AASHTO girder and multiplying that cross sectional area by 150 pcf to obtain an equivalent line load of 0.288 k/ft. This line load was by multiplied by 40 ft to account for the reactions from the girder on each side of the bent. A reaction of 11.52 kips was applied at each of the girder locations to simulate the girder self-weight. An image of the loading diagram of the first test performed on the Macon County bent can be seen in Figure 6-7. The soil springs along the length of the piles are graphically shown in this figure as well.

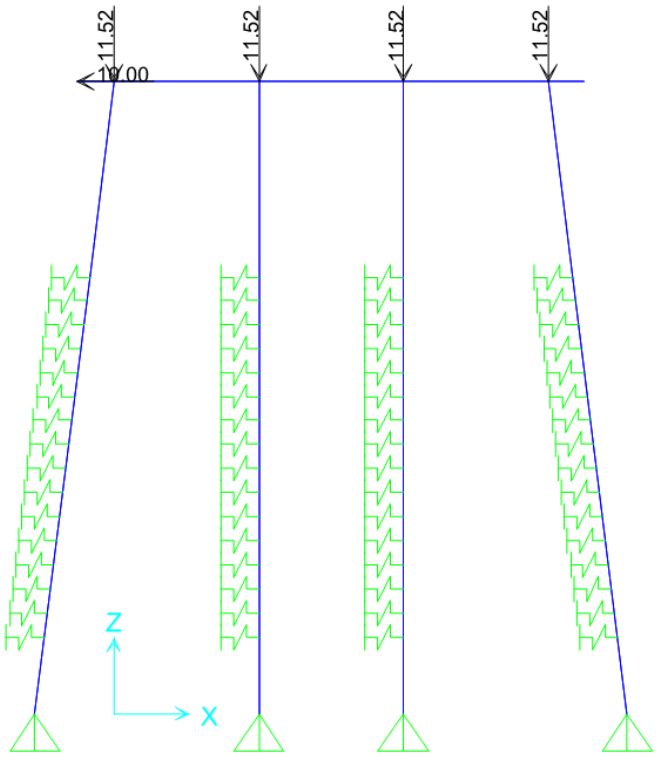

Figure 6-7 Loading Diagram for First Macon County Test

Additional loads needed to be applied for the second load test performed on the Macon County Bent. The weight of the bridge deck needed to be accounted for in this test. The deck load is transferred to the girders then the girders transfer the load to the bent at the bearing pad location. To correctly model this load transfer, point loads were applied at the girder locations. The deck loads were applied by taking the deck cross-section and converting it into an equivalent line load on each of the girders based on their tributary width. The deck cross section provided in the design drawings was used in order to determine deck thicknesses used in self-weight calculations as well as tributary widths used for the girder analyses. The equivalent line loads were then multiplied by the girder span to account for the reaction from the girders on the forward and back spans of the bent. The self-weight deck reactions applied were determined to be 20.77 kips at the exterior girders and 18.6 kips at the interior girders. The reactions are larger at the exterior girders due to

the deck thickening from 7 in. to 8 in. from the center of the exterior girders to the edge of the roadway at the location of the barrier.

The wheel loads from the load truck were also transferred from the deck to the girders to the bent. The centerline of the wheels of the load truck were not directly over the girders in either of the loading conditions where the load truck was on the bridge. A deck strip was first analyzed to determine the reactions on the girders in each of the truck positions. After these reactions were determined, they were applied to the girder at the location of the wheel axle. The point loaded girder was then analyzed as a simple span beam in order to determine the girder reaction on the bent.

The loads applied to the bent during each of the load test performed on the Macon County Bent with the deck in placed were assigned to different load patterns: dead, truck live, and lateral. Load combinations were built using the three different load patterns. Dead + Truck Live + Lateral was built for every lateral load increment. A summary of the girder point loads applied to the bent for each of the three tests performed on the Macon County Bent with the bridge deck in place can be seen in Table 6-3.

Table 6-3 Macon County Bent Loading Summary

Pile	P_{deck} (kips)	P_{girder} (kips)	$P_{truck\ centered}$ (kips)	$P_{truck\ at\ edge}$ (kips)
1	27.42	11.52	-1.65*	37.67
2	27.84	11.52	38.25	38.3
3	27.84	11.52	38.25	-3.53*
4	27.42	11.52	-1.65*	1.0

*Negative value indicates uplift reaction

Loads were applied to the US 331 Bent to simulate the loading conditions of the load tests performed. Similar to the Macon County test performed after the deck had been cast, self-weight loads, truck wheel loads, and static lateral loads were applied. Each of the gravity load cases were

applied as point loads at the girder locations. The method for calculating slab and girder self-weight was the same as the Macon County test, using tributary area of the girders to determine the girder reactions on the bent. The method for calculating girder reactions from the truck wheel loads was also the same as the Macon County test which consisted of analyzing a deck strip to determine the deck reaction on the girder then analyzing the girder to determine the girder reaction on the bent. All lateral loads were applied as static point loads applied at the centroid of the bent cap face. Load cases were created for self-weight, truck wheel loads, and lateral loads. Load combinations were created combining self-weight and truck loads with each of the lateral load increments. A summary of the girder reactions applied to the US 331 Bent can be seen in Figure 6-4.

Table 6-4 US 331 Bent Loading Summary

Pile	P_{deck} (kips)	P_{girder} (kips)	$P_{truck\ at\ edge}$ (kips)
1	22.54	9.79	0
2	19.24	9.79	0.1
3	19.24	9.79	-0.50*
4	19.24	9.79	1.87
5	19.24	9.79	40.45
6	22.54	9.79	26.87

*Negative value indicates uplift reaction

6.6 Analysis Results

The structural models were built in order to determine how well the models correlated with the results from each of the field tests. This section contains a detailed comparison of the results from the structural models created in SAP 2000 and the results from the field tests. Bending moments and cap deflections were used in order to determine how well the field test results correlated with the structural models.

6.6.1 Macon County Bent Without Deck

Bending moments and deflections from the SAP model of the Macon County bent without the bridge deck are compared to the bending moments and deflections from the field test in this section. The model for this test consisted of nine different lateral load cases from 10 kips to 75 kips, simulating the same loading conditions from the field test. The bent behavior from the SAP model correlated well with the field test results. The maximum cap deflection was within 12 percent of the maximum deflection predicted in the model. The deflected shape of the bent model at a scale factor of 200 can be seen in Figure 6-8. The figure depicts the deflected shape at the 75 kip load increment; however, the overall deflected shape of the structure remained the same for each loading increment.

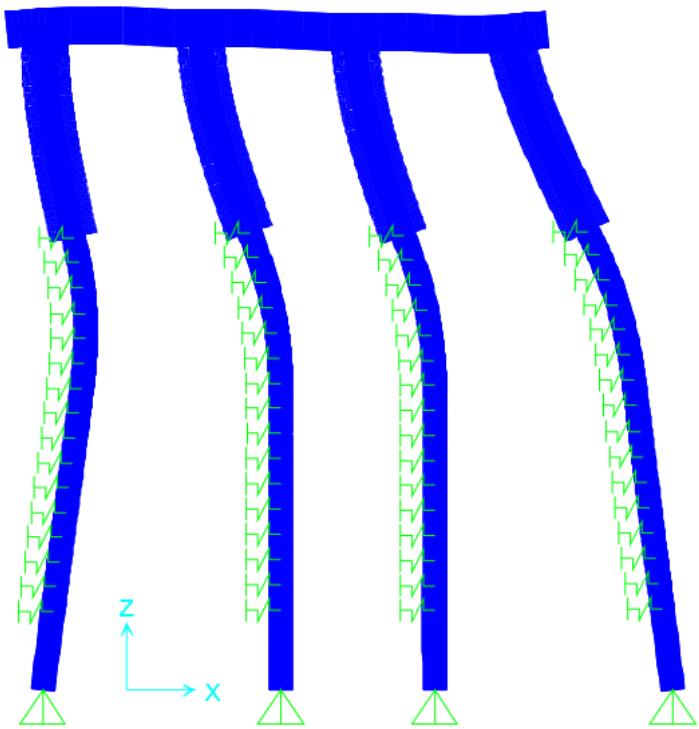

Figure 6-8 Macon County Bent with no Deck Deflected Shape at 75 kips

The bending moment diagrams from the SAP model for each of the piles at the 75 kip loading increment can be seen in Figure 6-9. Notably, the interior piles appear to take roughly 25 percent more moment than the exterior battered piles. The inflection point for each of the piles occurs at

or near the location of the ground surface specified in the model by the first soil spring. The rip-rap was not included in models created in FB Multipier by Skinner (2015); therefore it was not included in the SAP model. The comparison of the results shows the location of the inflection points to slightly vary between the field test and the model. The moment appears to dissipate around a depth of 20 feet for each of the piles in the model and actually reverses curvature a second time, though the moment magnitudes are seemingly negligible at these depths.

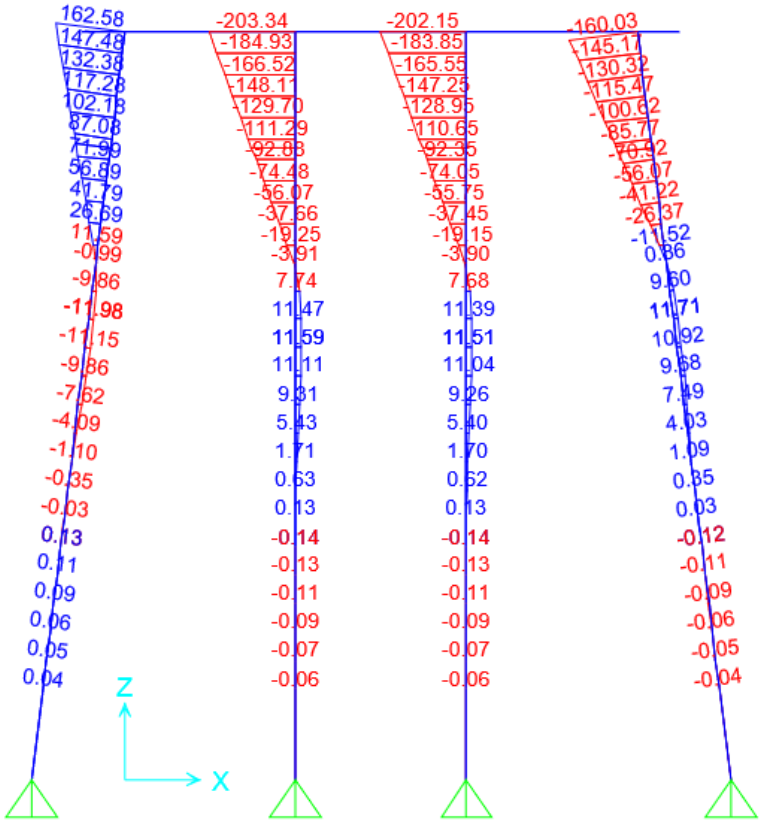

Figure 6-9 Macon County Bent with no Deck Moment Diagram at 75 kips

The moment diagrams for each of the four piles from the SAP model can be seen in Figure 6-10 through Figure 6-13. The data points from the calculated experimental results are also shown on these plots. For every pile with the exception of pile 4, the SAP model predicted higher magnitudes of bending moment than the calculated values. The field test bending moments

correlated well with the moments predicted in the SAP model aside from pile 1. The moments at the lowest instrumented section were very small relative the moments above grade due to the termination of the pile encasements. The location of the inflection point varied between the SAP model and the field test results. This variation of inflection point locations can be attributed to the exclusion of the rip-rap, which may provide a considerable amount of lateral resistance. The amount of lateral resistance provided by the rip-rap layer is highly uncertain which is why it was not accounted for in the model. Although the lowest instrumented section moment was calculated to be positive from the field test result and negative in the SAP models, it is clear that this instrumented section was near the inflection point of each of the piles.

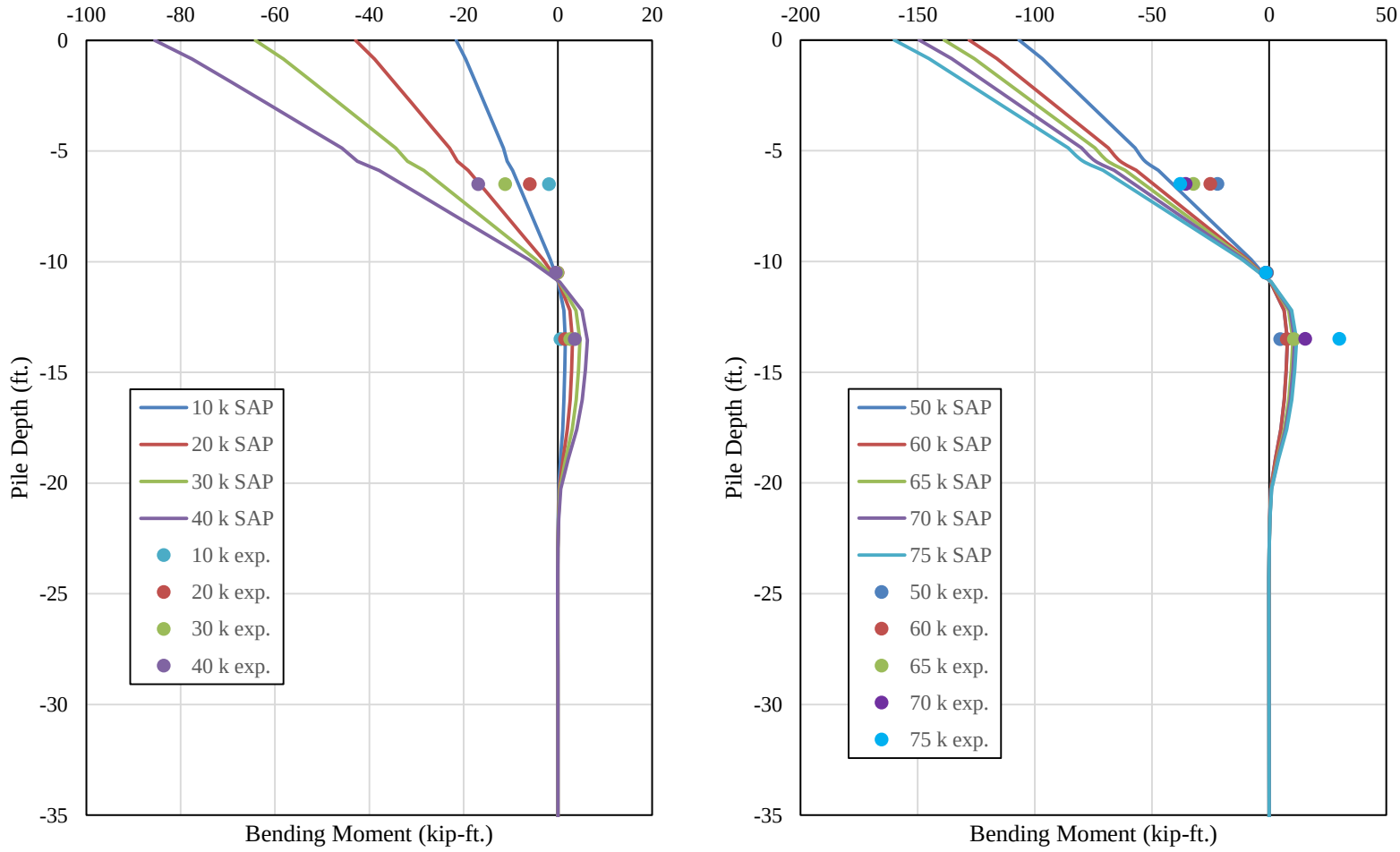

Figure 6-10 Pile 1 Bending Moment Comparisons

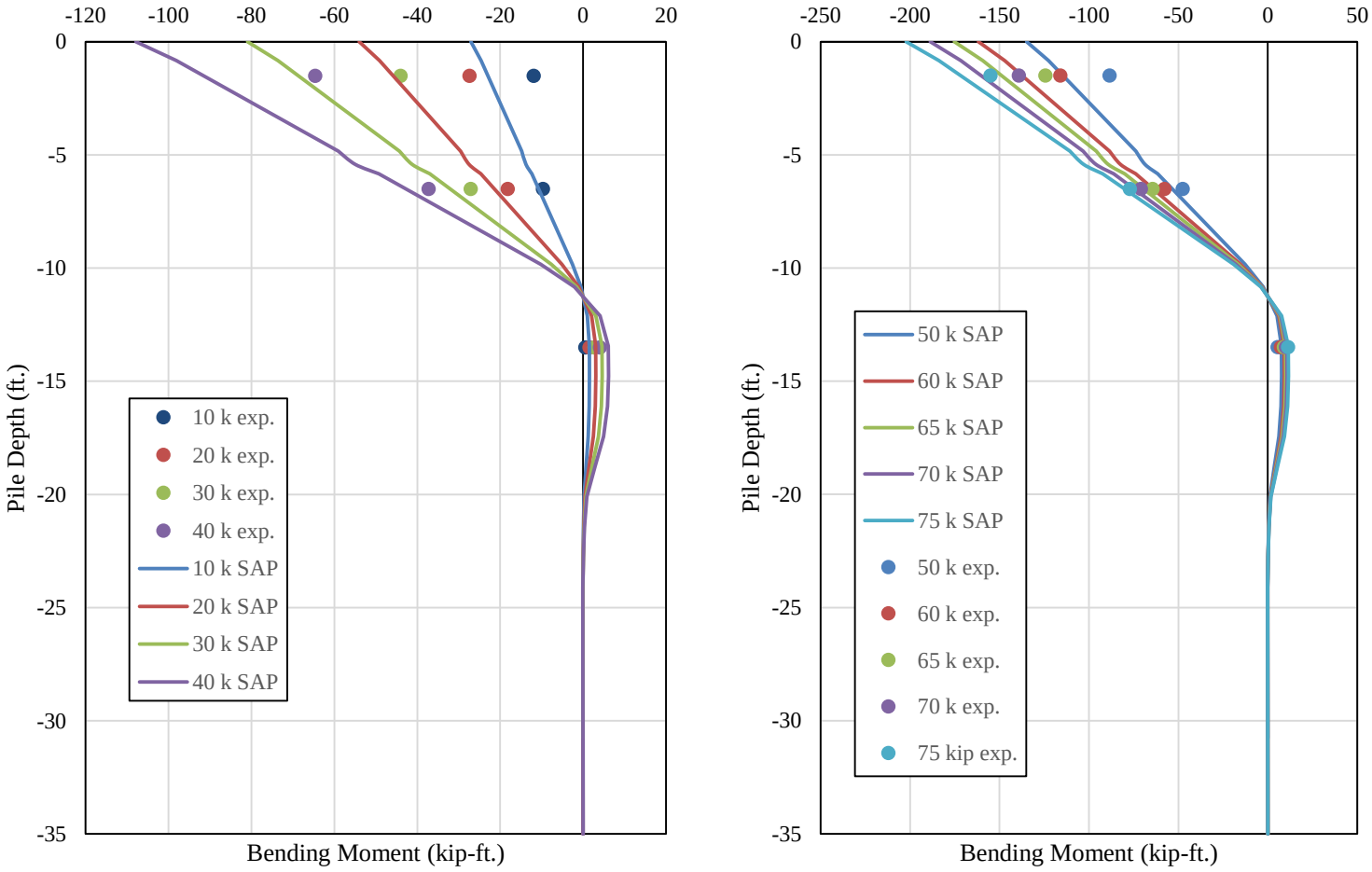

Figure 6-11 Pile 2 Bending Moment Comparison

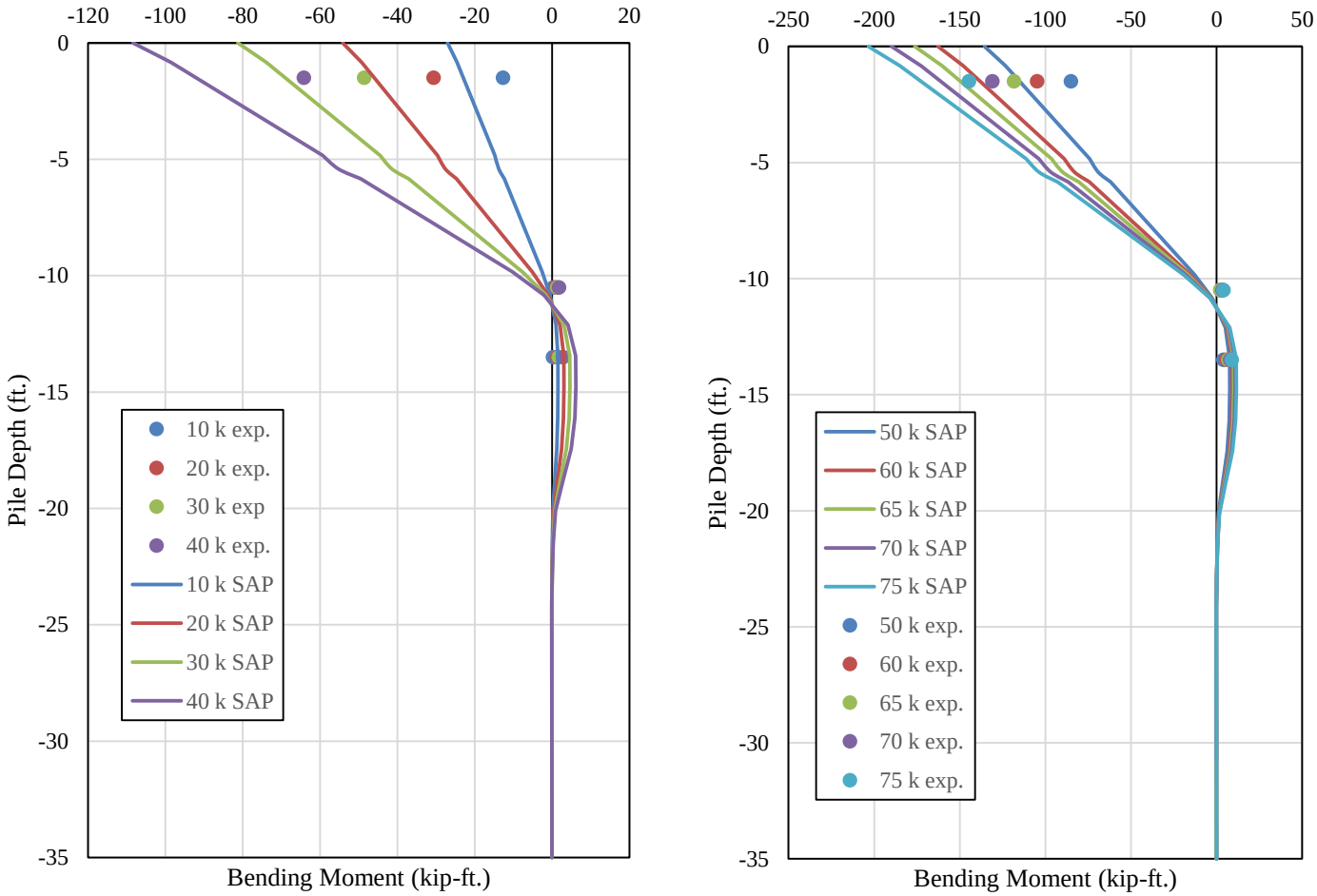

Figure 6-12 Pile 3 Bending Moment Comparison

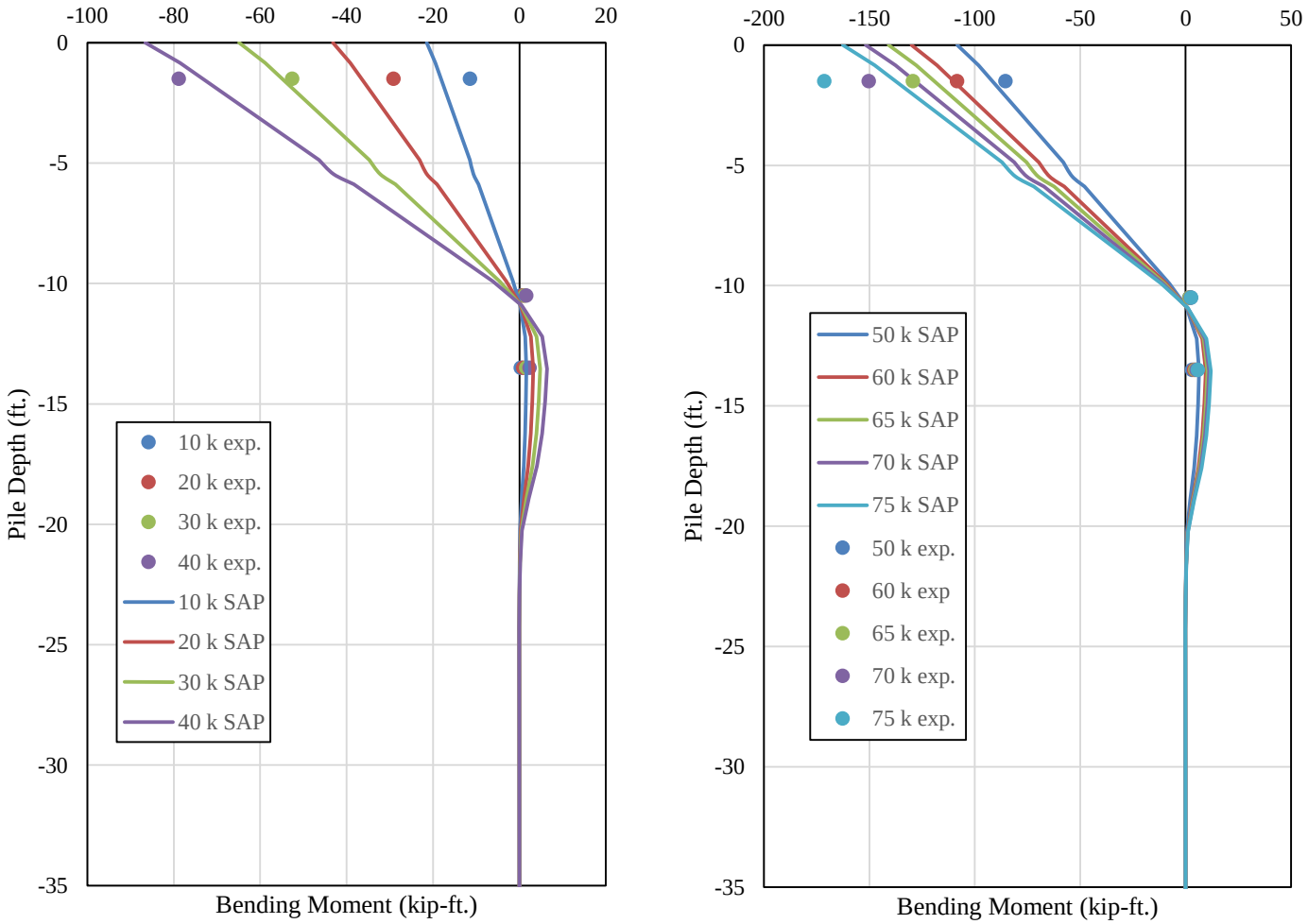

Figure 6-13 Pile 4 Bending Moment Comparisons

Axial forces versus lateral load for the lateral load cases from the SAP model are shown in Figure 6-14 through Figure 6-17. The axial forces shown in the figures below are from the lateral loads only, not including any self-weight of the structure. The axial force diagrams are constant over the length of the piles; therefore the axial forces are plotted against the applied lateral load as opposed to depth. Due to the large cross-sectional area of the encased pile sections, axial loads computed from measured strains were deemed to be unreliable and were not reported on. However, the axial force in the piles under the lateral load cases is of interest to designers. Most notably, the exterior battered piles carry the largest axial forces due to their batter. The interior pile axial forces are roughly 25 percent of the axial forces in the exterior battered piles. The leading pile has a compressive axial force and the leading pile has a tensile axial force which is to be expected due to the bent wanting to overturn under lateral loading. The magnitudes of these compressive and tensile forces are equal and opposite in sign.

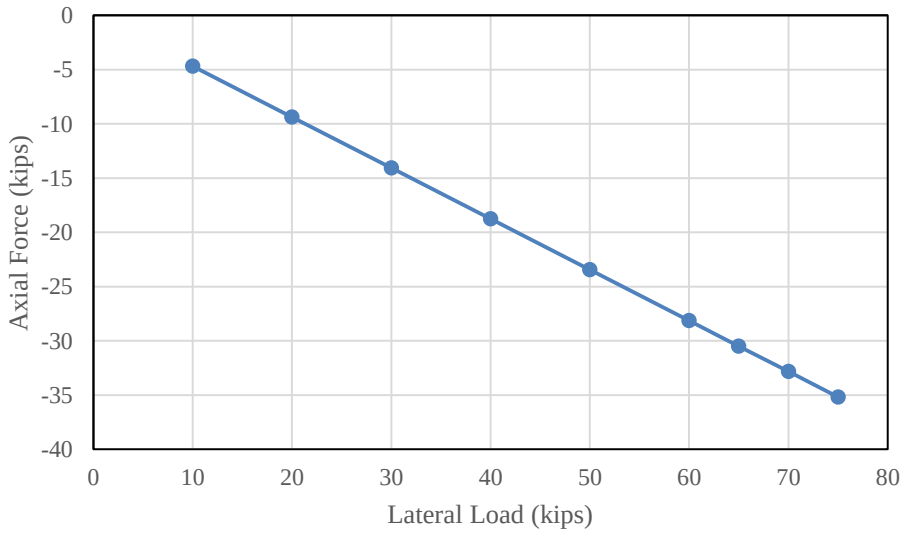

Figure 6-14 Pile 1 Axial Load versus Lateral Load

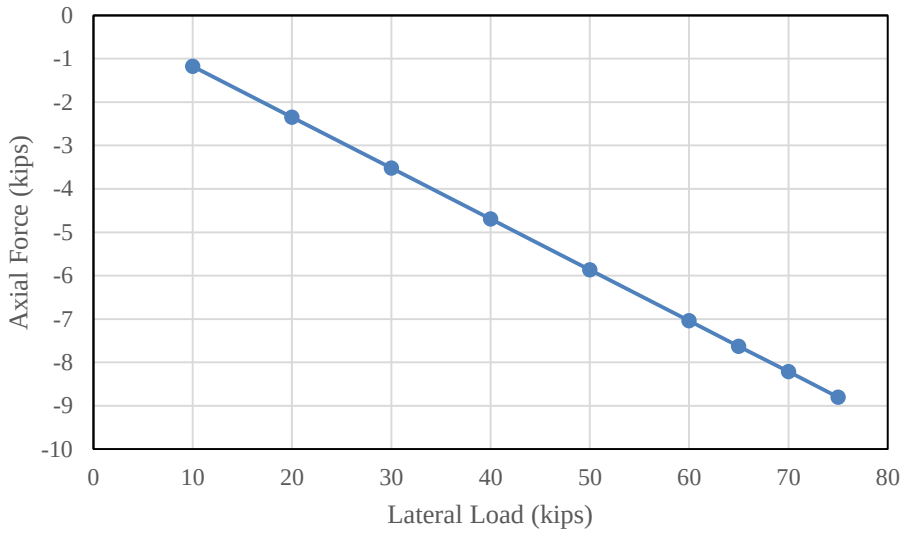

Figure 6-15 Pile 2 Axial Load versus Lateral Load

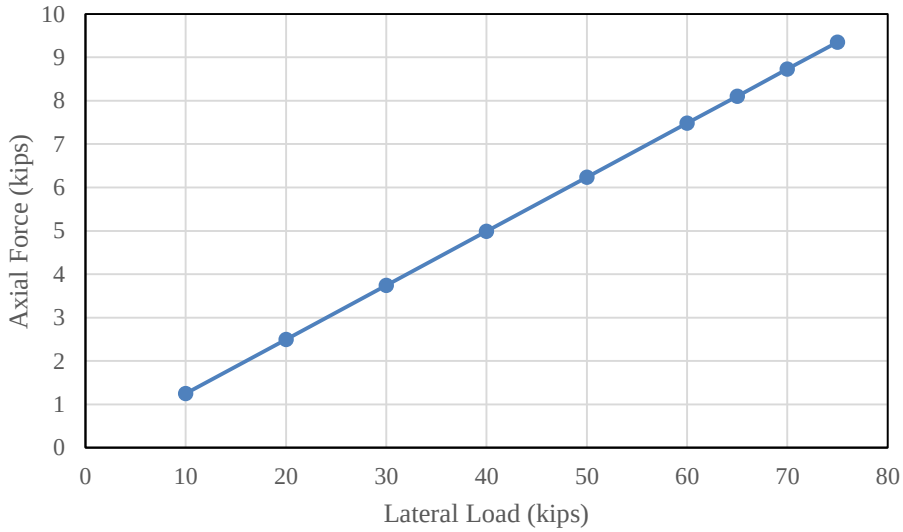

Figure 6-16 Pile 3 Axial Force versus Lateral Load

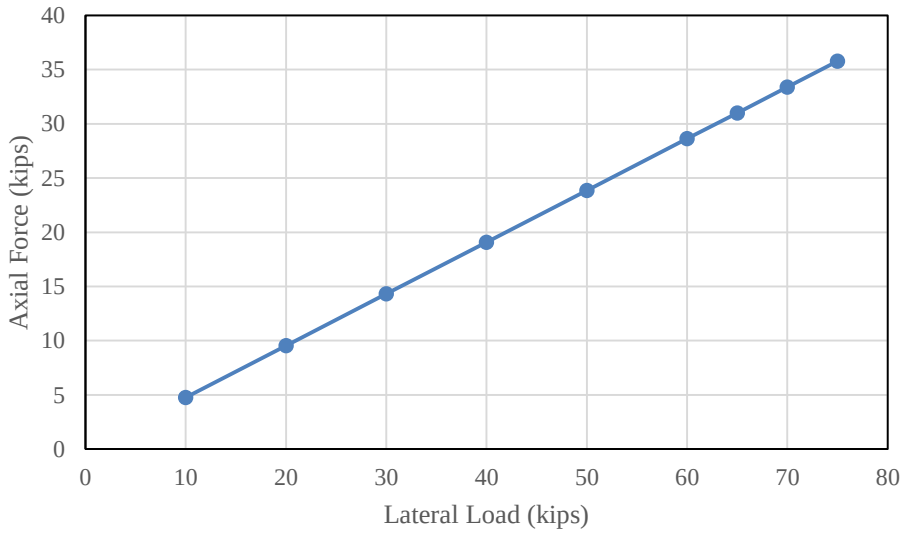

Figure 6-17 Pile 4 Axial Force versus Lateral Load

The load versus deflection from the Macon County test compared to the load versus deflection predicted from the SAP model can be seen in Figure 6-18. The model deflection was compared to the average deflection from the four wirepots used in the field test. The load-deflection responses from the field test and the SAP model correlated well throughout the majority of the load increments. The load-deflection from the SAP model is linear due to a linear elastic analysis being performed. The load-deflection from the field test is relatively linear with virtually no deflection at the 10 kip increment. This small amount of deflection could be due to the loading apparatus initially setting in, creating a small load effect at this increment. The deflection appears to increase linearly starting at the 10 kip increment throughout the rest of the test. The maximum deflection at 75 kips from the SAP model was within 12 percent of the average deflection from the field test.

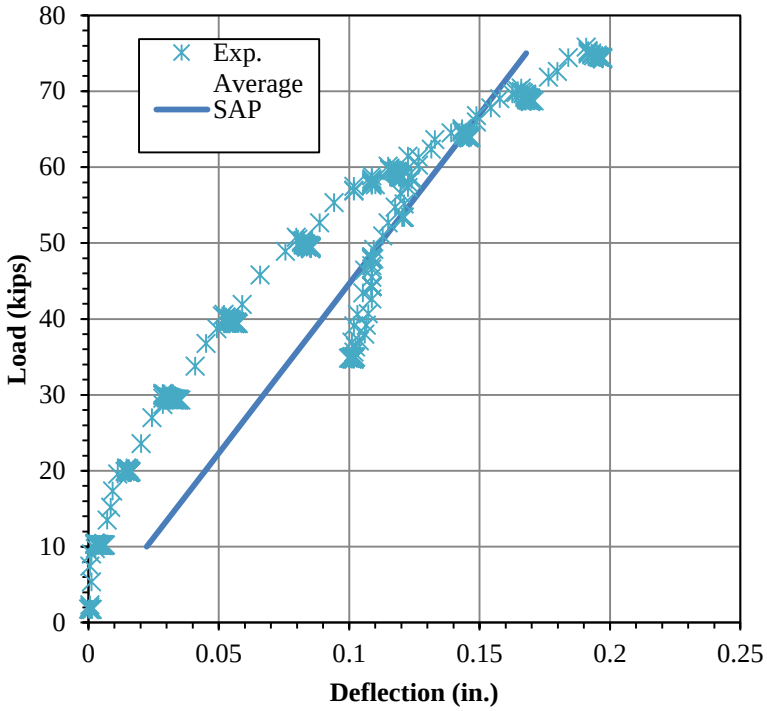

Figure 6-18 Load Deflection Comparison from Macon County Test with no Bridge Deck

6.6.2 Macon County Test with Deck

The bending moments and deflections for each of the load tests performed on the Macon County bent after the bridge deck had been cast are compared to the results from the SAP model created for the bent in this section. For this model, the same frame elements used in the model from the first load test were used. The magnitude of the springs used in the model for the first test were used again in the model with the bridge deck. For the models created for the bent in which the bridge deck was in placed, the additional stiffness provided by the bridge deck needed to be accounted for. It was apparent from the field test results that a portion of the lateral load was distributed to structural elements other than the test bent. The decrease in deflection under the same lateral load with the deck in place suggests that some of the lateral load is transferred to the adjacent bents. The load-deflection data from the field tests were used to approximate the additional lateral stiffness of the bent due to the bridge deck transferring the lateral load to the

adjacent bents in the bridge. The primary objective was to provide additional means of stiffness in the model so that the deflections from the field test correlated well with the model deflections. A spring was applied at the face of the bent cap in which deflections were measured in the field test in order to account for the additional stiffness provided by the bridge deck. To determine the magnitude of this spring, an average overall lateral stiffness of the bent for the load test without the bridge deck and the load test with the bridge deck without the addition of the truck load was computed. This stiffness was computed by taking the lateral load applied and dividing it by the bent deflection at each loading increment for each of the tests. The difference in these values was used as the applied spring for the bent model to account for the stiffness of the bridge deck. The overall stiffness of the bent without the bridge deck was determined to be 385 kip/in. and 588 kip/in. for the bent with the bridge deck. Therefore a spring with a magnitude of 203 kip/in. was applied to the node at the face of the bent cap on the trailing pile end (Pile 1).

A comparison of the bending moments from the SAP model and the field test results can be seen in Figure 6-19 and Figure 6-20. Due to the large variation in strains during the tests, the gages on Pile 1 were considered to be unreliable. Therefore, the field test results for Pile 1 are excluded from the figures below. Similarly to the results from the bent without the bridge deck, the SAP model predicted higher bending moments in each of the piles with the exception of pile 4. The results from the field test correlate well with the SAP model with the exception of the lowest gage on pile 3, in which the bending moments calculated from the field test results are significantly higher than the moments predicted from the SAP model.

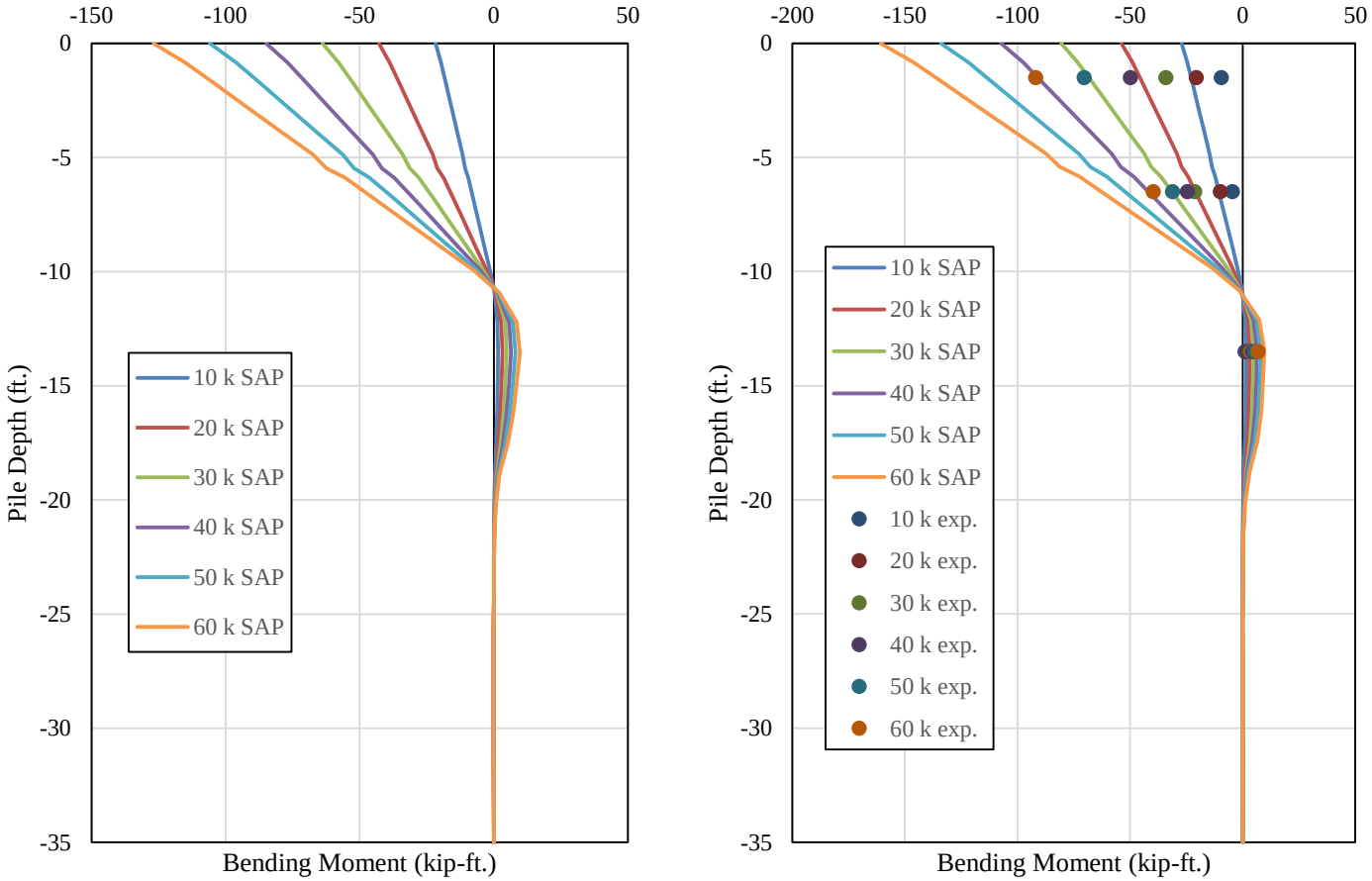

Figure 6-19 Pile 1 & 2 Bending Moment Comparisons with no Load Truck

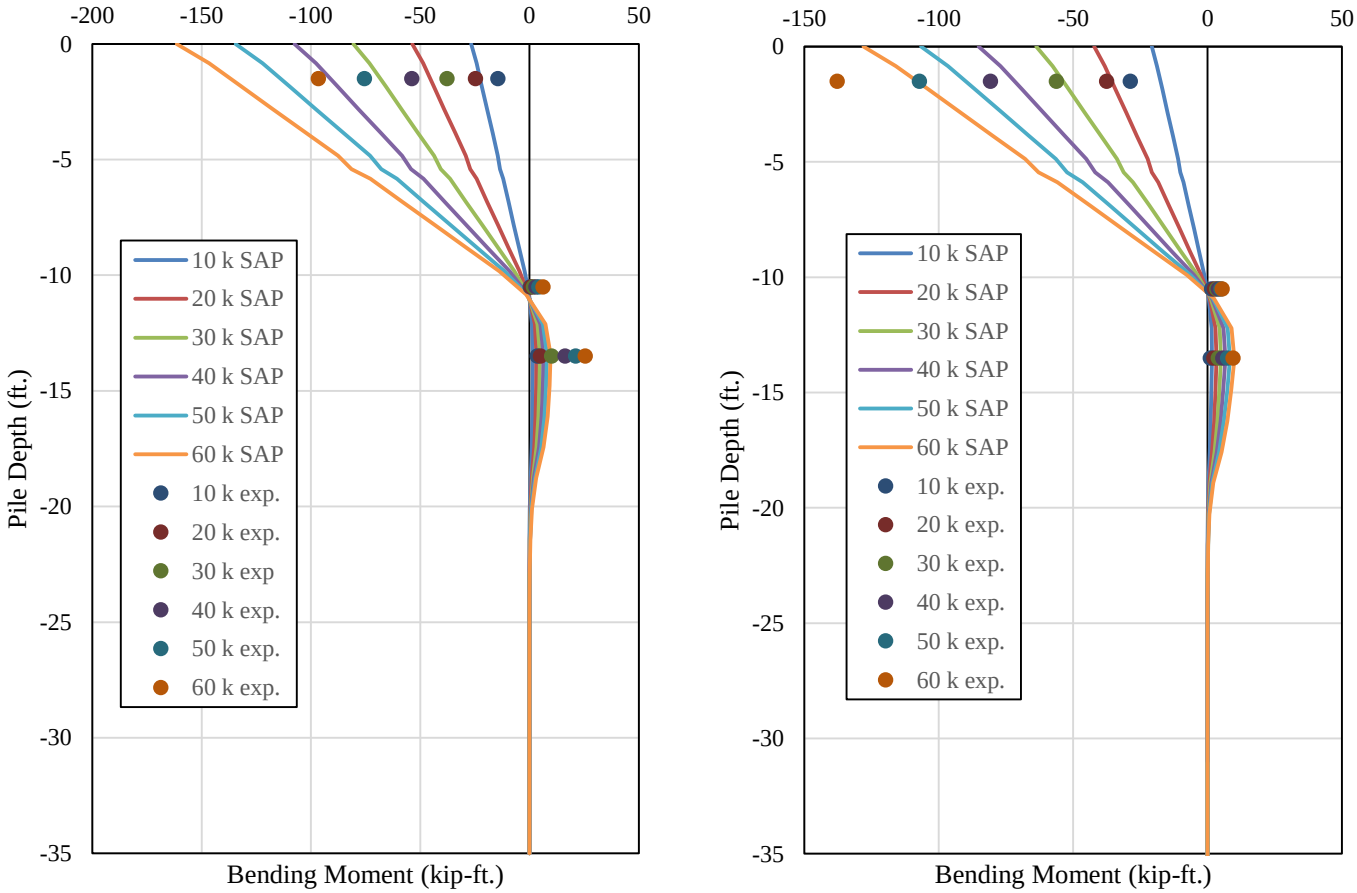

Figure 6-20 Pile 3 & 4 Bending Moment Comparisons with No Load Truck

The moments from the load test with the load truck centered over the roadway are compared to the moments predicted from the SAP model in Figure 6-21 through Figure 6-24. The results from the field test for Pile 1 are not included in these figures again. The SAP model predicts higher bending moments in each of the piles with the exception of Pile 4. Notably, the bending moment diagram from the SAP model for Pile 1 under the 10 kips loading increment predicted the location of the inflection point to be significantly higher than each of the other piles in the bent. Overall, the results from the field test correlated well with the results from the SAP model with the bending moment values varying from the field test by lower than 5 percent in some instrumented sections to as high as 40 percent. The lowest instrumented section in Pile 3 showed bending moment magnitudes significantly higher than the predicted values from the SAP model. However, the magnitude of these bending moments at this location is small relative to the bending moments at sections above grade.

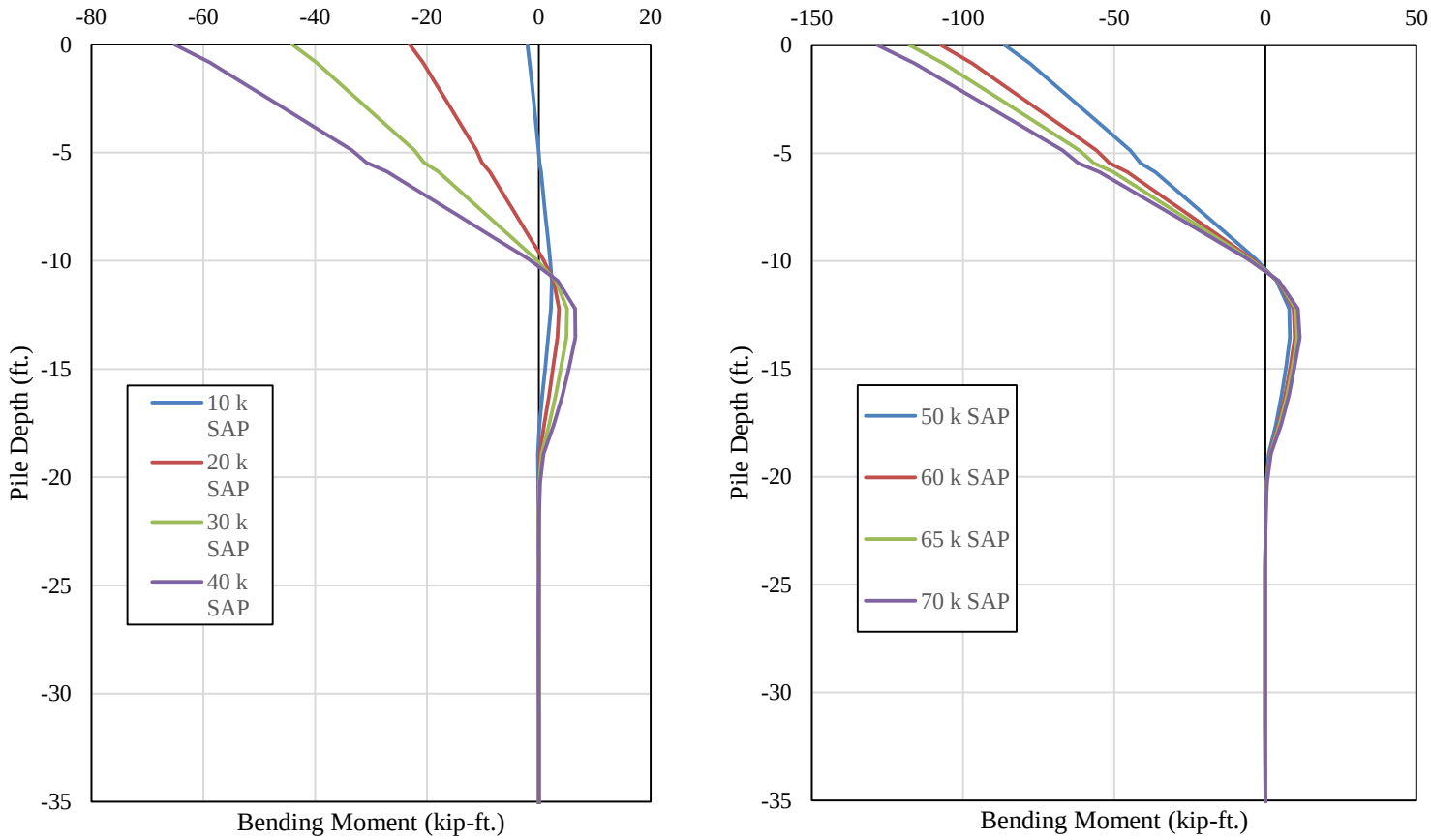

Figure 6-21 Pile 1 SAP Bending Moment Profiles with Load Truck Centered on Roadway

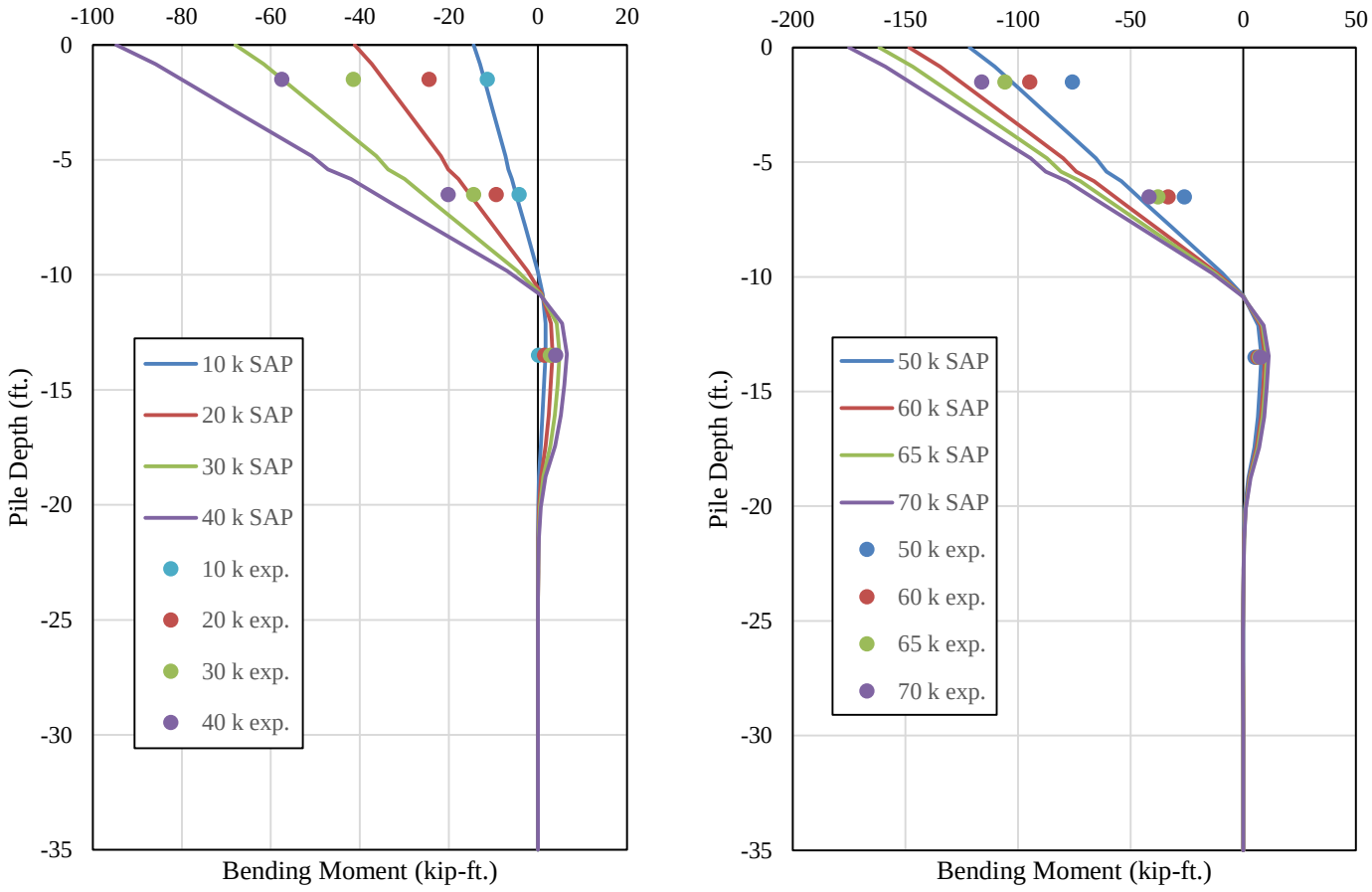

Figure 6-22 Pile 2 Bending Moment Comparisons with Load Truck Centered on Roadway

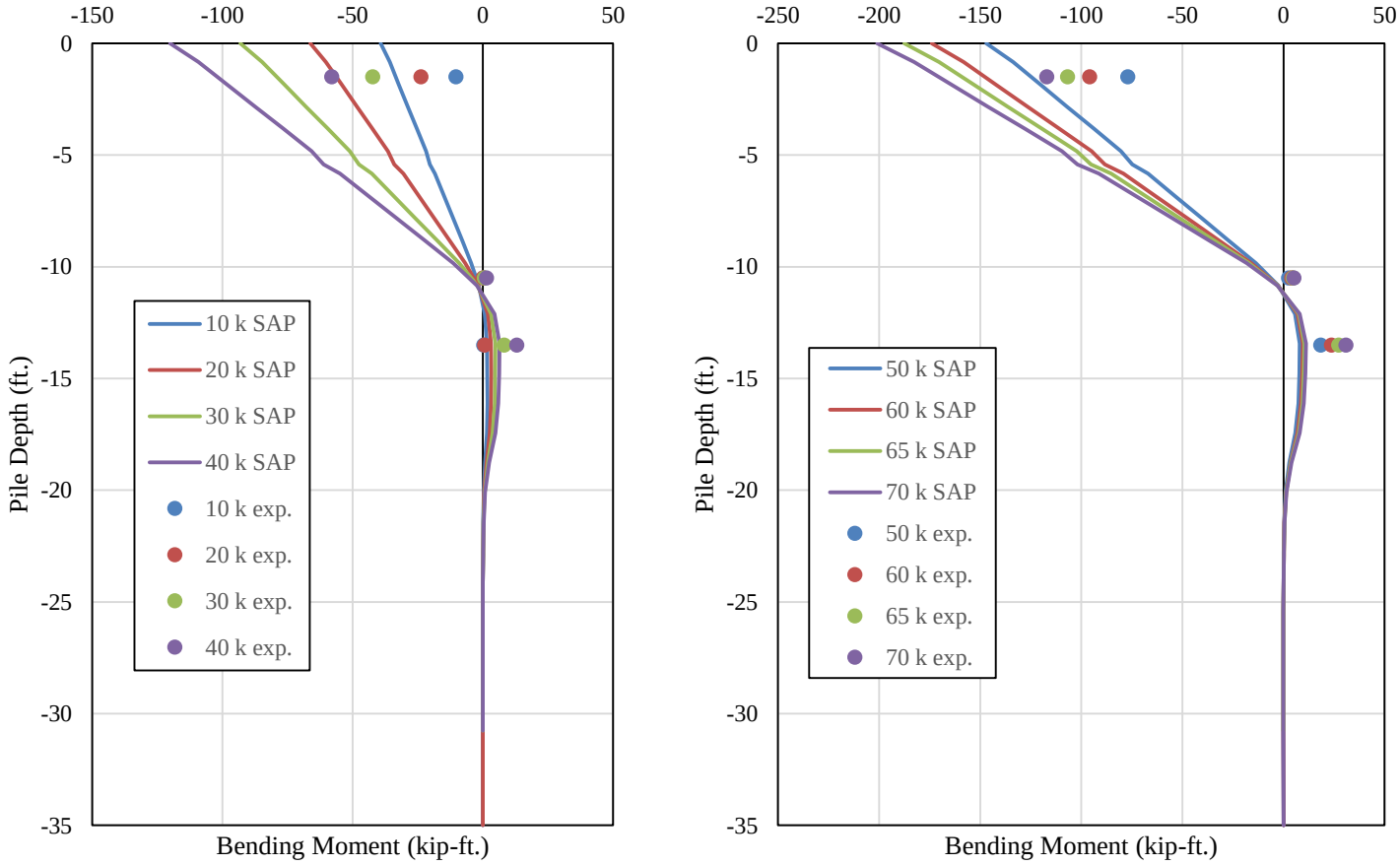

Figure 6-23 Pile 3 Bending Moment Comparisons with Load Truck Centered Over Roadway

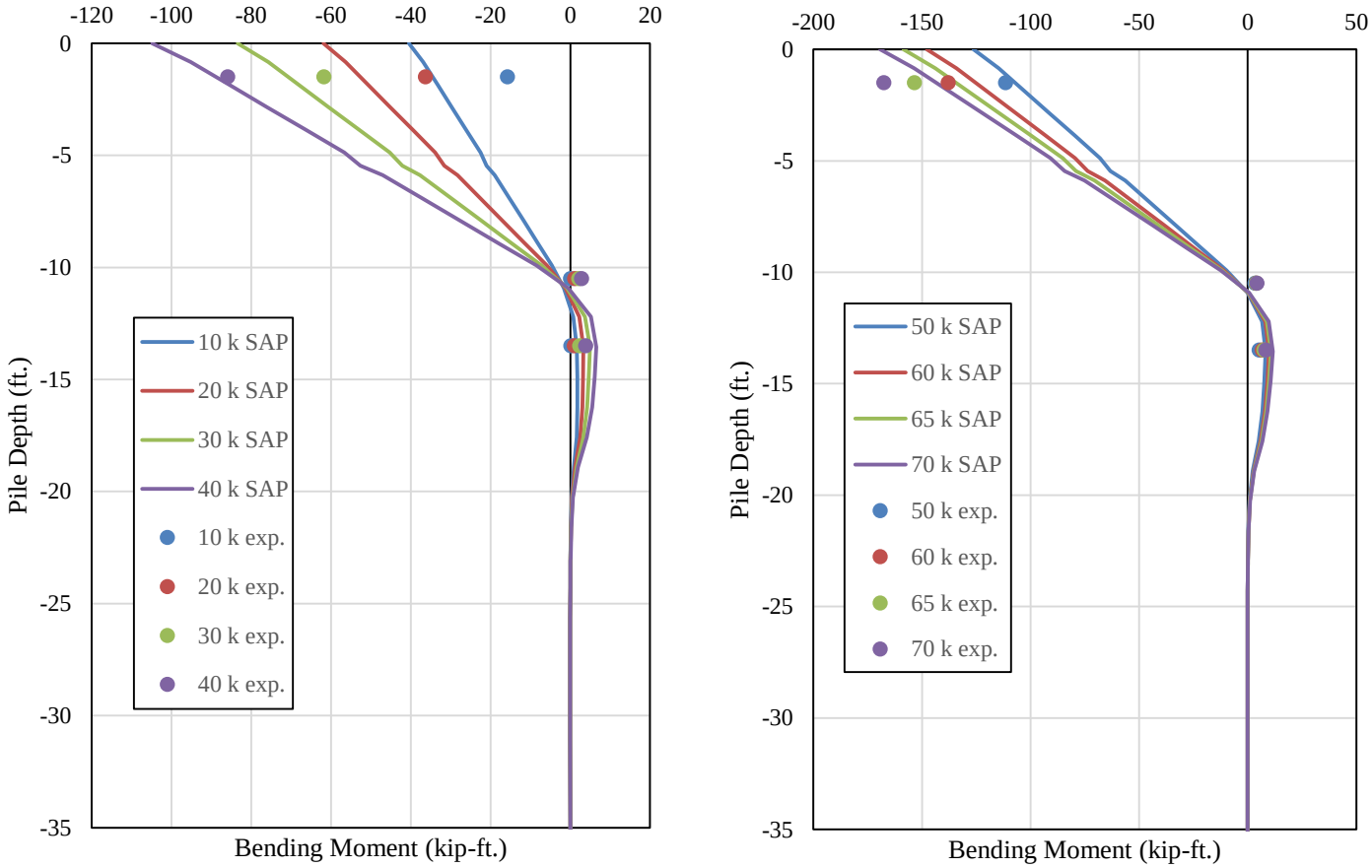

Figure 6-24 Pile 4 Bending Moment Comparisons with Load Truck Centered Over Roadway

The results from the load test with the load truck positioned at the edge of the roadway compared to the results from the SAP model can be seen in Figure 6-25 and Figure 6-26. The bending moments from the field tests compared to the bending moments from the SAP model shows the same trend as the previous test with higher predicted moment values from the SAP models with the exception of Pile 4 under higher loading increments. Results from the field test for Pile 1 are not included. Overall the results correlate well between the field test and the SAP model for lower load levels with the results from Pile 4 correlating significantly better at all load levels. The bending moments at instrumented sections were within 10-30 percent of the predicted values from the SAP model. The model predicted higher bending moments in the interior piles with smaller bending moments in the exterior piles. The results from the field test show bending moment values that are relatively similar for each of the piles, with the largest moment values occurring in Pile 4 which is the leading pile.

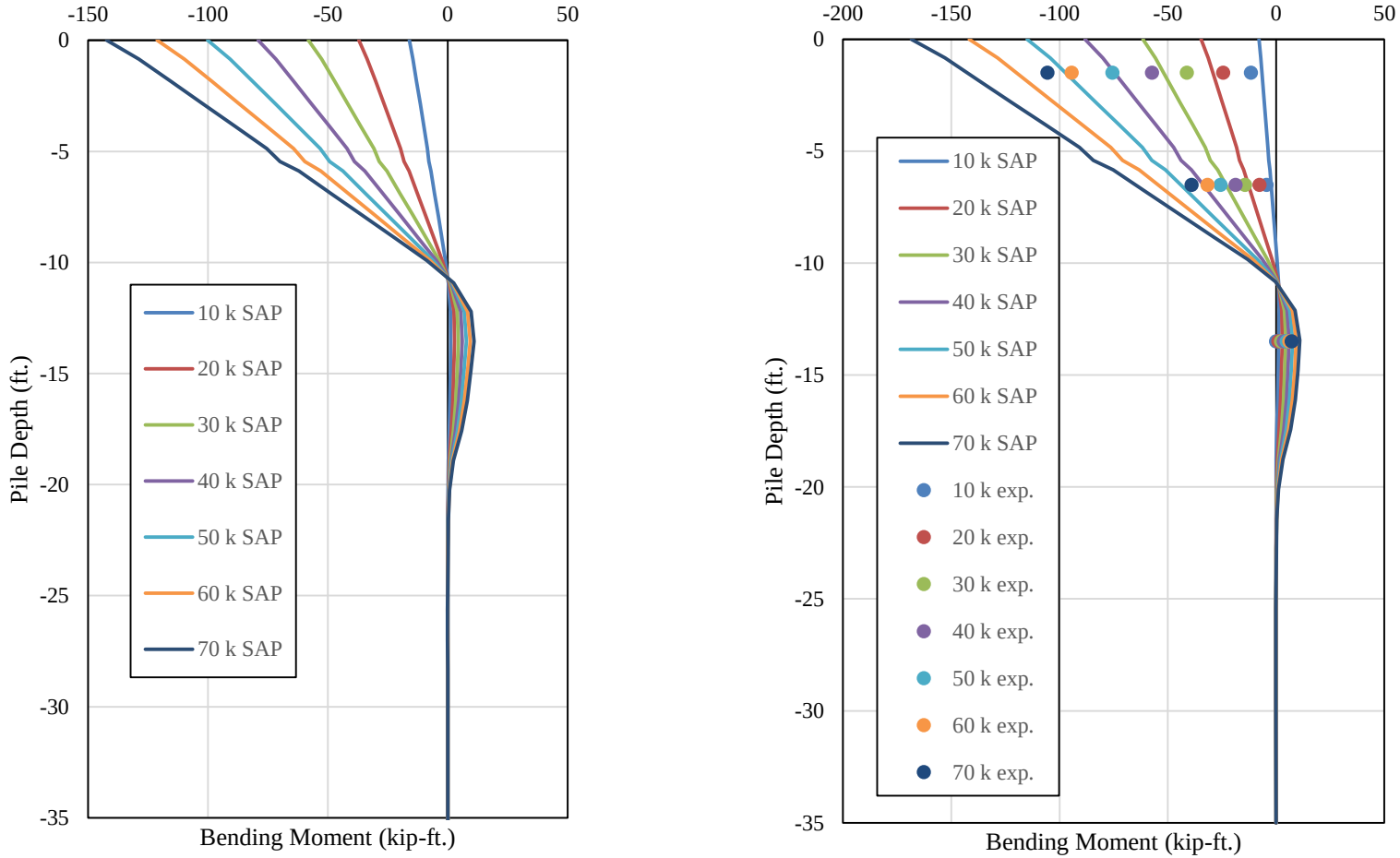

Figure 6-25 Pile 1 & 2 Bending Moment Comparisons with Load Truck Positioned at Edge of Roadway

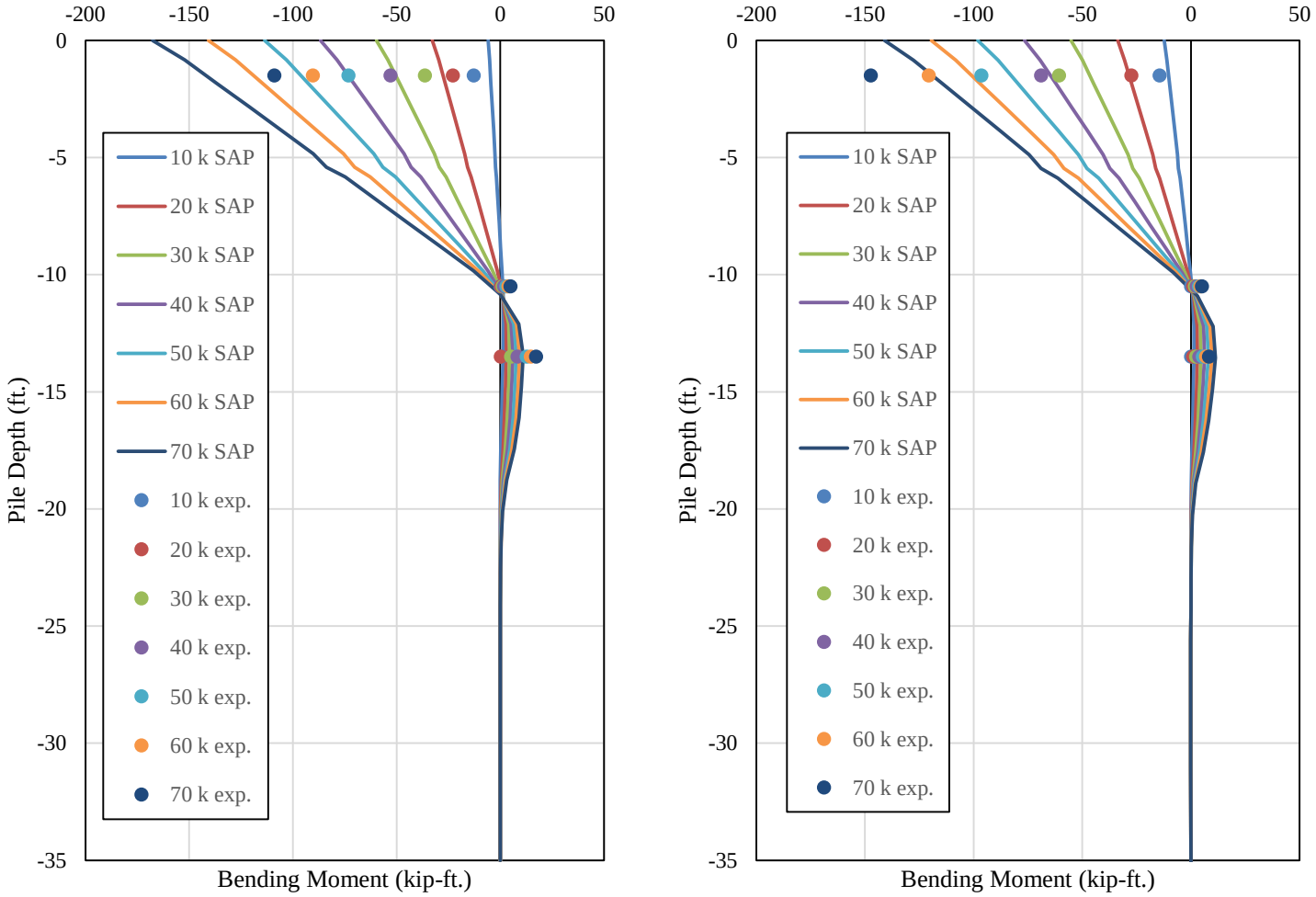

Figure 6-26 Pile 3 & 4 Bending Moment Comparisons with Truck Positioned at Edge of Roadway

Axial forces versus lateral load for each of the piles under the lateral load cases are shown in Figure 6-27 through Figure 6-30. Similarly to the axial forces plotted for the first Macon County test, the axial forces reported below are from the cases in which the lateral load was only applied. The self-weight of the structure and the wheel loads from the truck are not included in these plots. The axial forces are similar to the results from the model from the test without the bridge deck. The magnitudes of the axial forces are roughly 80 percent of the axial forces from the test without the bridge deck. This 20 percent loss can be attributed to a portion of the lateral load being transferred to other structural elements in the bridge. The overall bent behavior is consistent to the model from the first test with the exterior battered piles carrying larger axial forces than the interior vertical piles and the leading pile carrying a compressive axial force and the trailing pile having a tensile axial force. Similar to the load deflection response for the bent, the axial force appears to increase linearly with applied lateral force. This linear trend is due to no geometric or material non-linearity being specified within the model.

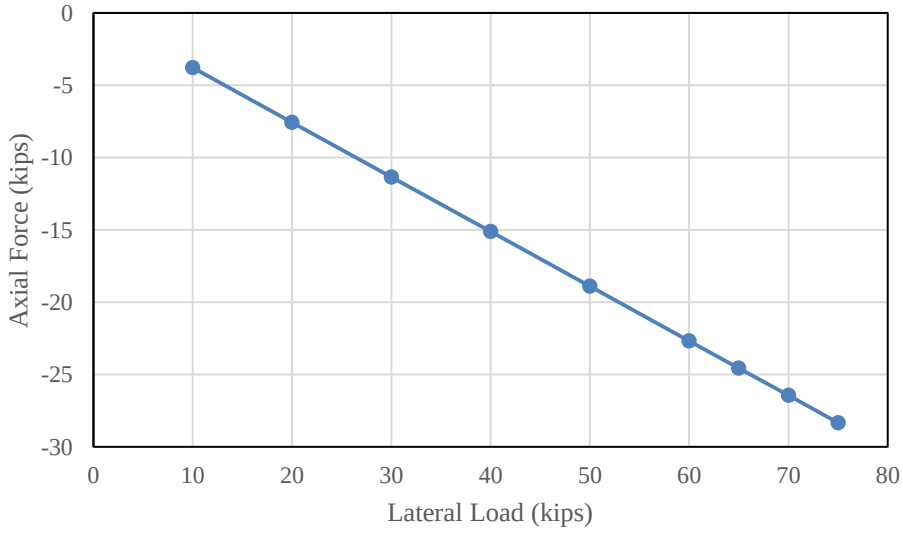

Figure 6-27 Pile 1 Axial Force versus Lateral Load

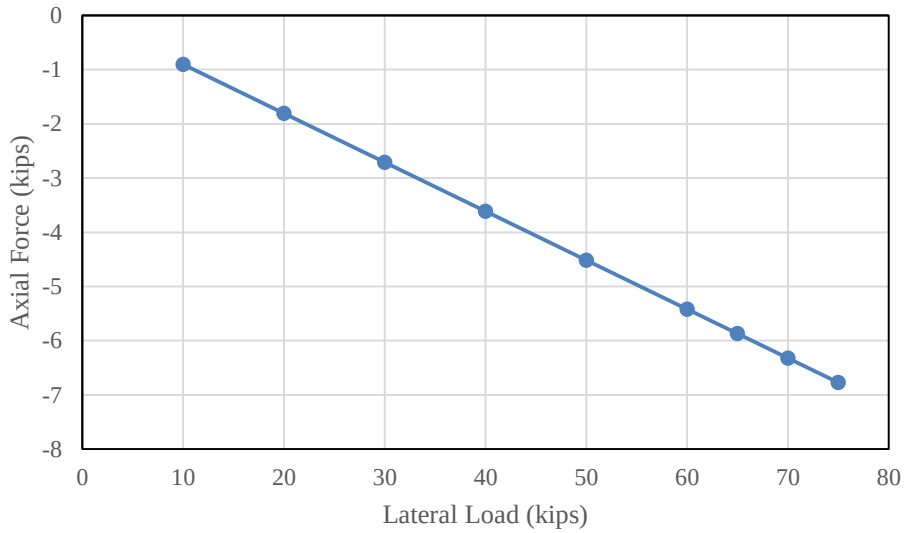

Figure 6-28 Pile 2 Axial Force versus Lateral Load

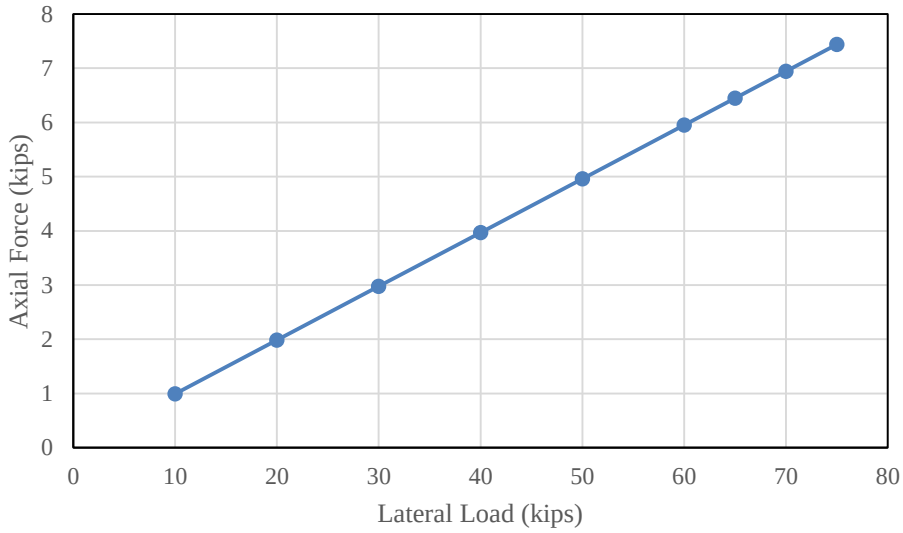

Figure 6-29 Pile 3 Axial Force versus Lateral Load

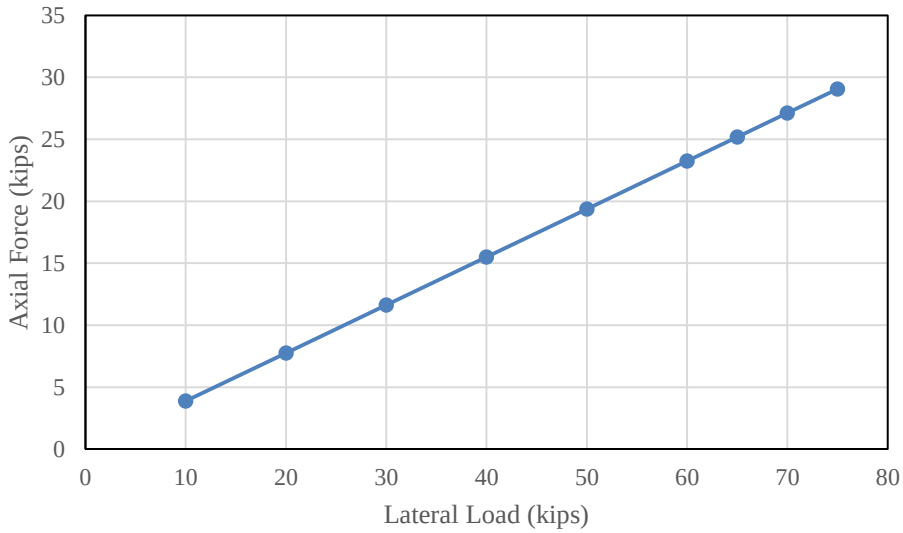

Figure 6-30 Pile 4 Axial Force versus Lateral Load

The objective of the SAP model was to provide a close correlation to the field results in terms of bent deflection. With the addition of the springs at the face of the bent cap, the deflection of the bent in the SAP model was 0.105 in. at the 60 kip loading increment with gravity loading simulating the condition without the load truck. The average deflection of the bent from the field test under these same loading conditions was 0.102 in., varying 3 percent from the predicted SAP deflection. The deflections from the field tests appear to be linear with the respect to applied load as shown in Figure 6-31; however the increase in deflection does not seem to begin until the 20 kip loading increment. The slopes of the load-deflection diagrams shown in Figure 6-31 appear to be very similar indicating the stiffness approximated in the model correlates well with the actual stiffness of the bent during the load tests. The SAP model predicts a linear load-deflection response which is to be expected. Notably, the deflections predicted by the SAP model do not vary significantly from the loading condition without the truck and with the truck centered over the roadway. However, the deflections are slightly smaller, roughly 5 percent, in the loading condition with the truck positioned at the edge of the

roadway compared to the other two loadings. The deflections from the field test were 10-15 percent greater in the test without the load truck compared to the both of the test with the load truck. These lateral deflections, however are very small in terms of the overall clear height of the bent, resulting in a ratio of nearly h/1200 if the clear height of the bent excluding the rip-rap is used.

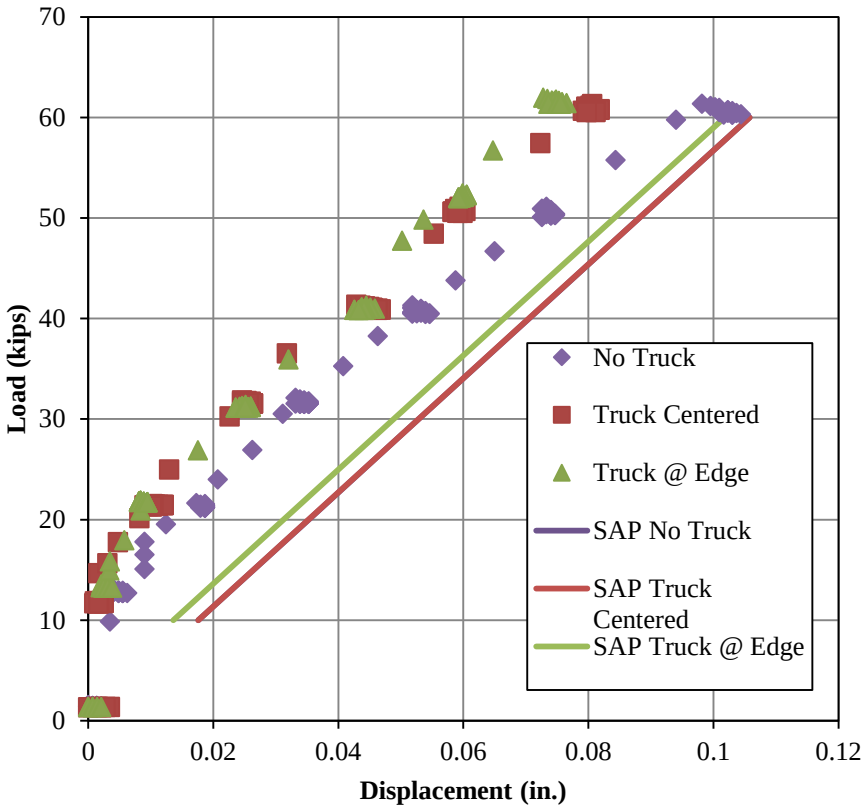

Figure 6-31 Load-Deflection Comparisons of Macon County Bent with Bridge Deck

6.6.3 US 331 Test

Bending moments and deflections from the US 331 test are compared to moments and deflections from the SAP model in this section. A number of uncertainties existed with the US 331 bent that made modeling the bent to simulate its behavior during the field tests fairly challenging.

The most significant uncertainties were material properties of the concrete used in the encasements and the bent cap and the level of additional lateral stiffness provided by the bridge superstructure during the load tests. An assumption had to be made regarding the concrete strengths of the encasements and the bent cap in order to approximate the modulus of elasticity to use for the materials of the frame elements in the structural model. A concrete strength of 5000 psi was determined to be acceptable for the encasements and the bent cap. The modulus of elasticity of the concrete was approximated using the empirical formula presented in chapter 5.

The additional lateral stiffness of the bridge superstructure and the simulation of load being transferred to the adjacent bents needed to be accounted for in the model. An approach similar to the one used for the Macon County bent was not used for the US 331 bent due to a lack of field test load-deflection data for the bent without the deck in place. No additional means of lateral stiffness were applied to the bent the take into the account the stiffness of the deck. However, it was decided to perform a displacement-controlled analysis in SAP to determine the correlation between the forces and moments from the model to the results obtained from the field tests. Non-linear load cases for each lateral load increment were created, and a limiting displacement was added to the node at the face of the bent cap in which deflections were measured in the field test. This non-linear load cases was used in load combinations including the self-weight and wheel loads from the truck, similar to the Macon County bent model. Arbitrary lateral loads had to be applied corresponding to each of the non-linear load cases; however, the displacement at the controlled node would be limited to the specified displacement in the load case. The average displacements at each load increment from each of the two field tests were used as the control displacements. The displacement increments are still referred to by the loading increment naming convention from Chapter 5.

Bending moment comparisons of the test with the load truck positioned over the edge of the roadway and the SAP model are shown in Figure 6-32 through Figure 6-37. The initial moment diagram from the SAP model represents the condition with just the load truck on the bridge. The shape of the moment diagram above ground varies from the exterior piles to the interior piles. The slope of the moment diagram in each of the interior piles is linear at higher lateral load levels (above 30 kips). The slope of the moment diagram for Pile 1 from the SAP model is concave up above ground and concave down for Pile 6. A kink in the moment diagram from the SAP models occurs below ground at each of the locations where springs are applied beginning at a depth of 14 feet below the top of the pile. The kink in the moment diagram appears to be dependent on the soil reactions at each of these spring locations. For every pile with the exception of Pile 5, the SAP model predicted higher moments at the location six inches below the bottom of the cap and the inflection point of the piles appears to be shifted down in the SAP model.

In each of the piles, the values of moment are positive at low load increments and begin to increase negatively as the magnitude of the applied lateral displacement increases. The transition from positive to negative bending moment is due to the gravity load applied to the bent and the location at which the load is applied. The truck is positioned over the piles expected to be in axial compression due to lateral load effect, therefore the magnitude of lateral load resulting in a transition from positive to negative bending moment is higher. The results from the field test appear to exhibit this behavior, but other than Pile 6, the initial positive moment values are significantly less than the predicted values from the SAP model. As a result, the maximum negative moments at larger applied lateral displacements are less than the moments calculated from the field tests.

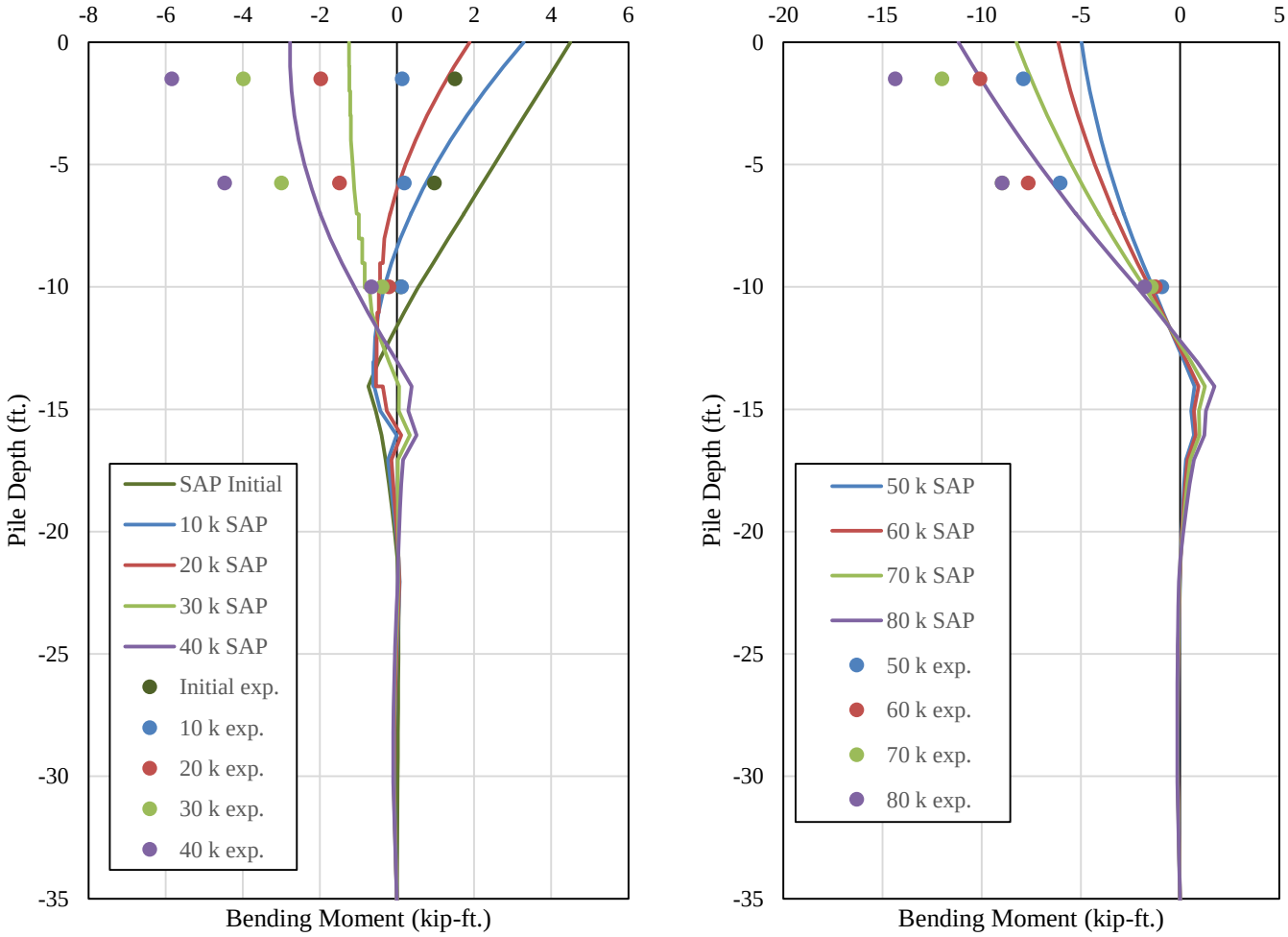

Figure 6-32 Pile 1 Bending Moment Comparisons with Truck at Edge of Roadway

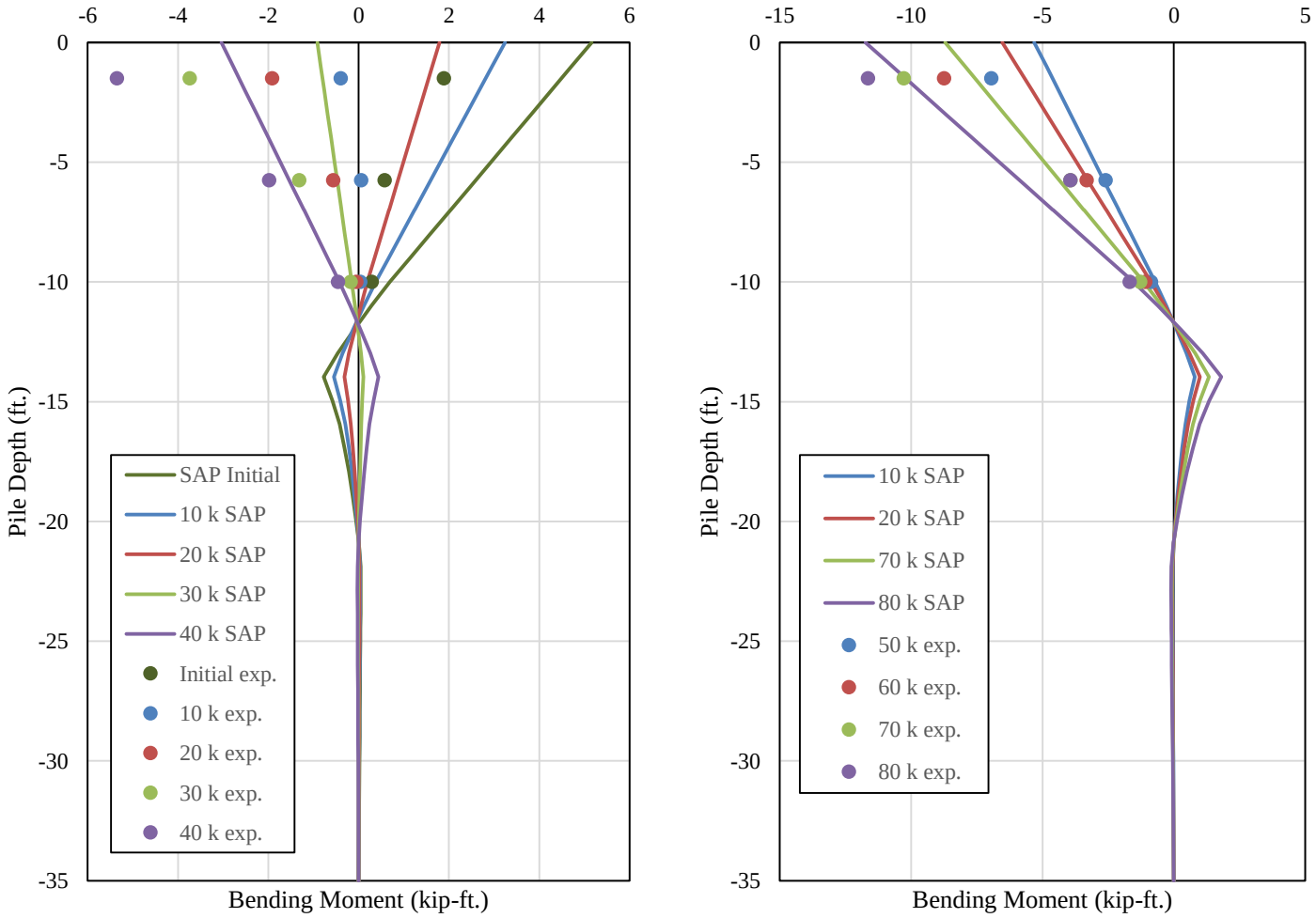

Figure 6-33 Pile 2 Bending Moment Comparisons with Truck at Edge of Roadway

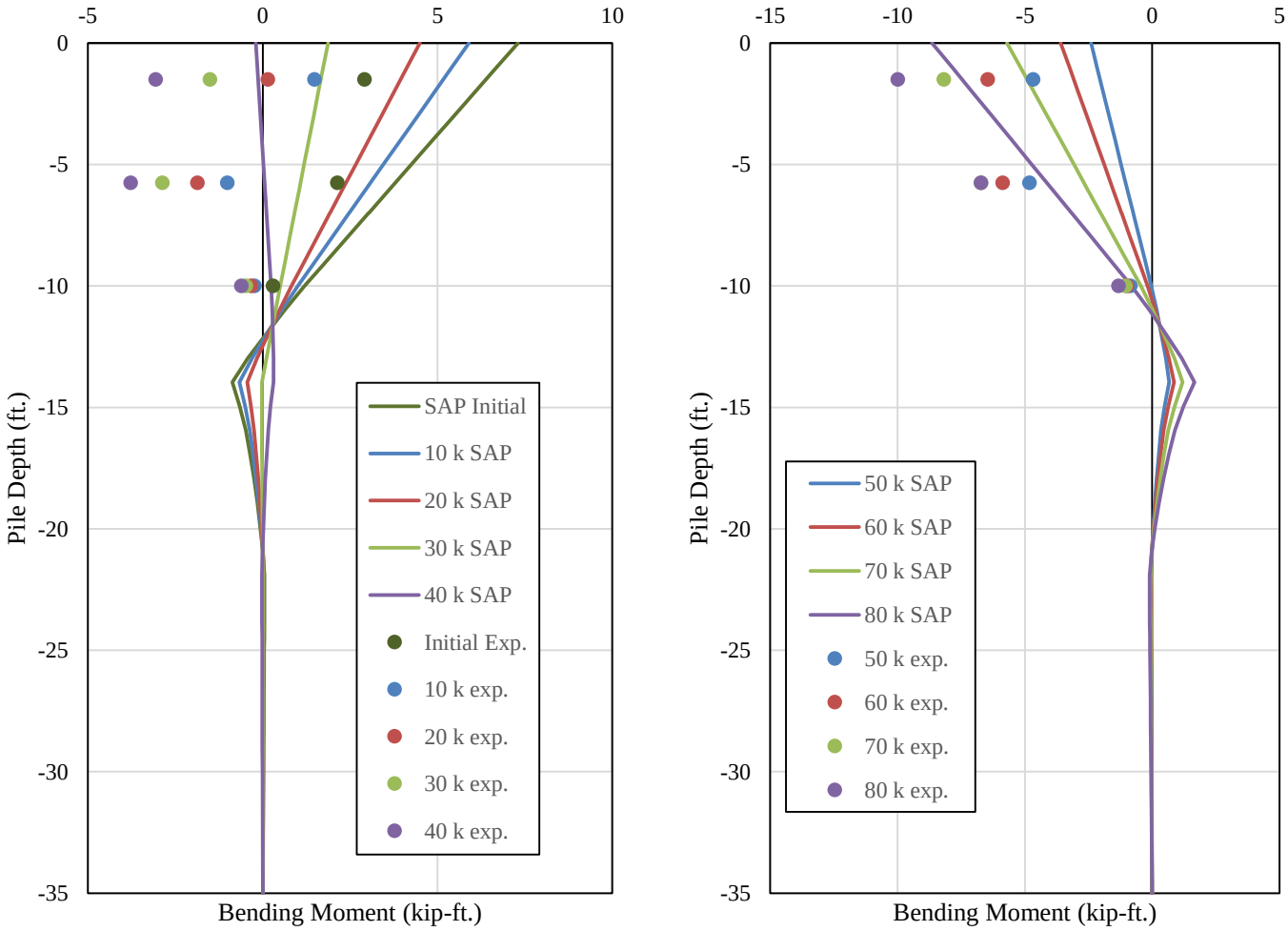

Figure 6-34 Pile 3 Bending Moment Comparisons with Truck at Edge of Roadway

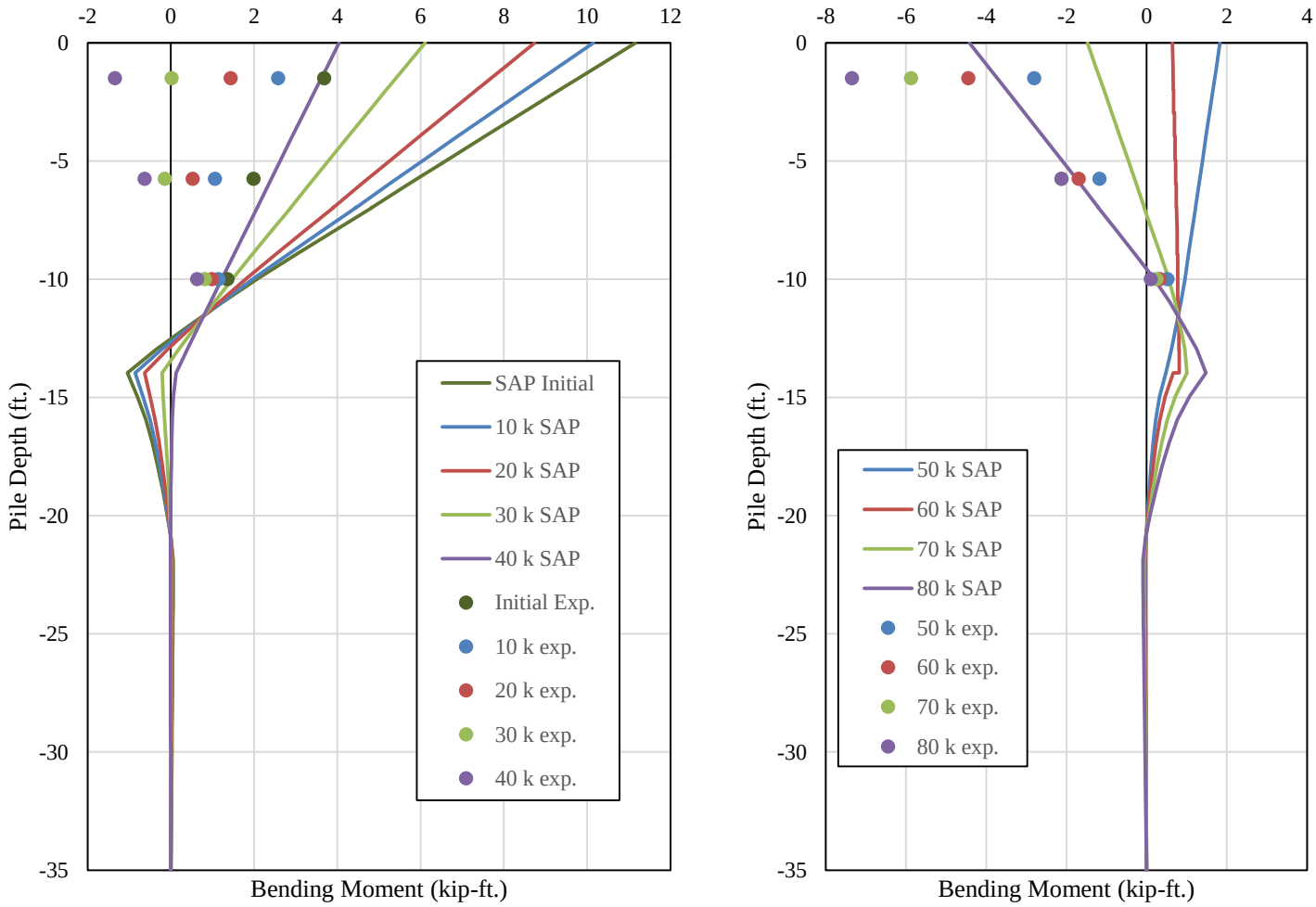

Figure 6-35 Pile 4 Bending Moment Comparisons with Truck at Edge of Roadway

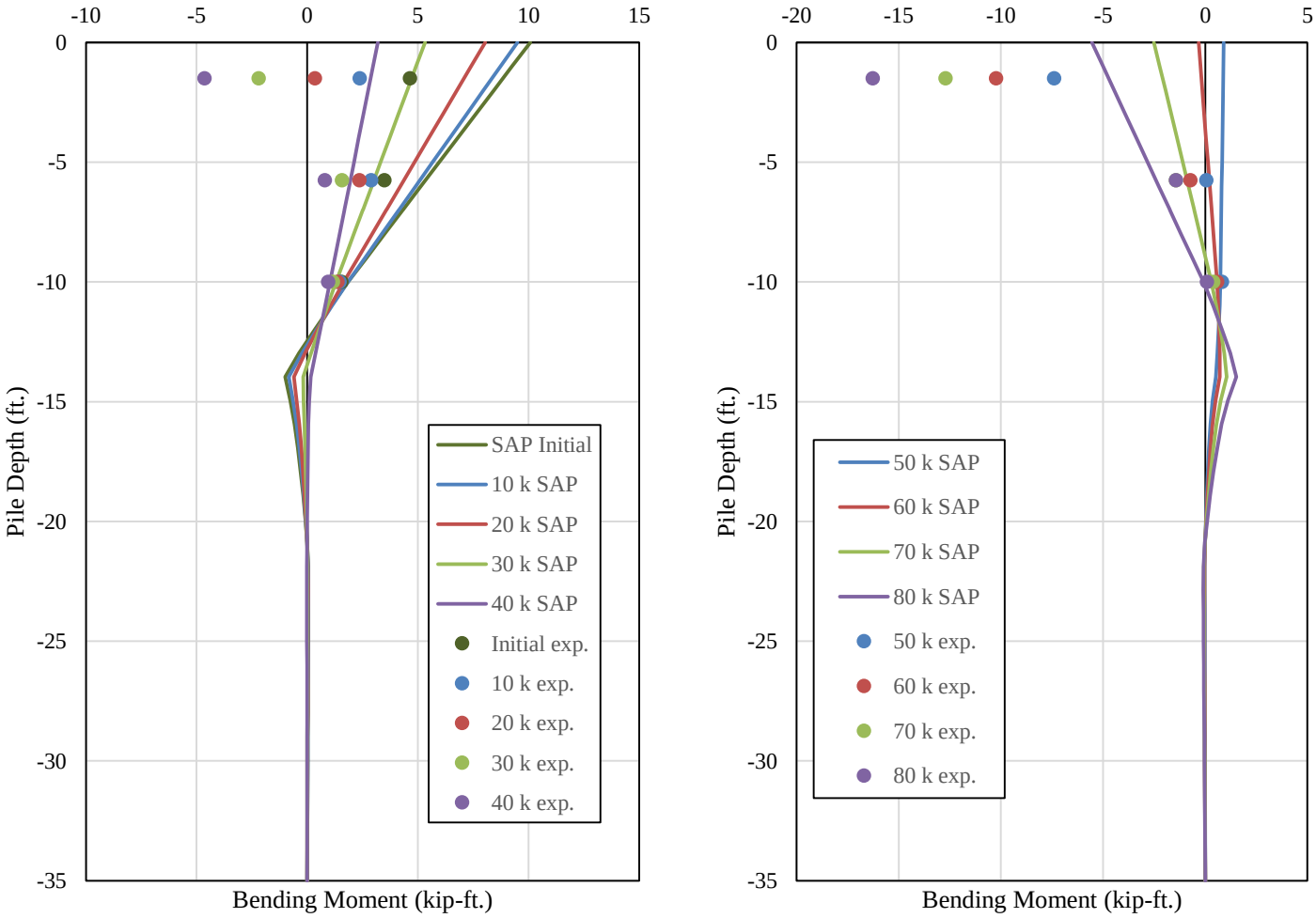

Figure 6-36 Pile 5 Bending Moment Comparisons with Truck at Edge of Roadway

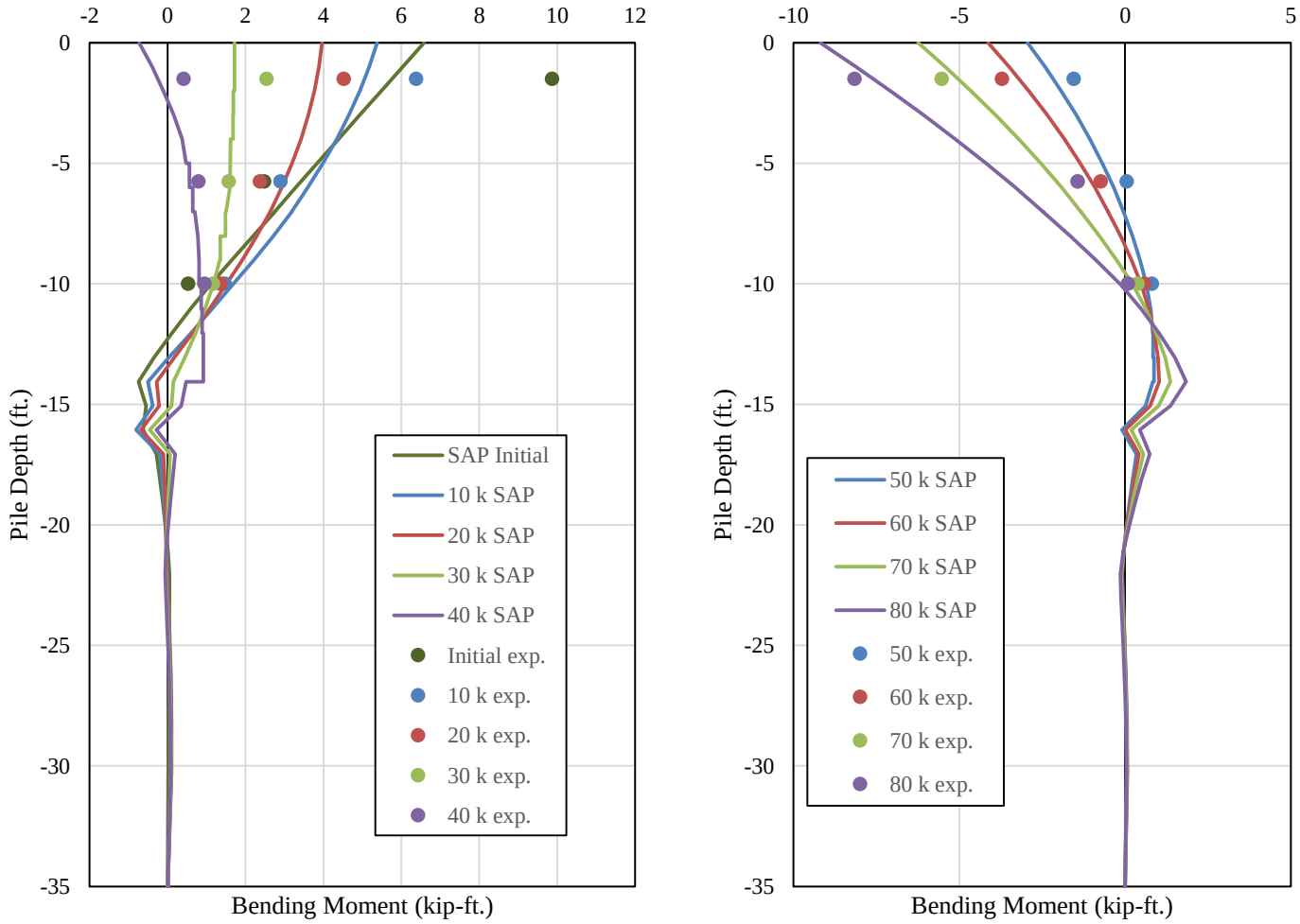

Figure 6-37 Pile 6 Bending Moment Comparisons with Truck at Edge of Roadway

The bending moments from the SAP model are compared to the results from the field test without the load truck in Figure 6-38 through Figure 6-43. The slope of the moment diagrams in the exterior piles in the SAP model was similar to the moment diagrams from the loading condition with the load truck at the edge of the roadway. For each of the piles, the maximum bending moment increases negatively as the magnitude of the applied lateral load increases. The kink in the moment diagrams in the SAP model at the spring locations occurs in this loading condition as well. Overall, the SAP model again predicted higher bending moments than the results from the field test at each of the instrumented locations, and the location of the inflection point appears to be higher in the field test results. The maximum bending moments predicted by the SAP model at the highest instrumented location ranged between 16-18 kip-ft. for the six piles in the bent compared to an average of 12-14 kip-ft. from the field test results.

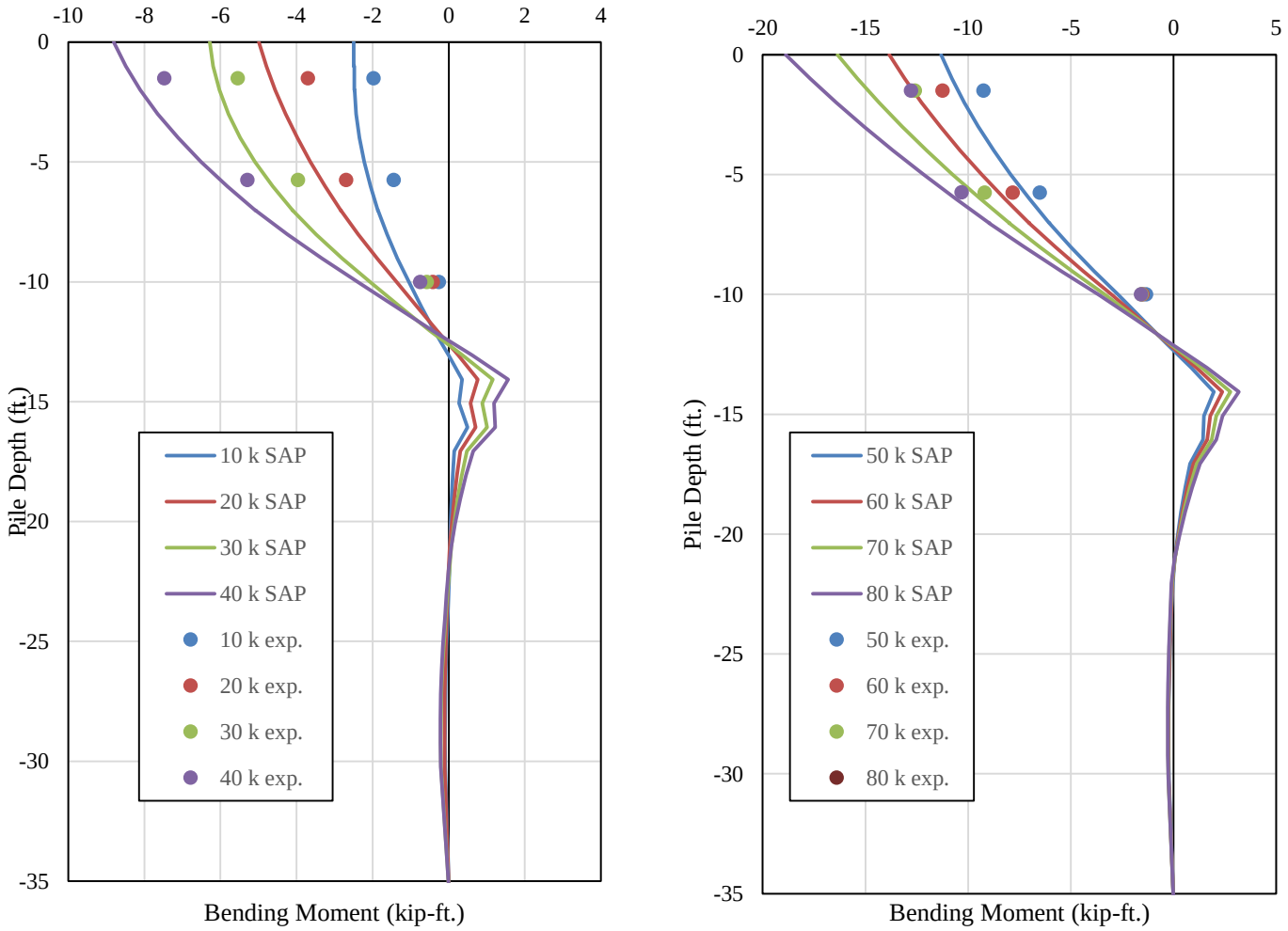

Figure 6-38 Pile 1 Bending Moment Comparisons with no Load Truck

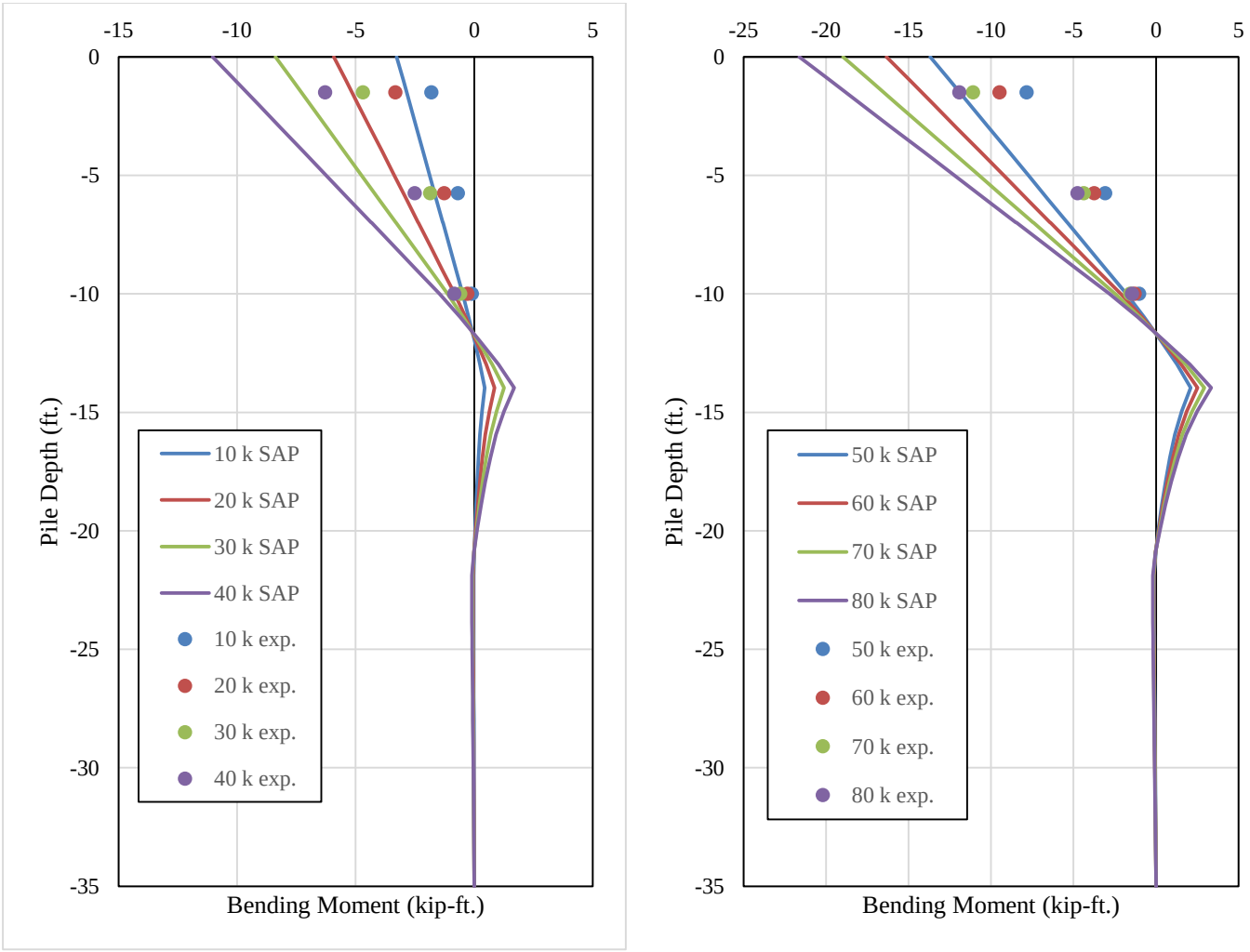

Figure 6-39 Pile 2 Bending Moment Comparisons with no Load Truck

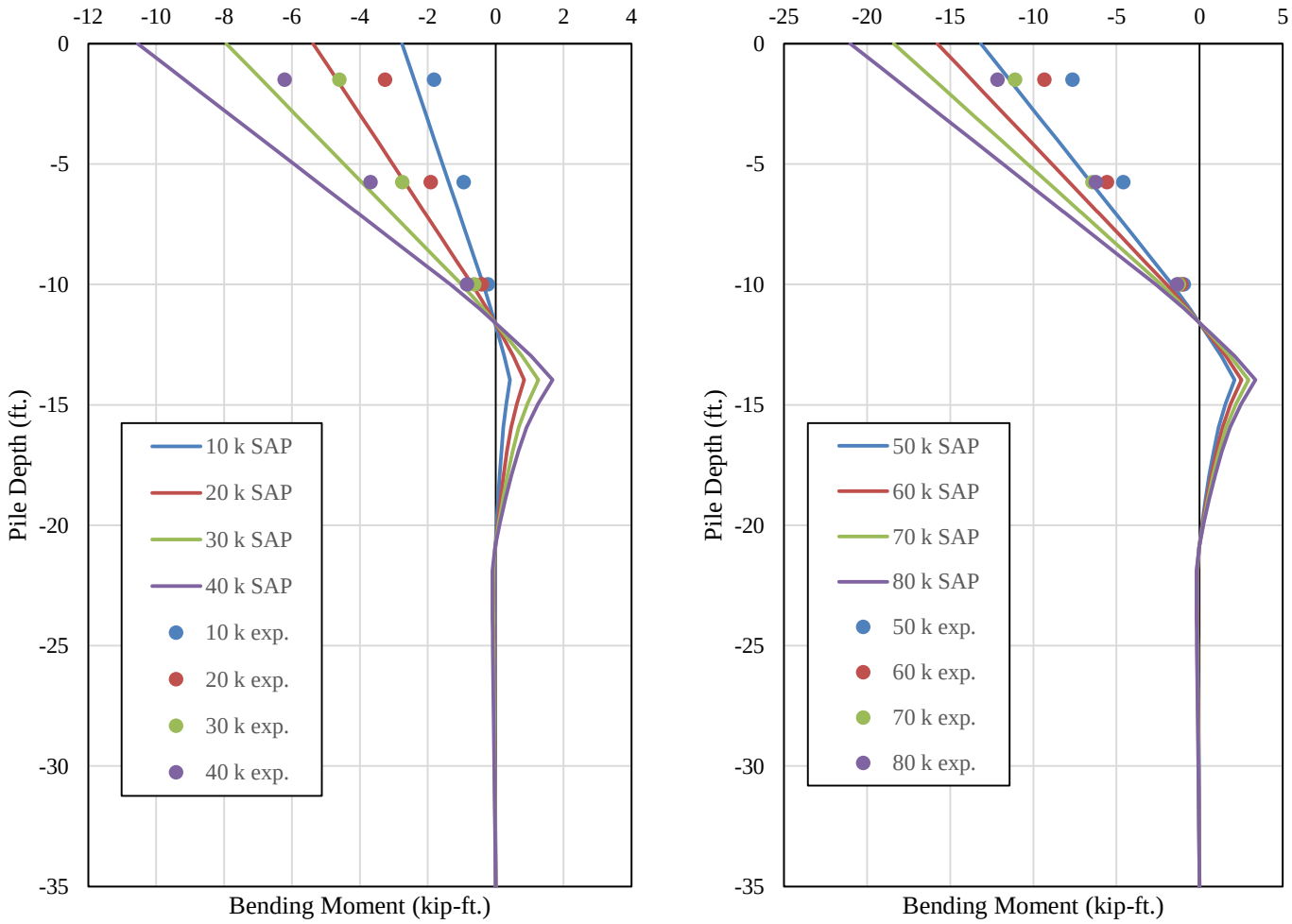

Figure 6-40 Pile 3 Bending Moment Comparisons with no Load Truck

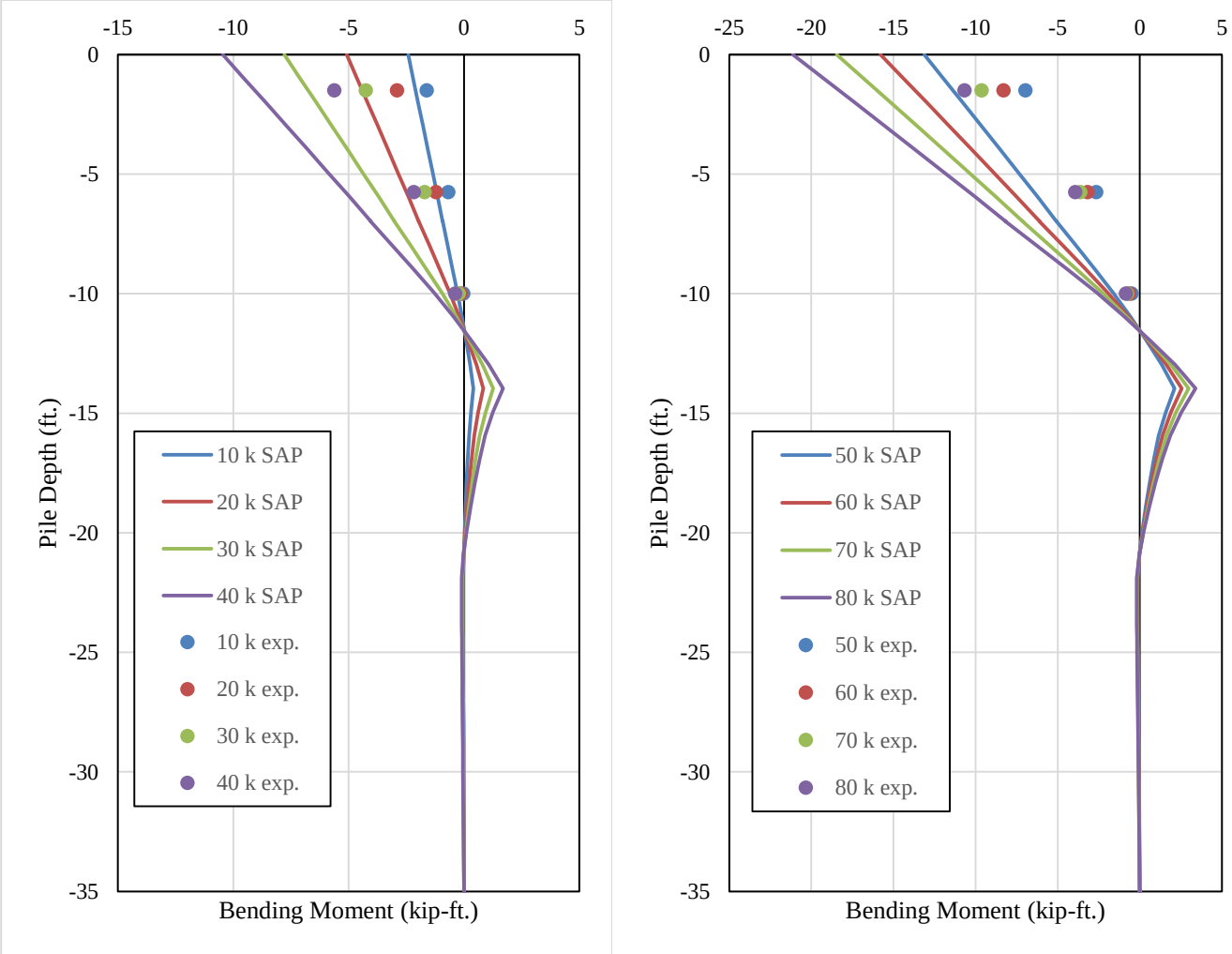

Figure 6-41 Pile 4 Bending Moment Comparisons with no Load Truck

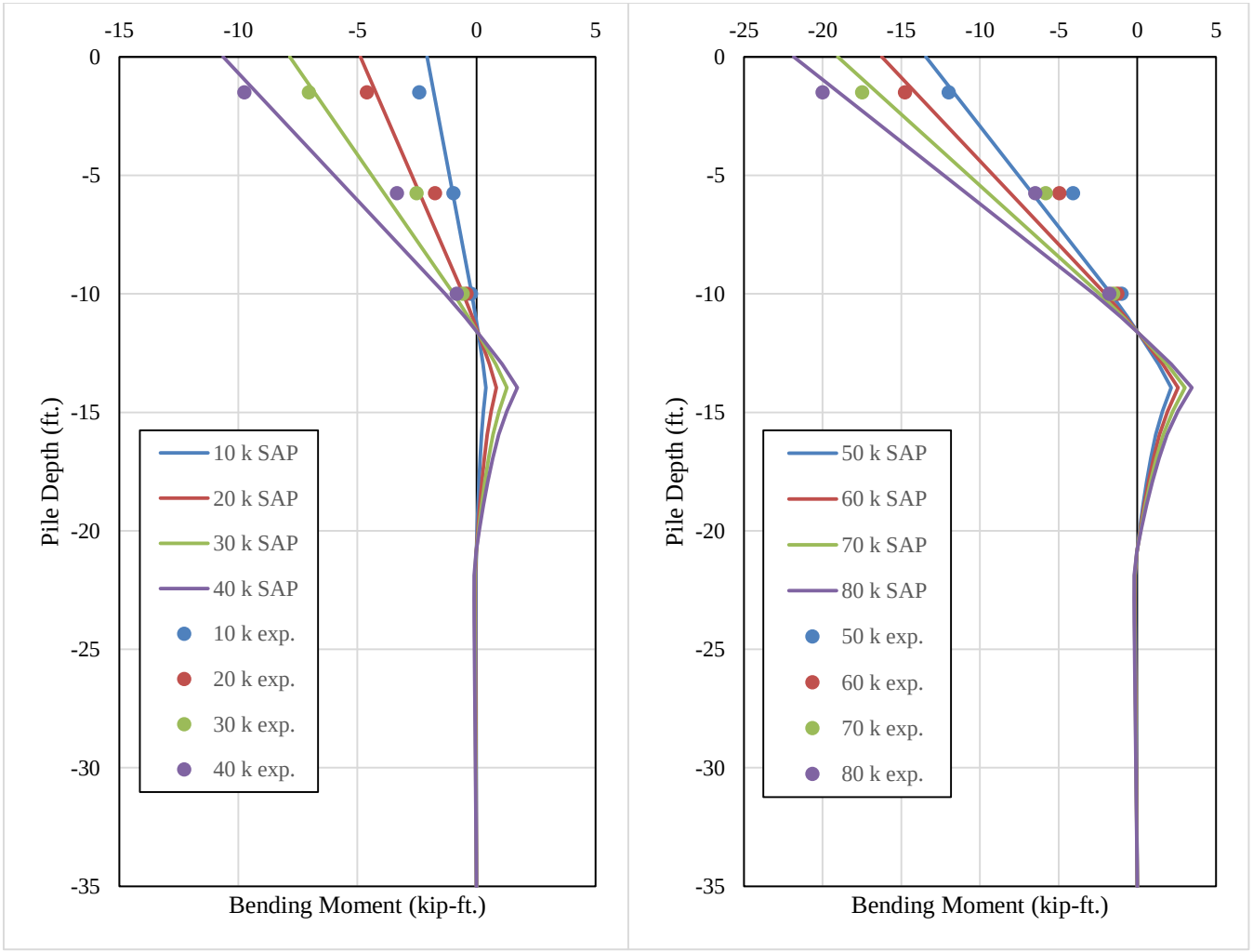

Figure 6-42 Pile 5 Bending Moment Comparisons with no Load Truck

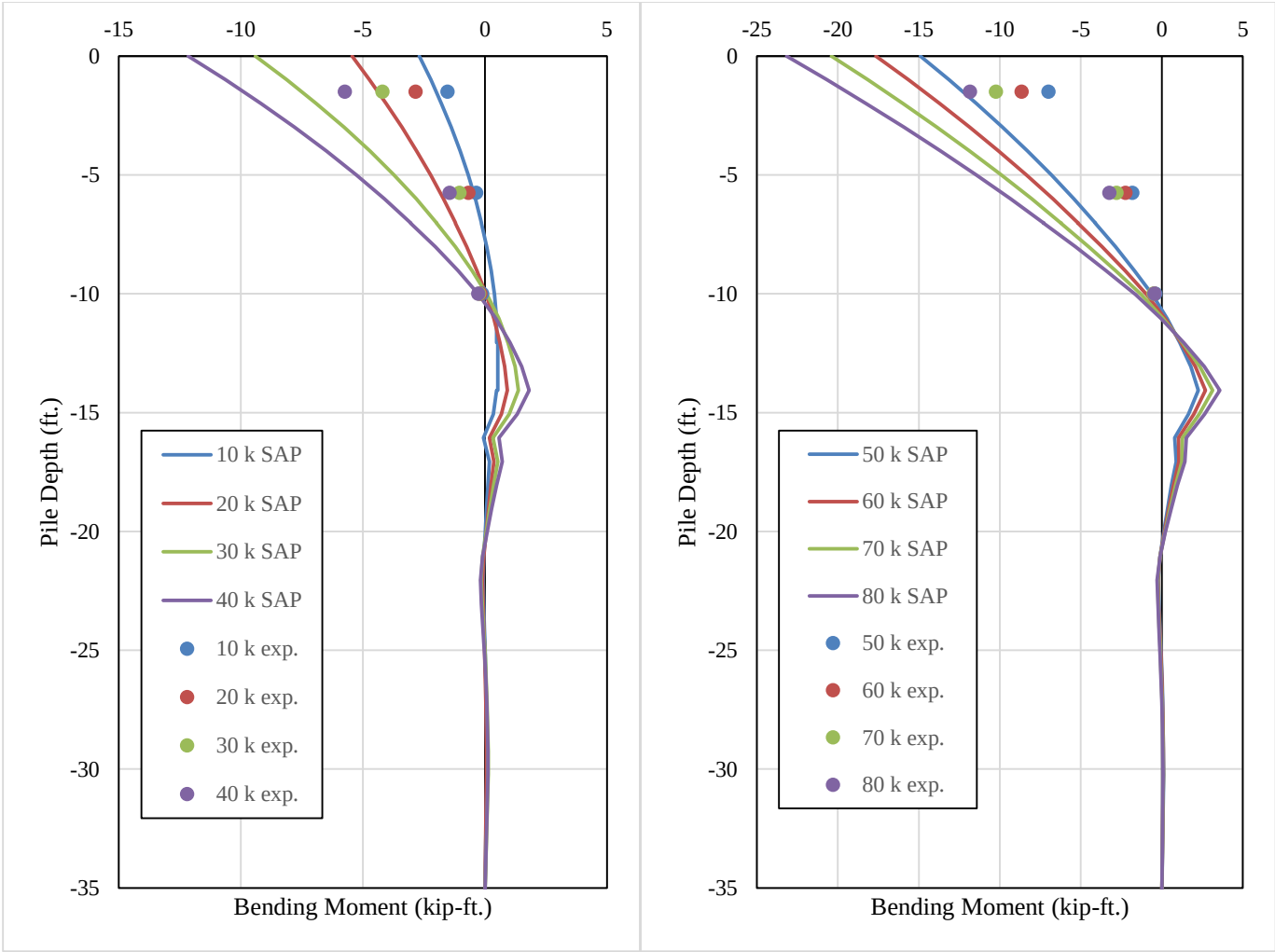

Figure 6-43 Pile 6 Bending Moment Comparisons with no Load Truck

Axial forces versus applied lateral load for each of the six piles are shown in Figure 6-44 through Figure 6-49. The axial forces computed from measured strains during the load test without the load truck are shown in these figures as well. The forces from the SAP model are the forces corresponding to only the lateral load being applied without the addition of the self-weight of the structure. The model and the field test results indicate that the exterior battered piles have the largest axial forces with the leading pile in axial compression and the trailing pile in axial tension. Notably, the axial force is plotted versus lateral load for the model forces, when in actuality a lateral displacement corresponding to the lateral load measured from the field tests was applied. The lateral displacements that were applied to the bent were not perfectly linearly; therefore the axial force does not increase linearly with applied displacements. The model predicted much lower axial forces than were calculated from the measured strains during the field tests. The large axial forces can be attributed to the large cross sectional area of the composite pile section. With a large cross-sectional area, small changes in strains can result in large changes in the axial force computed on the cross section. In terms of the cross-sectional area of the section, the axial forces computed from the measured strains in the field test are seemingly negligible. Overall, the field test results did not correlate well with the predicted axial forces from the SAP model. The leading pile was in compression and the trailing pile was in tension for both the model and the field test results; however, the magnitudes of these forces varied significantly.

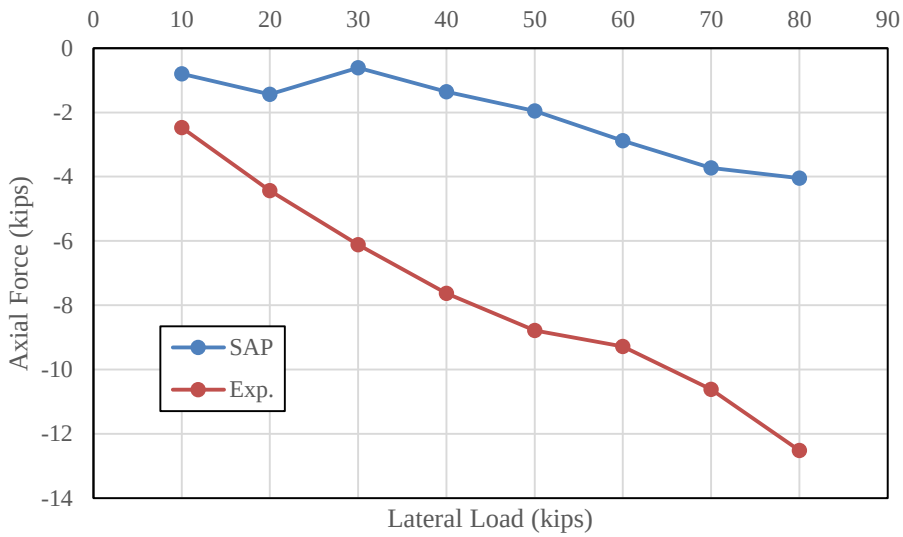

Figure 6-44 Pile 1 Axial Force versus Lateral Load Comparison

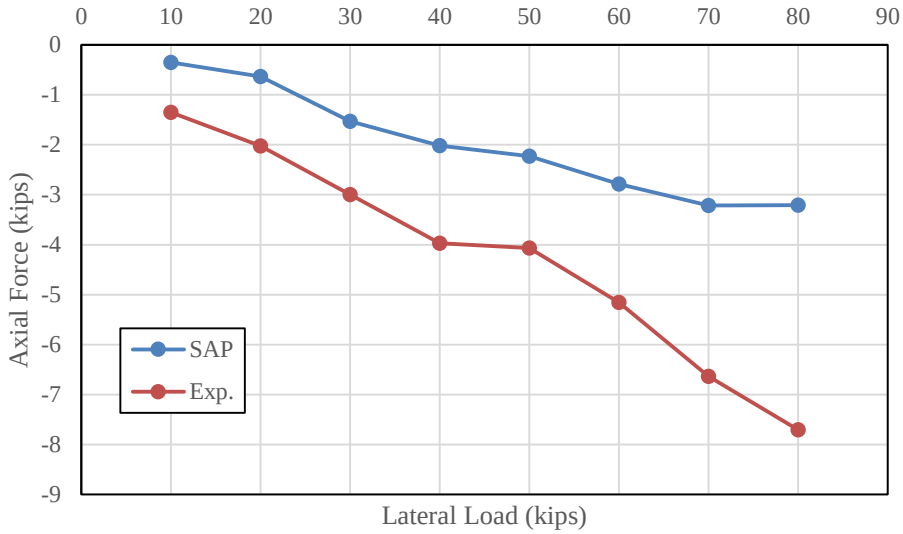

Figure 6-45 Pile 2 Axial Force versus lateral Load Comparison

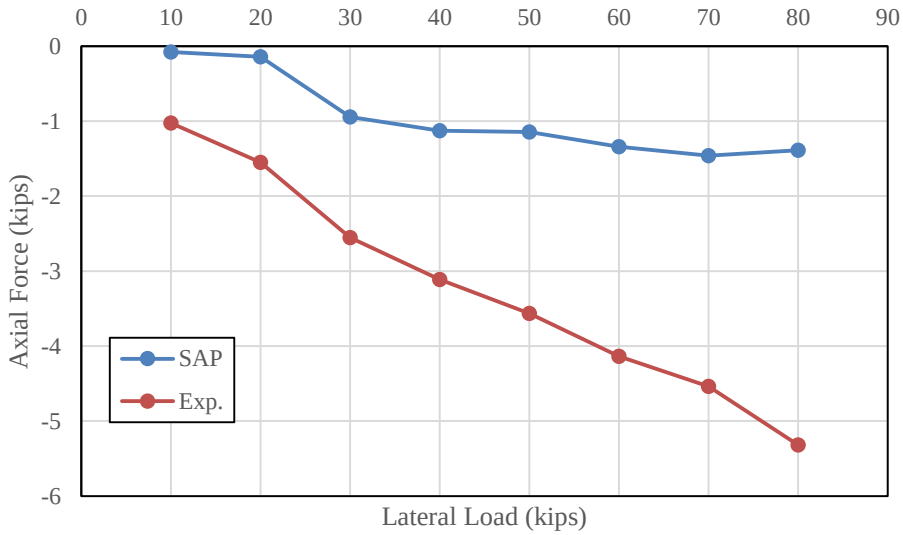

Figure 6-46 Pile 3 Axial Force versus Lateral Load Comparison

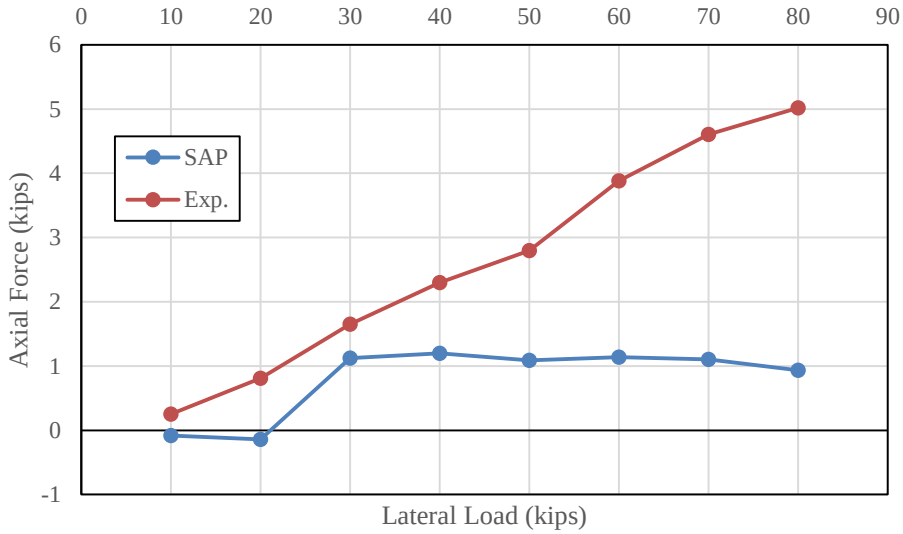

Figure 6-47 Pile 4 Axial Force versus Lateral Load Comparison

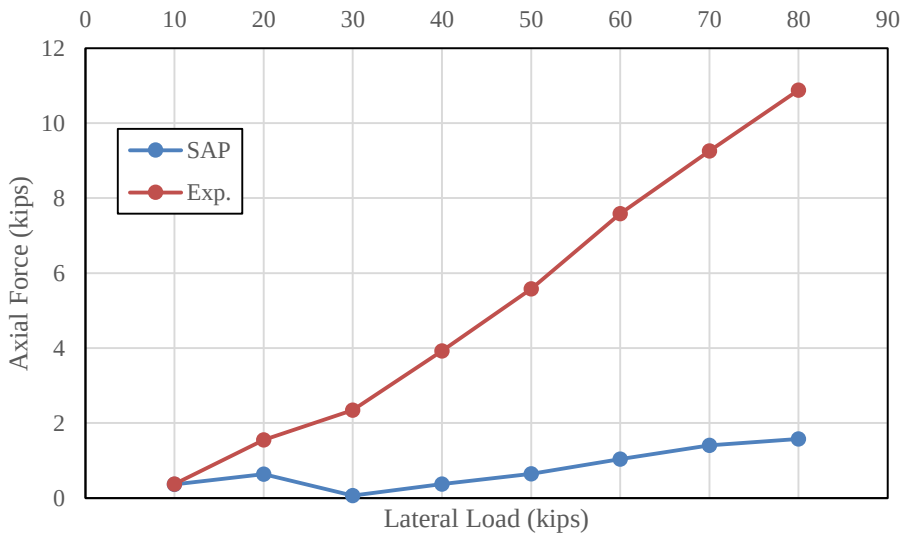

Figure 6-48 Pile 5 Axial Force versus Lateral Load Comparison

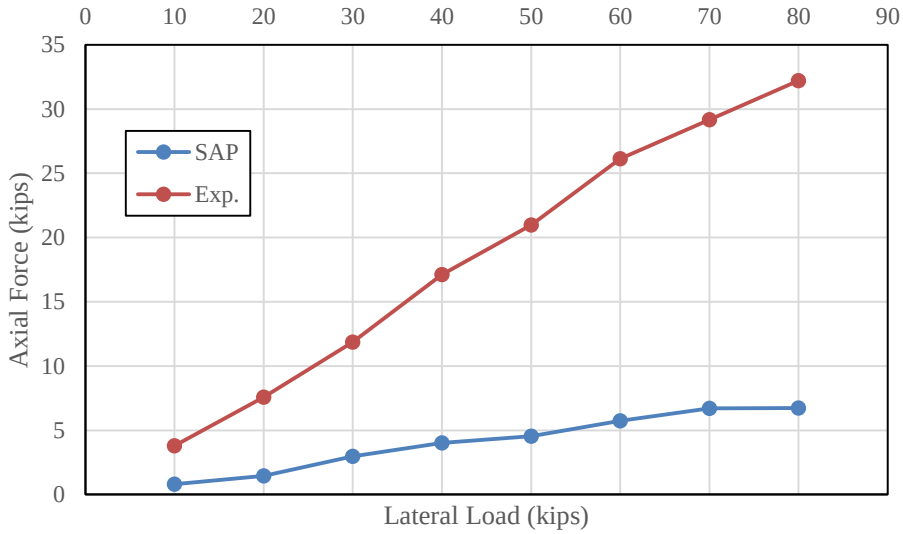

Figure 6-49 Pile 6 Axial Force versus Lateral Load Comparison

Deflections from the SAP model were applied to simulate the lateral load applied in each of the field test. Since these deflections were identical in the SAP model to the measured deflections in the field, they are not presented in this section.

6.7 Chapter Summary

The results from the SAP model created for the Macon County bridge correlated well with the results from the field test without the bridge deck. The model predicted a linear load-deflection response for the duration of the load test with the maximum deflection at the 75 kip varying from the measured deflection by 11 percent. The model seemed to over predict the magnitude of bending moments when compared to the results from the field test by 10-20 percent. The model clearly predicted that the bending moment dissipates significantly once the pile encasements are terminated, and the values of moment are very small at the below ground locations relative to the moments near the bottom of the cap.

The bridge deck provided an alternate load path in which the lateral loads were transferred to other structural elements in the bridge, most likely the adjacent bents. The transfer of loads into the adjacent bents was accounted for by applying a linear spring to the bent. The magnitude of this spring was determined using measured deflections from previous field tests. In the SAP model, the addition of the load truck had minimal effect on the load-deflection response of the bent, similar to the results from the field tests. The SAP model again over-predicted the values of bending moments at each of the instrumented locations. Overall the results from the field tests seemed to correlate reasonably well with the results from the SAP model.

A displacement-controlled analysis was performed to simulate the lateral load for the US 331 bent model. The measured displacements from the field tests were applied as nodal displacements at the face of the bent cap in order to determine how well the pile forces and moments correlated with the SAP model. For the test in which the load truck was positioned over the edge of the roadway, the bending moments at the top of the piles were positive at low load increments due to the effect of the load truck, and decreased in value becoming more negative as the applied lateral displacements increased. This transition from positive to negative moment was especially apparent

in the piles that were closer to the position of the load truck. The moments from the field tests showed the same trend, beginning positive and becoming more negative as the magnitude of the lateral load increased; however, the positive moment at lower load levels was smaller than predicted by the SAP model. As a result, the maximum negative moment at larger load levels was greater than the maximum negative moments predicted by the SAP models at applied displacements corresponding to the same lateral loads. For the load test without the load truck, the bending moments were negative moments at the top of the pile at all load levels, becoming more negative as the lateral load increased. The moments from the field test without the load truck correlated well with the SAP model under the same loadings. The SAP model over-predicted the moments in this test by 10-30 percent on average for each of the pile. As a result, the location of the inflection point predicted by the SAP model is lower than the apparent inflection point from the field test results.

The SAP models predicted the largest axial forces due to lateral load effects to occur in the exterior battered piles with the leading pile being in axial compression and the trailing pile being in axial tension. The interior vertical piles carried very roughly one fourth of the load that the battered piles carried. The axial forces increased linearly with applied lateral load in the SAP models created for the Macon County bent. The axial forces did not vary linearly with applied displacement for the US 331 model due to the displacements at corresponding with applied lateral loads in the test not having a linear trend. The magnitudes of the axial forces computed from measured strains from the US 331 tests were much larger than the axial forces predicted in the model which can be attributed to the large cross-sectional area of the pile sections.

Chapter 7 Summary, Conclusions, and Recommendations

7.1 Summary

The multi-span bridge with intermediate bents consisting of driven steel piles and a reinforced concrete cap is commonly used in the state of Alabama. Understanding the load transfer mechanism of these pile bents under lateral loading is necessary in order to provide efficient designs. The research in this thesis was performed to identify the lateral load transfer mechanism of pile bents through a series of lateral load tests performed on a new construction and in-service bridge.

From previous research, it has been found that a fully-fixed head condition at the connection of the pile to the bent cap is difficult to achieve in the field. Results from field testing indicated that the maximum bending moments in the piles due to lateral loads were developed near the top of the pile. Each of the bents that were tested consisted of piles that were encased in concrete. While these encasements are considered as non-structural elements, it was found through testing that these encasements provide a significant amount of lateral stiffness due their large moments of inertia. The addition of the bridge deck in the second Macon County test provided an alternate load path resulting in a portion of the applied lateral load transferred to other structural elements in the bridge. This portion of load being distributed to other elements within the bent was taken into consideration in analytical models created in SAP 2000. The models consisted of soil-pile interaction, composite section properties and applied loads which simulated the actual loads applied during the field tests. The results from the models correlated well with the results from the field tests in terms of bending moments and lateral displacements.

7.2 Conclusions

Based on the field testing of the Macon County Bent:

- The bent was very stiff under high lateral load levels without the addition of the bridge deck, deflecting less than 0.25” at a lateral load of 75 kips.
- The concrete encasements provide a large amount of additional lateral stiffness to the bent, even though they are not considered as structural elements.
- The encased pile sections did not appear to behave purely composite during the load test, with the measured steel strains exceeding the measured concrete strains at instrumented cross-sections where steel and concrete strains were measured.
- The largest bending moments appeared to be near the top of the pile and decreased linearly to around the ground surface.
- The addition of the bridge deck provided an alternate load path for the lateral load resulting in a part of the load being transferred to other structural elements of the bridge
- The addition of gravity load in the center of the roadway and at the edge of the roadway had little effect on the lateral stiffness of the bent.

Based on the field testing of the US 331 Bent:

- The bent was extremely stiff under large lateral loads, deflecting less than 0.1” in each of the tests with and without the load truck.
- Behavior of the steel piles during the test was unknown due to the inability to instrument the steel pile sections.
- The maximum bending moment appeared to occur near the top of the pile and decreased linearly towards zero at the ground surface.
- The calculated axial forces in the exterior piles were significantly higher than the axial forces in the interior vertical piles.

Based on analytical modeling of the tested bridges:

- Modeling soil-structure interaction through a series of linear springs appeared to provide a good representation of the soil behavior in the lateral load tests.
- The load-deflection from the SAP models was linear due to no geometric or material non-linearity being specified. The measured deflections correlated well with this linear assumption.
- The magnitude of bending moments was similar between the models and the field test results, varying by 5% in some cases to 40% in other cases.
- A fully-fixed connection between the pile head and the bent cap in the model produced similar results to the field tests in terms of deflections and bending moments.
- The addition of gravity loads from the load truck wheels had seemingly no effect on the lateral stiffness of the bent in the model.
- A displacement-controlled analysis for the US 331 model provided a more accurate approach to determine the correlation between bending moments in the model and bending moments from the field tests.

7.3 Recommendations

The following recommendations for further research were determined:

- When available, the use of inclinometers to determine pile deflected shape and rotations can provide better pile behavior over the entire pile length.
- The use of wirepots to determine vertical displacement of the bent under lateral load would monitor cap rotation.
- A cracked section analysis of the encased pile sections neglecting the concrete surface in tension would provide more accurate results.

- Stiffness modifiers in the SAP models to account for cracked section properties of the encasements should be used to model the composite pile sections.
- Providing instrumentation near the pile head within the cap can better monitor the behavior of the pile-to-cap connection.

References

American Concrete Institute (ACI). (2011). *Building Code Requirements for Structural Concrete (ACI 318-11) and Commentary (ACI 318R-11).* Farmington Hills, MI.

Bridge Software Institute (BSI). (2004). *FB-Multipier User Manual.* Gainsville: University of Florida.

AISC. (2011). *Steel Construction Manual.* Chicago.

ASTM International. (2007). D 3966-07 *Standard Test Methods for Deep Foundations Under Lateral Load*.

Bowles, J. E. (1996). *Foundation Analysis and Design, Fifth Edition.* New York: McGraw-Hill.

Broms, B. (1964a). Lateral Resistance of Piles in Cohesionless Soils, ASCE. *Journal of the Soil Mechanics and Foundations Division*, 123-156.

Campbell Scientific. (2015, September 14). *CR1000 Measurement and Control Datalogger*. https://www.campbellsci.com/CR1000

Broms, B. (1964b). Lateral Resistance of Piles in Cohesive Soils. *Journal of the Soil Mechanics and Foundations Division, ASCE*, 27-63.

Computers and Structures, Inc. (. (2011). *SAP User Manual.* Berkely, CA.

Ensoft. (2000). *GROUP 5.0: A program for the analysis of a gorup of piles subjected to axial and lateral loading* . Austin, TX: Ensoft Inc.

Gerber, T., & Rollins, K. (2009). Behavior of a Nine-Pile Group With and Without a Pile Cap. *International Foundation Congress and Equipment Expo*, 530-537.

Hetenyi, M. (1946). *Beams on Elastic Foundation.* Michigan: University of Michigan Press.

Hsiung, Y., & Chen, Y. (1997). Simplified Method for Analyzing Laterally Loaded Single Piles in Clays. *Journal of Geotechnical and Environmental Engineering, ASCE*, 1018-1029.

Mokwa, R., & Duncan, J. (2003). Rotational Restrain of Pile Caps during Lateal Loading. *Journal of Geotechnical and Geoenvironmental Engineering, ASCE*, 829-837.

Poulos, H. (1971a). Behavior of Laterally Loaded Piles: Part I-Single Piles. *Journal of the Soil Mechanics and Foundations Division*, 711-731.

Poulos, H., & Davis, E. (1980). *Pile Foundation Analysis and Design.* New York: John Wiley and Sons.

Reese, L., Isenhower, W., & Wang, S. (2006). *Analysis and Design of Shallow and Deep Foundations.* New York: John Wiley and Sons.

Richards, P., Rollins, K., & Stenlund, T. (2011). Experimental Testing of PIle-to-Cap Connections for Embedded Pipe Piles. *Journal of Bridge Engineering, ASCE*, 286-294.

Salgado, R. (2008). *The Engineering of Foundations* . New York: McGraw Hill.

Skinner, Z. (2015). *Theoretical Modeling and Lateral Load Testing of Driven Steel Pile Bridge Bents.* Auburn, AL: Auburn University.

Tonias, D. E., & Zhao, J. J. (2007). *Bridge Engineering: Design, Rehabilitation, and Maintenance of Modern Highway Bridges.* New York: McGaw Hill.

Weatherford and Associates (2013). *Bridge Over Old Town Creek on County Road 9, Project No. ACBRZ60157-ATRP(001).* Montgomery, AL.

Appendix A. Threaded Rod Calibration Data

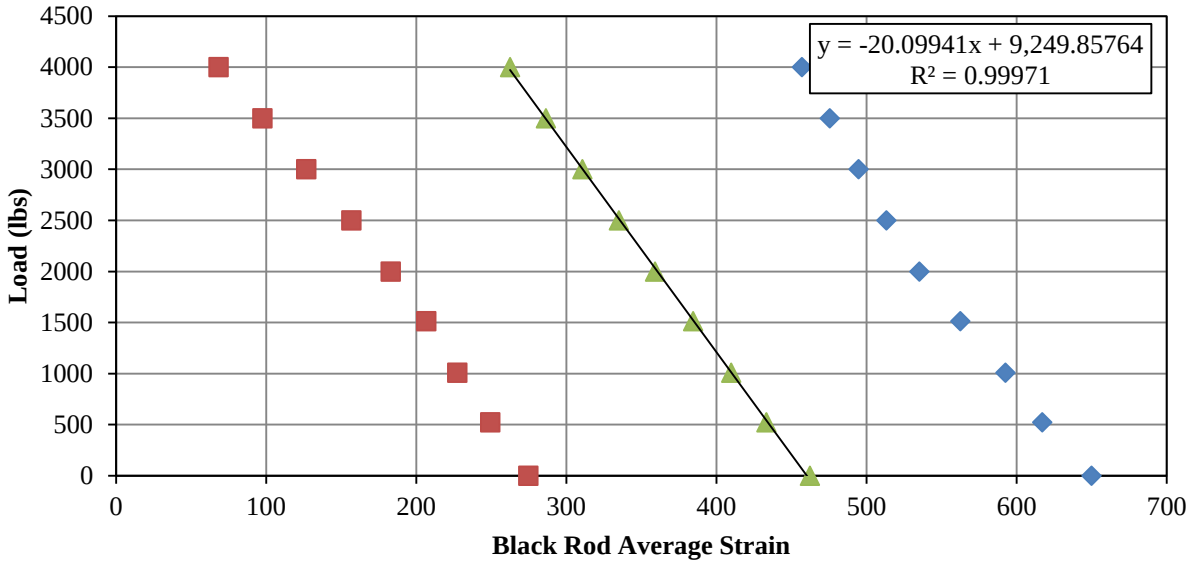

Figure A-1 Black Rod Calibration Data

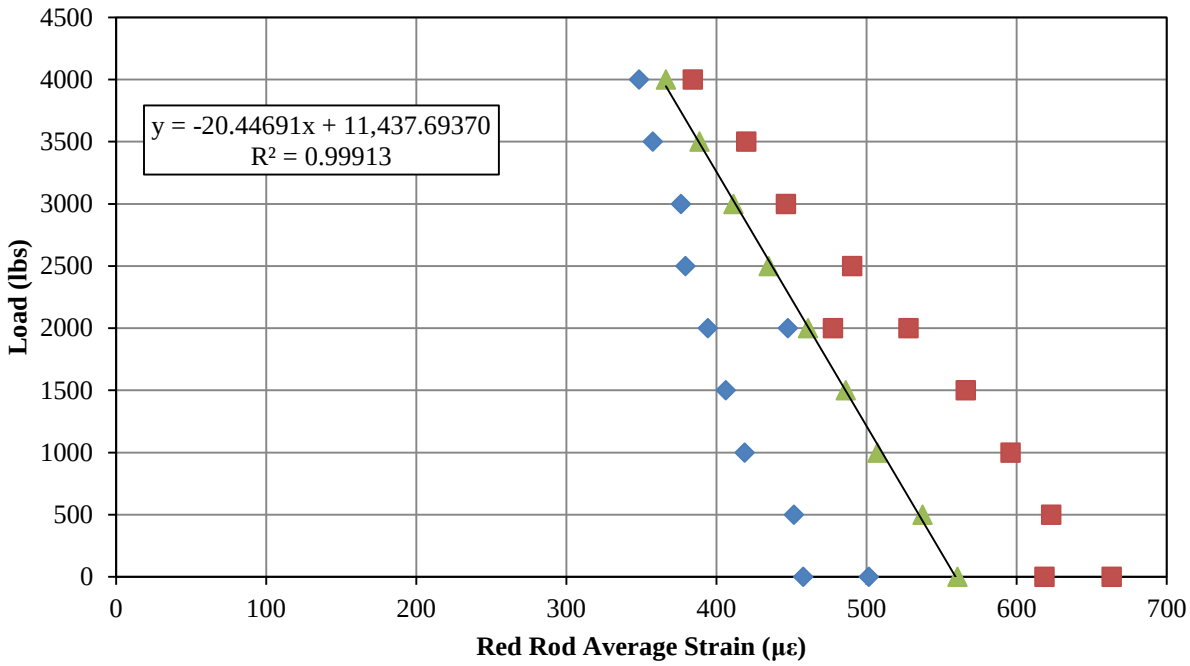

Figure A-2 Red Rod Calibration Data